Modelling the crashworthiness of specialist wheelchair devices

PAUL ROGERS

A submission presented in partial fulfilment of the requirements of the University of Glamorgan / Prifysgol Morgannwg for the degree of Doctor of Philosophy

This research programme was carried out in collaboration with the Rehabilitation Engineering Unit at Rookwood Hospital, Cardiff

November 2008

Abstract

A small percentage of wheelchair users are unable to transfer from their wheelchair to a vehicle during transportation. Reasons for an occupant to remain in the wheelchair during transport may be the inability to safely transfer to a vehicle seat, the occupant's requirement of a specialist postural management wheelchair seating system or reliance on life support equipment attached to the wheelchair. The Rehabilitation Engineering Unit at Rookwood Hospital deal with people who require either a specialist postural support wheelchair seating system, life support equipment or both. To cater for such equipment the wheelchairs have to be modified to some degree and sometimes completely custom made. In performing modifications to the wheelchairs the Rehabilitation Engineering Unit take on the manufactures responsibilities, one of which is to ensure that the wheelchair is safe for use in transport. Standard crash tests for production wheelchairs are destructive so are impractical to use for bespoke wheelchair designs meaning that the Clinical Engineers at the Hospital have to rely on their best engineering judgement as to whether a wheelchair design is crashworthy or not. It was proposed that by using computer crash simulation techniques an informed judgement of the crashworthiness of the bespoke wheelchair designs could be attained. A series of computer models of occupied wheelchairs were created and validated against physical crash data performed on surrogate wheelchairs. These validated wheelchair computer models were then used to examine a series of different crash scenarios that provided the Clinical Engineers at Rookwood hospital with an informed process for virtually assessing the crashworthiness of their wheelchair designs. The validation results showed that the wheelchair crashworthiness could feasibly be predicted by computer simulation. This thesis concluded that attaching equipment to the wheelchair can increase both its horizontal displacement and the forces on the tie-downs securing the wheelchair to the vehicle chassis. Skewed impact simulations also highlighted the poor lateral restraint ability of the 4-point webbing tie-down system and also the importance of sufficient lateral support on the wheelchair for occupant protection.

Acknowledgements

I'd like to thank my supervision team, consisting of Professor Steve Wilcox, Dr Alex Chong and Dr Colin Gibson for their help and support over the last few years.

My sincere gratitude to all the personnel at the Rehabilitation Engineering Unit, Rookwood Hospital, Cardiff who made me feel welcome and assisted greatly with their wheelchair and specialist seating knowledge.

ARUP for their software support, in particular Ian Bruce, Hazel Partridge and Brian Walker.

Kieran Forrington at Millbrook Proving Ground, Bedford for technical information.

Thanks go to Bob Appleyard and Q'Straint for supplying wheelchair tie-downs and seatbelts for testing, draft sketches for ISO 10542 and 16840 surrogate wheelchairs and invaluable knowledge of wheelchair crash testing.

Leyton Stevens at Invacare, UK for inviting me along to one of their wheelchair crash tests.

Dr Paul Mouser and Dr David Shearer for their invaluable advice and motivation.

To my friends and family for their encouragement.

And, last but certainly not least, to Elaine for her patience, understanding and support over the last 4 years.

Table of contents

List of figures

List of tables

Nomenclature

P-point	Centre point of a cylinder of 100mm diameter and 200mm length placed on a wheelchair seat so that the cylinder surface touches both the seat and seatback
H-point	Point between the hip joints of the dummy
X	Horizontal direction
Y	Lateral direction
Z	Vertical direction
$\{k\}$	Stiffness matrix
$\{\mu\}$	Nodal displacement matrix
$\{F\}$	Force matrix
μ	Nodal displacement
$\dot{\mu}$	First derivative of nodal displacement
$\ddot{\mu}$	Second derivative of nodal displacement
[C]	Damping matrix
t	Time
t_s	Time step
E	Young's Modulus
c	Speed of sound through a material
ρ	Material density
G	Shear modulus
υ	Poisson's ratio
g	Gravity
m_F	Mass over front wheelchair wheels
m_R	Mass over rear wheelchair wheels
m_{right}	Mass over right wheelchair wheels
m_{left}	Mass over left wheelchair wheels
m_{WC}	Total wheelchair mass

d_W	Distance between front and rear wheelchair axles
x_{RA}	Distance of centre of mass from rear wheelchair axle
w	Distance between mid-plane of rear wheelchair wheels
y_{RW}	Centre of gravity from rear right wheelchair wheels midplane
θ	Angle of wheelchair elevation during stability testing
$m_{F\theta}$	Mass over front wheelchair wheels at angle, θ
$m_{R\theta}$	Mass over rear wheelchair wheels at angle, θ
h	Height of wheelchair's centre of gravity above the ground
θ / s	Radians per second for pitching vehicle
z_R	Nodes at the rear of the vehicle chassis
z_F	Nodes at the front of the vehicle chassis
d_N	Distance between the front and rear vehicle chassis nodes
X_{WC}	Wheelchair horizontal P-point excursion
X_{knee}	Dummy knee horizontal excursion
X_{headF}	Front of dummy's head horizontal excursion
X_{headR}	Rear of dummy's head horizontal excursion
ε'	Uniaxial strain rate
$\sigma(\varepsilon')$	Stress at uniaxial strain rate
D	Cowper Symond's constant
q	Cowper Symond's constant
σ_0	Yield stress
k	Stiffness
x	Displacement
F	Force

Chapter 1 - Introduction

This work was conducted in collaboration with the Rehabilitation Engineering (RE) Unit at Rookwood Hospital, Cardiff who identified a need for virtual crash testing of their specialist wheelchair and seating systems and approached the University of Glamorgan for assistance. Although there are many other RE units throughout Britain who perform a similar service, and therefore are most likely to have similar issues regarding the crash safety of their equipment, only those of Rookwood Hospital's RE Unit will be considered in this thesis.

The Rehabilitation Engineering Unit at Rookwood hospital creates custom wheelchair and specialist seating systems for people with spinal abnormalities and people who rely on the equipment attached to their wheelchair, e.g. life support systems, specialised seating for postural management or environmental controls. The patient's dependency on these wheelchair systems means that the majority of the RE units client base must be transported in a vehicle while remaining seated in their wheelchair. Before a vehicle can transport an occupied wheelchair it must be retro fitted with an access ramp or lift, have chassis mounted load points, to attach the wheelchair, and have a B-pillar fitted (fixing point for upper seatbelt anchor), if one is not already available, see Figure 1.1.1. The standard recognised method for securing a wheelchair in a vehicle is by placing 4 webbing straps, known as tie-downs, to each corner of the wheelchair. These tie-downs are fixed to the vehicle chassis by cleats at one end and secured to the wheelchair by hooks, which locate at loading points, at the other. A three point seatbelt is fitted around the occupant that has its upper anchor point fixed to the B-pillar and lower anchor points fitted to the vehicle chassis. A typical setup of a wheelchair and occupant secured in a vehicle is shown in Figure 1.1.1.

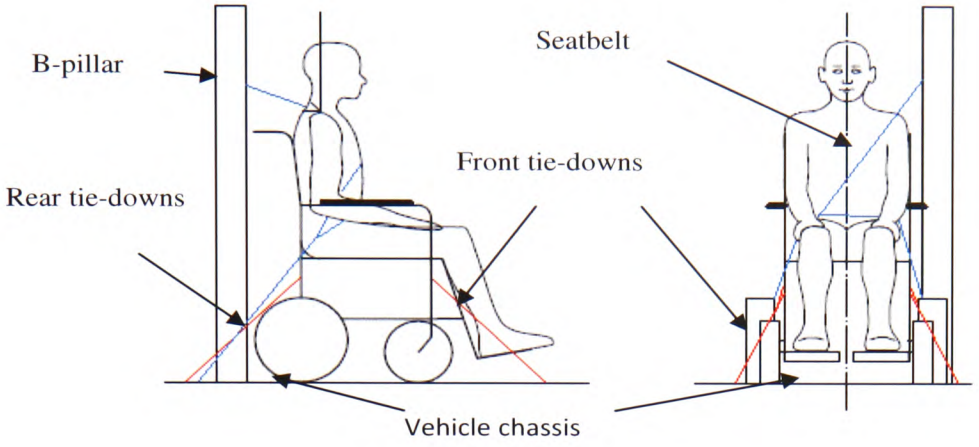

Figure 1.1.1 showing a typical setup of a secured wheelchair and occupant in a vehicle [1].

1.1 Occupant risk

The NHS has put forward proposals to provide people on life support with the freedom of wheeled mobility by attaching their life support equipment to a wheelchair. This gives an improved standard of life to the patient, frees up limited hospital beds and also reduces a significant cost burden on the NHS. Although the process of attaching life support equipment to a specialist wheelchair, and the associated care required, is not cheap it is readily offset against the cost of keeping someone in intensive care, currently in the region of £1200 per day [2]. An important consideration to take into account when attaching life support to a wheelchair is the increased risk to the patient.

Risk, in medical terms, is a measure of the probability and severity of harm. Clinical risk is described as hazards (potential sources of harm) to a specific patient resulting from a specific clinical investigation or treatment designed to produce a specific clinical benefit to that patient. In the case of the RE Unit at Rookwood Hospital the treatment to a patient is a wheeled mobility device and postural support system, issued to provide the benefit of improving mobility and posture.

As far as litigation is concerned Rookwood hospital take on the responsibility of the manufacturer as soon as they modify the wheelchair in a way that is not in accordance with the manufactures instructions. This is unavoidable if Rookwood are to deliver a

complete solution to their customers. As a result the RE Unit must carry out a risk assessment for each of the wheelchairs they issue. This risk assessment is primarily undertaken to ensure maximum safety to their clients, although it also helps to protect the department from litigation.

Part of the risk assessment process includes the ability of the wheelchair system to offer adequate protection to the occupant in the event of a crash while being transported in a vehicle. The current standard for assessing the crashworthiness of wheelchairs in transport is ISO 7176-19 [3]. This standard requires production wheelchairs to be physically crash tested to determine whether or not the wheelchair offers sufficient occupant protection. As the name implies, crash testing is a destructive test. The cost of crash testing is high (in the region of £12,700) due to both the test itself and the cost of the destructed test specimen, see Table 1.1.1. The testing cost can be easily justified for a mass produced wheelchair design but is unfeasible for the bespoke wheelchair designs that the RE Unit produce. There are also the impracticalities of destroying a one off wheelchair design as one would effectively have to make two identical wheelchair systems, one to crash test and one to issue to the patient. At present the RE unit have to use their engineering judgement as to whether their wheelchair systems are safe for transport or not. It has been proposed that a computer model of the wheelchair system and occupant could be virtually crash tested to aid the RE unit's risk assessment process. 'Virtual crash testing' is the process of creating a computerised representation of a physical event and using it to help predict the outcome of a physical crash. Virtual crash testing of the wheelchair and occupant in a crash would not only provide the RE unit with the confidence to issue their wheelchair systems for use in transport but ultimately improve the safety afforded to the occupant. It was hoped, therefore, that by using computer simulation an informed judgement of the wheelchair's crashworthiness and safety of the occupant can be attained.

Item		Cost (£)
Wheelchair		4000
WTORS		312.55
Life Support		
	Breas Ventilator PV 403	4898.58
	Leardal Suction Unit	757.88
	Oxygen cylinder	164.50
	Connection and fittings	100.00
Crash Test		2000.00
1 day for two members of staff		200.00
Transport, accommodation and expenses		300.00
Total		12,733.51

Table 1.1.1 showing the cost of physical crash testing using a custom made stretched wheelchair with typical life support equipment as an example

1.2 Injury

A surprisingly large amount of work [4-33] has already been carried out in the area of wheelchair crashworthiness. The vast majority of these studies have focused on specific areas of interest, such as tie-down and seatbelt forces and seat strength, for generic wheelchairs and not focused in detail on any specific model of wheelchair. This thesis looks at the feasibility of using computer crash testing to help predict the crashworthiness of specific one-off wheelchair systems in order to enhance the risk assessment process that the Rehabilitation Unit at Rookwood Hospital must carry out. Specific injury to the occupant, however, shall not be covered in this work.

The reasons for not including occupant injury in this thesis are two fold. Firstly the wheelchairs that the RE unit modify are designed in accordance with ISO 7176-19, which only requires that the occupant remain in a designated position during and after the crash event. It would be unreasonable to expect the RE unit, upon modifying the wheelchair, to improve upon the underlying safety of the wheelchair by considering the injury experienced by the occupant.

Secondly, quoting head, neck, chest injury criteria would serve little purpose as the Hybrid III Dummy model used in the crash simulations herein is not validated, although it is effectively identical to the validated version available at considerable cost [34]. Only the head acceleration of the physical dummy was recorded in the physical crash tests to aid validation against the computer simulated model. Furthermore, much has been written on the poor suitability of the Hybrid III dummy's neck to model rear and lateral impacts [35, 36].

It may well transpire that injury levels of the wheelchair occupant will have to be within certain limits in the future version of wheelchair crash safety standards. Indeed, this would be a desirable step forward in wheelchair occupant safety.

1.3 Wheelchairs transported in vehicles

There are a number of vehicles in which a wheelchair and occupant may be transported. The two main groups of vehicle can be classed as public (coaches and buses (M2 and M3 class vehicles)) and private (cars, taxis and minibuses, M1 vehicles). Each of these vehicles presents its own problems to the wheelchair user in terms of access and securement.

A very comprehensive study of the issues surrounding wheelchairs in public vehicles was conducted by the Transport Research Laboratory (TRL) for the Department of Transport [26]. The objective of the study was to identify the level of safety of wheelchair occupants on public transport compared to able bodied passengers. The report dealt with frontal impacts, although the wheelchair faced rearward in some scenarios, effectively making some of the tests rear impact. The computer modelling in the study was highly simplified and was used to investigate occupant excursions in order to examine possible body impacts with any part of the vehicle interior (secondary impacts). Having details of the occupants excursion in a frontal crash allowed an excursion envelope to be constructed. This envelope was used by the Department of Transport to ensure that there were no protruding parts in the area of the vehicle set

aside for wheelchair users. Those that could not be removed were adequately padded to reduce injury.

Another vehicle that often transports occupied wheelchairs is the ambulance. Levick *et al.* [37] conducted a preliminary study to compare the injuries sustained to a restrained and unrestrained occupant in the back of an ambulance. The results were as expected with the unsecured occupant being thrown around the vehicle interior. The results raise an important point about injury to other occupants in the vehicle if any part of the wheelchair or occupant securement system should fail. This also applies to medical or control equipment that might be attached to the wheelchair. The issue of occupied wheelchairs transported in vehicles is becoming more prevalent as the government have put forward legislation to ensure more disabled people have access to vehicular transport by encouraging manufactures to test their products for vehicle use. There are also financial incentives for taxi drivers who have taxis fitted with wheelchair attachment points [38].

This study will only consider the crashworthiness of wheelchairs and their occupants transported in private vehicles with a standard 4 point tie-down system and 3 point restraint harness (seatbelt) attached to a designated B-pillar. A typical vehicle is illustrated in Figure 1.3.2.

This thesis will begin by examining the existing literature related to wheelchair crash testing. The methodology of the practical and simulated experiments will be discussed followed by a detailed examination of the computer modelling approach and then the validation against the results obtained from the physical tests. Finally the overall feasibility of using this method of computer simulation to aid the risk assessment of the crashworthiness of custom wheelchairs will be concluded.

Figure 1.3.2 showing a wheelchair and occupant being loaded into a converted Citroën Dispatch (left) and the wheelchair secured into the rear of the vehicle with tie-downs attached to the vehicle chassis (right)

1.4 Aims

The aim of this thesis is to conduct an investigation into the feasibility of using finite element techniques to predict the crashworthiness of bespoke wheelchair devices.

Specific Objectives

- To validate a virtual computer generated model of an ISO 10542-19 wheelchair crash test with an equivalent physical crash test.
- Identify which parts of the wheelchair crash testing standard (ISO 7176-19) can be predicted using the virtual computer generated wheelchair model.
- Investigate the wheelchair model's ability to predict the following non-ISO standard loading conditions:
    - Crash forces applied in a rearward direction
    - Addition of life support equipment
    - Inclusion of vehicle pitching
    - Affect of pneumatic and solid wheels on the dynamic response
    - The effects of skewed impact on the wheelchair and occupant

Chapter 2 - Literature Review

The Literature review outlines the work that has been undertaken in the field of wheelchair crash testing and describes areas where further work is required. Literature concerning specific wheelchair crash studies, as well as broader papers covering current computer modelling techniques for crash testing, will be examined.

The literature review will review the current legislation governing the safe transportation of wheelchair users. These standards apply to both the manufacture of wheelchairs and the person responsible for transportation. The parts of the wheelchair system that affect its crashworthiness will be examined independently, i.e. seatbelt anchor orientation, seat back strength, seat to chassis interface, wheelchair tie-downs and wheel compression. There are a number of different crash orientations that the vehicle transporting the wheelchair and user could be subjected to. Literature pertaining to the effects that these different crash orientations has on the occupant and structure will be considered. The main tool for analysing the crashworthiness of the wheelchair and seating system will be computer simulation. A number of useful studies on both wheelchair and vehicle crash simulation have been reported elsewhere and their relevance to this body of work will be discussed. Computer simulation should be validated against physical test data and the techniques employed by others to do this will be described and commented on. Finally, a conclusion of the literature will highlight gaps in the current knowledge that this body of work aims to address. To this end the Literature Review explains how the work in this thesis is novel and how it benefits the wheelchair crashworthiness community.

2.1 Legality, Acts and Regulations

Current legislation regarding the safe transport of occupied wheelchairs is fairly crude in so much as specific injury to the occupant of the wheelchair is not considered, only that they remain upright and seated during and after a crash [1, 3]. The main standard to which wheelchair manufactures must comply is ISO 7176-19 (2001) [3]. ISO 7176 covers the standards to which manual and electric wheelchairs must be designed. Part 19 of this standard deals with wheelchairs that are to be transported in motor vehicles. The ISO 7176-19 standard only considers forward facing wheelchairs involved in a 48km/hr frontal impact. The standard does not cover rearward facing wheelchairs in a frontal impact or side or rollover crashes. Although not stated specifically the standard can also be assumed not to cover rearward impacts, as this is the same as a rearward facing wheelchair in a frontal impact.

A harness restraining both the pelvis and chest of the dummy is required for the ISO 7176-19 test, along with a four point tie-down securement system of the wheelchair. Other wheelchair securement systems are catered for but the four point tie-down system is used exclusively on the wheelchairs issued by the RE unit so will be the only one considered here. In order to pass ISO 7176-19 the wheelchair and occupant are monitored during and after the crash. The P-point[1] of the wheelchair, the rear and front of the head and the knee must not move more than the stated excursion distances during the test [3]. After the test the angle of the occupant's torso to the back rest must be no more than 45^0, viewed from any direction, and otherwise remain in an upright seated posture. The wheelchair must be intact and have no sharp edges. Furthermore, the main load carrying structure of the wheelchair must show no signs of failure and the wheelchair and dummy restraints should be able to be removed without the use of tools.

---

[1] The P-point is an arbitrary point on the wheelchair defined by ISO 10542 and 7176-19 [1,3]. It is found by placing a cylinder of 100mm diameter and 200mm length on the wheelchair seat so that the cylinder surface touches both the seat and seatback. The P-point is the centre point of the cylinder at this position.

ISO 10542-1 is used to test the occupant and wheelchair restraints. Crash testing, by its nature, is considered a destructive test and once a wheelchair or component is tested it must then be discarded. To reduce testing costs a surrogate wheelchair is used for the restraint and add-on equipment tests, (Figure 2.1.1). The surrogate wheelchair is rigidly designed in order to withstand repeated crash testing. One drawback to the surrogate wheelchair design is its high rigidity. This makes the wheelchair considerably stiffer than normal resulting in higher loads on equipment that is attached to it due to less energy being absorbed by deformation of the wheelchair structure [26].

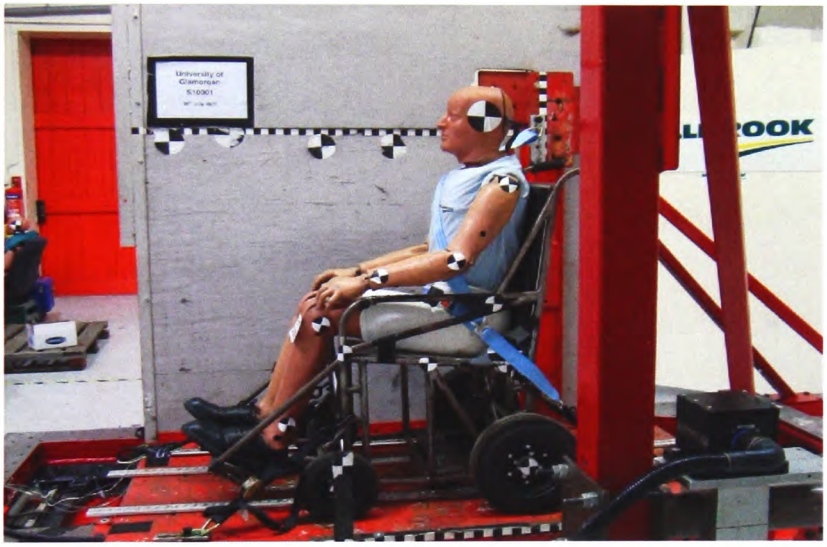

Figure 2.1.1 showing the ISO 10542 surrogate wheelchair and Hybrid II dummy secured to the crash test sled

The criteria for the wheelchair tie-downs and occupant restraint system (WTORS) to pass the dynamic crash test are similar to those of ISO 7176-19. The occupant must remain secured in the wheelchair seat after the crash and none of the WTORS should show any signs of failure or slip by more than 25mm [3].

Addition of any add-on components after crash testing nullifies the results of ISO 7176-19. ISO 7176-19 defines add on components as 'Hardware that is attached to the wheelchair frame subsequent to the sale by the wheelchair manufacturer, in a manner that requires the use of tools for removal, in order to enhance the design and/or

performance of the wheelchair'. Most of the components that the Rehabilitation Unit add to the basic wheelchairs would fall under this definition. The most common item to change on a standard wheelchair, however, is the seating unit. In order to remove the need for having to retest the crashworthiness of a wheelchair every time a new seat is added the ISO standard 16840-4 [39] has been proposed. This standard allows the seating system to be tested separately to the production wheelchair by attaching it to an ISO 16840 surrogate wheelchair, which is crash tested to the same parameters as those in ISO 7176-19. The ISO 16840 surrogate, as shown in Figure 2.1.2, differs to the ISO 10542-1 in that it has no seat. Instead it has two parallel bars onto which a variety of seating systems may be mounted. A further difference is the inclusion of aluminium bars attaching the front wheels and push bars to the main wheelchair frame. These aluminium bars deform, and are subsequently replaced, during each sled test and in doing so absorb some of the energy, giving a more realistic loading to the attached seating system and prolong the life of the surrogate wheelchair. This method removes the cost of destructively testing a wheelchair (the surrogate wheelchair can be reused) and provides a standard test base but is still quite costly [4]. A typical sled run costs around £2000, not including sensors and tie-down equipment or the cost of the wheelchair and seating systems.

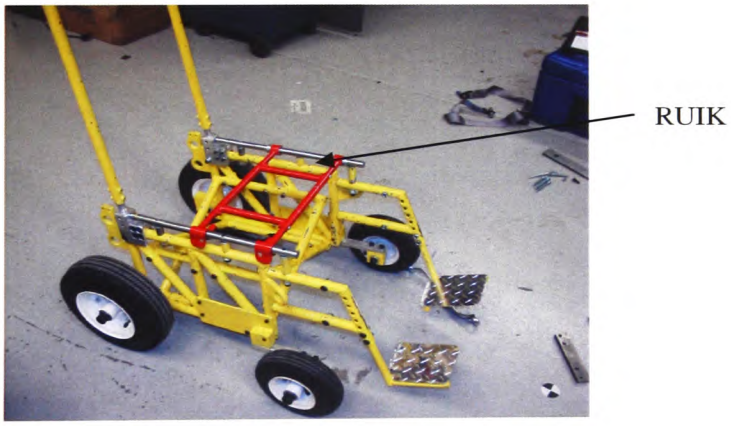

Figure 2.1.2 showing the ISO 16840 surrogate wheelchair with the Rookwood Universal Interface Kit (RUIK) shown in red.

The main limitation to the current ISO standards for wheelchair transport in vehicles is the lack of consideration given to the survivability of the occupant. The standards set

out maximum excursion limits for both the occupant and wheelchair but do not require the forces and accelerations that are imposed upon the occupant to be measured. There are methods of measuring the injury criteria [13, 15] that seated vehicle occupants are subjected to but as yet these haven't found their way into these standards. It should also be noted when comparing wheelchair crashworthiness with automotive seating crashworthiness, that the wheelchair, unlike the vehicle seat, is not primarily designed for vehicle transport.

2.2 Specific parts of the wheelchair system and their effects on crashworthiness

The main parts that affect the crashworthiness of the wheelchair in transport are the seating system, attached to the wheelchair chassis, the tie-downs securing the wheelchair to the vehicle chassis, the seatbelt restraining the occupant of the wheelchair and the occupant themselves. Each of these parts will be discussed in depth in the following sub-sections.

2.2.1 Seating

There are many different types of wheelchair seating systems ranging from the simple sling seat (canvas seat), as found in many hospital wheelchairs, to the custom made postural support wheelchair seats, which are contoured to fit an individual patients geometry. Any seat that is to be used in transport must be able to withstand crash forces. In tests conducted by the Transport Research Lab (TRL Ltd.) [26] it was found that a manual wheelchair, which was crash tested to ISO 7176-19, deformed under load which absorbed some of the energy resulting in reduced spinal compression of the occupant. The surrogate wheelchair, in an identical test, did not deform, resulting in much higher spinal loads. It could therefore be said that testing seating systems with a surrogate wheelchair, specified by ISO 16840, produces a worst case scenario.

An alternative seat testing method that has been used is to apply equivalent static loads, similar to those experienced in a crash, to the seat via a mould of the buttocks and thighs of a Hybrid III dummy [7, 22, 23], a Hybrid III dummy being the standard anatomical test dummy used in automotive crash testing. Applying static loads is far cheaper as most engineering laboratories have tensile-compressive test machines that can easily be adapted for such experiments.

By using the equivalent static load test method described above, Bertocci *et al.* [7] examined the crashworthiness of 'drop seats'. Drop seats are seats that are 'dropped' into position on two supporting rails attached to the wheelchair chassis and secured using metal hooks or slings. An equivalent static load of 16,65kN was applied to each seat. This load originated from earlier work by the same author in which load cells were used on a standard sled test setup to measure the downward force produce by a Hybrid III dummy in a frontal crash at 48Km/hr [8]. They found that the softer seats withstood more force than the stiffer ones due to greater seat deflection, consequently, absorbing more energy. The shortcomings of this paper, as conceded by the authors, were the use of equivalent static loads to represent the dynamic loads exerted in a crash and the simplification of attaching the seat to a test rig instead of an actual wheelchair. It is uncertain if attaching the seats to a solid test rig would give representative failure results. The deformation of the wheelchair chassis, in a crash would absorb energy, thus decreasing the load acting on the seating system. Such wheelchair chassis deformation, however, could cause the seating attachment hardware to fail prematurely. A further limitation of using equivalent static loads is that the effect of strain rate in the material is not considered. Increasing the rate of strain of a metal can cause an increase in its yield strength and ultimate tensile strength [40, 41].

A similar series of tests to those of Bertocci's *et al.* [7] were conducted by Ha *et al.* [22] where almost identical experimental procedures were used to examine the crashworthiness of wheelchair back supports and attachment hardware. These authors identified two methods for simulating the loading of the seat backs; from a rear crash (assuming the wheelchair was facing the front of the vehicle) and from rebound

after a frontal crash. In a frontal crash the occupant is thrown forward and restrained by the seatbelt. The occupant is then forced back onto the seat back by the stored energy in the seatbelt; this effect is called 'rebound'. Ha *et al.* found that all of the five commercial seat backs, that were tested, failed to withstand the load applied to them (10.55kN). All failures were as a result of failure of the attachment hardware.

Using the same test procedures, as those used for testing seat back strength [22], Ha *et al.* [23] investigated the crashworthiness of sling seats and sling back supports. As with Bertocci's *et al.'s* [7] static seat strength analysis, Ha *et al.* found that the sling seats could withstand a greater force than solid seat supports and attributed this to the less stiff material being able to absorb more energy. The criterion that Ha *et al.* set for a seat to pass was that the maximum force applied to the seat must be withstood for 5 seconds without failing. Work published by Ha *et al.* and others does not explain where the 5 seconds time limit comes from although it is most probably from the US Federal Motor standard for seating systems, FMVSS 571.207 [31, 42], which specifies a 5 second static test duration. Ha *et al.* tested six seat backs and six seat bases and found that in both cases 4 of the 6 specimens passed. In the same study of wheelchair sling seat and sling back crashworthiness Ha *et al.* [23] claimed that the greatest force on the seat back occurs when the occupant rebounds onto the seat back in a frontal crash rather than when the occupant contacts the seatback in a rear crash, with the same acceleration. This is contrary to his opinion in his previous paper [22]. What makes this change of opinion strange is that in both instances he used the same validated computer model to predict a value for the rebound force in a frontal crash. Generally rear impacts are conducted at lower accelerations than frontal ones due to the excessively high load that the occupant exerts on the seat back. Also the most common injury associated with rear impacts is the phenomenon of whiplash which occurs at lower speeds and impact accelerations [43, 44].

A useful study conducted by Warner *et al.* [45] examined the different behaviour of rigid and yielding car seats in rear impacts. Similarly to Ha *et al.'s* [22, 23] finding, the authors determined that the yielding, or deformable, seat backs provided significant

improvement in occupant safety. Rigid seatbacks were found to offer greater protection to the occupant in more severe rear impacts but as these were statistically far less likely to occur Warner *et al.* [45] agreed that the advantages of the yielding seat backs at the more common lower impact accelerations outweighed those of the rigid seat backs at higher accelerations.

A very useful experiment conducted by Bertocci *et al.* [8] was to find the seat loadings and shear forces in a frontal crash. Four load cells were positioned under a solid seat pan on a surrogate wheelchair then crash tested with a Hybrid III Anthropomorphic Test Dummy to SAE J2249 [19] (The crash test criteria of the Society of Automotive Engineers (SAE) J2249 is equivalent to those in ISO 7176-19). Four tests were carried out, two with the rear securement points located at 32mm above the centre of gravity of the wheelchair assembly, in accordance with SAE J2249, and the remaining tests with rear securement points at 164mm above the centre of gravity. The downward seat loads, for the range of rear securement point location, varied from 17.019kN to 18.682kN. The maximum shear forces were found to be from 4.424kN to 6.717kN. These values were subsequently used in many seat analysis projects [22, 23].

A problem that the RE Unit at Rookwood face, when determining crashworthiness of their wheelchairs and the possible injury to the occupant, is the varying postural position of each occupant. The majority of Rookwood's clients have postural abnormalities that the unit try to correct/accommodate through custom made moulded seats. Any posture deviating from normal seating geometry can put the occupant at greater risk in a crash [46, 47]. In his paper 'Effect of Seat Stiffness in Out-of Position Occupant Response in Rear-End Collisions' Benson *et al.* [46], through a series of sled tests, examined the upper and lower neck forces and moments of a Hybrid III male dummy seated out of position in seats of varying stiffness. The tests showed that the upper and lower neck forces and moments increased when the dummy was lent forward, where the distance between the back of the head and the head rest was greater than the normal seating position. Increased seat stiffness caused increased upper neck loads but had little effect on the loads of the lower neck.

The uncertainty with this series of tests was that the seat stiffness was varied by using different makes of seat. Each seat design would have different geometries affecting the results. A more scientific approach to the experiment would have been to use the same make of seat throughout and vary its stiffness by reinforcement. Such an approach was taken by Prasad *et al.* [44] who took a standard car seat and welding steel brackets to the back of it in order to increase stiffness. Prasad *et al.* found that stiffening the conventional seat caused an overall increase in neck moment related injuries, such as whiplash. It also increased lumbar and thoracic spine loads.

Kang and Pilkey [47] also looked at out of position occupants and found that the excursion of the head and chest of the occupant were not too dissimilar to that of normally seated occupants, as long as the shoulder belt stayed within the shoulder joint. If the shoulder belt slipped outside the shoulder joint then the occupant's head and chest excursion more then doubled.

Warner *et al.* [45] looked at the effects of out of position occupants in rear crashes and found a marked difference in the results when compared against those of normal seated occupants. They found that the occupant tended to contact the seat back at a higher distance from the seat base, which increased the influence of 'ramping', where the occupant slides up the back of the seat. This in turn increased the chance of head injuries against the roof of the vehicle, exaggerated neck and head hyperextension[2] and also increased the rebound off the seat back forward and upwards.

2.2.2 Tie-Downs

This thesis does not concern itself with different types of tie-downs and assumes they are attached correctly to the wheelchair in accordance with ISO 10542-1. It is, however, necessary to understand the way in which they are used and the effect they

[2] Hyperextension means the movement of a limb or body part beyond the normal limit.

have on the behaviour of a wheelchair in a crash. It was also necessary to test the tie-downs to obtain material properties, as described in Chapter 3.

The straps that attach the wheelchair to the transporting vehicle are called tie-downs. The most common arrangement of tie-downs is the four point strap type where four webbing straps are attached from 4 separate tie-down points on the wheelchair to four anchor points on the floor of the vehicle (Figure 1.1.1). These tie-downs must also be crash tested.

Hunter-Zaworski and Zaworski [24] examined the different methods of securing wheelchairs on public transport. The guidelines they used to assess the merits of each system came from the American Disability Act [48]. Hunter-Zaworski and Zaworski also made an interesting observation about the type of tyre used on the wheelchair and noted that a pneumatic tyre will compress, storing energy, during a crash and then release it, causing upward motion of the wheelchair [24, 47]. The effects that the tyres have on the crashworthiness of wheelchairs and the issue surrounding the accurate modelling of them will be discussed later in this Chapter.

One of the main differences encountered between wheelchair systems is their mass. More often than not this difference in mass also affects the centre of gravity of the wheelchair. Bertocci *et al.* [15] examined the effect that the position of the tie-down anchor points, with respect to the centre of gravity of the wheelchair, had on the injury of the occupant in a crash. The authors used 3 injury significant values; head, chest, and neck. They also stated that abdominal injuries could be more significant than neck injuries but as they couldn't capture the biomechanical response in this region the abdomen wasn't considered. This stance was justified by stating that the combined interaction between the head, neck and chest had a greater potential for injury than that of the abdomen. Bertocci *et al.* chose not to include injuries to lower limbs but to concentrate on those that were a risk to life. It was found that the optimum position for the tie-down points was between 38mm and 64mm above the wheelchair's centre of

gravity as the produced the best compromise between forward and rearward wheelchair rotation during a frontal crash.

A study by Kang and Pilkey [47] also looked at the optimum rear tie-down location and found it to be level with the centre of gravity. Unlike the work conducted by Bertocci *et al.* [15], Kang and Pilkey didn't examine the forces and excursion of the individual body parts (head, chest and knees) but rather the work examined the rotation and excursion of the wheelchair, the loads on the rear wheels and the forces that were applied to the lap belt to make a decision as to where the optimum height of the tie-downs should be.

The occupant of the wheelchair can also affect the requirements of the tie-down system. The mass and posture of the occupant will affect the centre of gravity of the wheelchair and hence alter the optimum position of the tie-down anchor points.

2.2.3 Seat Belts

Once the wheelchair is attached to the chassis of the vehicle (with suitable tie-downs) the occupant can then be secured. The usual securement method is a three point harness with one point mounted on the B-pillar (see Figure 1.1.1), positioned behind the shoulder of the occupant, and the other anchors mounted to the vehicle chassis. Occupant securement systems favoured by some manufactures incorporate the seatbelt system into the wheelchair seat.

The method of restraint that the occupant uses, as Hunter-Zaworski and Zaworski [24] note, can also affect the demands on the wheelchair tie-downs. If the occupant uses a seatbelt system that is built into the wheelchair the tie-downs then not only have to restrain the wheelchair but also the occupant [24, 49]. Most seatbelt systems used by wheelchair occupants tend to be a three point harness, similar to a car seatbelt, secured to a separate support post (B-pillar) and the floor of the vehicle. The advantage of this system is that the occupant's securement, and hence excursion, is controlled

independently of the wheelchair. In a frontal crash the occupant's forward excursion is restrained by the seatbelt and their downward excursion restrained by the seat base. The forces required to restrain an occupant in an inbuilt belt seat are transferred directly through the wheelchair seat and wheelchair tie-downs. This means that both the wheelchair and the tie-downs undergo a greater loading in a crash and have to be adequately reinforced. The advantage of an inbuilt seatbelt system, as claimed by Van Roosmalen and Bertocci [32], is improved belt fit and consequently a decreased risk of occupant injury. The integrated seatbelt also removes operator error when fitting an independent seatbelt around the occupant and wheelchair. Van Roosmalen and Bertocci based these conclusions on static tests of the in-built belt seat system; the tests should ideally have been verified with a dynamic loading test. The tests were also not compared with a wheelchair with a standard separate seatbelt securement, i.e. a 3-point seatbelt harness with an upper anchor point attached to a B-pillar and lower anchor points mounted to the vehicle chassis. A further oversight made by these authors was that the potential problems associated with having a heavier chair, that would be necessary to support the inbuilt seatbelt system, were not mentioned. An inbuilt belt system would require strengthening of the chair to chassis interface [7, 16], increasing the demand on the tie-downs and other issues associated with a heavier wheelchair, such as a bigger motor in the case of a powered wheelchair.

A much better study of integrated seatbelt seats was conducted by Park and Park [49], although car seats, as opposed to wheelchair seats, were examined. These authors compared the performance of the proposed belt integrated seat with a conventional car seat and found that the belt integrated seat significantly reduced seatbelt slack and hence occupant excursion. This would mean a lower chance of secondary impact between the occupant and the interior of the vehicle. As a result of the decreased excursion the load on the right shoulder (the shoulder over which the seatbelt passed) and the pelvis acceleration were found to be higher than that on a conventional seat. Chest acceleration, however, was found to be less.

None of the specialist seating systems produced by the RE Unit incorporate in-built seatbelts although they do have postural support straps. These straps are used to aid the occupant's posture and prevent them from falling out of their wheelchair in normal non-transport use. ISO 10542-1 require these postural support straps to have a maximum breaking force of (1kN) [1]. It is actually the buckles that are designed to fail at this force. If the postural straps do not fail in a crash then there is a danger that the motion of the occupant in a collision will be resisted by these postural support straps and transfer the force to the seating system assembly and subsequently the wheelchair as opposed to the vehicle seatbelt and chassis. This would result in an excessively high load on the wheelchair seat that it was not designed for.

The setup of the non-integrated seatbelt seat has a considerable effect on the kinematics of the occupant, in particular the position of the upper shoulder anchor point, attached to the B-pillar. It was shown, in a series of computer simulations conducted by Bertocci *et al.* [6], that varying the X, Y and Z coordinates of the upper seatbelt anchor point can have marked differences in the occupants head acceleration. The computer simulations used a Hybrid III dummy and adjusted each coordinate independently of each other to find the optimum anchor position. The study noted that both the X (fore and aft) and Y (side to side) coordinates of the anchor point were often un-adjustable due to the geometry of the vehicle and the solid fixture of the seatbelt post. The Z direction (floor to ceiling) could, however, be adjusted. The study found that positioning the seatbelt too high above the shoulder resulted in increased head acceleration whereas positioning the seat too low caused excessive head excursion in the Y-direction. The optimum height of the seatbelt anchor was found to be that which produced an angle of 55^0 to the horizontal. Only direct frontal crashes at zero degrees were considered. How this optimised frontal crash anchor point affects protection in offset crashes [50-53] was not discussed. The work produced by Bertocci *et al.* [6] went on to influence the recommended seatbelt shoulder anchor point location in both ISO 7176-19 and ISO 10542-1.

2.2.4 Dummies

Crash test dummies are used in vehicle impact testing to examine the motion and assess injury of the occupant. Crash test dummies were first used in the 1940s for jet plane ejector seat tests. Later these dummies were used by the Ford Motor company when they began using seatbelts in their vehicles. Since then dummies have become far more biofidelic and many different models, designed for different types of impact, now exist. Most of these dummies are made with a metal skeleton and outer layers consisting of rubber and foam. The weight distribution is matched to an equivalent human. The joint configurations of the limbs, neck and body are modelled to have the same range and limits as a normal human so as to accurately portray the movement of a human in a crash [54].

Each new dummy design is validated against tests using cadavers (dead bodies) [55-57]. Advancement in dummy design is ongoing as different parts of the dummy are examined in isolation and improved on. One such case is that of the lower limbs. Wheeler *et al.* [55] identified a need for a more biofidelic lower limb model, so conducted a series of tests using the lower limbs from cadavers, human volunteers and several existing crash dummy leg designs. The results showed that the Thor-LX model was far more life like than the other dummy models tested. During the tests the cadaver lower legs were fitted with an achillies tensioner to represent muscle tension. The lack of muscle tension is one of the draw backs with using cadavers and dummies. Cadavers are still used in certain cases where specific injuries need to be examined. Kallieris *et al.* [58] used cadavers to find the differences in injury severity from using active or passive driver restraint systems. The cadavers were autopsied after each test to find the exact injury caused by the different restraint systems. Such detail would be hard to replicate with a dummy [17, 55, 56, 58].

The most common dummies, and the ones referred to by ISO crash test standards, are the Hybrid II and III dummies. The Hybrid III range is mainly used in car tests where a greater amount of data is required. The Hybrid II series is often preferred for wheelchair testing due to them being cheaper and more robust. Accelerometers can be

attached to both series of Hybrid dummy but the Hybrid III's have significantly more output channels as well as a more biofidelic neck [59]. The biofidelity of the neck is most noticeable in rear and side impact tests but these tests are not presently required by wheelchair crash test standards. These dummies come in 3 different sizes; female 5^{th}, male 50^{th} and male 95^{th} percentile. All wheelchair crash test standards require the use of the 50^{th} percentile dummy, based on a male who has the a weight and height equal to or above 50% of the male population [54].

The next stage in the crash test dummy evolution was the finite element model. As with the physical dummies being compared to cadavers so the computer dummies were compared to the physical dummies. As can be appreciated, creating a computer model of a man made test dummy is considerably easier than making a computer model of a complete human body. It also makes validation of the said computer model easier, as well as taking less computational time to process. Creating accurate computer dummies has allowed a great deal of crash tests to be conducted virtually. This virtual crash testing has a massive advantage over traditional physical tests as once the computer model to be tested has been created and validated it is relatively quick and cost effective to test a number of different crash configurations. It is also a very powerful tool during product design as aspects of crash safety can be addressed before manufacture. The disadvantage of modelling computer dummies on physical dummies is that the computer model will not be any more biofidelic than the physical version that it's modelling. The Human Model for Safety research program created a biofidelic occupant computer model and validated it against cadavers, effectively cutting out the middle step of using a physical dummy [56]. The same process was used by Oshita *et al.* [60] in the validation of their Total Human Model for Safety. Unlike previous models this computer dummy was a model of the actual human form with complete skeleton, tendons, internal organs and realistic skin covering. This would seem to indicate the sorts of computer dummies of the near future but for now such dummies are very demanding in computer resources. This issue of processing cost is important in virtual crash testing when considering the type of dummy to use as there is a danger that over complication of the dummy can lead to it being the controlling

factor in the time that a simulation takes to solve. Ideally the computer dummy should be able to mimic the behaviour of a human in a crash whilst using the minimum number of elements. Such a model was produced by Kirkpatrick *et al.* [61] utilising rigid bodies in all but the most critical parts of the dummy, i.e. the neck, spine, head and abdomen. The dummy was similar to those used in MADYMO™ or the Articulated Total Body [62] model in its construction and was designed primarily to model occupant kinematics. The simple design approach of Kirkpatrick *et al.* [61] meant that the occupant model was not the determining factor in the time required to process the crash analysis simulation. Kirkpatrick *et al.* [61] also produced a 5^{th} and 95^{th} version of their simplified dummy by simply scaling the 50^{th} model up or down. This method is flawed as the weight distributions between the different percentile models are not scalable [63].

A further consideration of the dummies is the direction of the crash applied to the vehicle they are seated in, i.e. front, side or rear impacts. As mentioned previously, the Hybrid III dummy range is designed for high speed frontal impacts and is the industrial standard for such tests. The trade off of having a realistic neck model for high speed impacts is that the dummy's neck is overly stiff at lower impacts [64]. As mentioned previously when discussing whiplash, it is sometimes desirable to analyse the motion of the occupant at lower impact speeds. A study was conducted by Fast *et al.* [65] to look at the merits of using a four point postural restraint harness over a simple pelvic waist belt. The study rolled a number of wheelchairs down a ramp with a curb at the bottom. The acceleration of the head was recorded at each impact. Fast *et al.* [65] found that higher accelerations occurred with the four point harness than the waist harness. The four point harness greatly restricts the movement of the dummies upper body so the head must decelerate to zero velocity over a shorter distance than with the pelvic strap. From the recorded head acceleration a value of Head Injury Criteria (HIC) was found to predict serious injury. The values found may have been higher than for an actual occupant as the Hybrid III dummy used in the test has an overly stiff neck at lower impact speeds. Fast *et al.* [65] thus concluded that pelvic straps should be used over four point harnesses. The excessive stiffness of the Hybrid dummy neck was also

discussed by Szabo *et al.* [36] who examined the effects of low speed rear impacts (8-13km/h) on human volunteers and the Hybrid III dummy. The results showed that the neck of the Hybrid III dummy was indeed poorly suited for low speed impacts due to its excessive stiffness. A similar study, conducted by Hell *et al.* [43], also found higher head accelerations in dummies when compared to human volunteers. Hell et al's. [43] study went further by comparing male and female volunteers. It was found that women, on average, tended to have higher peak head acceleration than men. This was attributed to the women generally having a smaller neck circumference than men. The cause of the peak accelerations was found to be predominately due to the distance between the head and head rest [13, 36, 43].

The test device for human occupant restraint (THOR) dummy is more biofidelic than the Hybrid III and is better suited for identifying precise areas of injury due to its higher number of built in sensors. The THOR dummy also contains a more complete spine and pelvis which allows the dummy to adopt a variety of seating postures [54, 66]. Being able to represent a variety of different postures would be useful for the RE Unit as many of their clients have spinal abnormalities that could affect them in a crash, as mentioned in Section 2.2.1 on seating. The improved biofidelic nature of the THOR model was unnecessary in this project and as it is more suited to detailed investigation into specific injuries. The cost of the THOR dummy is also a lot higher than that of the Hybrid III. A further reason for not using the THOR dummy is that current wheelchair safety standards specify the use of a Hybrid II or III dummy when performing the wheelchair crash tests.

The dummies used to investigate rear impacts have a far more biofidelic neck to enable them to deal with injuries that are particularly associated with rear impacts, e.g. whiplash. The Biofedelic Rear Impact Dummy (BioRID) is one such dummy. The same argument applies to side impact dummies. The nature by which the head moves relative to the body, via the neck, in side impacts is very different to fore and aft motion in front and rear impacts. Dummies like the EuroSID and BioSID (Side Impact Dummies) have necks designed to closely replicate this side to side motion [54]. Side

and rear crash testing is currently not required for wheelchairs in transport. It should be mentioned that many of the RE Units clients have superior rear and side support over able bodied vehicle occupants due to the specialist moulded seating, used for postural correction and support, which the RE Unit produce.

2.3 Different crash orientations

All the standards for wheelchair crashworthiness currently issued are for frontal impacts, due to such impacts being the most common [52]. As a result the majority of published work produced has concentrated on frontal impacts.

Crash tests are carried out to agreed standards so that tests may be repeatable at different laboratories and the results obtained can be usefully compared. All wheelchair crash tests, for example, are for frontal impacts. The nature of such standardisation means that there is an inevitable gap between simulated laboratory crash tests and actual crash scenarios. Otte [50] compared legislated crash tests with actual accident analysis of cars involved in traffic accidents. He found that the current impact simulations only cover 34% of actual situations of road traffic accidents. The results showed that out of the recorded impacts investigated frontal impact accounted for 52.2% of the impact directions, with lateral impacts accounting for 32% and rear impacts accounting for 15.6%. When the types of frontal impact were examined it was found that very few were directly head-on. As a result Otte [50] concluded that offset impacts, with two-thirds overlap, between the front of the vehicle and the barrier, should be favoured. He also recommended that as lateral impacts make up approximately one third of all collisions more emphasis should be put on crash testing in this direction. Zaouk *et al.* [67] concur with Otte [50] and found that the most common injury producing crash direction was between 10 and 2 o'clock, with 12 o'clock being head on.

Otte [50] went on to state that vehicle versus vehicle crash tests should be given preference as the deformation of the second vehicle would affect the forces of the

occupant in the first. This is especially relevant with SUV (sports utility vehicles/ four wheel drive trucks) to car impacts where the vehicle crush tube orientation and stiffnesses differ [51, 68]. If vehicles of similar height impact into each other then both vehicles crumble zones act as they should and dissipate a large amount of the energy involved. If there is misalignment of the crumple zones or crush tubes, due to one vehicle being significantly higher than the other, then the crumple zones will work far less efficiently, causing larger accelerations to be experienced by the occupants. This paper is very useful as it identifies the most likely crash scenarios. The current wheelchair test standards only require a frontal impact test meaning that many possible weaknesses in the wheelchair securement system go unnoticed. Lateral and rear crash testing is of particular relevance to the Rehabilitation Department, at Rookwood hospital, due to the auxiliary equipment that is attached to the wheelchairs. This additional equipment could potentially cause secondary impact injuries to the occupant and other users of the vehicle if inadequately secured [50].

2.3.1 Skewed and offset impacts

According to Otte's [50] study of vehicle accident statistics 32% of recorded impacts were lateral. Otte [50] points out that vehicular lateral impacts offer the least protection for occupants due to the 'limited deformation path', meaning that there is a reduced crumple zone on the side of vehicles hence less distance for the energy of an impact to be absorbed resulting in higher accelerations exerted on the occupants. Buzeman *et al.* [69] also found side impacts to be less common but more injurious. The actual mechanism of a side impact also differs from a frontal crash. Gallacher *et al.* [70] discussed the creation of a simplified side impact model, explaining that in a frontal crash the forces are exerted on the occupant by the seatbelt whereas in a side impact it is the vehicle structure that applies the load onto the occupant when it intrudes into the occupant compartment. This side impact definition was expanded upon by Aekbote *et al.* [71] who developed a 4 stage side impact test rig and associated computer simulation model. The door was first accelerated into the dummy, the reaction between the door and the dummy is the second stage before both

door and dummy are accelerated together and finally the door and dummy are decelerated until they separate. This effect is described for occupants using the vehicle seats and not for wheelchair occupants, although the effects would no doubt be similar. Seatbelts, for able bodied and wheelchair passengers, are primarily designed for frontal impacts and have limited effect in controlling sideways excursion. The same is true for wheelchair tie-downs. They are effective in both frontal and rearward impacts but, due to their small angle with the X-plane, offer limited stability in side impacts.

2.3.2 Rear impacts

Rear impact crash testing, like those of side impacts, are not compulsory for wheelchairs at present. Despite this a number of studies have been conducted on wheelchair seat back strength, many of which were discussed in the Section on seating [22, 23, 44, 46]. A far greater volume of work has been conducted in the automotive industry and many of the findings are directly applicable to the wheelchair occupant. The main focus for rear impacts is cervical spine distortion, resulting in the common complaint of whiplash. O'Neill [72] explained that whiplash occurred where the torso was accelerated forward and the head, if unsupported, lagged behind. This effect initially caused an 'S' shape in the neck before the head suddenly bends backwards causing the whiplash injury. O'Neill attributed most whiplash injuries to poor head rest setup where the head rest is too low or the gap between the head rest and the back of the occupants head is too large. This is where some of Rookwood's patients have an advantage over able bodied vehicle occupants. Rookwood's clients often have custom made head rests that are either part of the seat or mounted separately to the wheelchair. Such head rests are at the correct height to offer maximum postural support so should provide a good level of protection to the occupants in a rear crash. When fitting such head rests the Clinical Engineer should be aware of its potential use in a vehicle situation and take steps to ensure that the head rest protects the occupants head in a crash and that the head rest and mounting is strong enough to withstand crash forces.

2.3.3 Pitching

Physical crash testing of the wheelchair is performed by attaching the wheelchair to a sled, which sits on rail tracks. The sled is fired down the tracks at crash accelerations. The physical crash test method will be discussed further in Chapter 3.

The sled, onto which the wheelchair is mounted in both FEA simulations in the literature and physical crash tests, only has one degree of freedom and is restrained in Y and Z directions as well as all degrees of rotation. This is certainly not the case in a car crash. Although the car itself is restrained to some extent in the Z-direction by the road, the chassis of the car, onto which the wheelchair is fixed, is able to move in all degrees of freedom due to the suspension and tyre compression of the vehicle. It has been shown by Suh *et al.* [73] that the movement in the Z-direction of a car in a frontal collision, known as pitching, can have a considerable effect on the kinematics of the occupant [73, 74]. Warner *et al.* [45] also acknowledged the short comings of sled tests to produce vertical and pitching motion when considering severe rear crash impacts. The authors found the majority of high impact rear crashes came from larger vehicles impacting into smaller ones. This caused the larger vehicle to override the smaller one introducing vertical excursion and pitching, which in turn increased the injury to the occupant. DeLeeuw [75] addressed this deficiency of the sled by creating a sled that incorporated a pitching function of +/- 10^0. This was achieved by mounting an additional sled on top of the main one. The top sled was attached via 4 hydraulic actuators that simulated the pitching and yaw of the vehicle chassis. The problem of controlling the hydraulic actuators was overcome by creating a computer model of the whole sled system so that the signal to the actuators could be controlled accurately. Deleeuw claimed to observe a 40% difference in Head Injury Criteria between tests including and excluding pitch and yaw of the sled. A similar problem exists for computer simulation of crash tests. When analysing the occupant cockpit, or indeed a secured wheelchair, it would be very computationally expensive to model the whole vehicle, to which the chair or wheelchair is attached, in order to obtain the correct pitch and yaw. Traditionally the item to be examined would be simply accelerated in the horizontal plane while being fixed in the lateral and vertical plane, much like the sled

test. Babu *et al.* [76] overcame this problem by running a computer simulation of the vehicle without the interior and the displacements of the nodes surrounding the cockpit were recorded at regular timesteps. These nodal displacements were then applied to a separate model of just the vehicle interior so as to apply the pitch and yaw without the need of running the whole model of the vehicle. A very similar study was carried out by Suh *et al.* [73] where by the cockpit of a vehicle was simulated independently from the rest of the vehicle. Unlike Babu *et al.* [76], Suh *et al.* [73] only mention the effect of pitching as an after thought and do not comment on the differences that including it would make. The addition of pitching could be readily applied to wheelchair crash analysis to gain a more realistic understanding of the behaviour of the wheelchair and occupant in a crash.

2.4 Computer Modelling

Although there have been a reasonable number of papers published on computer crash simulations of wheelchairs it is still worth looking at other relevant crash test papers for both motor vehicles and trains in order to gain a better understanding of the modelling process.

Car manufactures have been using computer crash testing for many years and as car safety standards become more rigorous so computer crash simulation becomes more vital to ensure that the vehicles produced meet these standards. It should be pointed out at this juncture that computer simulation in no way replaces physical crash testing. Indeed all crash testing legislation stipulates that physical crash tests must be performed [1, 3, 39]. Computer simulation provides the engineer with an insight into the potential outcome of costly destructive crash tests. Normally a full range of crash tests will be carried out using computer simulation before any physical testing begins [77]. When dealing with cars the cost of producing full working prototypes is much higher than the cost of producing the finished production vehicle, due to economies of scale. The cost of wheelchair production is much lower but the same principals apply. Problems arise in the case of the RE Unit at Rookwood Hospital

where the specialist bespoke wheelchairs they produce are one offs. It is unfeasible for the RE Unit to produce two of every wheelchair they design in order to crash test one of them. The cost of these wheelchairs is still considerable when one takes into account the life support equipment used, the customised postural seats produced for the occupant and environmental control equipment.

Apart from predicting the outcome of crash tests, computer simulation often enables the engineer to examine the crash event in greater detail than would be possible from physical testing. One of the draw backs of the physical tests is the limited views that video cameras filming the crash can allow. Computer simulation enables any part of the model to be viewed at any angle, where any part of the model that obscures the view can be hidden with ease [53, 78]. Computer modelling can also be used for optimisation of the wheelchair system. For example, Bertocci *et al.* [6] used computer simulation to find the optimum position of the seat belt upper anchor point by constructing a simple wheelchair, occupant and seatbelt model and then altered the location of the upper seatbelt anchor point in the X, Y or Z directions while the other two directions remained fixed. Repeated simulations were performed and the head, chest and abdomen accelerations and displacements, from which injury criteria could be derived, were measured until the optimum position was found. The main expense here would have been the time taken for the creation of the finite element model. A similar series of tests using physical sled testing would have been extremely expensive due to the test equipment and the destructive nature of the physical tests.

2.4.1 Finite Element Analysis (FEA) – An introduction of basic concepts

So far computer simulation and finite element analysis have been mentioned but what do these terms actually mean? This Section will briefly describe the finite element analysis process, how it works and why it is so important to engineers and mathematicians.

Finite element analysis (FEA) works by taking a geometry and discretizing it, that is breaking it down into small parts called elements. The elements that make up the geometry are called a mesh. Boundary conditions and loads are applied to the mesh (pre-processing). The model is then processed, or simulated, and then the results of the simulated model are examined (post-processing).

Simple mechanics problems can be readily described and solved using appropriate algebraic equation. When problems become more complex it is desirable to break the problem down (discretize) into smaller sections that can be solved with relative ease. Problems that can be broken down into a specific number of smaller parts are termed discrete and are well suited to being solved by computer. Other problems that cannot be broken down to a finite number of parts but require an infinite subdivision are described as continuous. Although simple continuous problems can often be solved by simultaneous equations, more complex problems cannot. This difficulty was overcome by treating the continuous problems in a similar way to the discrete problems, by subdivision. A small subdivision of a continuous problem could be sufficiently approximated to allow the problem to be solved, effectively approximating the continuous system to a discrete one. Ray W. Clough is credited with coining the term 'finite element' meaning a finite number of subdivisions, or elements, of a continuous problem [79, 80]. The finite elements that result from the division of the continuous problem (discretization) are joined at their corners by nodes. The combination of elements and nodes is called a mesh. It is important that the mesh is fine enough, i.e. the elements are small enough, to capture the areas of interest within the analysis.

FEA processes can be divided into Linear and Non-Linear. Linear finite element analysis assumes static loading, where the load is constant over a long period of time. It also assumes that there is little change in the stiffness of the structure being analysed and that the deformation of the structure is small. Static problems, where the aforementioned assumptions hold true, can be readily solved using linear matrix algebra of the form:

$$[K]\{u\}=\{F\} \qquad \text{- } \textit{Equation 1}$$

where [k], {u} and {F} are the global stiffness matrix, the displacement vector and force vector respectively.

These equations are then solved to give the values of nodal displacement. From the displacements of the nodes and the properties of the model's material, the stresses in the geometry can be found [79-82].

2.4.2 Non-Linear FEA

Crash events cannot be analysed using linear FEA due to the large displacements of the model, multiple contacts (causing changes in the structures stiffness) and non-linear material behaviour (plastic deformation of materials or inherently non-linear materials such as foam), i.e. the linear analysis assumptions do not hold true. Such non-linear analysis events are termed 'dynamic' and take the form of dynamic equilibrium:

$$[M]\{\ddot{\mu}(t)\}+[C]\{\dot{\mu}(t)\}+[k]\{\mu(t)\}=\{F(t)\} \qquad \text{- } \textit{Equation 2}$$

where [M], [C] and [k] are the mass, damping and stiffness matrices respectively with μ as the displacement, therefore $\ddot{\mu}(t)$ and $\dot{\mu}(t)$ denote acceleration and velocity respectively.

The most common method of solving non-linear problems is an iterative technique called the Newton-Raphson method. The load on the model is applied in increments. At each time step the equilibrium of the model is calculated by the difference between the external loads applied and the internal forces of the model. This allows the linear approximations, governing the behaviour of the model, to converge to the non-linear solution.

2.4.3 Implicit and explicit solvers

The two main types of solver, for non-linear analysis, are implicit time integration and explicit time integration.

The implicit method, adopted by programs such as Ansys, is the Newton-Raphson algorithm. The Newton-Raphson algorithm uses a series of linear approximations to describe the non-linearity. This is achieved by examining the difference between the internal and external element forces, called the out-of-balance load vector. Using a linear solution the program checks for convergence tolerance between these two values. If the difference is greater than the pre-defined convergence value the program re-examines the out-of-balance load vector and updates the stiffness matrix. Convergence is rechecked and the process repeated until the convergence tolerance is satisfied [83]. The assumption made in this method is that the acceleration over each iteration is linear. When this method is used to solve impact problems a very small time step is required and the stiffness matrix [K], in the dynamic equilibrium equation, Equation 1, must be inverted. These combined effects result in very intensive CPU usage and therefore long simulation times [84].

The explicit method, as used by programs such as LS-Dyna, works by dividing the acceleration into a large number of time steps and assuming the acceleration over each timestep is constant. The explicit method requires far more timesteps than the implicit method but does not have to invert the stiffness matrix, meaning that each calculation is simpler to compute. It also has the advantage of not relying on convergence to solve so is far more robust [84, 85].

When dealing with highly non-linear finite element problems, due to multiple contacts and materials, it was found that the explicit finite element method was more stable [86]. This makes explicit solvers, such as LS-Dyna, more suitable to highly non-linear analysis, e.g. crash simulations.

The main finite element algorithm to use the explicit method is LS-Dyna. LS-Dyna is the industry standard for use in vehicle impact analysis. Ansys comes with the ability to use the LS-Dyna code but is not well suited to many of the more common features that LS-Dyna offers for crash analysis. It was decided to use a specialist pre and post processing software package that was specially tailored to crash simulation, thus facilitating the use of LS-Dyna. After a market review the most appropriate package for the project's requirements was the Oasys™ Pre and Post Processing bundle, produced by ARUP PLC [87]. The only limitation of the Oasys™ package was a lack of mesh generation capabilities. A license of Hypermesh™ was procured to take care of all meshing work.

2.5 Computer modelling of vehicle impacts

A number of papers have been written on the subject of crash testing motor vehicles and wheelchairs. Although the aims of the majority of these simulations differ from the aims of this project they still contain many useful modelling techniques that can be utilised.

Two useful papers that discuss the FEA technique for modelling vehicle impacts from start to finish was written by Zaouk *et al.* [53, 88]. The authors set out to model a Dodge Neon but due to copyright infringement issues were unable to obtain any geometric or material data from the manufacturer. Instead the author was forced to measure each part of the vehicle using a coordinate measuring machine and digitizer. Many parts that were not critical to the crash behaviour of the vehicle were simplified. Zaouk *et al.* [88] advised caution when measuring sheet metal parts as paint, or other coatings, add to the thickness but not to the strength of the sheet metal. Another useful modelling tip was to apply a point at each spot weld location to aid their addition during the pre-processing stage. Once the geometry of the vehicle was captured the model was meshed. When creating the mesh the minimum time step during processing must be considered. The minimum time step is the smallest amount of time that the solution breaks down into. The smaller the time step then the greater number of

calculations that need to be performed. The time step[3] is controlled by the time taken for a sound wave to travel through the smallest stable element in the model. In his model Zaouk *et al.* [88] restricted the smallest element to 7mm across, therefore ensuring a timestep of no less than one microsecond. Material data was also collected for the car. This was found by a series of tensile tests at 3 different strain rates, quasi-static, low rate dynamic and high rate dynamic. Zaouk *et al.* [88] didn't specify the exact values of the strain rates although Cunat [41] defined them as low strain rate (quasi-static, e.g. tensile testing) = 10^{-5} to 10^{-1} s^{-1}, medium strain rate (low rate, e.g. car crash strain rates) = 10^{-1} to 10^{2} s^{-1} and high strain rate (e.g. car crash to ballistic) = 10^{2} to 10^{4} s^{-1}. The results were converted into true stress against true strain, a form that could be used with the LS-Dyna material model of 'Piecewise Linear Isotropic Plasticity'.

In a paper investigating the aspects of the simulation of automobile seating using LS-Dyna, Williamson [74] discussed the techniques for seat and occupant modelling and the problem of seatbelt interaction with the seatback. When modelling the seatbelt around the seated dummy Williamson found that using shell elements, as opposed to beam elements, better distributed the contact forces across the dummy. Seatbelt beam elements were still used where the seatbelt didn't come into contact with the dummy to cut down on processing time and to enable the correct function of the seatbelt retractors and slip rings [74, 87]. This particular method of seatbelt modelling was also endorsed by Song *et al.* [89]. Song *et al.* also discussed the importance of ensuring that the contact between the seatbelt and occupant allowed both horizontal and vertical movement of the seatbelt. An undesirable complication in frontal crashes is submarining, where the seatbelt rides up over the iliac crest (the high sides of the pelvis) causing the pelvis of the occupant to move underneath the lap belt resulting in severe abdominal injuries. This is often caused from either a loose or poor fitting

[3] Time step, $t_s=d/c$ where d= the shortest diagonal distance across the element and c= the speed of sound through a material ($c=(E/\rho)^{1/2}$, where E=Young's Modulus and ρ =material density).

seatbelt or from low friction between the occupant and the seat. It is important that the contact between the seatbelt and occupant can capture this behaviour should it occur [7, 9, 11, 47, 89, 90].

Gavelin [91] carried out very similar work to Williamson [74] by conducting an isolated study of a belted occupant. The aim of Gavelin's work was to examine seats with integrated seatbelts and the effect that the seat stiffness and seatbelt properties had on the occupant. Gavelin concluded that integrated seatbelt seats were advantageous in offset frontal collisions where the A or B pillars of a vehicle can be damaged. He also found that the occupant had a tendency to rotate towards the impact zone in an offset frontal crash while wearing a 3-point seatbelt. Gavelin's work could have been improved upon by considering vehicle's intrusions and secondary impacts between the occupant and vehicle interior. A physical validation of the model would have also been of benefit.

One of the main differences between the crash response of a wheelchair and a standard vehicle seat is the compression and rotation of the wheelchair wheels. In a dynamic crash test of a wheelchair assembly, the manner in which the tyres of the wheelchair deform strongly influences the behaviour of the wheelchair and occupant. The way in which the wheelchair and wheels compress is not that different to the behaviour of the wheels on a car in a frontal crash test. Williams *et al.* [92] observed that their model of a vehicle in a frontal crash was significantly affected by both the make-up of the tyres and suspension. Williams constructed a tyre model and modelled the internal air pressure by using the airbag function in LS-Dyna. This is a common method for modelling car tyres and has been used by number of people [12, 92-100]. The FEA tyre model was then validated by impacting the tyre into a solid surface and measuring the reaction forces. Video footage of the impact was also compared. Wheelchair wheels are far simpler in their construction than motor vehicle tyres but this method for representing the internal pressure is still valid for both.

2.6 Validation of computer simulation

The two main methods for validating computer models against physical crash tests are analysis by high speed video cameras and readings from accelerometers. The disadvantage of video cameras, as mentioned by Zaouk *et al.*, [53] is that they tend to be setup to capture the behaviour of the occupant in physical crash tests and cannot see through door panels or other objects obscuring the view of interest.

Zaouk *et al.* [53] also advised against 'tweaking' the computer model to match the physical tests. There are two reasons for this; firstly there may be a genuine fault with the model that will be overlooked if other parts of the model are adjusted to compensate. As an example Zaouk *et al.* found that the omission of three spot welds was enough to cause the computer model to differ noticeably from the physical tests. Secondly that no two physical crash tests will produce the exact same results due to the high number of variables involved. This is also a reason why there is no standard method for computer simulation validation [53].

A different method of validation was taken by Williams *et al.* [92] who validated individual components of their model of a Caterham 7 light weight sports car. Many of the parts considered to have a large influence on the crash behaviour of the car were tested to investigate their individual behaviour. To ensure robustness of the simulation process the physical component tests were then modelled virtually. This gave the authors the opportunity to check how well the FEA software and model represented the real life component behaviour before the entire car model was assembled, ensuring a far higher degree of accuracy between the simulation and physical model.

2.7 Materials

When carrying out a Finite Element Analysis it is important that the correct properties of the material are entered. The type of material information required and the way in which the FE model behaves is down to the material model used. LS-Dyna has a wide

range of material models available to the user from a simple elastic isotropic (properties the same in all directions) model that has linear elasticity to more detailed orthotropic (properties vary in each direction) models that describe plasticity and failure [101].

In the case of crash impacts the rate at which the strain of the material changes has an effect on its physical properties. Movement of dislocations within steels is time dependant, therefore at high strain rates yielding is resisted causing an increase in both yield and ultimate strength [102, 103]. As Bleck *et al.* [40] point out in a paper on high strain rates in car body steels, failure to include strain rate effects can lead to over estimating the car body deformation in a crash.

The strain rate sensitivity of steels is related to their tensile strength, with high strength steels being less effected [40]. The range of strain rates typically found in automotive crash tests are between $10^{-1}s^{-1}$ and $10^{2}s^{-1}$ [40, 41]. Cunat [41] explained that steels which are highly sensitive to strain rate effects are desirable in the automotive industry due to increased resistance to deformation at high strain rates. As a point of interest Cunat identified Austentic stainless steel as being especially useful in automotive applications as its deformation under load is readily predictable and it also has high energy absorption properties.

There are several ways of modelling the effects of strain rate within LS-Dyna, five of which were examined by Dietenberger *et al.* [103]. These were as follows:

'Piecewise Linear Plasticity' – requires full stress-strain curves at different strain rates to be entered. LS-Dyna calculates the strain rate on a particular element then reads off the value of stress from an appropriate graph.

'Plastic Kinematic Hardening' – This model is isotropic and scales the yield stress for the required strain rate by using the Cowper-Symonds equation[4].

'Piecewise-Linear with Cowper Symonds' – This model uses a single stress-strain curve taken at a quasi-static strain rate and uses it in conjunction with the Cowper Symonds equation to predict the behaviour at different strain rates.

'Simplified Johnson-Cook' – This model is both strain rate and temperature dependant so can model material softening from plastic dissipation.

'Modified Zerilli-Armstrong' – This is an improvement on the Johnson-Cook model and models strain and strain rate hardening as well as materials softening effects. The model works by utilising the mechanics of dislocations through the crystal lattice.

Dietenberger *et al.* [103] carried out a frontal crash test of a truck using each of the five strain rate models and compared the results against the simulation with no strain rate effect and physical crash test data. From examining the results produced it appeared that the inclusion of strain rate effects had a significant effect but that the difference between the different types of strain rate models was minimal. Dietenberger *et al.* are unclear in their discussion of the results and claim that the difference between the effects with and without strain rate was relatively small, despite their results showing a considerable increase in internal energy of the test specimen with included strain rate effects. The increased internal energy can be shown as an increase in area under the stress-strain graph, implying that the material can absorb

---

[4] Cowper Symonds stress at uniaxial strain rate, $\sigma(\varepsilon') = \sigma_0 \left[1 + \left(\frac{\varepsilon'}{D} \right)^{\frac{1}{q}} \right]$

Where: σ_0 = Yield stress, D = constant (s^{-1}), q = constant, ε' = uniaxial strain rate (s^{-1}). Typical values for mild steel are D=1300 and q=5 [41. Cunat, P.J. *Stainless Steel Properties for Structural Automotive Applications.* in *Metal Bulletin International Automotive Materials Conference.* 2000. Cologne: Euroinox..

more energy at higher strain rates. Presumably the effects of the Simplified Johnson-Cook and Modified Zerilli-Armstrong models, with their inclusion of plastic dissipation representing the effect of heat loss through crack propagation in ductile materials, would be more pronounced in fatigue situations, as apposed to high strain rate situations where failure is rapid.

A better explained study of LS-Dyna's strain rate modelling ability was conducted by Gokstrop *et al.* [104]. Practical stress-strain data from aluminium tensile test specimens were measured for two different strain rates using a Hopkinson Bar. The Hopkinson bar works by placing the specimen in the middle of the bar and putting a collar around the outside of the specimen. One end of the bar is struck while the other end is held rigid. A compressive shock wave travels down the bar, bypasses the specimen through the collar, then reflects off the fixed end and travels back through the bar as a tensile shock wave. This reflected shock wave applies a dynamic tensile load to the test specimen, whose strain values are then read from attached strain gauges. The Hopkinson strain rate experiment was then modelled virtually and the results compared. The authors found that a visco-plastic model in LS-Dyna produced the most accurate results when compared to the physical test data. Plasticity models are time independent and use an equation, such as Cowper Symonds, to scale the plastic yield stress to account for the strain rate effects. A disadvantage with using the Cowper Symonds equation is that it assumes constant strain rate sensitivity. This is in fact not the case as steel's sensitivity to strain rate tends to decrease with increased strain [105]. The visco-plastic model is time dependant and uses the strain rate to directly calculate the stresses and strains in the plastic region. The visco-plastic model is not a standard model in LS-Dyna. Of the standard LS-Dyna material models used the Johnson-Cook model gave the best results. Gokstrop *et al.'s* [104] results, like those of by Dietenberger *et al.* [103], show a fairly close agreement between all the different models used and the accuracy of the results required should also be taken into account when choosing the correct strain rate model to use [84].

2.8 Literature summary

From the review of the literature it can be seen that a considerable amount of work has been carried out on the effects that various parts of the wheelchair system have on both the wheelchair and occupant behaviour in a frontal crash. These include the orientation of tie-downs with respect to the centre of gravity, the position of the seatbelt angle and anchor point location, and the stiffness of the seat. Far less work has been carried out on rear impacts and none on side or skewed impacts, as far as the author is aware. Work on the rear crashworthiness of wheelchairs has mainly revolved around static testing of wheelchair seat backs.

All the work using computer simulation to model the crashworthiness of wheelchairs discussed so far has looked at specific parts of the wheelchair system. By constructing a more detailed model of several wheelchairs this thesis will tie many of these individual studies together and produce robust computer models that can predict the crashworthiness of the whole wheelchair system.

The computer simulation work reviewed has not taken into account the pitching of the transporting vehicle or examined the effects of skewed impacts on the crashworthiness of transported wheelchairs. The wheelchair model herein will be used to investigate the effects that both the pitch of the vehicle and behaviour in a skewed impact has on the crashworthiness of the wheelchair and occupant. The literature reviewed has also not examined the effects that adding life support equipment has on the crashworthiness of wheelchairs.

Chapter 3 - Methodology

In this Chapter both the process of the physical crash tests, undertaken in order to generate the necessary empirical data required for validation, and the experiments to determine the material properties for non-standard parts, are discussed. The material properties found were applied to the relevant components making up the complete wheelchair assembly and occupant model, whose construction is described in the ensuing Chapter.

As with the majority of computer simulations it is necessary to have empirical data to compare virtual computer generated predictions to. Finite Element software, LS-Dyna in particular, can solve the simulations presented to them but may produce inaccurate or even erroneous results if the choice of modelling parameters are not carefully made. Comparison with empirical data allows the engineer to assess the accuracy of the results and make amendments to the model as necessary.

3.1 Physical Crash Testing

Due to funding restraints it was only possible to conduct two full wheelchair crash tests; an ISO 10542-1 frontal 20g and rear 10g crash test, both of which were carried out at Millbrook Proving Grounds (www.millbrook.co.uk). It was decided to conduct both tests using the rigidly constructed ISO 10542 surrogate wheelchair [1] in order to eliminate the possibility of structural failure of the wheelchair. The rigid surrogate wheelchair allowed for the movement of the dummy, the behaviour of the seatbelt and tie-downs and the compression of the wheels in a crash situation to be examined in isolation of the wheelchair chassis deformation. Due to the rigid structure of the ISO 10542 wheelchair the FEA model wheelchair chassis could be modelled as a rigid body, decreasing both the modelling and run time.

The surrogate ISO 10542 wheelchair was designed for repeated testing of wheelchair tie-downs and occupant restraints (WTORS). It was manufactured from 22mm diameter steel tubing with a simple sheet steel seat welded to it, as illustrated in Figure 3.1.1. Additional steel sections were welded to the wheelchair frame to achieve a desired weight of 85kg and a centre of gravity of 142mm +/- 25mm horizontally from the rear axle and 287mm +/- 25mm vertically from the floor, in line with ISO 10542-1 [1].

Figure 3.1.1 showing the ISO 10542 wheelchair

Sled testing is used to crash test parts without full scale destructive vehicle testing. Standard vehicle crash testing drives a vehicle into a solid barrier where high speed video cameras, load cells and accelerometers capture the behaviour of the vehicle and its occupants. If only the behaviour of the occupant and/or seat is of interest then the occupant and vehicle seat can be mounted on a sled that can be fired down a track with a crash pulse styled on a passenger car travelling at a desired constant speed impacting into a rigid barrier [106]. Sometimes the vehicle shell (often referred to as the 'body in white') is also attached to the sled with the seat and occupant to examine secondary impact of the occupant with the vehicle interior. The crash pulse describes the change in acceleration over time from the moment the vehicle contacts the solid barrier until it comes to rest. The crash pulses used in this study were 20g and 10g pulses. These values refer to the maximum acceleration that must be achieved by the pulse for a certain duration (>15ms in the case of the 20g pulse), where 'g' is the acceleration due

to gravity, so the 20g pulse is in fact equal to an acceleration of 20 x 9.81m/s^2 = 196.2m/s^2. An acceleration of 20g was chosen for the frontal test as this was the acceleration required for all ISO frontal wheelchair crash tests. It was also the same acceleration used by the majority of automotive impact tests and represents a vehicle's deceleration upon hitting a solid barrier while travelling at 48 km/hr (30mph) [1, 107].

An acceleration of 10g was chosen for the rear impact test for several reasons. Firstly, a crash pulse of 10g is used in ISO 17373 [107] for evaluating occupant head and neck interactions with seat/head restraint designs in motor vehicles and is believed to be optimum for producing whiplash in the occupant [43, 44]. Secondly, a crash pulse of 20g on the majority of production wheelchairs would be excessively aggressive and cause catastrophic failure, according to conversations with engineering personnel at Millbrook [108]. Although an acceleration of 10g is not as injurious as higher accelerations it is certainly more common [45]. From a validation point of view the acceleration used in the physical tests made little difference as it was straight forward to adjust the crash pulse of the computer simulated model.

3.1.1 Methods of physical crash testing

There are two main methods of applying crash accelerations to the sled. The first is to take the sled up to the required velocity then use a series of dampers to decelerate the sled at the required rate [28]. The second method works in reverse by accelerating the sled from rest to the velocity before the impact using an acceleration equal and opposite to the deceleration experienced during the impact in the first method. The second method of accelerating the sled is preferred as it allows greater control of the acceleration characteristics and ensures that the position of the occupant doesn't change before the crash acceleration begins [109]. The acceleration is achieved by a HYGE™ pneumatic ram. This ram, shown in Figure 3.1.2, consists of two halves whose volume can be altered to produce the desired crash pulse. The two chambers are divided by a fixed plate with a hole in the middle of it. The end of the piston sits in the front chamber, of fixed volume, and has a contoured pin attached to the back of it that passes through the hole and into the rear chamber (load volume chamber). An O-ring

around the pin seals the two chambers from each other. The front chamber (set volume chamber) is filled with nitrogen and acts as a damper. The maximum pressure ratio between the load and set volume is 6:1, any higher and the O-ring seal will release and cause the ram to fire prematurely. The ram is fired by applying compressed air to the O-ring, this blows the seal between the pin and the load volume chamber.

As the pressure in the load volume chamber begins to force the piston, the shape of the pin provides the compressed air with a variable area on which to act. Varying any part of the cylinder and pin affects the crash pulse but in general the shape of the crash pulse is controlled by the contoured shape of the pin, the peak acceleration is controlled by the pressure in the rear chamber (load volume chamber) and the duration of the pulse is governed by the volume of the rear chamber [28, 110]. When the pneumatic cylinder is charged a safety bolt securing the sled in its initial position is released and the cylinder fired, see Figure 3.1.2. The duration of interest lasts as long as the stroke length of the cylinder. After this the sled continues down the run way where it comes to a safe stop.

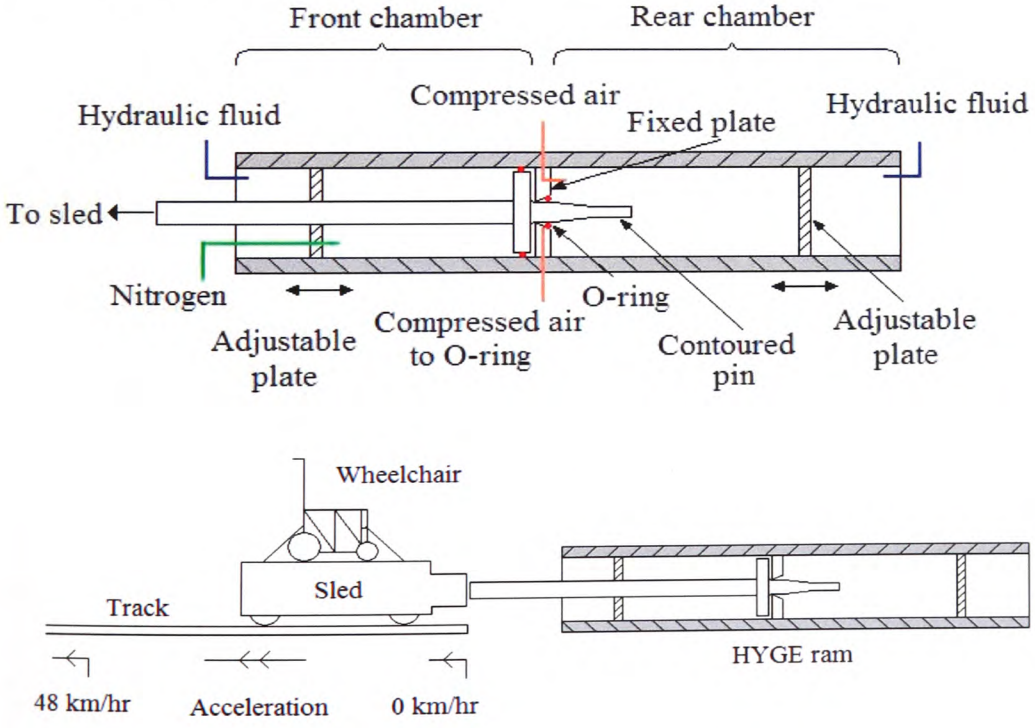

Figure 3.1.2 showing the cross section of the HYGE pneumatic ram (top) and the HYGE ram and sled setup (bottom)

The crash pulse measured from the pneumatic cylinder is shown in Figure 3.1.3. This crash pulse was used to control the motion of the virtual sled onto which the computer model of the wheelchair was attached. The LS-Dyna software allows for complete load curves to be entered. When inputting such data curves the sample rate must not be greater than the minimum timestep. The acceleration curve was therefore regularised to a lower sample rate.

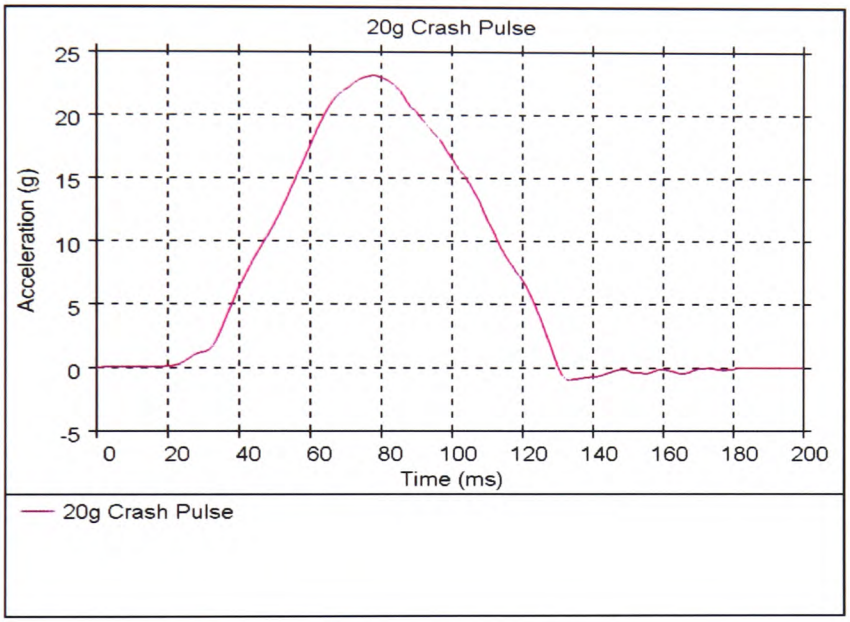

Figure 3.1.3 showing the crash pulse from the HYGE pneumatic ram

As there are differences in sled crash test equipment between various test centres it would be unreasonable to expect them to produce exactly the same acceleration curve. To ensure a certain level of consistency between these different test centres an acceleration corridor is specified in ISO 10542-1 [1]. The acceleration corridor is the area under the acceleration versus time graph, into which the acceleration curve used must fit. The acceleration corridor required for ISO 7176-19 and ISO 10542-1 is shown in Figure 3.1.4 [26].

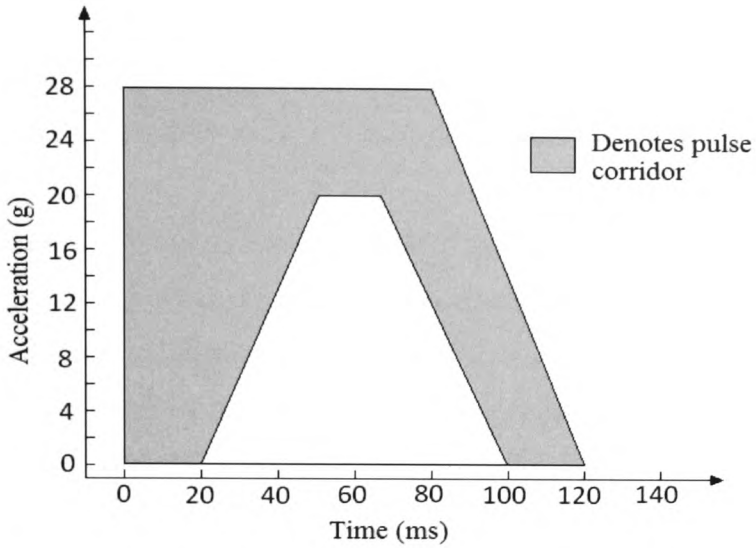

Figure 3.1.4 showing the crash pulse corridor as specified by ISO 7176-19 [3] and 10542-1 [1]. The acceleration curve used must fit into the greyed area of the graph. Note the acceleration is in multiples of g (9.81m/s^2)

In the sled tests conducted a Hybrid II dummy was used. Hybrid II dummies have largely been superseded by the Hybrid III for automotive applications. The Hybrid III has more sensor location points and is more biofidelic. The more robust Hybrid II dummy is predominately used in wheelchair sled testing by Millbrook Proving Ground because such crashes tend to be more damaging to the dummy than tests conducted using car seats. Also, the current wheelchair crash safety standards do not require any sensors on the dummy and the Hybrid II dummies are far cheaper than the Hybrid III dummies.

3.1.2 Crash test setup

The physical wheelchair frontal sled test was setup as shown in Figure 3.1.5 and Figure 3.1.6. The dummy was clothed, to better simulate the friction between the seat and occupant, and then positioned on the wheelchair. The seatbelt and tie-downs were attached in accordance with ISO 10542-1. The seatbelt upper shoulder anchor point was attached to the B-pillar, which represents the B-pillar in a car. The seatbelt passed over the shoulder of the dummy, across its chest and down to a buckle at the side of

the opposite hip. From here the belt continued down to an anchor point on the sled while another part of the belt passed from the buckle, across the front of the dummy's pelvis and back down to another anchor point on the sled.

The tie-downs were webbing straps with cleats at one end, which were secured into brackets mounted on the sled, and hooks on the other end that connect them to specially designated parts of the wheelchair frame. The angles and lengths of both the seatbelt and tie-downs were measured for use in the finite element models.

Markers were placed on the dummy and wheelchair and the distance between these markers and a high speed camera, mounted out to the side of the sled, was measured. These distances were then used in the video editing software (MOVAIS Pro) to measure the movements of the wheelchair and dummy.

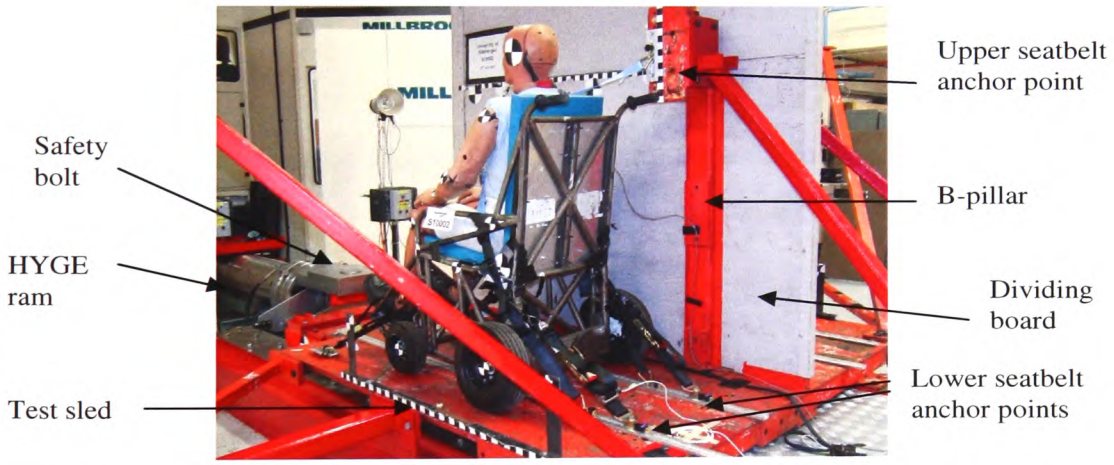

Figure 3.1.5 showing the test sled with the ISO 10542 surrogate wheelchair, Hybrid II dummy and HYGE pneumatic ram

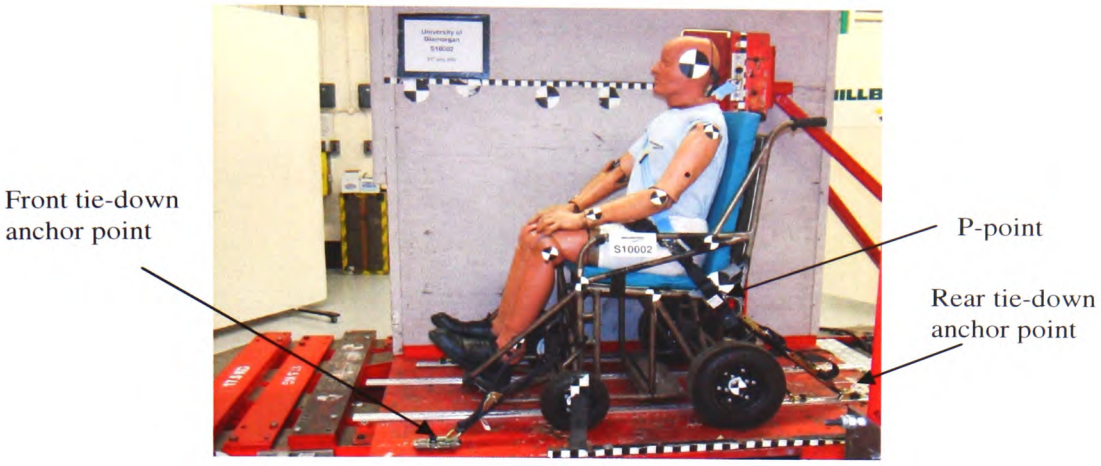

Figure 3.1.6 showing the setup of the ISO 10542 surrogate wheelchair and Hybrid II dummy

Two accelerometers (Endevco 2262CA) were placed in the dummy's head to record X, and Z accelerations (with the X-axis being in the horizontal direction of sled travel and the Z-axis being the vertical direction). Seatbelt load cells (FGP FN 4090) were placed on the upper shoulder belt and on one of the rear tie-downs to measure the tensile load. These load cells were of light weight aluminium construction, adding minimal weight to the seatbelt. A high speed camera was mounted on a boom attached to the side of the sled. The camera could acquire 1000 frames per second and was triggered when the pneumatic cylinder fired. Data of the vertical and horizontal motion of the head, knee and P-point (see Figure 3.1.6) were measured after the test by video capture software at a sample rate of 200Hz (sample period of 5ms). Still photos were also taken before and after the crash.

The rear crash test of the ISO 10542 surrogate wheelchair was setup in the same way as the frontal crash but with the wheelchair facing the opposite direction. The pin in the pneumatic cylinder, controlling the pulse shape, was changed to provide a 10g crash pulse, modelled on a vehicle impact at 15km/hr into a rigid barrier, as shown in Figure 3.1.7.

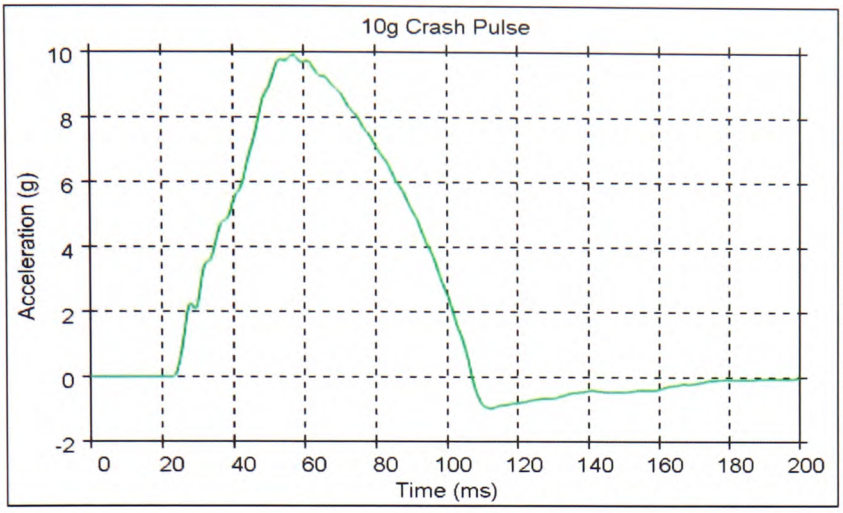

Figure 3.1.7 showing the crash pulse from the pneumatic cylinder form the rearward 10g sled test

The accelerometers and force sensors used in the practical experiment to record the accelerations of the dummy's head and axial force in the tie-downs and seatbelt were subject to a large amount of noise. Before the recorded signal could be analysed this noise had to be filtered out. Filters remove unwanted noise from the signal, e.g. high frequency background noise. When applying digital filters it is important to take into account the transfer function of the filters and the aliasing effect of digitizing the data from an analogue signal. If the sampling rate is less than the Nyguist frequency then erroneous data can be generated. It is therefore desirable to have the sample rate far higher than the highest frequency contained in the signal (i.e. sampling frequency $> 2f_{max}$). The common frequency rates of interest in crash testing are between 60-1000Hz so a sample rate of 10 kHz ensured that the aliasing effect was avoided. The filters have an effect on all the signal data, not just on the frequency range being filtered. The amplitude or time delay maybe affected by the filter so a compromise must be made when choosing a filter.

The acceleration and force data from the simulations in this study were passed through a C60 low pass filter. Low pass filters allow low frequency signals but reduce higher frequencies above a certain cut off frequency. The reduction of these higher frequencies is achieved by reducing the amplitude of the signal, or attenuating it. The C60 low pass filter has a cut off frequency of 100Hz, meaning that any signal of

frequency of 100Hz will be reduced by 3dB. Higher frequencies will subsequently be attenuated by a greater extent.

The equivalent accelerometer and load cell readings from the computer simulated sled tests were also filtered using the C60 low pass filter that was built into the T/HIS post-processing software, the graph of which is shown in Figure 3.1.8.

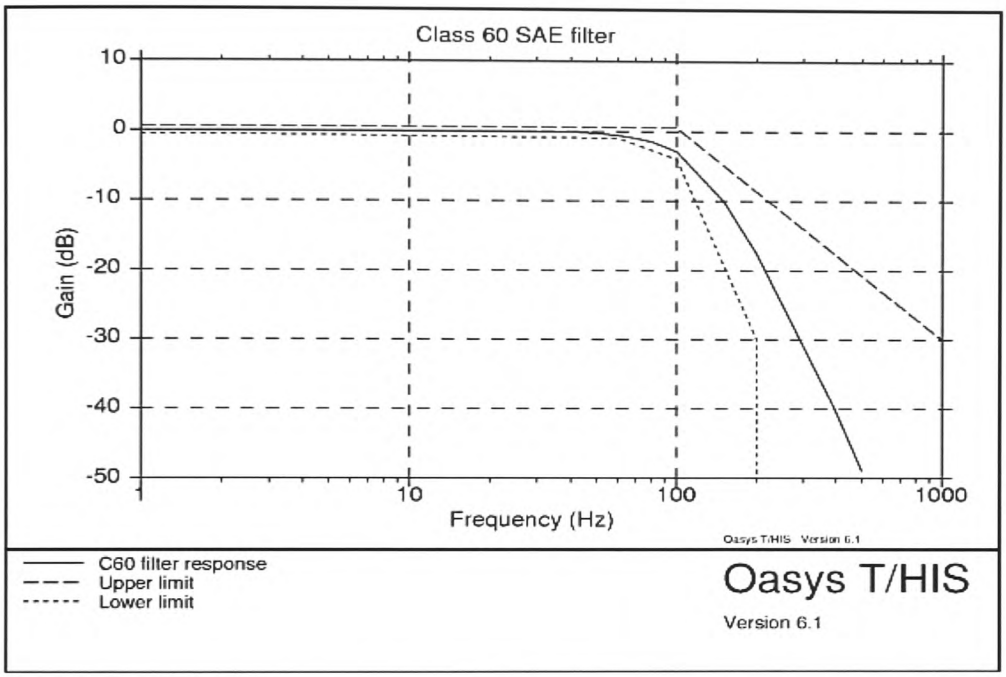

Figure 3.1.8 showing the C60 low pass filter used for head accelerations and axial force data [87].

3.2 Material testing

To enable a finite element model to accurately predict the behaviour of a wheelchair and occupant, in a crash scenario, the material properties for the test item must be gathered from either manufactures, literature or testing. Material properties for parts, such as steel tubing, were readily available from literature and their behaviour well documented. More data-obscure parts, such as cushion foam and tie-down webbing, had to be tested to determine their physical characteristics.

The remaining section of this Chapter is subdivided into three tests carried out to find the properties of the cushion foam used in the seats produced by the RE Unit, the stiffness of the tie-down straps that secure the wheelchair in place and the behaviour of the wheelchair wheels.

3.2.1 Cushion Foam

The RE Unit use Polyurethane foam (VC 55085) for their carved foam cushion seats. This foam is used for to its machinability and its ability to compress in such a way that it doesn't distort the carved shape, reducing the chances of pressure problems for the occupant. The RE Unit measure the contours of their patients requiring postural support using a Contour Body Measurement (CBM) rig. Data from the rig is modified as necessary then sent to a milling machine, which carves out the negative of the patients body contour. The carved cushion helps manage the patient's posture and prevents pressure sores.

Objective:

To find the stress strain properties of the seat foam. The stress against strain properties of the foam was necessary in order to accurately model the foam's behaviour under loading in LS-Dyna.

Method:

The seat foam sample was machined into 12 80x80x40mm cubes and placed one at a time into compression plates fitted to a Hounsfield H10KW tensile test machine, see Figure 3.2.1. The Force against displacement results were recorded using the attached plotter. These results were then converted into stress against strain results.

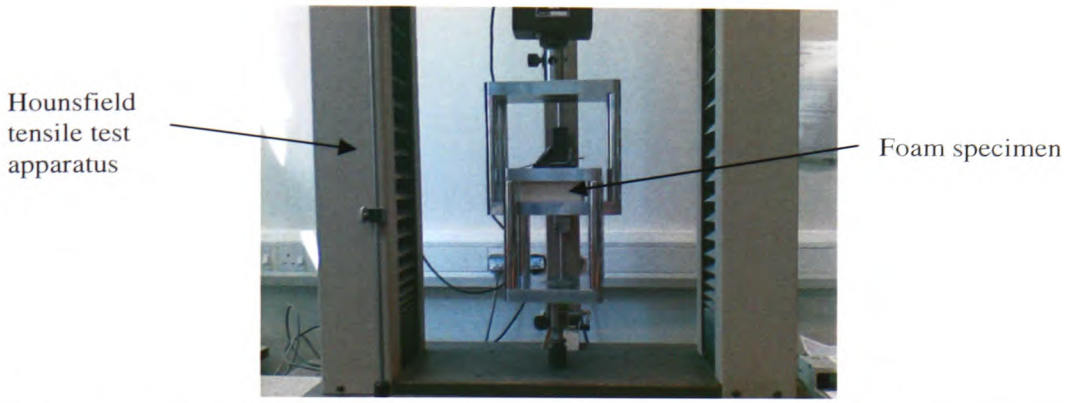

Figure 3.2.1 showing the Hounsfield tensile test apparatus used for testing foam compression

Results:

The results from all 12 specimens were plotted and a curve of best fit of all the data points was found. The R^2 value for the best fit curve was 0.97, indicating a good agreement with the results obtained.

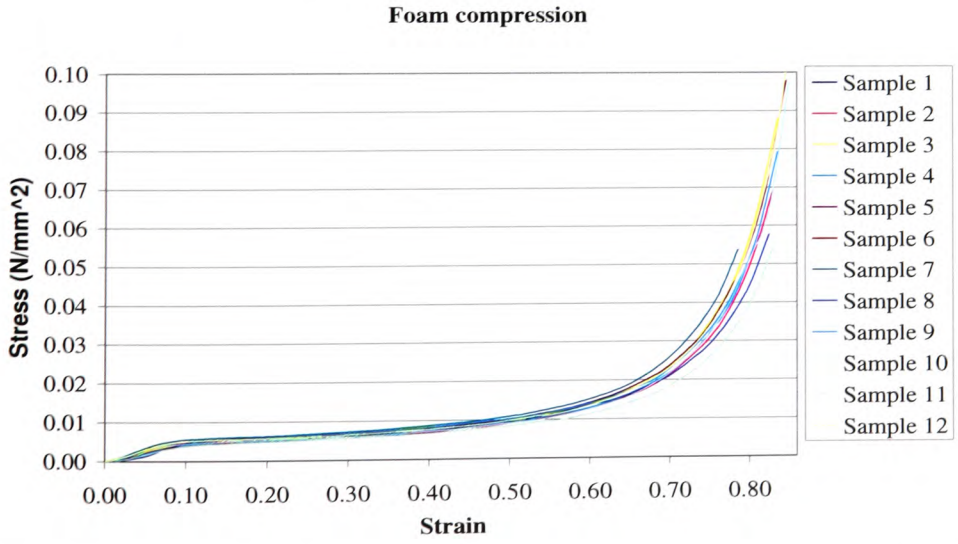

Figure 3.2.2 showing the stress against strain results for the Polyurethane (VC 55085) foam

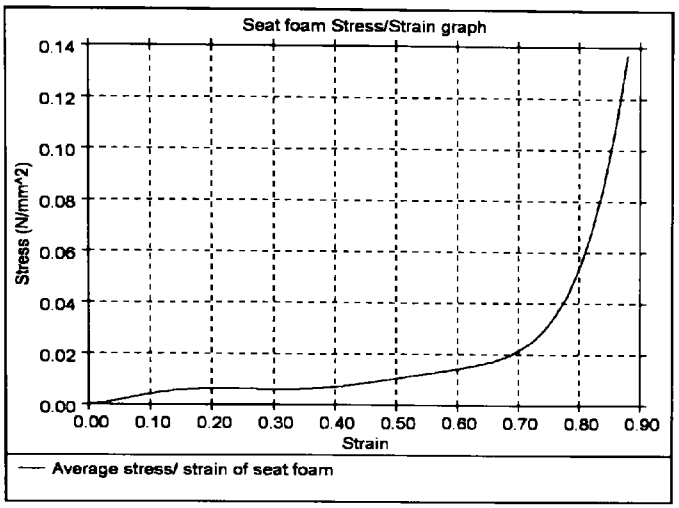

Figure 3.2.3 showing the average stress against strain curve of the seat foam before the addition of artificial stiffening

The density of the foam was supplied by the manufacture (CARPENTER Ltd.) and was given as 55 kg/m^3.

Discussion:

After the initial increase of stress with strain the foam continues to compress at a roughly constant stress due to the closure of the voids within the foam. This closing of voids within the foam also accounts for the small amount of lateral expansion during longitudinal compression, resulting in a low value of Poisson's ratio [87].

The stress strain curve was exported from Excel into T/HIS, the post-processing and data management tool used for LS-Dyna, where it was converted into a format that could be read by LS-Dyna. The foam material data was used with LS-Dyna's 'Mat_Low_Density _Foam' material, which was used to describe the loading behaviour of the seat foam.

3.2.2 Tie-down experiment

The tie-downs attach the wheelchair to the vehicle chassis. In a crash it is the tie--downs that restrain the movement of the wheelchair. It is therefore important to accurately model the stiffness of the tie-downs in order to be able to predict the movement of the wheelchair in a crash.

The complete tie-downs consist of webbing, steel clamps and hooks. The webbing is doubled up in some parts and singular in others. This would tend to suggest that the minimum stiffness of the tie-downs would be that of just a single strip of webbing material. It is far more probable that the stiffness of the complete tie-down assembly is considerably higher. From performing simple hand calculations on the data received from the webbing manufacturer it was found that the strain calculated was significantly higher than the strain observed in the wheelchair sled experiments and because of this the tie-downs were tensile tested as a complete unit.

Finding the stiffness of the tie-downs as a whole allowed for modelling simplifications, namely representing the tie-downs as a series of beam elements. The 1D seatbelt elements in LS-Dyna, which were used to model the tie-downs, required a graph of force against strain to be entered along the mass per unit length of the material.

Objective:

To find the force versus strain relationship of the tie-downs used to secure the wheelchair to the sled. A force versus strain graph was required for the LS-Dyna finite element material model in order to accurately model the physical characteristics of the tie-downs.

Method:

Two spigots were machined to enable two load rings to be attached to an Instrom 8502 tensile test machine. The tie-down was attached between these two rings and a force

applied at a rate of 5kN/min. The force versus displacement of the loading head was recorded by the Introm software.

Both the rear and front tie-downs were tested. The rear tie-down webbing was 50mm wide and the front tie-downs were 26mm wide.

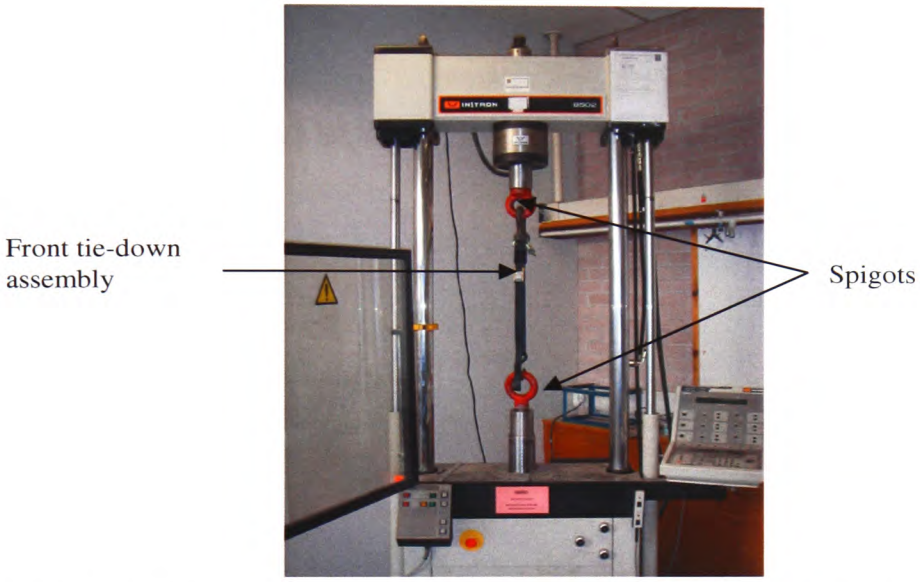

Figure 3.2.4 showing a front tie-down mounted between two load hooks in the Instron tensile test machine

Results:

Two rear and two front tie-downs were kindly supplied by Q'Straint, manufactures of tie-downs and seatbelts for transporting wheelchair devices (www.qstraint.com). The average of the two results for the front and rear tie-downs were used.

Rear tie-downs:

The rear tie-downs were tested to failure. The hook that attached the tie-down to the wheelchair failed at 33.2kN in the first test and the steel shackle attaching the anchoring cleat and the material webbing failed at 29.6kN in the second test. The graph of force against strain for both tests showed a gradual increase in stress as the initial slack in the system was taken up (Figure 3.2.5). At a strain of 0.025 there appeared to be some slippage of the belt system. This same pattern was seen in both

tests conducted and was assumed to be the belt tightening mechanism locking in place under load. In the first test, after this initial 'bedding in' of the clamping mechanism, the force-strain curve showed good linearity up until a force of 30kN where upon the hook began to deform. The angle of the stress strain curve eased off until the stress began to decrease with strain until the eventual failure of the metal hook (Figure 3.2.6). Before the hook failed some of the webbing was heard to rip, visual evidence of this can be seen in Figure 3.2.7. The second test showed similar linearity after the bedding in of the locking mechanism but failed more suddenly. The failure of the shackle in the second test occurred at the weld where weld porosity was observed. Both tie-downs failed above their predicted maximum load in the frontal crash test.

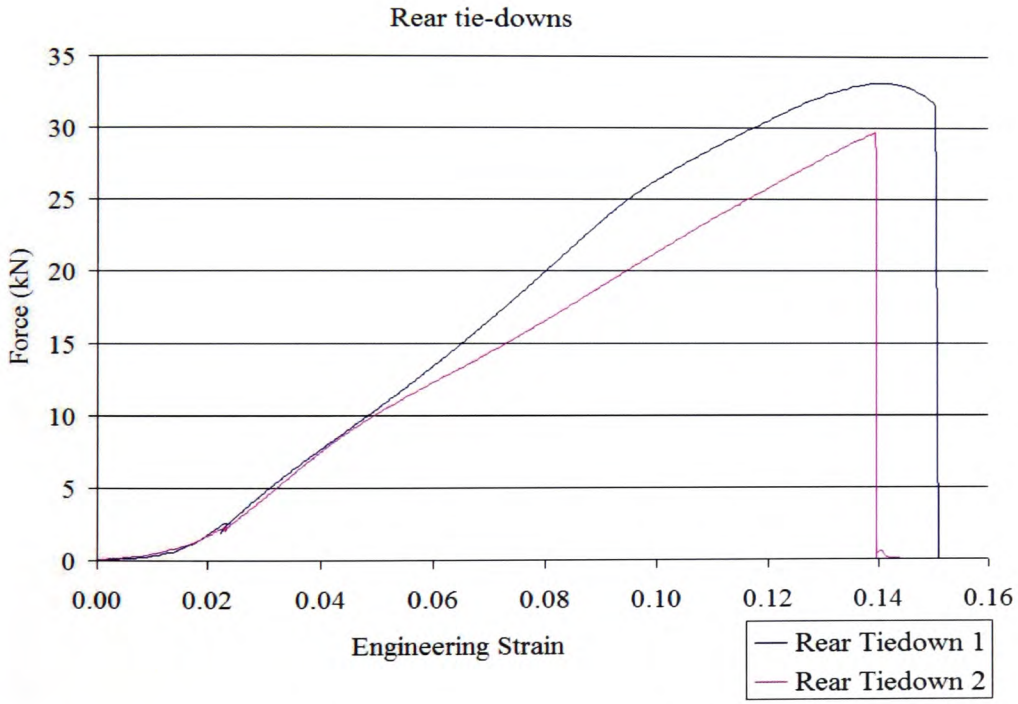

Figure 3.2.5 showing the stress against strain curve for the rear tie-down tensile test

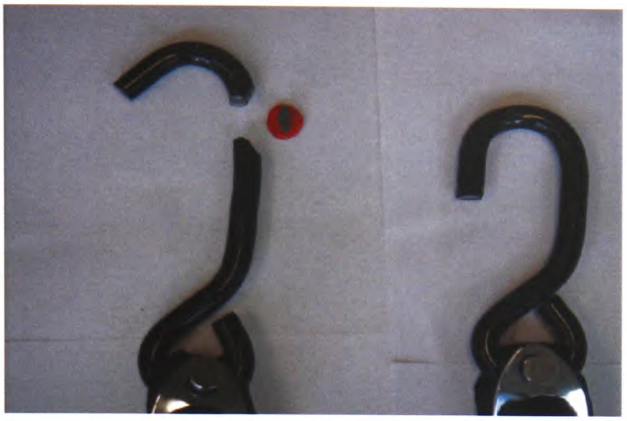

Figure 3.2.6 showing the broken tie-down hook (left) against a non-deformed hook (right)

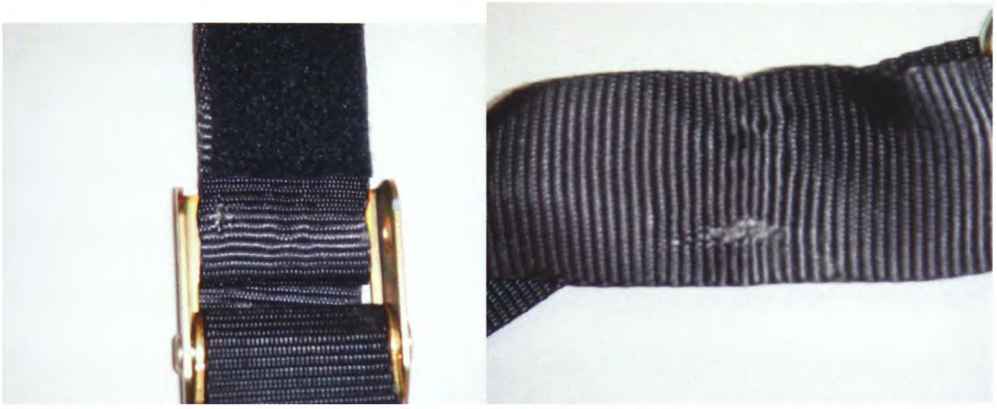

Figure 3.2.7 showing damage to the webbing strap at the tightening mechanism (left) and near the triangular metal linkage (right)

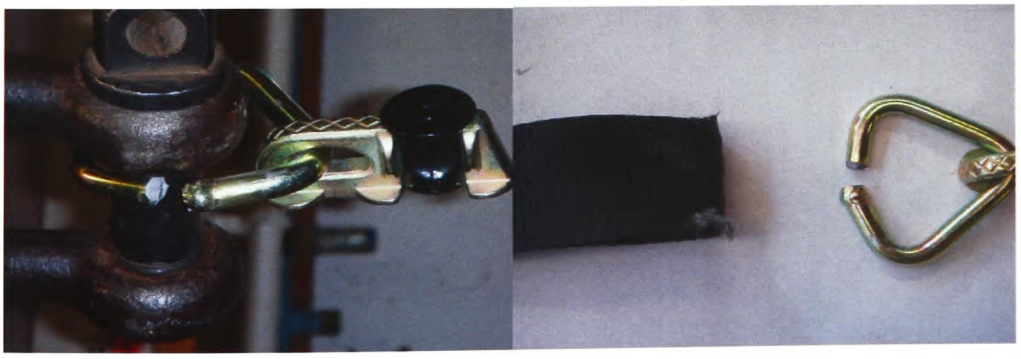

Figure 3.2.8 showing the broken triangular metal link. The figure on the left shows the large diameter of the shackle that contributed to the failure of the link. The figure on the right shows damage to the webbing where is slid out from the link and tore on the sharp edge

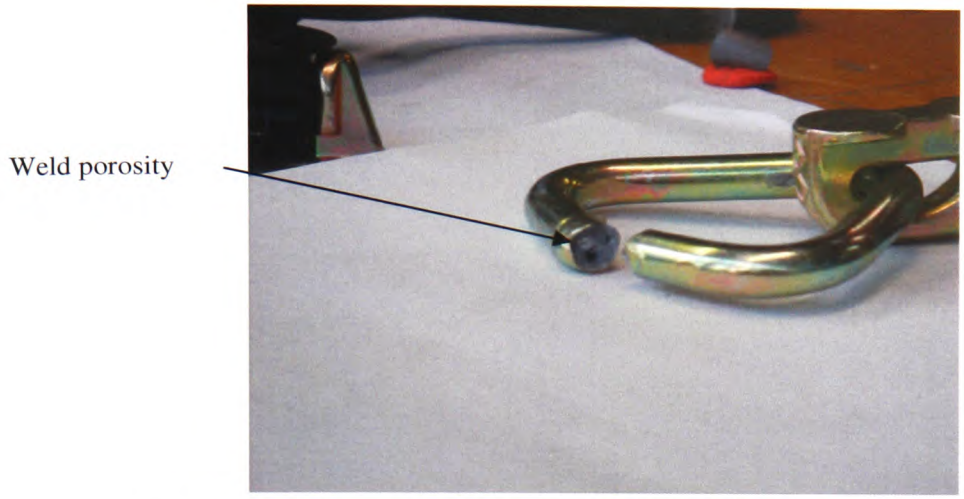

Figure 3.2.9 showing porosity in the weld of the rear tie-down shackle

Front tie-down:

The first of the front tie-downs failed due to the stitching on the webbing strap breaking at a load of 18.9kN. The second test failed in the same way but at the higher force of 20.7kN. As with the rear tie-down experiment the force strain graph of the front tie-downs, in Figure 3.2.10, also showed slippage as the webbing clamp locked. The webbing clamps on the front tie-downs had a different design to the ones on the rear tie-downs. They worked on a camming principal, whereby a sharp knurled face bedded into the webbing strap as load was applied (Figure 3.2.12). At around 8kN both graphs became linear up until their respective failure loads.

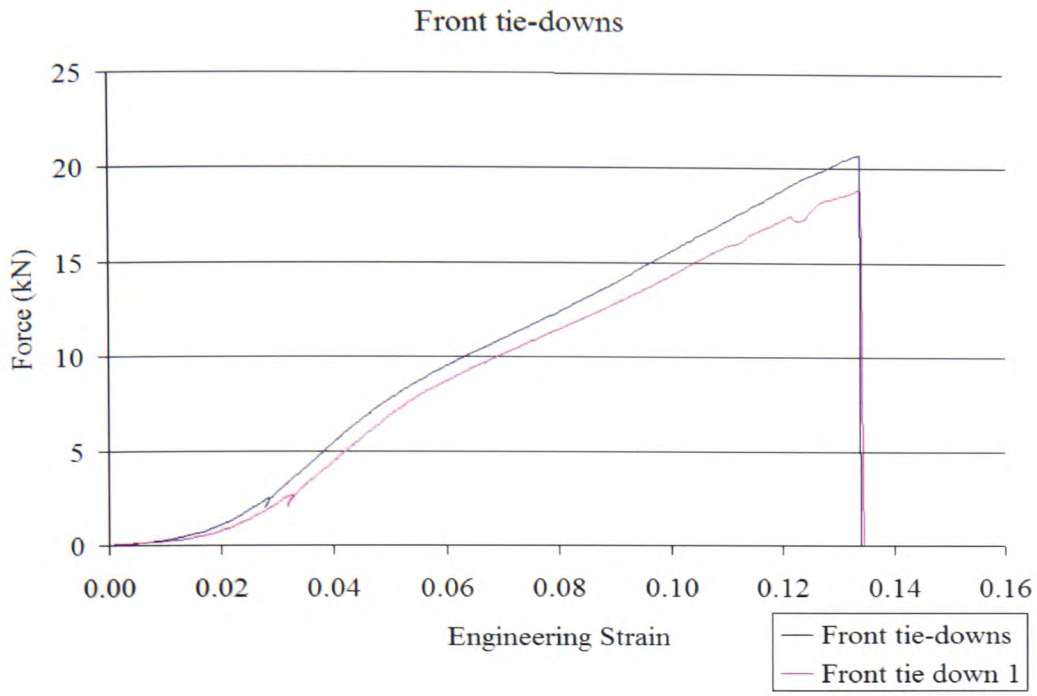

Figure 3.2.10 showing the stress-strain curve for the frontal tie-downs

Figure 3.2.11 showing where the stitching of the front tie-down webbing strap failed (left) compared to an undamaged front tie-down (right)

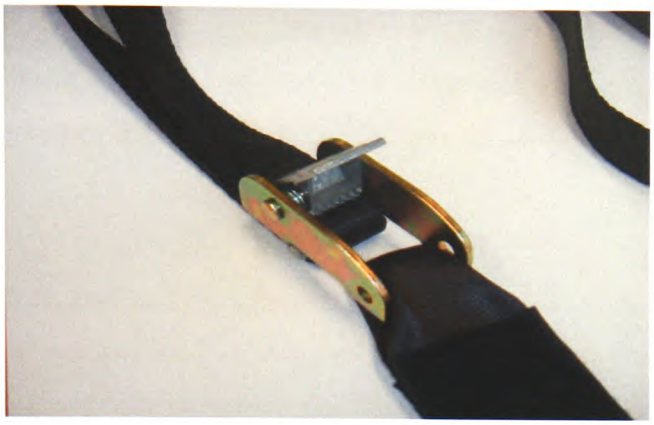

Figure 3.2.12 showing the front tie-down clamp cammed in to lock the webbing strap in place

Discussion:

From the literature the highest load experienced by the rear tie-downs in a frontal 20g wheelchair crash test was 21.03kN and the highest load on the front tie-downs was 8.76kN [14, 28]. These values compare favourably with the failure loads of the rear and frontal tie-downs tested as shown in Table 3.2.1.

	Max. load experienced in frontal 20g crash from literature (kN)	Min. failure load from experiment (kN)
Rear tie-down	21.03	29.6
Front tie-down	8.76	18.9

Table 3.2.1 showing the maximum tie-down loads experienced by the tie-downs in a frontal 20g crash, from the literature, compared to the minimum failure loads from the experiment

Due to limitations in test equipment the tie-downs could only be tested statically. Although not ideal the resulting force/ displacement curve still gave useful material properties that were used in the computer model. The mean value of both the front and rear tie-downs were used.

The failure mechanism of the tie-downs during the static test was of limited interest as the tie-downs themselves are designed to withstand frontal 20g wheelchair crash forces and are tested to ISO 10542-1 [1].

The material model used to represent the tie-downs in the computer simulation was 'MAT_SEATBELT'. This material model had no stress in compression. The material properties required for this model were mass per unit length and a graph of force against strain.

A virtual version of the practical tensile tie-down test was created to examine how faithfully the simulated predictions matched the results from the practical tensile test. The simulated results were expected to be very close, as the load versus strain data from the practical experiments were put directly into the material model of the tie-downs to describe their behaviour. A similar technique of testing individual parts against their equivalent FE model was used by Williams *et al.* [92] to validate their model of a Caterham 7 motor car.

Seatbelt elements were created that had a total length equal to the tie-downs in the practical experiment (612mm for the rear and 580mm for the front). One end of the tie-down was restrained and a load over time applied to the other end. The seatbelt elements were given a density of 1.01×10^3 kg/m^3, which equalled a mass per unit length (1 metre) of 50.5 $\times 10^3$ kg for the 50mm wide rear tie-downs and 26.3×10^3 kg for the 26mm wide front tie-downs. Both tie-downs had a thickness of 1mm. The computer modelling of the tie-downs will be discussed in more detail in Section 4.3.3.

The output of the simulation was plotted as force against strain. This graph was then compared with the one obtained via experimentation and is shown in Figure 3.2.13.

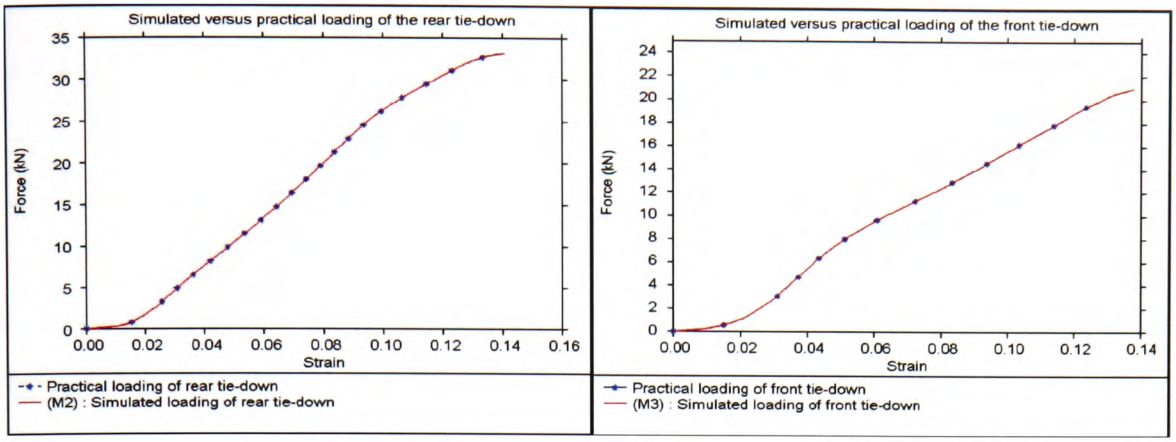

Figure 3.2.13 showing the practical and simulated force against strain graphs for the rear tie-downs (left) and front tie-downs (right)

As expected, the results showed that the simulated results perfectly match those obtained from practice.

Summary

Both the rear and frontal tie-downs failed at loads higher than values recorded from frontal crash tests (see Table 3.2.1), therefore are expected to survive the actual crash test. The experiment could be improved by testing at strain rates equivalent to those experienced in a standard 30mph crash test. The practical experiment was modelled using FEA and found to produce identical results.

3.2.3 Compression of Spectra wheel

Aim:

The aim of this experiment was to validate the FEA model of the Invacare Spectra wheelchair rear wheel against physical tests. It would have also been desirable to test the surrogate wheelchair wheels in a similar fashion but these could not be sourced. During the physical crash tests the compression of the wheelchair wheels had a considerable effect on the motion of the wheelchair assembly and consequently affected the kinematics of the occupant.

Method:

A simple compression test was performed on the wheel using an Instrom 8502 tensile test machine. A test rig was constructed to fix the wheel in place by its axle. A flat plate was then used to compress the tyre. Both force and displacement were measured from the compression plate. The test setup is shown below in Figure 3.2.14.

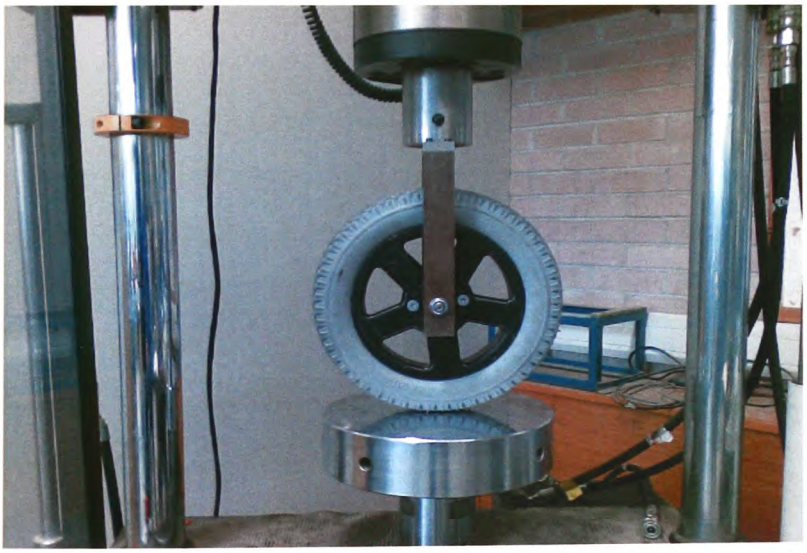

Figure 3.2.14 showing the experimental setup of the Spectra wheel compression test

The pneumatic wheelchair wheel was tested at 5 different pressures, to simulate different operating pressures and ensure the robustness of the FEA model, and in addition a solid wheelchair tyre was also tested. Solid wheels are used by the RE unit on some of their wheelchair designs. The solid wheels had exactly the same geometry as the pneumatic wheels and were made by removing the tyre's inner tube and filling the tyre up with Microcellular Polyurethane (MCP) foam, making the tyre resistant to punctures and stiffer than the pneumatic tyres. The load was applied at a rate of 1000mm/min as this was the fastest feed rate at which the measuring software could record sufficient data. All tests were subjected to a 25mm compression. The practical experiment was recreated in LS-Dyna and the results from the practical and simulated experiments compared.

Computer models

The objective of the FE wheel model was to faithfully reproduce the behaviour of the actual wheelchair wheel while not being too processor intensive. This was achieved by several simplification steps found from existing literature on car tyre modelling [95, 96, 100, 111]. Models of both the pneumatic and solid tyres were produced, each requiring slightly different modelling techniques.

Computer model of the Pneumatic tyre

The rim and hub of the wheel were made from rigid shell elements, as they had very little effect on the behaviour of the wheel compared to the tyre compression. The tyre model was made from deformable fully integrated shell elements, which are recommended for large deformations [112]. The standard Belytchko-Tsay shell elements are very efficient, and hence set as the LS-Dyna default shell element, but can form artificial weak points if badly distorted and hence under predict stiffness [85]. The cross section of the actual tyre had a variable wall thickness. This was modelled by dividing the tyre wall up into several 'bands' of shell elements, each with a different wall thickness [98, 100, 113], see Figure 3.2.15.

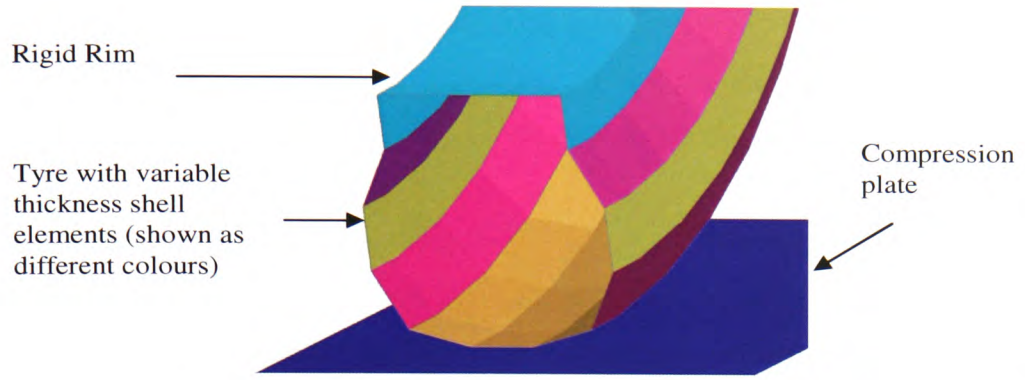

Figure 3.2.15 showing the cross section through the meshed tyre. The different colours depict the different shell thicknesses

The actual tyre was constructed from a rubber and fabric inner layer that was covered by a further rubber layer of varying thickness, which also incorporated the tyre tread. The tyre bead had six strands of steel wire running through it. Testing each different material layer of the tyre would be very difficult as they are all bonded together and vary in thickness throughout their cross section. The tyre composite was also anisotropic. Reid [98] also encountered this problem with his model of automotive tyres so took material properties for the tyre were therefore taken from existing literature. The material properties used for the tyre model are shown in Table 3.2.2.

Component	Density (kg/m^3)	Young's Modulus (MPa)	Poisson's Ratio	Shear Modulus (MPa)	Shell thickness (mm)
Rim (rigid)	$7.85x10^3$	$210.0x10^3$	0.30	N/A	6.0
Tyre wall	$1.10x10^3$	30.0	0.45	10.34	2.5-4.5
Tyre Tread	$1.10x10^3$	30.0	0.45	10.34	6.0

Table 3.2.2 showing the material properties used for Spectra wheel model

The shear modulus, G was found from the following equation:

$$G = \frac{1}{2}\left(\frac{E}{(1+\upsilon)}\right)$$

Where G=Shear Modulus

E=Young's Modulus

υ=Poisson's Ratio

Although stated previously that the material making up the tyre wall was anisotropic (material properties were direction dependant) it was assumed to be isotropic (material properties the same in all directions) for purposes of model simplification.

The air inside the tyre was modelled by using the 'Airbag' function within LS-Dyna [85]. This function, originally designed to model airbag deployment in motor vehicle crash analysis, had a simple volume-pressure setting that allowed an inverse relationship between volume and pressure to be assigned to a defined volume. The volume, in this case, was made up from the inside wall of the tyre and the rim. Segments, which are used to define the faces of the contacting surfaces, were used to define the volume between the inner tyre wall and the rim. It was assumed that the volume didn't leak and that there was no temperature or mass flow. The pressure in the tyre changed with the relative volume, with the relative volume being the current volume divided by the initial volume [85]. For model stability it was recommended that the pressure be ramped up over a period of time. For this simulation the pressure was increased gradually over the first 20ms [87].

Due to the large differences in stiffness the contact relationships between the tyre and rim and between the tyre and compression plate where setup using SOFT=1. Self contact (AUTOMATIC_SINGLE_SURFACE) was used on the tyre to check for self contact as the tyre compressed in on itself. Further details regarding contact and the 'SOFT' function are discussed in Section 4.2.3.

During preliminary runs of the pneumatic tyre the shell elements of the tyre tread arched up away from the compressing plate. This phenomenon was also observed by Reid [98] who found it to be caused by an excessively stiff tyre material and described the process as 'cupping', see Figure 3.2.16. Reducing the stiffness of the tyre wall and creating a variable thickness tyre wall, as described above, successfully eliminated the problem. The total mass of the pneumatic tyre wheel was measured as 2.1kg. Due to geometric simplifications mass had to be added to the finite element model to equal that of the physical wheel.

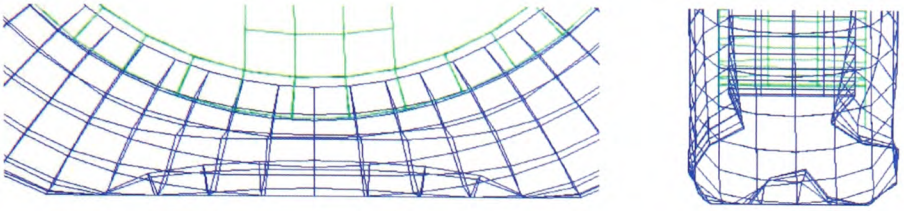

Figure 3.2.16 showing 'cupping' of the tyre shell elements during compression

Solid tyre:

The solid tyre was modelled from solid elements using the 'LOW DENSITY FOAM' material model that allows the behaviour of the foam to be controlled by inputting a stress-strain curve. The solid tyre model was formed by 'spinning' 2D quadrilateral elements about the wheel axle to form 3D hexahedral elements. The solid tyre model had far more elements than the pneumatic tyre model and hence had a longer run time. The solid foam elements were initially coated with shell elements given the same properties as the rubber tyre wall, as used in the pneumatic tyre model. Initial runs of the tyre model took over 10 hours to run. This was an unacceptable run time and would have made the eventual run time of the wheelchair, with 4 wheels, far longer than necessary. The stiffness of the tyre wall and the foam within the tyre combined to give the tyre its stiffness. In order to decrease the run time, and remove the problem of cupping that was also observed, the model was simplified by coating the solid foam with Null Shells[5] and increasing the stiffness of the foam to compensate for the removal of the tyre wall rubber, Figure 3.2.17. This approach successfully simplified the model and massively decreased the run time to 18.27 minutes.

---

[5] Null Shells are placed over the top of solid elements of soft materials to aid contact with surfaces of significantly higher stiffness's. The null shells are given a greater stiffness than the underlying elements and a very low density (10.0×10^{-9} kg/m^3) in order to prevent contact penetration without interfering with the behaviour of the under lying solid elements.

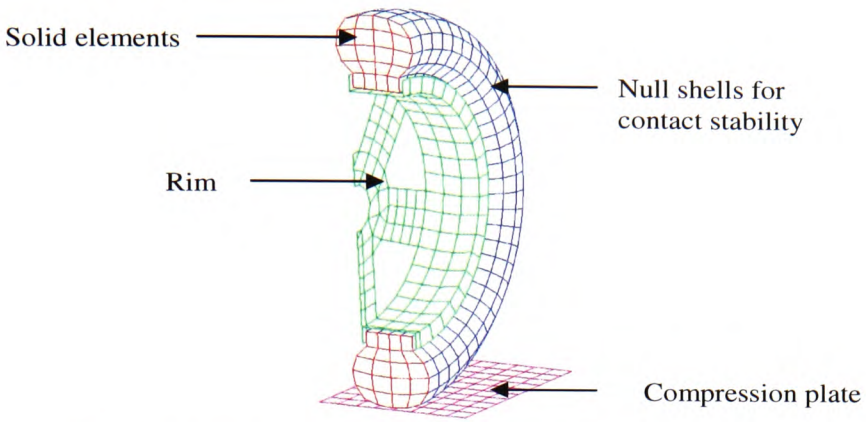

Figure 3.2.17 showing a cross section of the solid tyre model

Gravity was applied to both models and, like the airbag, was ramped up over the first 20ms. The compression plate only began moving after this initialisation time. Ramping up the gravity and airbag pressure over time helped to decrease model oscillations. The simulation was set to record the displacement of the compressing plate and the contact force between the plate and tyre.

Results:

Results of Pneumatic tyre

The FE tyre model appeared to mimic the behaviour of the physical tyre well and showed no undesirable element deformation. A comparison of both the virtual and actual pneumatic wheels under the same compressive force is shown in Figure 3.2.18.

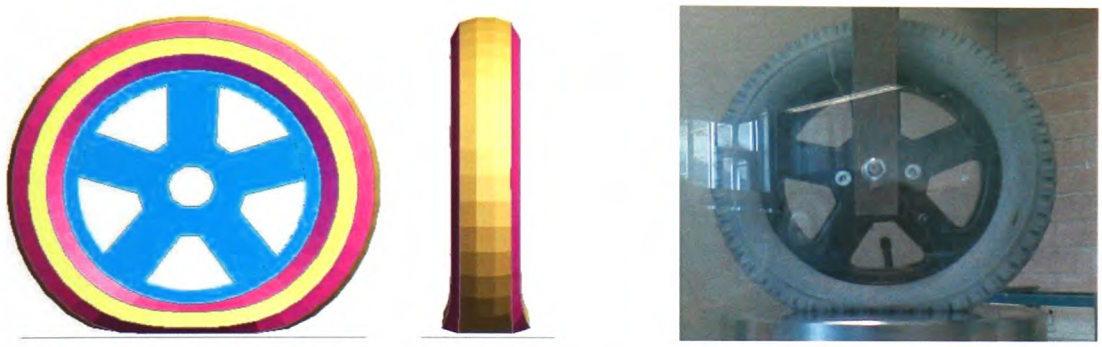

Figure 3.2.18 showing the compression of the FE model wheel (left) compared to the physical compression test (right)

The results were recorded as force against displacement. The graphs, in Figure 3.2.19 and Figure 3.2.20, show the results for each different tyre pressure. A line of best fit through the force against deflection graph was used to find the stiffness, which is equal to the gradient of the linear trend line. The results from the graph are summarised in Table 3.2.3. The simulation of the tyre model was visually inspected to ensure that there was no excessive deformation of the model elements that could lead to erroneous results.

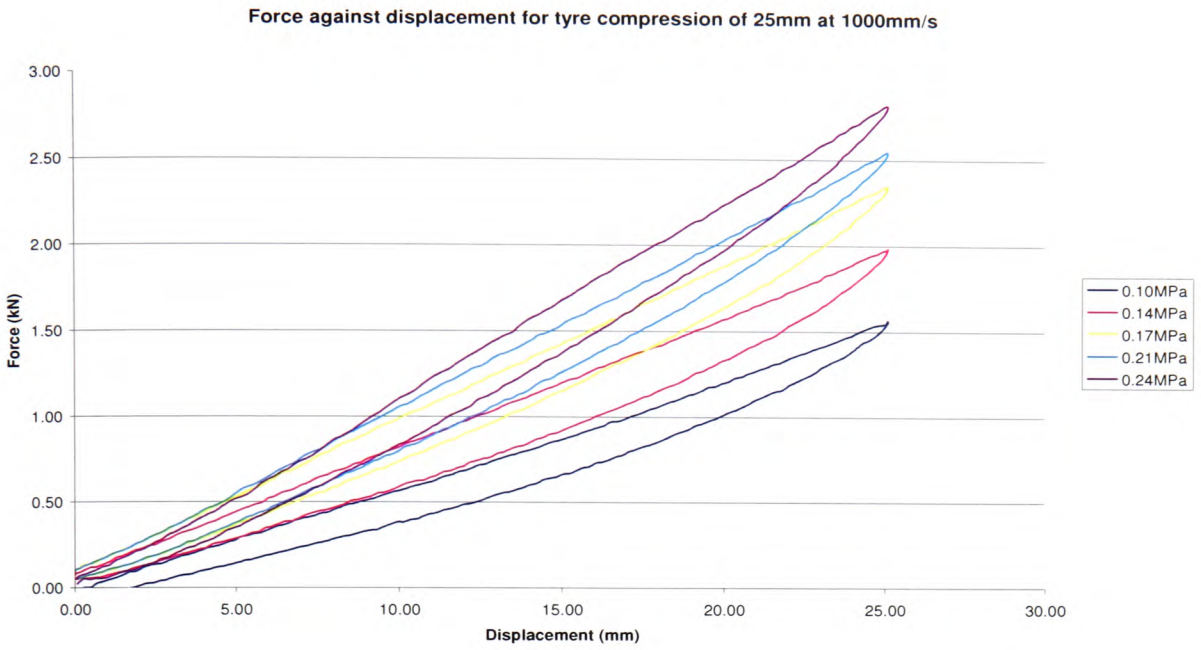

Figure 3.2.19 showing the force against displacement for the practical pneumatic wheel compression test

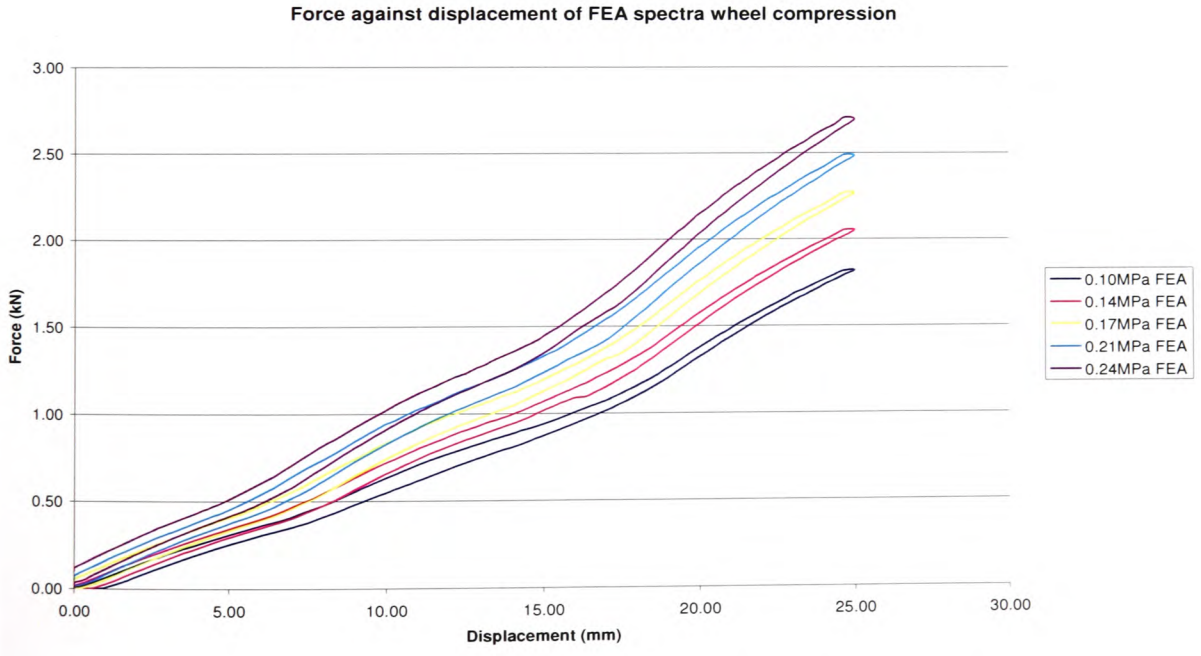

Figure 3.2.20 showing the force against displacement for the finite element model of the pneumatic wheel compression

Pressure (MPa)	Pressure (psi)	Experimental Max Force (kN)	FEA Max Force (kN)	Practical Stiffness (KN/m)	FEA Stiffness (KN/m)	% stiffness difference
0.103	15	1.56	1.82	62.10	71.00	14.3
0.138	20	1.98	2.05	75.50	80.30	6.36
0.172	25	2.34	2.26	89.70	88.60	1.23
0.207	30	2.54	2.48	98.30	96.80	1.53
0.241	35	2.81	2.69	112.70	104.60	7.19
					Mean % error	6.12

Table 3.2.3 summarising the results from the practical pneumatic wheel compression test

Results of Solid tyre

The total mass of the solid tyre wheel was measured as 3.1kg. The force against displacement graph, as shown in Figure 3.2.21, shows a reasonable correlation between the practical and simulated compression tests. The graph also shows a larger degree of hysteresis than observed in the pneumatic tyre compression tests. The highest load at the maximum compression of 25mm was 6.3kN, considerably higher than that of the pneumatic tyres tested.

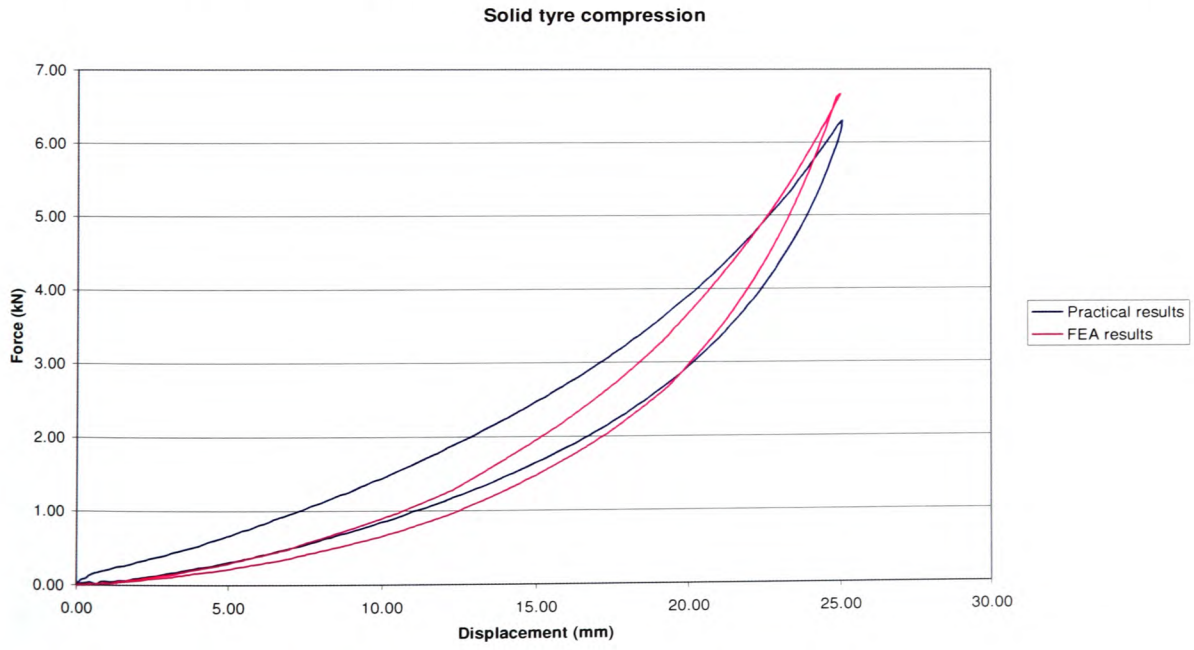

Figure 3.2.21 comparing the force against displacement curves for the practical and virtual compression of the solid tyre wheels

From visual inspection of the solid tyre model, illustrated in Figure 3.2.22, the foam elements compressed without excessive deformation.

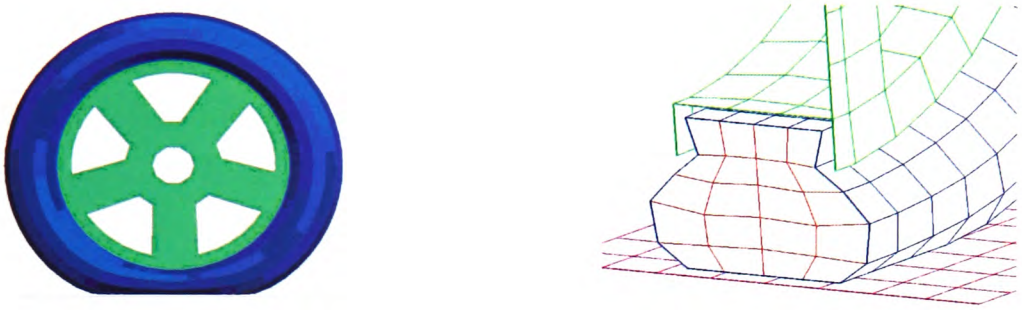

Figure 3.2.22 showing the compression of the solid tyre model with a cross section view of the deformed solid elements on the right

Known sources of error

The pressure in the tyre during the practical compression test was only measured to an accuracy of +/- 0.01 MPa. The Instrom's internal measurement system had a percentage error of 0.69% at full scale as per the certificate made on 12/09/2007) and was used to measure both displacement and force instead of using independent gauges. In the FEA simulations the tyre pressure was ramped up before loading began. The initial gap between the loading plate and the tyre was fixed so higher initial tyre pressures caused a slight initial load as the tyre expanded into the loading plate.

Discussion

The graphs of force against displacement for the practical compression of the pneumatic tyre show hysteresis curves. The loading section of the curves demonstrate good linearity and compare favourably with the results obtained from the FEA simulation. The unloading of the pneumatic tyre, however, was less linear, requiring less force per displacement than the loading cycle. This is typical hysteretic behaviour of rubber. The FEA results do not show the same hysteresis curve because a simplified material model was used to save on processing time. If detailed comparison of the tyre was required then a more precise material model could be used. In this instance the primary concern was to capture the absorption of energy during the tyre compression

with as simplified wheel model as possible. From examining the overall model predictions it was felt that this objective was satisfactorily achieved.

The stiffness of both the practical and theoretical results were taken from the loading part of the curve only. The simulated and practical results of the pneumatic tyre were reasonably close, with a mean percentage error of 6.12%.

The practical results of force against displacement for the solid tyre show a parabolic curve, a loading property more associated with foam and rubber than the more linear air compression of the pneumatic tyres. The solid tyre was also considerably stiffer, having a maximum compressive force at 25mm compression of 6.3kN compared with 2.8kN for the pneumatic tyres. The FEA results showed reasonable agreement with those from experimentation, having similar maximum force values and a parabolic load curve shape. The practical results were stiffer at lower forces. This is most probably due to the modelling simplification of just having the foam tyre without a rubber tyre wall. The foam tyre was coated with null shells that provided contact stability only.

Conclusion

Both pneumatic and solid FEA models agreed well with the physical tests carried out on the wheels. Although improvements to both models could be made it was decided that the small increase in accuracy would not justify the large increase in processing time.

3.3 Methodology summary

Accurate material properties are essential if meaningful FEA results are to be achieved. The process of testing sub components of the wheelchair system has the added advantage of checking the behaviour of these parts against their equivalent FE model before complete assembly. The next Chapter will discuss the modelling process and how these results were used to create the various FE models of the complete wheelchairs.

Chapter 4 - Modelling of wheelchair systems

4.1 Modelling overview

This Chapter looks in detail at the process that was used to construct the computer models of the wheelchairs examined in this thesis. The flow chart in Figure 4.1.1 shows the process involved in modelling. Each part will be discussed briefly followed by a more thorough explanation of the Finite Element pre-processing used to create the models.

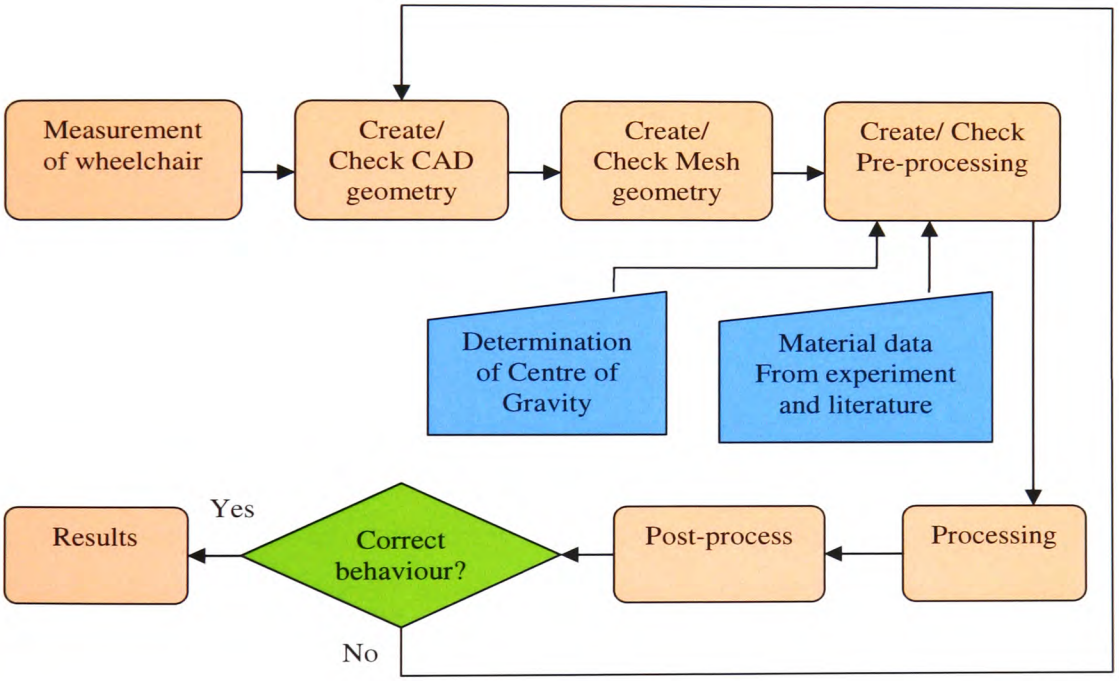

Figure 4.1.1 showing the modelling process

The modelling process firstly involved taking a CAD geometry, turning it into a finite element model and then applying representative loads and boundary conditions to it. Accurate CAD drawings were not available for either of the surrogate wheelchairs or indeed the production wheelchairs used by the Rehabilitation Engineering Unit. Each part of the wheelchairs, therefore, had to be accurately measured and reproduced as

CAD models in SolidWorks. The CAD models were saved in an IGES file format (Initial Graphics Exchange Specification) then imported into the meshing software (Hypermesh™).

The CAD geometries were meshed using Hypermesh™, supplied by Altair. The meshing process breaks down the geometry into small parts, called elements. The combination of these elements is referred to as the mesh. The completed mesh had boundary conditions and loads applied to it using pre-processing software. The pre-processing software used was Primer, part of the Oasys™ suite of programs produced by ARUP. Primer, along with D3Plot (post-processor) and T/HIS (results viewer) contained many features especially tailored for crash analysis. Primer is designed specifically with LS-Dyna in mind and incorporates all the main features of LS-Dyna, aiding the production of the LS-Dyna keyword file. The keyword file is the command script that is sent to the LS-Dyna program for processing. It contains node and element details along with material properties, element formulation and boundary conditions. This file can be written by hand but this soon becomes impractical when dealing with models containing large numbers of elements.

Each critical part of the model, such as the wheels, tie-downs and seat, were simulated independently to ensure correct function. This approach allowed for the separate parts to be checked, refined and in some cases, validated prior to complete system simulation. Williams *et al.* [92] used a similar approach for their model of a Caterham 7 motor vehicle and claimed to validate the entire model by testing the individual parts separately. Although each individual part can be checked before assembly it by no means ensures that the assembly as a whole will function correctly. Further validation of the fully assembled models was therefore conducted, as detailed in Chapter 5.

4.2 Modelling Procedures

4.2.1 CAD geometry

The CAD drawing involved two stages, the first being the construction of the wheelchair geometry as shown in Figure 4.2.1.

Figure 4.2.1 showing from left to right the ISO 10542 surrogate wheelchair, the ISO 16840 surrogate wheelchair and the Invacare Spectra Plus production wheelchair with Rookwood seatpan attached

The CAD drawing was then modified to simplify the meshing process. The modification involved the removal of any non-critical detail from the model, e.g. chamfers and rounded edges from non-critical parts, and alteration for shell element meshing. Shell elements were used to model thin parts by modelling the part as a single surface. SolidWorks, however, requires all parts produced to have a thickness. The meshing software can automatically calculate the mid-plane (the plane in the centre of the part parallel to the top and bottom faces) of such parts, but where complex connections between parts occur this automated mid-plane method can leave gaps at the joints, as illustrated in Figure 4.2.2(b). Gaps such as these make it very difficult to create a continuous mesh. Some of the wheelchair frames, which had complex tube joints, were therefore undersized so that their outside surface became their mid-surface, When exporting the geometry into the meshing software the outside surface could then be used directly as the mid-plane without causing any gaps between joints, Figure 4.2.2(c).

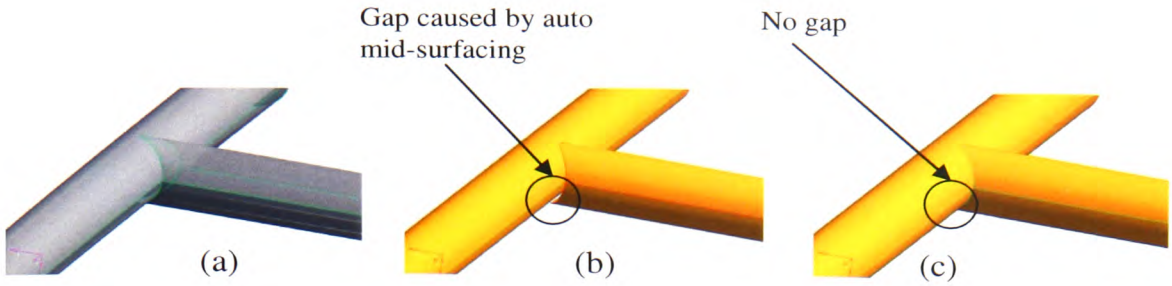

Figure 4.2.2 showing the CAD geometry (a), the extracted mid-plane with gaps (b) and the outer surface extracted without gaps (c)

4.2.2 Meshing

The goal in creating a good FE model is efficiency. The model must be accurate enough to represent the behaviour of interest while not being excessively large, i.e. the number of elements should be kept to an acceptable minimum.

The number of elements used to make up the mesh effects the run time. The elements used for 2D and 3D parts were shell and solid elements. Shell elements are used in parts with limited thickness and exhibit plane stress, i.e. the stress does not change through the thickness. Solid elements are used in non-thin parts that cannot be simplified to 1D or 2D representations or require greater detail, e.g. seat cushions. The shell elements are primarily quadrilateral and the solid elements are cubic, or hexahedral. To mesh non-rectangular shapes the quadrilateral and hexahedral elements must deform to some extent to allow them to tessellate. Excessive deformation of the quadrilateral and hexahedral elements can lead to erroneous results. The types of deformation are termed aspect ratio – ratio of length and breath, taper, skew and warp. The ideal shape for the quadrilateral and hexahedral elements would be a square and cubic respectively [114]. In order to minimise element deformation, and aid element tessellation, triangular, for 2D, and tetrahedral, for 3D, elements may be incorporated into the mesh. These triangular and tetrahedral elements must be limited to 5% of the total elements used in the mesh for LS-Dyna as they tend to be stiffer and too many can produce erroneous results [85].

There are several ways of ensuring good efficiency of the FE model and many of these are through simplification of the model geometry. Parts of the system that are not of direct interest, such as the test sled and rigid frame of the surrogate wheelchairs, can be modelled more crudely, using larger elements. The areas or greater interest are meshed with a higher density of elements. A certain amount of trial and error is required when deciding on the correct mesh density to use. It is usual to carry out a number of runs to examine the sensitivity of the model to various mesh densities. In this instance much of the mesh refinement was done at the individual part level, e.g. wheels, seat-pan and frame, before the complete wheelchair was assembled, helping to ensure a successful run of the complete assembly.

Parts that were not expected to deform were treated as 'rigids'. Rigid parts are defined in LS-Dyna by applying the 'MAT_RIGID' material to the elements of the part. The rigid parts do not deform and any forces or motion applied to them are summed together and applied at the parts centre of mass. Constraints, such as displacements and boundary conditions, may be directly applied to rigid bodies at the centre of mass [112]. Material properties must still be added to the rigid part; the density is required for mass calculations and the Young's Modulus and Poisson's Ratio are required for contact stiffness calculations.

4.2.3 Pre-processing

Part of the process of capturing the wheelchair's geometry was finding its centre of gravity. If the model is accurate enough and the same densities for the materials are entered then the centre of gravity should be the same as the measured value. Often there is a small difference in the location of the centre of gravity that can be adjusted by redistributing the mass across the nodes of the model during pre-processing. For the surrogate wheelchair models the ISO standards 10542-1 and 16840-4 [1, 39] specified the mass of the wheelchairs and their centres of gravity with allowable tolerances. The production wheelchair's centre of gravity had to be empirically identified. This was achieved by first measuring the weight of the wheelchair under each wheel when level, to find the centre of mass, then measuring the weight again after inclining the

wheelchair. The test was conducted with the rear brakes on so the wheelchair was assumed to pivot about the point where the rear tyres contacted the ground. This setup of this experiment is shown in Figure 4.2.3.

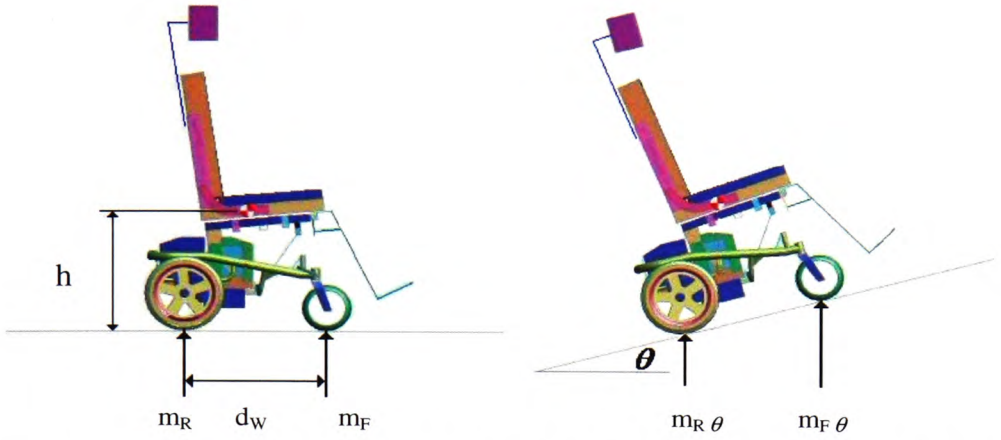

Figure 4.2.3 showing the method of calculating the centre of gravity for the Spectra Plus production wheelchair

Weight of production wheelchair (Invacare Spectra Plus) when level:

Mass over front wheels = 14.7kg (m_F)
Mass over rear wheels = 55.4kg (m_R)
Mass over right wheels = 36.0kg (m_{right})
Mass over left wheels = 34.1kg (m_{left})

Total mass = 70.1kg (m_{wc})

Distance between front and rear wheel axis = 583.0mm (d_w)
Taking moments about the rear wheels; $m_{wc}\, x_{RA} = m_F\, d_w$
Where the centre of mass from the rear wheel axle, x_{RA} = <u>122.5mm</u>

Distance between the right and left rear wheels = 460.5mm (w)
Taking moments about the right wheel; $m_{wc}\, y_{RW} = m_{left} w$
Where the centre of mass from the right wheel is, y_{RW} = <u>224mm</u>

The centre line between the two rear wheels lies 230mm from the right wheel, meaning that the lateral centre of gravity from the centre line is 6mm towards the right wheel.

The front of the wheelchair was raised up by 110mm producing an angle of 9.2^0 to the horizontal.
Mass over front wheels: 11.2kg ($m_{F\theta}$)
Mass over rear wheels: 58.9kg ($m_{R\theta}$)

Calculation to work out the height of centre of gravity from the ground, h:

$$h = \frac{m_{wc}x_{RA} - m_{F\theta}d_W}{m_{wc}Tan\theta} = \frac{70.1\times122.5 - 11.2\times583}{70.1\times Tan9.2^0} = \underline{\underline{182.0mm}}$$

As the radius of the rear wheel is 158mm, this is equal to a centre of gravity height of 24.0mm above the rear axle. As the lateral position of the centre of gravity was only 6mm from the centre line it was decided, in the interest of model simplification, to assume that the centre of gravity was directly on the centre line. The overall position of the centre of gravity was therefore 122.5mm forward of the rear axle and 24.0mm above the rear axle. A similar method was presumably employed by Caldicott and Shapcott [115] for their 'software-based stability assessment system'.

Modelling Contact

Another important task during the pre-processing phase is the setting up of contacts. Contact surfaces are used to prevent predefined surfaces of the model from passing through each other. Many different types of surface contact exist and the right one must be chosen for the specific application. The majority of contact types used in this study are penalty based contacts. These contacts function by specifying a slave and master side of predicted contacting surfaces. During simulation, the position of these master and slave sides are checked at each time step. If the surfaces are found to come into contact with each other a force is set up between the nodes of the surface elements to resist penetration. For solid elements the outside edge of the element is taken as the

surface and for shell elements the surface is taken at a certain distance away from the mid-plane, depending on the thickness specified for that particular shell element.

The two most common contact problems arise from large differences in stiffness between contacting surfaces and the rate at which these surfaces come into contact. The contact distance between two shell elements is half the thickness of the slave surface plus half the thickness of the master surface. If the time taken for a node of the slave surface to travel the contact distance is less than the minimum time step of the simulation process then the node can travel past the mid-plane of the master surface before being identified. When the penetrating node is identified the force setup to resist its motion pushes it away from the wrong side of the shell's mid-plane, increasing apparent penetration. Both the contact stiffness and contact distance should be adjusted within the contact definition to try and eliminate such problems.

In solid element contact, the solid elements are coated with either shell elements or segments. Segments define the area that will take part in the contact, useful if only a small area of a larger part is to come into contact with another part. When a solid is coated with shell elements the properties of the contact, i.e. the contact stiffness, is obtained from the shell elements and not the solid elements that they overlay. The most common example of this application is when modelling foam. A layer of 'null' shell elements are placed over the solid foam elements. The null shells have a very low density but a relatively high Young's Modulus (typically density=10.0×10^{-9} kg/m^3 and Young's Modulus = 10 GPa). Since foam has a very low Young's Modulus, and hence low Bulk Modulus[6], the higher Young's Modulus of the null shells increases the contact stiffness between the foam and contacting surfaces allowing for a stable solution [85].

Contact between nodes can be defined in a number of ways within LS-Dyna by using the 'SOFT' function. The default value of SOFT=0 uses the stiffness of the contacting

[6] The amount that a material compresses under a given pressure with units of N/m^2

nodes to setup the contacting stiffness and does not take into account the mass attached to the nodes. This can cause stability issues if the contacting node, attached to a low density element, contacts a higher density element, e.g. foam contacting steel. The relationship that governs this is as follows:

Unstable if the contact stiffness, $k \succ \frac{m(dt)^2}{4}$

where m = mass, dt = timestep

Setting SOFT=1 automatically determines the contact stiffness, k, so that $k \prec \frac{m(dt)^2}{4}$.

This ensures contact stability between surfaces of different mass densities and stiffness's, e.g. tyre to load plate contact described in Chapter 3.

The final part in pre-processing is selecting the output information. Recording unneeded information can result in excessive file sizes and prolong the run time. The sample rate for the graphical output of the data can be controlled and is usually set to between 500-200Hz. The time history output data is normally sampled at a higher rate, in the order of 10kHz, to reduce the chance of aliasing during any subsequent filtering of the signal [87], as mentioned previously in Chapter 3.

4.2.4 Processing

Once the pre-processing is complete the LS-Dyna keyfile, generated by the pre-processor, is sent to the processor, in this case LS-Dyna, to run. LS-Dyna processes the file and outputs a series of binary files containing graphical and time-history results [87].

4.2.5 Post-processing

The two programs used for post-processing were D3Plot and T/HIS, both part of the Oasys™ suite of software. D3Plot displays the output from the '*.ptf' files which

contain details of the movement/deformation of the part. The movement of the part can be animated, allowing visual checks on correct model behaviour, such as correctly functioning boundary conditions, part deformation and penetration detection. Any anomalies are noted and corrected in the pre-processor or by mesh refinement. Minor mesh refinement can be carried out in the pre-processor but major re-meshing of a part must be conducted using the separate meshing software.

T/HIS is a graphical display program that displays the graphs of the data requested. All data is recorded against time but the software has many tools allowing graphs to be combined, multiplied, subtracted and translated. The software also includes standard data filters, such as Channel Filter Classes (CFC) 60, 180, 1000 [87].

4.3 Details of common wheelchair components

The modelling of the three wheelchairs used in this study (ISO 10542 surrogate, ISO 16840 surrogate and Invacare Spectra Plus) will be discussed individually. Prior to this, parts common to all wheelchair models will be considered. The way in which the wheelchairs were fixed to the sled, in an actual test setup using tie-down straps, is common to all the wheelchair models, as is the positioning of the occupant, application of the seatbelt and modelling of the wheels. The process of creating the wheels has been dealt with in Chapter 3 on Methodology so will not be repeated here.

4.3.1 Sled

The sled, or vehicle chassis, is the base onto which the wheelchair is mounted. The sled was modelled with rigid shell elements. The B-pillar (see Figure 3.1.5 in Chapter 3), where the upper shoulder belt anchor point was attached, was omitted in favour of an extra node relationship that was used to fix the upper shoulder anchor point to the sled. The extra node function allowed a defined node to be related to a rigid body as if it were physically attached. This decreased the total number of elements required and allowed for more flexibility if the upper seatbelt anchor point

needed to be moved. The bottom seatbelt mounting points and the tie-down mounting points were modelled in the same fashion.

The crash pulse graph, as described in Chapter 3, was applied to the sled using the 'BOUNDARY_PRESCRIBED_MOTION' function in LS-Dyna. The crash pulse curves are shown in Figure 3.1.3 and Figure 3.1.7 in Chapter 3. The onset of the acceleration pulse was delayed by 20ms to allow time for the gravitational force on the model and wheel pressure curves to reach their maximum value. Both these values were ramped up from zero to improve model stability. The air pressure in the tyres was found to be particularly susceptible to oscillations caused by neglecting to ramp up the pressure over time.

4.3.2 Wheels

The behaviour of the wheels is extremely important with regards to the motion of the wheelchair in a crash and as such it is important to model them as accurately as possible. The method of generating the FE models of the wheels was discussed at length in Chapter 3.

The joint between the wheel and frame was achieved by use of a 'REVOLUTE_JOINT' [85]. Joints can only be applied between rigid bodies and allow movement in the direction specified whilst restraining translation and rotation in all other directions. The revolute joint requires two pairs of nodes to define it with one pair of nodes being attached to a rigid body part of the frame and the other pair being constrained via the extra node function to the rigid rim of the wheel.

From published literature of modelling car tyres, the coefficient of friction defined between the tyre and road surface varied from 1.0 to 0.5 [96, 100, 111, 116]. Higher performance tyres tended to have a higher friction coefficient so the lower value of 0.5 was deemed to be more appropriate for wheelchair tyres. The model showed little sensitivity to tyre friction so determining the true friction of the wheelchair tyres was deemed unnecessary.

4.3.3 Tie-downs

Following on from the brief discussion in Chapter 3 the modelling process required for the tie-downs will be considered in more detail here. One dimensional, single degree of freedom, seatbelt elements were used to model the tie-downs as they produced zero force if the strain became negative, i.e. they modelled tension only. The force was calculated from the positive strain between the two nodes that define the element. The force acted along the axis between the two nodes and in the opposite direction to the direction of strain. The stiffness of the seatbelt elements were defined by inputting a mass per unit length instead of a density value. Unlike beam elements, the seatbelt elements did not require a third orientation node to define them [85].

When attaching the seatbelt elements to the wheelchair frame the diameter of the attaching hook was taken into account to allow for the correct attachment point, as shown in Figure 4.3.1. For simplification the metal hooks and vehicle cleats were omitted and the webbing tie-downs assumed to be attached directly from vehicle chassis to wheelchair frame. This was a valid simplification as the load versus extension characteristics of the tie-downs were measured experimentally with the hooks and cleats attached, as described in Chapter 3. A node was placed at the point where the tie-down attached to the frame and was joined to the frame by the 'EXTRA_NODE' function in LS-Dyna, which associated the node specified with a particular rigid body, i.e. the surrogate wheelchair frame.

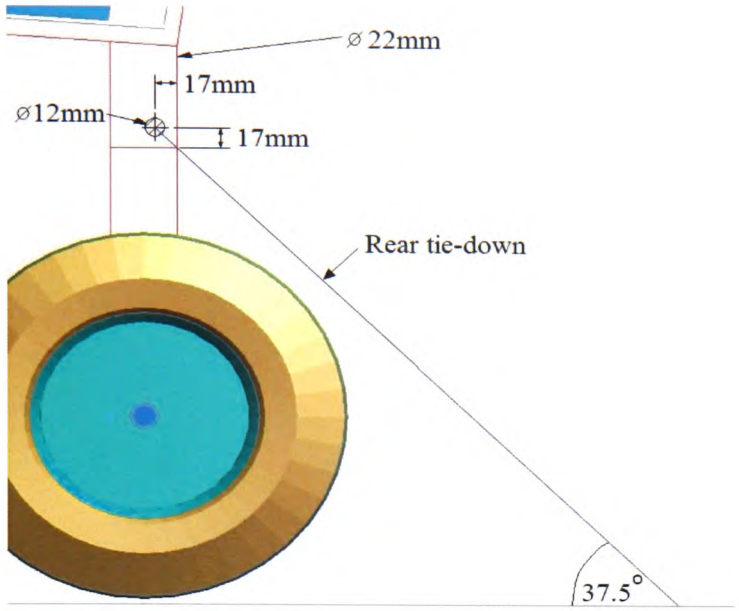

Figure 4.3.1 showing the spacing between the tie-down hook and the wheelchair frame

The orientation of both front and rear tie-downs were taken from ISO 10542-1 and the Q-Straint manual accompanying the Q-Straint tie-downs, itself taken from the aforementioned International Standard. The tolerances of the tie-down orientation, shown in Figure 4.3.2, allowed for different configurations of wheelchair and vehicle interior.

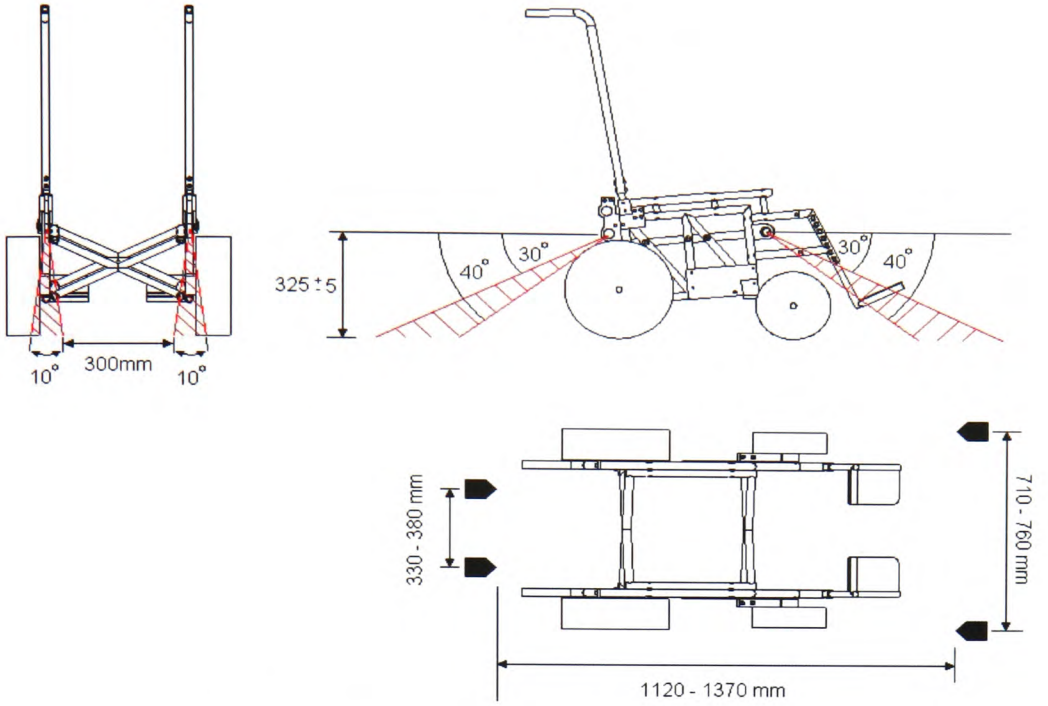

Figure 4.3.2 showing the tie-down location and angle, taken from ISO 10542-1 [1]

The angle of the front and rear tie-down angles horizontal to the sled were measured from the ISO 10542-1 test setup as 30.0^0 and 37.5^0 respectively.

4.3.4 Seat and cushions

In the case of the ISO 10542 surrogate wheelchair, modelling the seat was relatively straight forward as it consisted of two sheets of aluminium bolted to the chassis. For all subsequent wheelchair models the standard Rookwood seat-pan was used, as illustrated in Figure 4.3.3. This was constructed from various sheet aluminium parts and could therefore be completely modelled by shell elements. The seat-pan consisted of a seat base and back rest connected together by two bolts. Two arms were positioned between the base and back to lock them in position. These arms were found to deform excessively at stresses well below the expected yield limit of the material. The mesh density on the arms was increased and fully integrated shell elements were used to adequately capture the stress distribution across the supporting arms, resulting in more realistic behaviour.

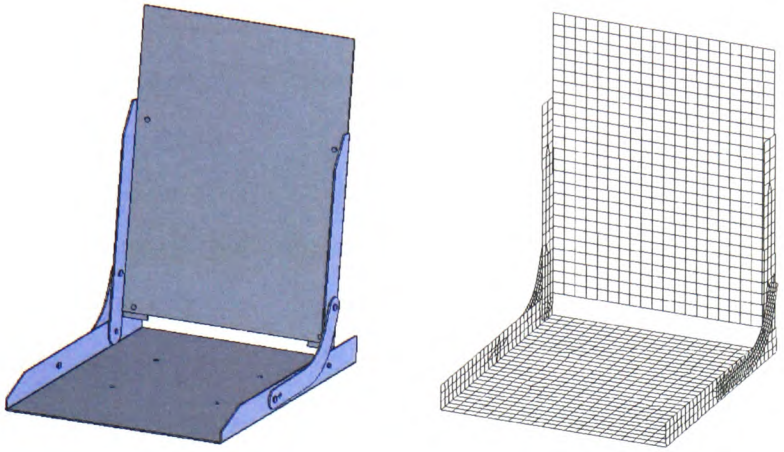

Figure 4.3.3 showing the CAD drawing (left) and meshed model (right) of the Rookwood seat-pan

Both seats had foam cushions onto which the dummy was positioned. The foam cushions were modelled from solid hexahedral elements and the LS-Dyna 'MAT_LOW_DENSITY_FOAM' material applied. The foam material required a graph of stress against strain to describe its behaviour. This was measured experimentally, as discussed in Chapter 3. As the foam material was relatively soft it underwent a large amount of deformation. This deformation can result in 'negative volume' errors whereby the solid elements modelling the foam compress to zero volume. Such an error causes the solution of the model to fail. A recommended method for improving the robustness of the foam material was to stiffen the stress-strain curve of the foam material at 80% strain to give a final stress value of 100 MPa at 100% strain. This prevented the foam elements from collapsing in on themselves [84]. A further modelling technique to aid foam material contact with far stiffer materials, such as the dummy and the seat base, was to coat the solid foam elements with null shell elements, as described previously.

Once the geometry of the seat was created the dummy had to be seated in it correctly. It was necessary to account for the pre-compression of the seat cushions in order to correctly simulate the initial position of the dummy and the resistance to forward motion the compressed cushions would cause in a crash. It is most common to position the dummy using the H-point, which point lies between the two hip joints [85, 87, 112]. The dummy was positioned into the un-deformed seat cushion. The first

method of moulding the seat cushion around the dummy was to perform a pre-run where the dummy was moved away from the seat then pushed back in, causing the seat foam to compress, see Figure 4.3.4. The output file of the compressed seat foam elements could then be entered back into the original file to produce a compressed seat profile [74, 87]. An alternative method has been produced by the ARUP group in their LS-Dyna pre-processing software 'Primer' [87]. The so called 'seat squash' function works in a similar way to the previous method but is carried out within the pre-processor as opposed to being run through LS-Dyna. Unlike the previous method the 'seat squash' function only rearranges the seat cushion mesh to mould around the dummy and does not calculate the internal stresses in the foam. As a result this method is significantly quicker. Williamson [74] claimed that including the stress initialisation of the foam cushion, by performing a pre-run, reduced the likelihood of error terminations due to negative volumes of the foam elements. This problem was not encountered during the creation of the models in this study so the quicker method of compressing the seat foam in the pre-processor was adopted.

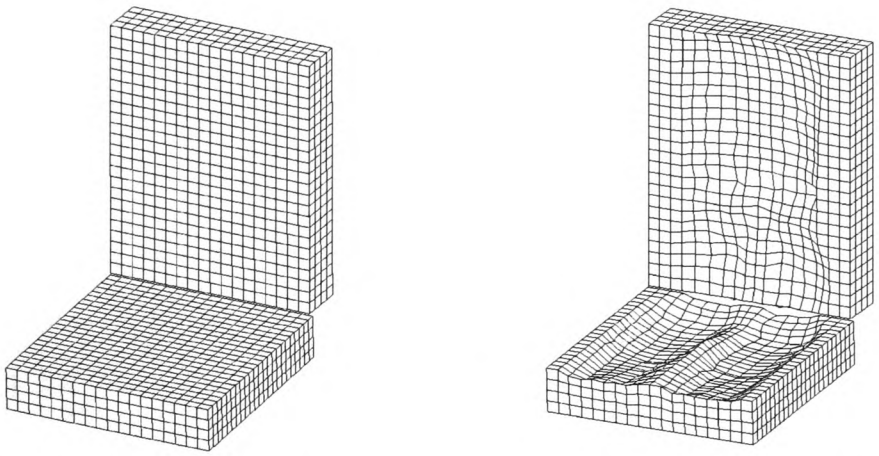

Figure 4.3.4 showing the seat cushions before and after pre-compression

4.3.5 Seatbelt

The seatbelt securing the dummy in the wheelchair seat was a 3-point harness with one upper shoulder anchor point and two floor anchor points. The seatbelt was attached in accordance with ISO 10542-1, as illustrated in Figure 4.3.5.

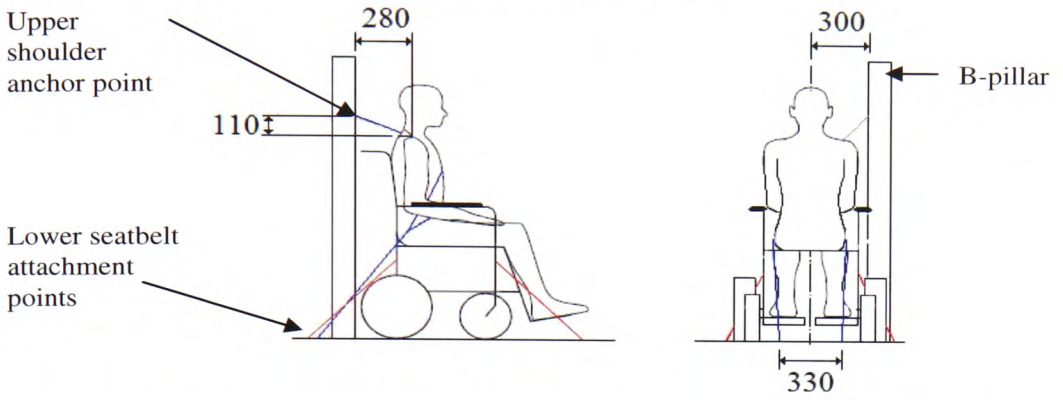

Figure 4.3.5 showing the upper shoulder seatbelt anchor position with respect to the top of the shoulder measured from the practical setup [1]. All dimensions in mm

The seatbelt was fitted to the dummy using an algorithm within Primer, the pre-processing software. The fitting was achieved by selecting a number of points on the dummy and wheelchair that defined the path of the seatbelt, through which a spline was fitted. The fitting of the spline was then improved by moving the points of the spine closer to the dummy. Penetration between the dummy and the spline was checked at each step, or iteration, until penetration occurred. The spline was then moved back out from the contacting surface until zero penetration was achieved. Once the path was set it could then be meshed with a combination of 1D and 2D seatbelt elements. The 2D seatbelt elements used were a fabric material that, like 1D seatbelt elements, produced zero stress with negative strain (i.e. they did not model compression).

2D shell elements are more robust when applying contact between surfaces and so were used where the seatbelt contacted the dummy. They also better model the actual interaction between the occupant and seatbelt by distributing the load over an area, as opposed to a single line in the case of using 1D elements. ID elements, however, are

faster to solve and were therefore used for non-contacting parts of the seatbelt. The contact applied in LS-Dyna between the seatbelt and occupant was in the form of 'AUTOMATIC_SURFACE-SURFACE', with the slave side of the contact as the seatbelt and the master side being the dummy null shells.

1D seat belt elements are in effect discreet elements and as such are not able to cope with node to node contact. This presented a problem where the 1D seatbelt came into contact with beam elements, such as the surrogate wheelchair frame. In this situation either 2D seatbelt elements must be used or the beam elements must be replaced by shell elements. A third option was to coat the discreet 1D seatbelt elements with null beam elements. It was found that the best solution was to replace the parts of the wheelchair frame, which came into contact with the 1D seatbelts, with shell elements. The issue of belt contact with non-occupant parts is more pronounced in wheelchair simulations than automotive scenarios due to the large distance between the seatbelt floor anchor points and the wheelchair seat and the number of items the belt is fitted around, i.e. seat cushion, seat base and wheelchair frame. Car seatbelts, in comparison, are anchored far closer to the seat and so the seatbelts predominately come into contact with the seat and occupant only.

4.4 Wheelchair systems

The following Section examines the specific modelling procedures for the three wheelchairs under consideration, namely the ISO 10542 surrogate, the ISO 16840 surrogate and the Invacare Spectra Plus wheelchairs (referred to as the 'Spectra' herein).

4.4.1 ISO 10542 surrogate wheelchair model

The frame geometry of the ISO 10542 surrogate wheelchair was measured and drawn in Solidworks along with the various metal plates that were used as both structural supports and ballast to achieve the correct mass and centre of gravity, in accordance

with ISO 10542-1 [1], see Figure 4.4.1. The tubing making up the frame was mild steel of 22mm outer diameter and 18mm inner diameter. The surrogate wheelchair was designed to be rigid so the beam elements making up the FE model of the wheelchair frame were assigned the 'MAT_RIGID' material property in LS-Dyna, causing them to be treated as rigid bodies.

The frame was modelled out of Hughes-Liu beam [85] elements that were given the cross section of the tube. The Hughes_Liu beam formulation is the default used in LS-Dyna. It can model both circular and rectangular cross sections as well as accepting different cross section formulations. The disadvantage of this type of beam element is that the integration of the beam formulation takes place at the centre of the element so, in the case of bending, the yield point will be shown at the centre of the beam as opposed to the edge, i.e. the formulation will over-estimate the force that causes the material to yield. As the beam was treated as rigid this wasn't an issue [85].

The seat and backrest of the surrogate were made of sheet aluminium being 6mm and 3mm thick respectively. These were also treated as rigid and were modelled from Belytschko_Tsay shell elements, the default LS-Dyna shell element formulation with one in-plane integration point and two integration points through its thickness. These shell elements are far quicker to solve than the more comprehensive fully integrated shell elements.

The ballast parts of the surrogate wheelchair were modelled from solid elements to ensure correct mass and centre of gravity. These were also treated as rigid. The solid elements used for these parts were default hexahedron elements with a single integration point at their centre. The single integration point makes these elements quick to solve but they do not tolerate bending if only one element thick. If bending is expected on a part then more than one layer of solid elements should be used. Alternatively fully integrated solid elements can be used, where each element has eight integration points [85].

The rigid parts of the frame, seat and ballast were attached by using the 'CONSTRAINED_RIGID_BODIES' relationship in LS-Dyna. This connects the rigids bodies together and treats them as one body.

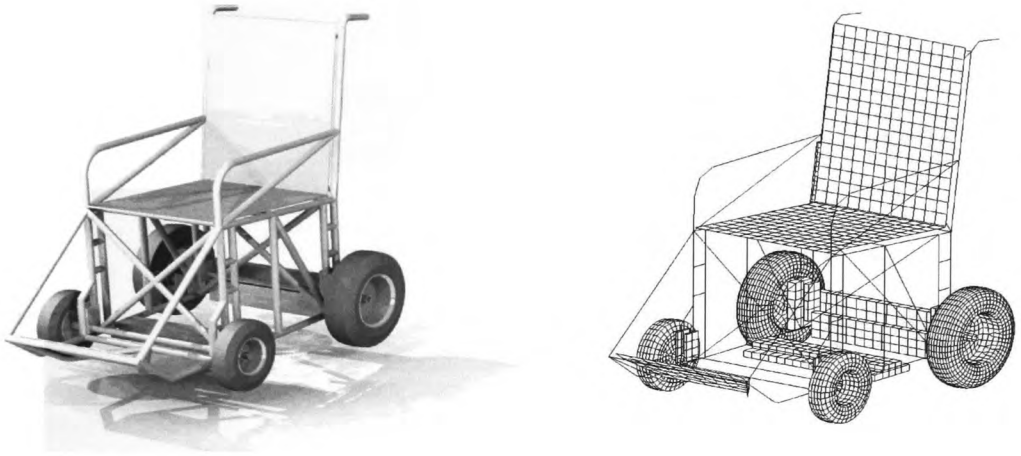

Figure 4.4.1 showing the CAD (left) and FEA (right) models of the surrogate 10542 wheelchair

Mass and centre of gravity checks

The mass and centre of gravity of the surrogate wheelchair, as specified in ISO 10542-1 is 85kg +/-1kg at a position of 142mm+/-25mm forward of the rear axle and 126mm+/- above the rear axle. It was important that the computer model of the surrogate matches that of the physical surrogate wheelchair if it was to respond in the same way. The geometry of the surrogate wheelchair and the densities of the materials used were matched as close as possible but further manipulation of the model was required in order to achieve the tolerances given in ISO 10542-1 [1] and illustrated in Figure 4.4.2. This was made easier in the ISO 10542 surrogate wheelchair model as the ballast steel blocks attached to the bottom of the wheelchair could be adjusted slightly to achieve the correct mass and centre of gravity. An alternate method, available in the pre-processing software, distributes mass through the specified parts of the model until the required mass and centre of gravity are achieved [87].

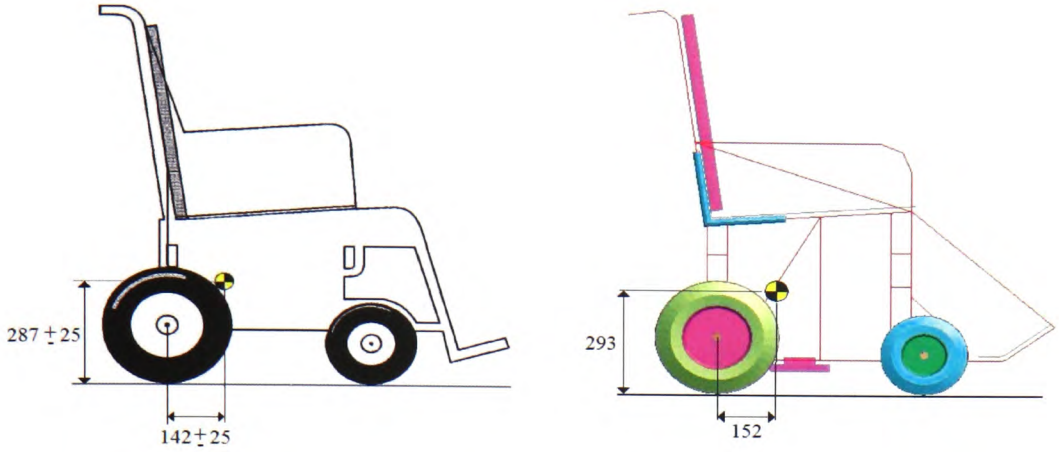

Figure 4.4.2 showing the centre of gravity of the ISO 10542 standard surrogate wheelchair (left) [1] as compared with the ISO 10542 computer model (right). All dimensions in mm

4.4.2 Construction of ISO 16840 surrogate wheelchair frame

The reason for modelling the surrogate ISO 16840, shown in Figure 4.4.3, wheelchair was for further validation of the modelling process since data already existed from tests previously carried out by the RE Unit. These tests were conducted to establish the crashworthiness of the Rookwood Universal Interface Kit (RUIK)[7], illustrated in Figure 4.4.4, which was used to attach the seat-pan to the wheelchair frame.

The ISO 16840 surrogate wheelchair was designed for crash testing aftermarket wheelchair seats. Like the ISO 10542 surrogate wheelchair the ISO 16840 surrogate is built to endure repeated crash tests but does not have a seat. Instead it has two parallel bars onto which different seating systems can be mounted. A further difference of the ISO 16840 surrogate is the use of aluminium bars to attach the front wheels to the main steel frame. These bars deform in the crash test, absorbing energy and in doing so increase the life of the main steel chassis. When creating the FEA model of the ISO 16840 surrogate wheelchair these aluminium bars were modelled using solid elements to capture the correct deformation behaviour under load.

---

[7] Roach G.R. International patent application filed 11.02.04 "Wheelchair and seat interface apparatus" International Publication No. WO/2004/071364 published on 26.08.04 priority data: 0303069.9 GB filed 11.02.03 & 0303132.5 GB filed 12.02.2003.

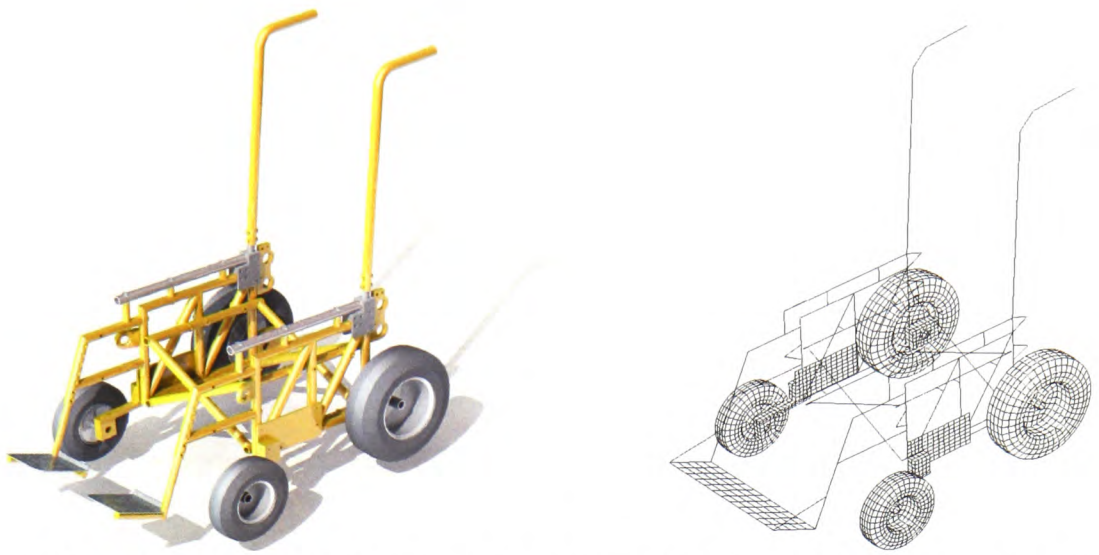

Figure 4.4.3 showing the CAD (left) and the FEA (right) models of the ISO 16840 surrogate wheelchair

The setup of the sled, tie-downs, occupant and seatbelt were the same as described for the ISO 10542 surrogate wheelchair setup.

4.4.3 Modelling of RUIK clamping system

The RUIK consists of a tubular frame that attaches to the wheelchair chassis and a clamping unit that attaches to the underside of the seat-pan, see Figure 4.4.4. From the physical crash test to assess the crashworthiness of the RUIK, conducted by the RE Unit, it was observed that only the tubular frame part deformed. This part was therefore modelled using deformable shell elements and the clamping unit modelled with rigid solid elements.

The idea behind the RUIK was to be able to attach any seat to any wheelchair chassis. The female part of the RUIK, as shown in Figure 4.4.4, had telescopic arms that adjust to the size of the wheelchair chassis. The FEA model was constructed so it could also be adjusted without having to be re-meshed. This was achieved by using a Tied-Contact in LS-Dyna (CONTACT TIED SHELL EDGE TO SURFACE BEAM OFFSET) relationship between the telescoping arms and the main body [85]. The Tied-Contact, in this instance, worked by finding the nodes on the shell element's

surface of the RUIK that 'contacted' nodes on the telescopic arms according to the desired contact tolerance. The 'BEAM-OFFSET' function within the contact definition treats the penetrating nodes as if they are connected by beam elements, allowing moments to be transferred between the surfaces. The Tied-Contact is checked at the beginning of each simulation so the telescopic arms can be adjusted without having to reapply the contact.

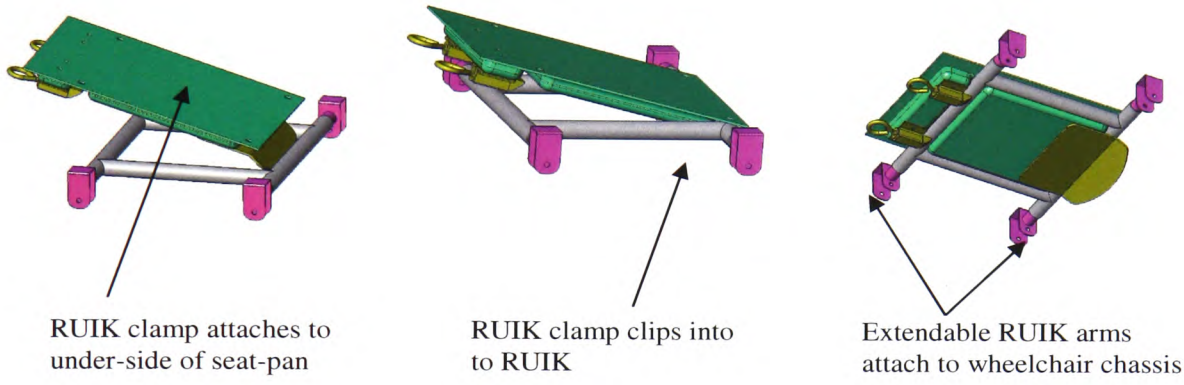

Figure 4.4.4 showing the RUIK and RUIK clamp arrangement, which is subject to Design copyright Cardiff & Vale NHS Trust

4.4.4 Construction of Spectra Plus wheelchair model

The Invacare Spectra Plus wheelchair is the most common electric wheelchair chassis issued by the RE Unit. The main frame consists of a bent circular cross section tube, on to which the motor and gear box housings (for the rear wheels) and the front casters, are attached, see Figure 4.4.5. Two lugs on the main tube connect to the rear of the square section tube seat mount. The front of the seat mount is attached to the main tube with an actuator that controls the angle of the seat mount by rotating about the rear lugs. Seat angle adjustment is used for medical requirements of some occupants and also for occupant comfort.

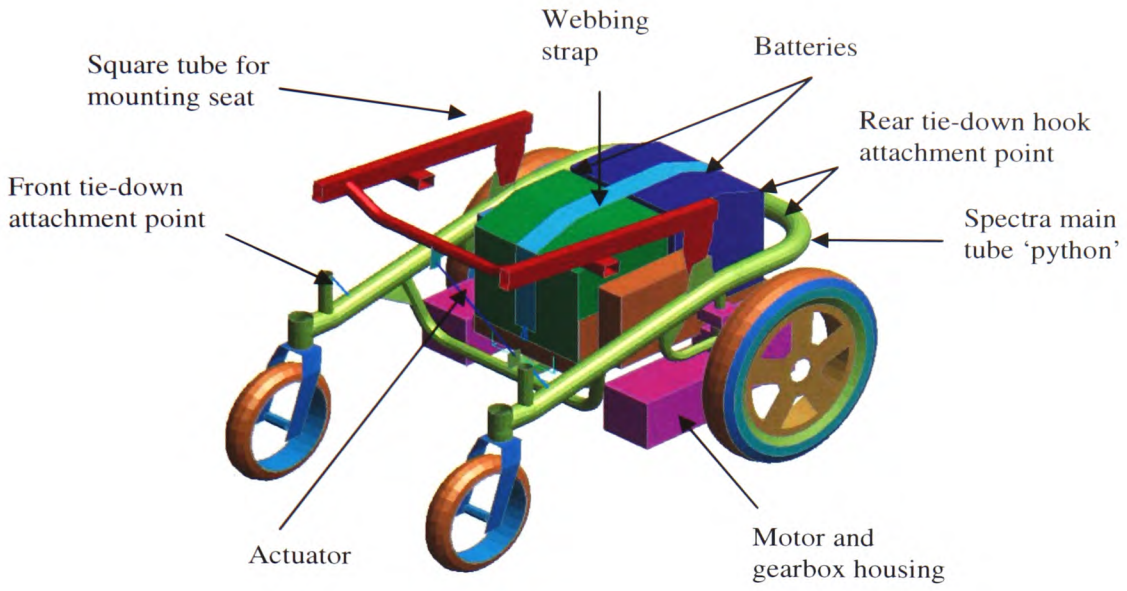

Figure 4.4.5 showing the FE model of the Invacare Spectra Plus chassis

The two batteries for the motors and actuator were positioned inside the main frame in a wire cradle. The motor and actuator controllers were mounted on to each side of this cradle. The batteries were held in position by a webbing strap. It was important to model the restraint of the batteries accurately as part of the ISO 7176-19 crash standard requires that the batteries do not move outside of the wheelchair footprint during a frontal crash. The batteries and controllers were modelled as rigid with the appropriate mass. There were dedicated tie-down mounting points at the front of each arm of the main tube. The rear tie-down hooks attached directly to the rear of the main tube. The Spectra frame was modelled in far more detail than the surrogate wheelchair, due to its greater complexity, and consisted mainly of shell elements. The batteries, motor and gear box houses and controllers were modelled as rigid solid elements and given mass and centres of gravity from measurement. The actuator was modelled as a simple beam element for simplification. In reality the actuator may provide a certain amount of damping in a crash but it was decided to assume it to be rigid to model the worse case scenario and for simplification. The circular cross section of the main Spectra tube, shown as green in Figure 4.4.5, required a fine mesh at points where other circular sections joined.

The main Spectra frame was found to deform excessively during initial simulation runs. The cause of the premature failure was found to be inadequate mesh density where the tubes supporting the motor housing joined onto the main tube. Increasing the mesh density around the join allowed the forces to be correctly transmitted to the main tube without excessive deformation, see Figure 4.4.6.

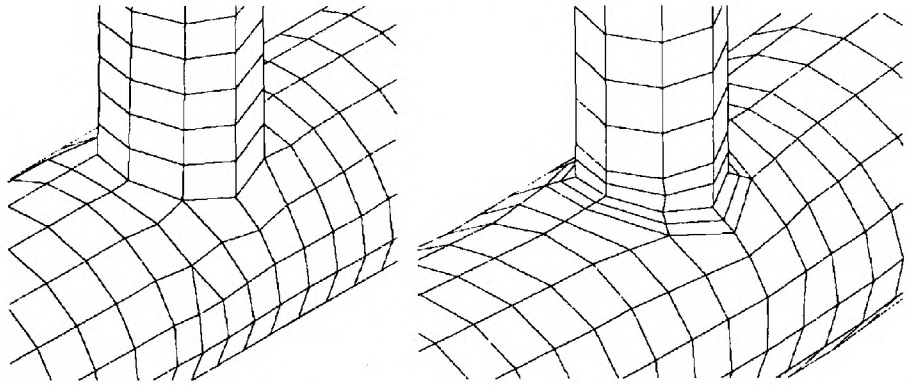

Figure 4.4.6 showing the increased tube mesh density at circular tube joints.

The seat-pan was attached to the Spectra chassis with the RUIK. The rest of the setup was as previously described for the surrogate ISO 10542 wheelchair. The complete Spectra wheelchair, seat-pan and occupant is shown in Figure 4.4.7.

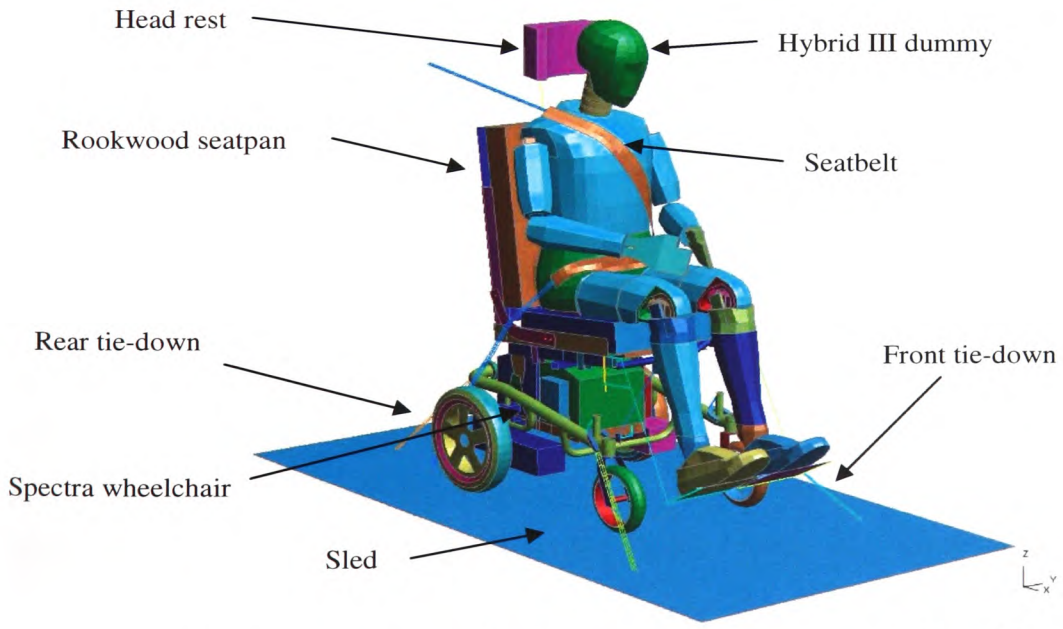

Figure 4.4.7 showing the complete Spectra, seat-pan, occupant and seatbelt setup

Many of the welded and rigidly attached components were joined to each other by using LS-Dyna's 'Tied_Contact' relationship. This form of join works using the penalty method in the same way as contact surfaces. Two surfaces are defined and the distance between them checked. Any nodes that are found to overlap are 'bonded' together. In the case of shell elements the thickness of the shells are taken into account. The surfaces can therefore either share a midplane or have a physical distance between them. LS-Dyna requires that the type of tied contact be defined, i.e. either midplane or separated. This method of joining parts is useful as the joint is maintained if either part has to be remeshed. A limitation of this joining method, that was discovered, was that one part will not allow other parts to be joined on opposite sides. When the joint is formed the shell normals are automatically adjusted so that the master and slave sides point towards each other. If another part is added to the opposite side of the master part the normals of the master side cannot be adjusted to face the new slave part as they are already facing the first slave part.

4.4.5 Tie-Down position for Spectra chair

The rear and front tie-downs were positioned in accordance with ISO 7176-19. The rear tie-downs had a length of 490mm and were at an angle of 39.5^0 to the horizontal. The distance apart of the anchor points on the sled were 330mm. The front tie-downs had a length of 509mm at an angle of 33.9^0 to the horizontal. The distance apart of the anchor points on the sled were 735mm.

The tie-downs were modelled with a simplified hook attached to the wheelchair frame. The hook itself is of little interest as it is tested to ISO 10542-1 by the manufacturer and its energy absorption by deformation has previously been taken care of in the tie-down material experiment where the tie-down webbing and hook were tested. The hook is included to simulate the loading on the frame only. Also, unlike the surrogate wheelchairs, there is no specific attachment point for the rear tie-down hooks on the Spectra wheelchair, as previously mentioned. The rear tie-down hooks are therefore free to slide along the main tube.

4.5 Further Modelling Considerations

In this Section the modelling requirements of the different crash scenarios will be discussed. These include the life support attached to the wheelchair, producing the pitching effect in a frontal crash and creating a skewed impact.

4.5.1 Modelling life support equipment

Apart from the seat sizes and cushion geometries another parameter that makes the RE Unit's wheelchair systems unique is the ancillary equipment attached to them. The example made available to study by Rookwood Hospital had an oxygen cylinder and suction pump attached behind the seat between the two push arms, see Figure 4.5.1.

Figure 4.5.1 showing the attachment of an oxygen cylinder (left) and a suction pump (right) to the back of a Spectra wheelchair

The equipment and attaching frame were measured, weighed and their centre of gravities found. A CAD model of the assembly was drawn and from this a simplified finite element mesh was created. The combination of life support equipment depends on the patients particular medical needs. The oxygen cylinder can be used to supply supplementary oxygen or used in combination with a ventilator unit. The ventilators used are positive pressure ventilators (PPV's) that introduce oxygen to the lungs via an

endotracheal tube. The suction unit removes fluid build up from the lungs and is a manual device operated by the carer, although in a very few instances they can be operated by the patient. A range of typical life support equipment carried on a wheelchair was modelled in CAD and shown in Figure 4.5.2.

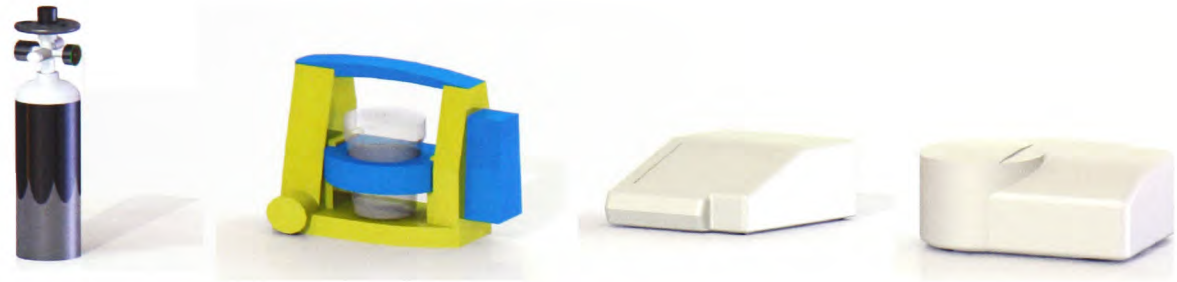

Figure 4.5.2 showing a selection of life support equipment; from left to right: Oxygen cylinder, Suction pump, two different types of ventilator

It is beyond the scope of this study to examine the effects of crash forces on life support equipment and possible harm that could be caused to a patient using such a system. The current range of equipment used in conjunction with wheelchairs is described by the manufactures as portable, meaning that they can be used when moving the patient short distances, i.e. from one ward to another. The equipment was not necessarily designed to be used for extended periods in a wheelchair environment and certainly not built with crash safety in mind. The life support equipment will therefore be treated as simple lumped mass, as illustrated in Figure 4.5.3.

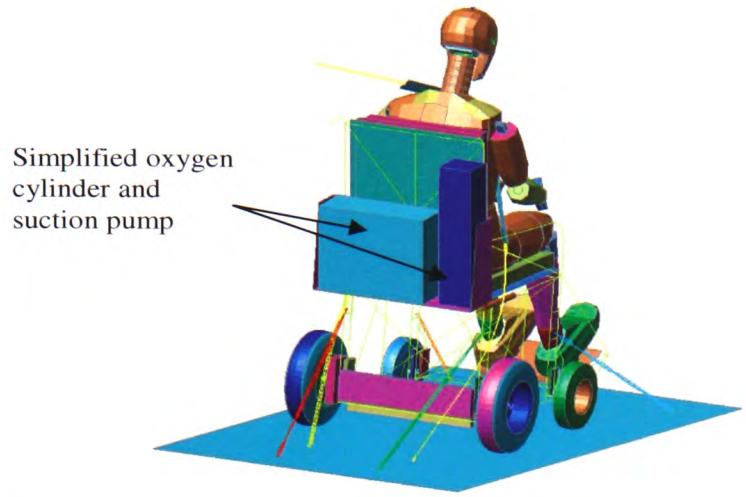

Figure 4.5.3 showing the simplified model of the oxygen cylinder and suction pump on the bracket mounted between the two push handles

4.5.2 Vehicular Pitching

The current ISO standards for wheelchair safety specify that the crashworthiness of the wheelchairs must be assessed by the use of sled testing. Sled testing is also the method used for assessing wheelchair crash safety in the available literature. As Warner *et al.* [45] point out; sled tests are not a true representation of the behaviour of a vehicle chassis in a crash. The sled is fixed in the horizontal plane and an acceleration applied to it, as previously discussed. In an actual frontal crash the vehicle pitches forward due to compression of the front tyres and suspension as well as the deformation of the front of the vehicle. From studies of motor vehicle crash test literature it was found that the inclusion of pitching tended to increase the injury to the seated occupants. No study, as far as the author is aware, has been conducted to investigate the effects of pitching on wheelchair's and their occupants.

In order to study the pitching effect on wheelchairs transported in motor vehicles it was first necessary to find the variation in the pitch angle with time for a typical vehicle in a frontal crash. Automotive companies are understandably reluctant to release detailed crash data on their vehicles so it was decided to conduct a simulation

of a standard 48km/hr frontal vehicle impact and measure the vehicle pitch angle against time.

A model of the Chevrolet C2500 Pickup Truck was downloaded from the National Crash Analysis Centre [117]. The FEA model consists of 10,500 elements allowing it to be run on a desktop PC. Vehicle models more closely resembling those usually associated with wheelchair transport were available but contained greater detail and consequently far more elements, making them impractical to run on the computer resources available.

The truck model was setup to impact into a rigid wall at 48km/hr by applying an initial translational velocity to the truck body and an angular velocity to the wheels. The screen shots in Figure 4.5.4 show the truck as it impacted into the rigid barrier where the pitching angle of the truck can be clearly seen in the last two frames.

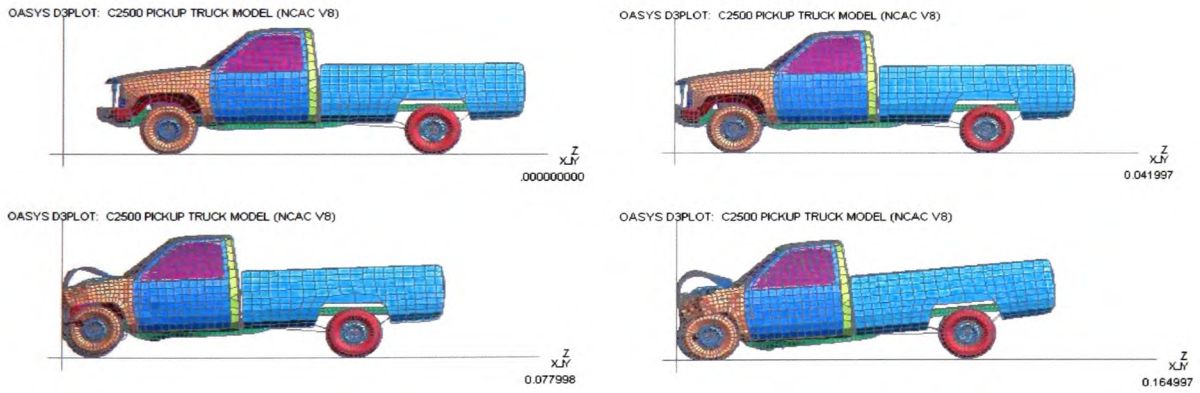

Figure 4.5.4 showing screenshots of the truck impacting a rigid wall at 48km/hr

Four nodes at each corner of the rear of the truck were assigned to record the displacement and acceleration history of the truck chassis. These 4 nodes represented each corner of the area where the wheelchair would be attached and would go on to describe the area of the sled. The nodal displacements were plotted and, for simplification purposes, the average of the two front and two rear nodal displacements were taken to eliminate the slight yaw effect from the small rotation about the X-axis.

The Z-displacement of the nodes was used to find the rotation (θ) about the Y-axis of the rear of the truck per second, using:

$$\theta / s = Tan\left(\frac{z_R(t) - z_F(t)}{d_N}\right)$$

Where $z_R(t)$ is the displacement of the rear chassis nodes against time, $z_F(t)$ is the displacement of the front chassis nodes against time and d_N is the distance between the front and rear nodes. The rotation of the truck chassis against time was plotted, as shown in Figure 4.5.5.

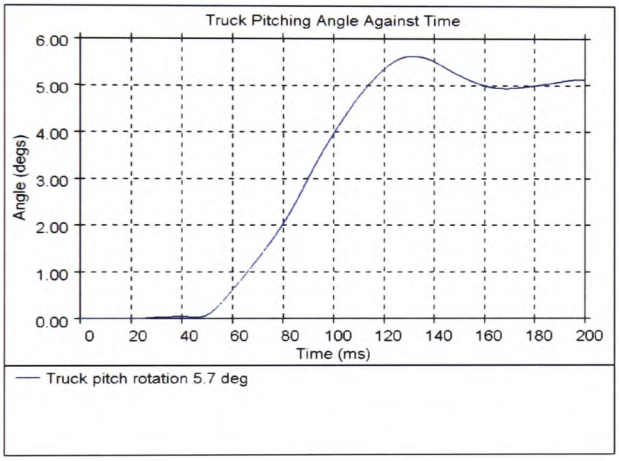

Figure 4.5.5 showing the rotation of the truck chassis

The horizontal acceleration of the truck chassis was also recorded and compared to the 20g crash pulse recorded from the physical wheelchair crash tests and that used in the simulated wheelchair crash tests. The general shape of the two acceleration graphs agreed well, as shown in Figure 4.5.6, although a higher peak acceleration of 32.2g was recorded for the truck chassis as compared to the peak acceleration of 23.1g for the practical crash pulse.

To aid comparison between simulated sled tests, with and without pitching, it was decided to use the 20g crash pulse from the practical experiments as the horizontal

acceleration and apply the recorded chassis rotation of the truck to simulate the pitching effect. This was deemed to be a reasonable method as the horizontal crash pulse of a vehicle will depend on the energy absorbing abilities of its crumple zone and is therefore largely independent of the rotation of the vehicle chassis.

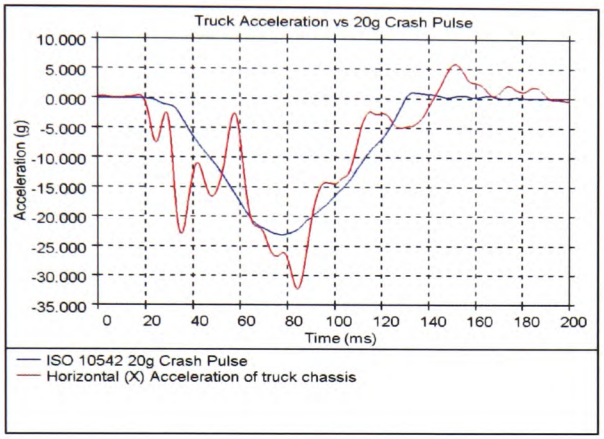

Figure 4.5.6 showing the horizontal acceleration of the truck chassis as compared with the ISO 10542-1 20g crash pulse

The vertical acceleration of the 4 nodes was also recorded. The rear axle of the truck acted as a pivot which is why the maximum peak of the rear of the chassis in Figure 4.5.7 was positive and the peak of the front of the chassis at the same time was negative at 62ms.

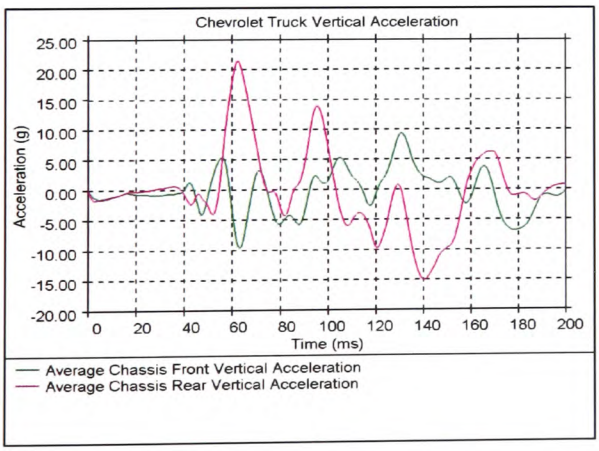

Figure 4.5.7 showing the Vertical Acceleration at the front and rear of the truck chassis

From discussion with personnel at Millbrook Proving Ground [108] the pitching angle can be far greater in other vehicles. The Ford Explorer, for instance, has been recorded to pitch by up to 12.5^0 [108], see Figure 4.5.8. It was decided to include this higher pitching angle in the simulations to help examine the effects that varying the degree of pitch had on the wheelchair and occupant. As the rate of pitching for the Ford Explorer was unknown the pitching curve for the Chevrolet Truck was scaled up in proportion to a maximum angle of 12.5 degrees.

Figure 4.5.8 showing the pitching during a frontal crash of a Ford Explorer at 55.6km/hr, [118]

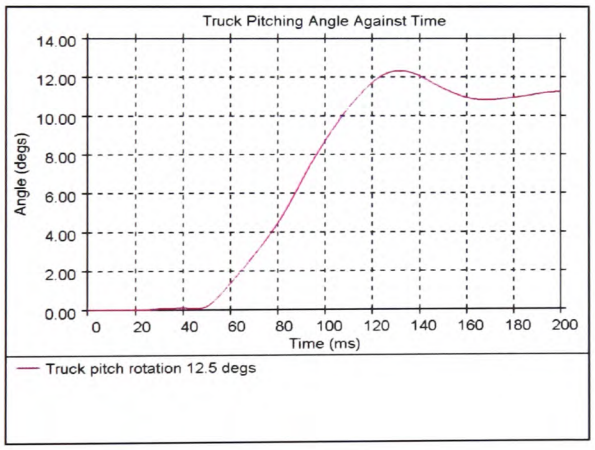

Figure 4.5.9 showing the pitch angle of the Chevrolet truck scaled up to 12.5^0 to match that of the Ford Explorer

The pitching of the truck was applied to the sled by using the 'BOUNDARY_PRESCRIBED_MOTION' function in LS-Dyna. The graphs in Figure 4.5.5 and Figure 4.5.9 of radians against time were used directly as a means to rotate the rigid body of the sled. A secondary prescribed motion was used to apply the

horizontal acceleration. All prescribed motions for a rigid body are applied at its centre of mass so the centre of mass of the sled was therefore the axis of rotation.

4.5.3 Skewed Impact

Skewed wheelchair impacts have had very little attention in the literature reviewed and no computer modelling undertaken, as far as the author is aware. All crash test work undertaken, and especially that in the field of wheelchair safety, is predominately head-on frontal collision based. This is indeed the most common cause of serious injury [50, 52, 67] but should by no means be focussed on exclusively as the only way of improving crash safety. Indeed it could be argued that all but a few crash scenarios have some lateral component to them.

A skewed impact angle of 60^0 from the longitudinal mid-axis of the vehicle was chosen as this has been found to be the most common angle of skewed impact [50]. An assumption made when looking at the skewed impacts was that they acted through the centre of gravity of the wheelchair and occupant. In reality, the position that the lateral impact occurs on the transporting vehicle, relative to the wheelchair and occupant, will alter the dynamics of the wheelchair as the vehicle will tend to rotate about the point of impact. For example, if a wheelchair and occupant were positioned in the centre of a vehicle the rotation they would experience depends on whether the vehicle was struck laterally in front or behind the location of the wheelchair.

The same 20g frontal crash pulse was used in the skewed simulations and was applied along a vector directed through the wheelchair and occupant's centre of gravity in a direction 240^0 to the front of the vehicle. As with the frontal and rear sled test simulations the skewed simulations accelerated the wheelchair and occupant away from the impact point.

The different levels of protection that a left or right shoulder 3-point seatbelt gave the wheelchair occupant were investigated. The fitting algorithm used to fit the seatbelt over the occupant, as described previously, generates a spline between prescribed

points, which is then moved closer to the occupant until a desired level of contact has been achieved. As the wheelchair was symmetrical it was found that reflecting the skewed impact direction was easier than re-applying the seatbelt over the opposite shoulder. This had the added advantage of ensuring the path and fit of the seatbelt was identical in both cases.

Aerial shots of the Spectra wheelchair and dummy in Figure 4.5.10 show the crash pulse direction vector at 240^0 representing a 60^0 skewed impact towards the dummy's right shoulder and a crash pulse vector at 120^0 representing a 300^0 skewed impact towards the dummy's left shoulder.

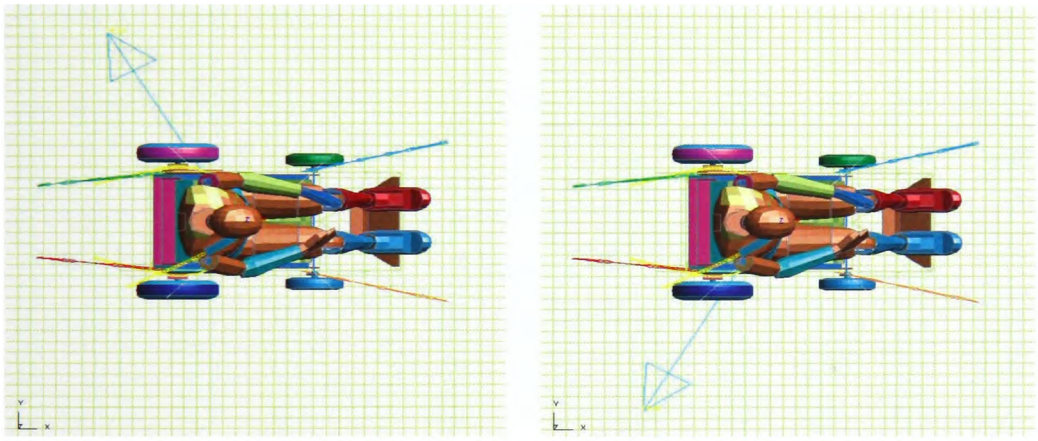

Figure 4.5.10 showing the lateral vectors applied to the sled. The left image represents a 60^0 lateral impact on the right hand side of the dummy and the image on the right represents a 300^0 lateral impact on the left hand side of the dummy

4.6 Modelling summary

The computer models of the wheelchairs described herein underwent many simulation runs to get them working correctly. This proved to be an invaluable learning process as well as creating a robust representation of the wheelchairs that required little modification to examine a host of different crash scenarios. The next Chapter will look at the frontal and rear ISO 10542 surrogate wheelchair models and compare them with emprical data obtained from physical crash testing. The ISO 16840 surrogate wheelchair computer model will also be compared to video footage of the equivalent physical crash test.

Chapter 5 - Validation

This Chapter examines the behaviour of the frontal and rear crash tests, performed at Millbrook Proving Ground in accordance with ISO 10542-1, using the ISO 10542 surrogate wheelchair and Hybrid II dummy and compares them with the equivalent simulated computer runs. The comparison will show that the simulated model is capable of predicting the behaviour of both the wheelchair and occupant in a frontal and rear sled crash test. A qualitative comparison of a frontal ISO 16840-4 [39] test with the RUIK clamp against an equivalent simulation is also discussed.

The process of confirming that the computer representation of a physical event is sound comprises of two parts; Verification and Validation. The American Society of Mechanical Engineers produced an informative guide [119] for both verification and validation and clearly make a distinction between the two. Verification is the determination that the FE software used to solve the finite element model (in this case LS-Dyna) accurately computes the mathematics that the model describes. Validation, on the other hand, is the process of ensuring that the FE model created reliably predicts the behaviour of the physical system being investigated.

The most common method of software verification is to compare a number of standard simulation models with hand calculated predictions. This is often a useful way to become more familiar with the inner workings of the software and instil confidence in its use. Due to LS-Dyna's wide use in industry and countless publications its verification will be confidently assumed [61-63, 73, 74, 76, 78, 120-125]. The validation of the various models herein, however, must be demonstrated.

There is no industrial standard on crash model validation so the decision of whether or not a simulated model faithfully reproduces the behaviour of its physical equivalent is up to the judgement of the engineer [53]. Most crash models are designed to allow the engineer to analyse how changes in the design parameters will affect various parts of

its performance in a crash, without having to perform expensive destructive testing. Put another way, the purpose of a crash model, or any simulation model for that matter, is to predict the behaviour of a system where no current data is available. These analyses are comparative in nature, with the simulation model first being compared to a standard physical crash test and then to another simulation incorporating a certain design change. Zaouk *et al.* [53, 88] point out that the information required from the model should be born in mind when deciding whether or not a model is sufficiently validated. They also warn against excessive 'tweaking' to get the simulated model to match the physical model. These are both very pertinent points, especially in crash test validation where the number of variables that may affect the results are large.

The errors and repeatability of the physical crash test should be kept in mind when validating. From discussions with the engineers at Millbrook Proving Ground it is common for identical crash or sled tests to produce different results [108]. If a simulation is 'tweaked' to one particular physical crash test it may be to the detriment of its comparability with other similar tests. It is therefore far better to observe the trends between the physical and simulated results and, where disparities occur, check for errors in the model or understand the cause of such errors. Ideally a number of identical physical crash tests would have been conducted and the average results used to validate against a simulated model but due to the high cost this was impractical.

Again, the acceptable error in the validation results must be judged on the results required. Kirkpatrick *et al.* [93], in their study of railroad passenger cars, describe their accelerometer readings as being 'close' and showing 'general agreement' with the equivalent physical test results. In their paper on crash simulations of wheelchair occupants, Kang *et al.* [47] use the percentage difference between peak values to validate their model. In the authors opinion this method is fine but does not indicate if the peaks occurred at the same time or whether the shape of the acceleration or displacement curves had a similar trend. Moumni *et al.* [126] went further and compared peak values at specific time periods with each other.

Zaouk *et al.* [53, 88] recommended performing part validation and then full scale validation. The part level validation, as discussed in Chapter 3, ensures that individual components behave correctly before being assembled into the complete model. Williams *et al.* [92] dispensed with full scale validation and instead relied purely on just the part validation. This would seem to be an unreliable method as the loads, boundary conditions and interaction between different parts, when assembled together, could be considerably different to when tested at component level.

The technique of validating computer simulations against physical tests using only video footage has been used in several papers [10, 49, 92, 127], where snapshots at a number of time intervals were compared. The current wheelchair crashworthiness standards require only limited information about the dummy and wheelchair, namely that the maximum displacements of the dummy and wheelchair remain in a specified displacement envelope [1, 3, 39]. It was decided, however, that in the interest of achieving a robust validation model that a comprehensive range of data between the physical and simulated model should be compared. In actual tests carried out at Millbrook Proving Grounds, accelerometers were placed in the dummy's head, to quantify head acceleration, and load cells attached to the rear tie-downs and upper shoulder seatbelt to record forces developing in these components. The readings from these, along with head, P-point and knee displacements, were compared with the equivalent readings from the simulation model.

The data recorded from the practical tests was reported by Millbrook Proving Ground as being filtered by a C1000 filter, in line with recommendations in ISO 10542-1. When the data from Millbrook was later analysed, however, it was found that frequencies in the order of 1000Hz and above were not present. Also when comparing the simulated data, filtered to C1000, with the practical data, reported as being filtered to C1000, the difference between the two signals was considerable. The simulated data was run through a C60 filter instead that produced a far better match with the practical results and so was used for all results [87, 106].

The frontal 20g crash tests, in accordance with ISO 10542-1, will be considered first. The snapshots in Figure 5.1.1 compare video footage of the physical crash test, on the left, with the computer simulated crash test, on the right. The video snapshots, used for visual comparison, were taken at meaningful events, such as maximum head excursion or full tyre compression, rather than at fixed time intervals. This made the images more meaningful and easier to compare and analyse.

5.1 Frontal crash validation

Practical 20g Frontal impact	Time (ms)	Simulated 20g frontal impact
	0	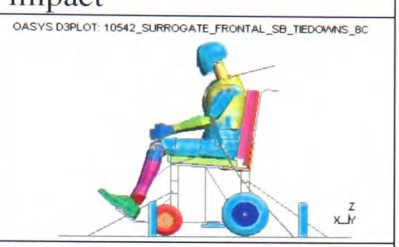
	88	
	100	
	144	
	174	
	200	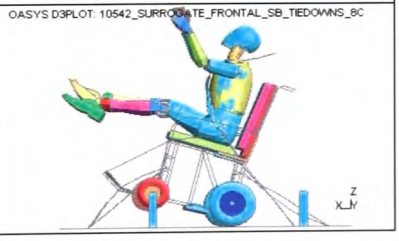

Figure 5.1.1 showing the comparison between the physical and simulated 20g frontal crash test using the ISO 140542 surrogate wheelchair

The video stills in Figure 5.1.1 show good correlation between both the wheelchair and occupant excursion. The large green webbing strap, which can be seen in the video stills of the physical crash test, was a standard precaution to prevent the dummy from 'flying off' in the event of seatbelt or tie-down failure.

The sled test at Millbrook Proving Grounds, as discussed in Chapter 4, works by assuming that the test item, at constant velocity before the impact, will be in equilibrium just as if it were stationary. The sled is accelerated from stationary to simulate the deceleration of a vehicle from constant velocity resulting from an impact. It therefore makes sense to describe the motion of the wheelchair and occupant with regards to the sled test as opposed to the deceleration crash event that it represents. As the sled accelerated down the track (from left to right in the screen shots) it slid from underneath the wheelchair, whose wheels were free to rotate. The tension in the rear tie-downs increased, forcing the wheelchair downwards, due to the angle of the tie-downs, until the rear wheels fully compressed at 88ms (second row of Figure 5.1.1). During this time the wheelchair slid from underneath the dummy until the seatbelt came tight across the dummy's chest (third row of Figure 5.1.1). The energy stored in the compressed rear wheels and rear tie-downs was released causing the wheelchair to move and rotate backwards (in the same direction as the sled motion) while the dummy's head and limbs continued to move in the opposite direction, until the dummy's maximum head horizontal motion occurred at 120ms (third and forth rows of Figure 5.1.1). The stored energy in the seatbelt and dummy's chest forced the dummy backwards as the front tie-downs came tight, at 164ms (forth and fifth rows of Figure 5.1.1), causing the wheelchair to rotate forwards and the front tyres to compress. The energy stored from the compressed front tyres and extension of the front tie-downs, as well as the dummy's back contacting the seat back, rotated the wheelchair rearwards again, as shown in Figure 5.1.1 at 174ms and 200ms.

The dummy used in the physical tests was a Hybrid II dummy whereas the dummy used in the simulation was a Hybrid III dummy. The most striking difference between the two is the neck angle and the head position, see Figure 5.1.2. The Hybrid II dummy

is much more upright whereas the Hybrid III adopts a more typical 'slouch', seen in most human occupants, especially when holding a steering wheel in a car, which these dummies were primarily designed for.

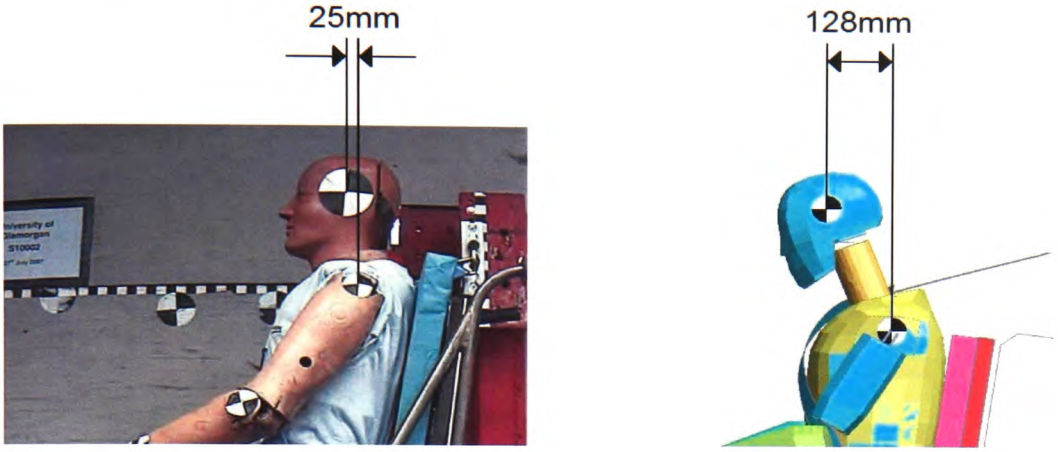

Figure 5.1.2 showing the Hybrid II dummy used in the practical experiments (left) and the Hybrid III dummy used in the computer simulations (right)

A second considerable difference, observed from the screenshots in Figure 5.1.1, is that the simulation becomes out of phase with the practical results at around 144ms. The cause of this was attributed to a lack of damping in the model of the wheelchair tyres and slippage of the rear tie-downs in the practical experiment, which was not accounted for in the simulation. This also ties in with the hysteretic loading of the pneumatic tyres as observed during the tyre compression experiment in Chapter 3. The tyres used a simple constant volume-pressure relationship to describe the pressure in the tyre that did not take into account any energy loss from heating of the tyre or air leakage during full tyre compression. Such a simplification is common place in many automotive crash models, where a vehicle's mass is far greater and normally has suspension present [117]. A more complex air pressure model for the wheelchair tyres may improve the rebound effect. The modelling simplification made was to assume that the loading and unloading curves of the tyre were the same.

From the graphs it can be seen that the general trends of displacement against time are similar for both the practical and simulated tests. Differences between some of the graphs do exist and the cause of these will be discussed below.

The head horizontal excursion in the model had a peak value of 250mm as compared to 335mm recorded in practice. The peak P-point horizontal excursion from the simulation, of 89mm, was considerably closer to the practical value of 98mm, which would indicate that the considerable difference in the head horizontal displacements was independent of the motion of the wheelchair.

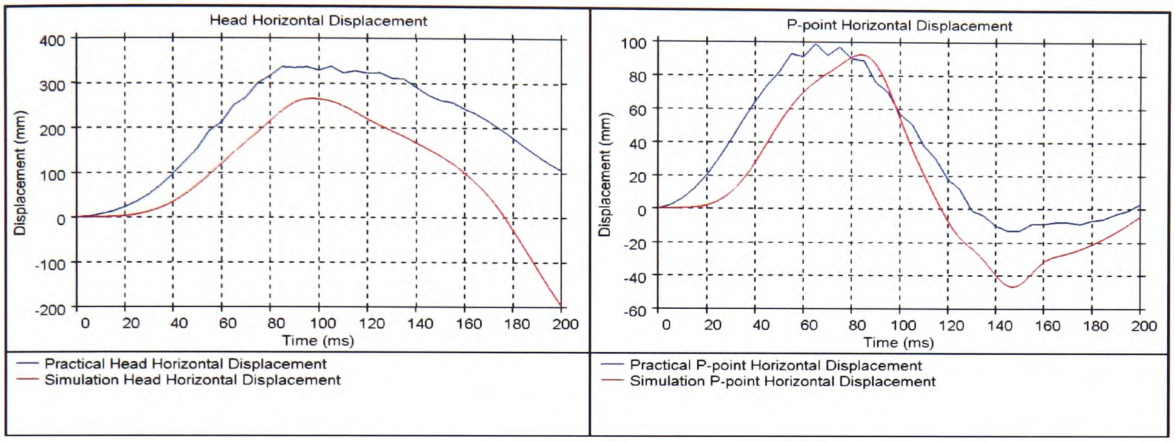

Figure 5.1.3 showing the Head and P-point horizontal displacement for the physical and simulated frontal crash test

The significant difference in head horizontal displacement, as illustrated in Figure 5.1.3, can be attributed to the difference in the Hybrid II and Hybrid III dummies geometry. The horizontal shoulder to head distance for the Hybrid II dummy was measured as 25mm compared to 128mm for the Hybrid III dummy, this can be seen in Figure 5.1.2. The difference in shoulder to head distance of 103mm meant that the simulated Hybrid III dummy's head had less distance to travel before reaching the maximum horizontal position when compared to the Hybrid II dummy, from the practical results.

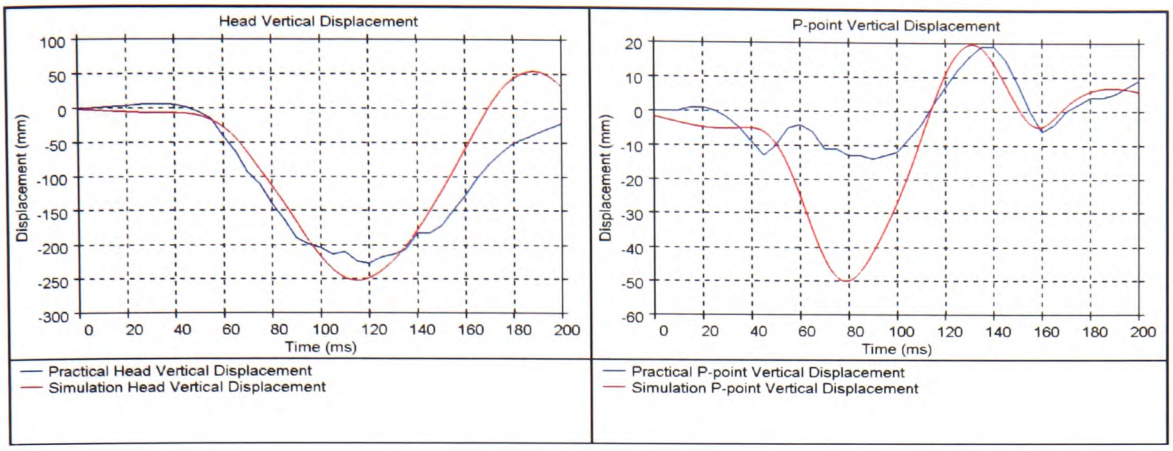

Figure 5.1.4 showing the vertical displacement of the Head and P-point of both the physical test and model

The vertical head displacement was very close to that recorded in practice despite a very large difference in P-point vertical displacement between simulation and practical results, as can be seen in Figure 5.1.4. Although the two minimum peaks of the vertical P-point displacement differ considerably the trends and maximum peak are very similar. The component controlling the vertical movement of the wheelchair was the rear wheels. The large negative peak, observed in the simulated vertical P-point displacement was -48mm and occurred at 80ms, at the point of full rear tyre compression. The minimum value recorded for the practical test, at this point, was -14mm, despite the screenshots, in Figure 5.1.1 at 80ms, showing the rear wheels of both the practical and simulated wheelchairs fully compressed.

Both simulated and practical rear tyres were observed to 'bottom out' with the practical rear tyres being compressed by 25mm and the simulation tyres compressed by 64mm. It is proposed that this difference in compression was due to the surrogate tyres having a very thick solid rubber tread. The exact thickness of the tread could not be determined without cutting into the tyre. Due to this lack of dimensional data the cross section thickness of the Spectra wheelchair wheels was used when modelling the surrogate wheels. Although a significant increase in tyre tread thickness may not account for all of the difference between the theoretical and practical vertical P-point values it would go some way to explain the difference and is likely to account for the

noisy head vertical acceleration, as compared to the practical results, from the lack of cushioning that a thick rubber tread would provide.

This hypothesis was tested by increasing the tyre tread thickness from 6mm to 20mm. The nature in which the tyre tread was modelled was also altered. The modified model maintained the shell elements at the tyre wall but used two layers of solid elements to describe the tyre tread. A diagram of the cross section of the altered tyre model is shown in Figure 5.1.5, where the increased thickness of the tyre tread can be seen. The complete model was re-run and a reduction in the vertical P-point was observed, see Figure 5.1.6. The increased tyre tread thickness had little effect on most of the measurements, with the notable exception of the head vertical acceleration, which decreased due to the damping effects that the thick rubber tread had when the tyre 'bottomed out', Figure 5.1.6. The previous simulation, with the thinner tyre wall, matched the practical head vertical acceleration very closely. It was suspected that the stiffness of the physical tyre's rubber tread was stiffer (possibly due to wire reinforcement or the use of a different rubber compound), producing less cushioning and resulting in a higher acceleration on the dummy's head.

It may be observed that the compression of the wheels is larger than the vertical displacement of the P-points. This was due to the P-point being forward of the rear wheel axle. At full rear wheel compression the front wheels of the wheelchair rose up, reducing the vertical displacement of the P-point with respect to the rear wheel axle. This rotation was not as pronounced in the model, further contributing to the large disparity between P-point values.

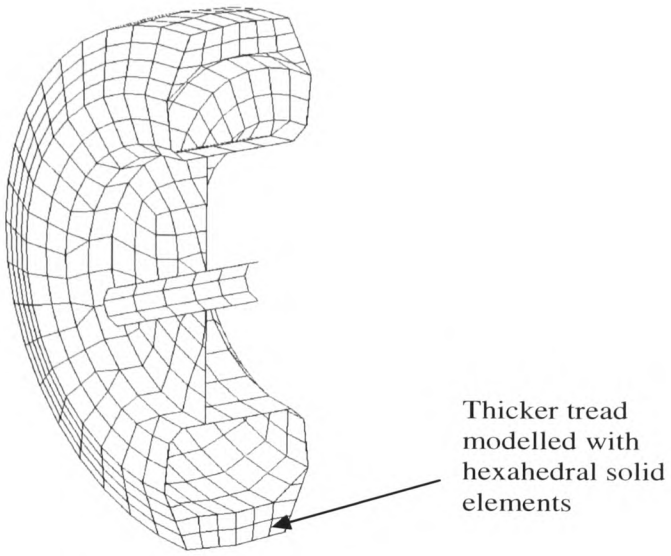

Figure 5.1.5 showing the modified tyre wall of the surrogate wheelchair rear wheel

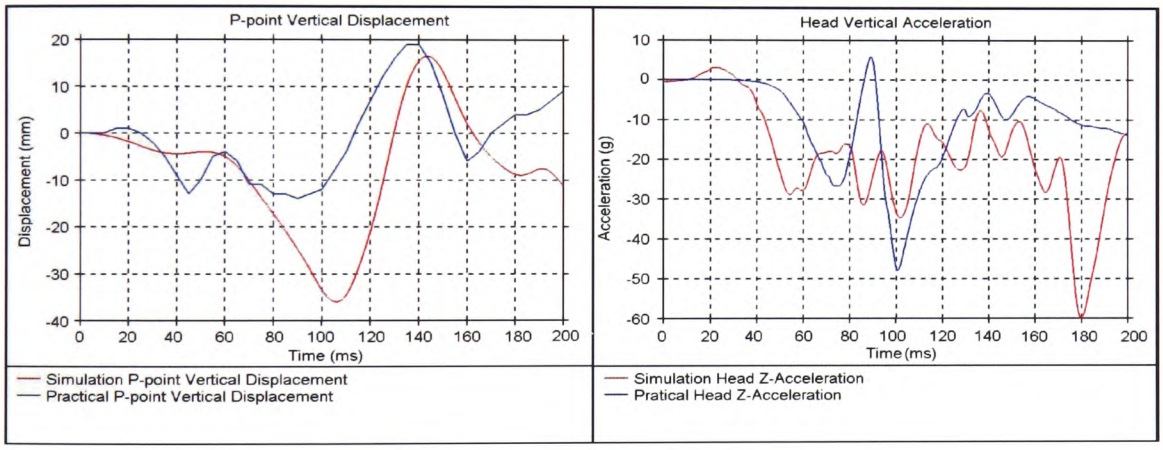

Figure 5.1.6 showing the change in P-point vertical displacement (left) and head vertical acceleration (right) due to increasing the tyre tread thickness from 6mm to 20mm

The head horizontal and vertical accelerations are shown in Figure 5.1.7. The general shapes of the graphs correspond well to those obtained during the practical experiment. The maximum negative value for the simulation head horizontal acceleration has a high peak value at 120ms of -28.5g, which is higher than the practical peak acceleration of -18g. The difference in these peak values is partially due to the different hybrid dummies used. Values of 33g, for the horizontal head acceleration of a hybrid III dummy in a surrogate wheelchair, were recorded by Bertocci *et al.* [10] which is closer to the peak simulated value obtained.

The graph of the vertical head acceleration between practical and simulated results was in close agreement, although the points of minimum and maximum acceleration for the simulation occured 14ms before that of the practical. Again, this phase shift most probably results from differences between the two hybrid dummies. The compression of the tyres, as discussed previously, would also have an affect.

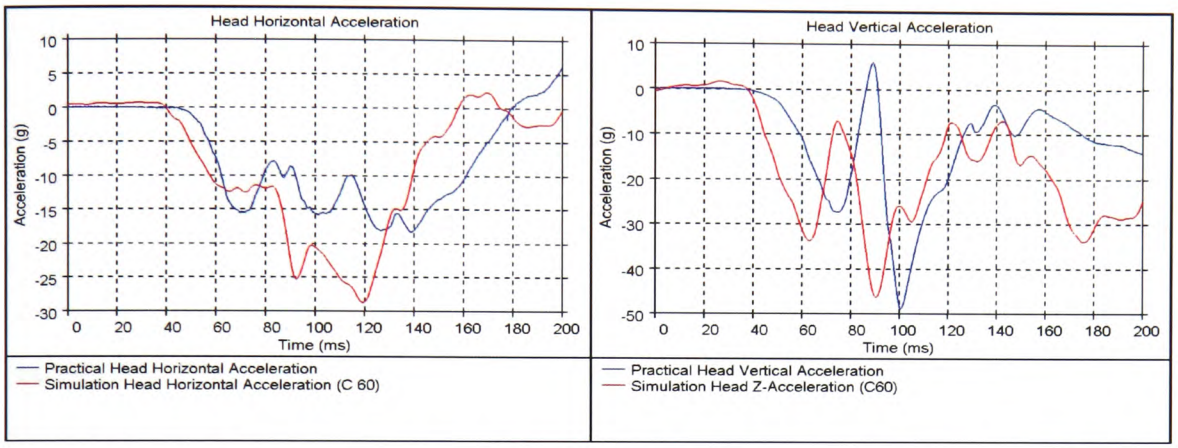

Figure 5.1.7 showing the comparison of displacements and accelerations for the practical and simulated ISO 10542-1 20g frontal crash test

The simulated maximum horizontal excursion of the knee, as shown in Figure 5.1.8, was 34mm less than the practical displacement. The simulated P-point value, however, was 10mm less than those measured in practice. This would seem to imply the seat belt around the dummy was slightly too stiff or that the friction between the dummy and seat was a little too high.

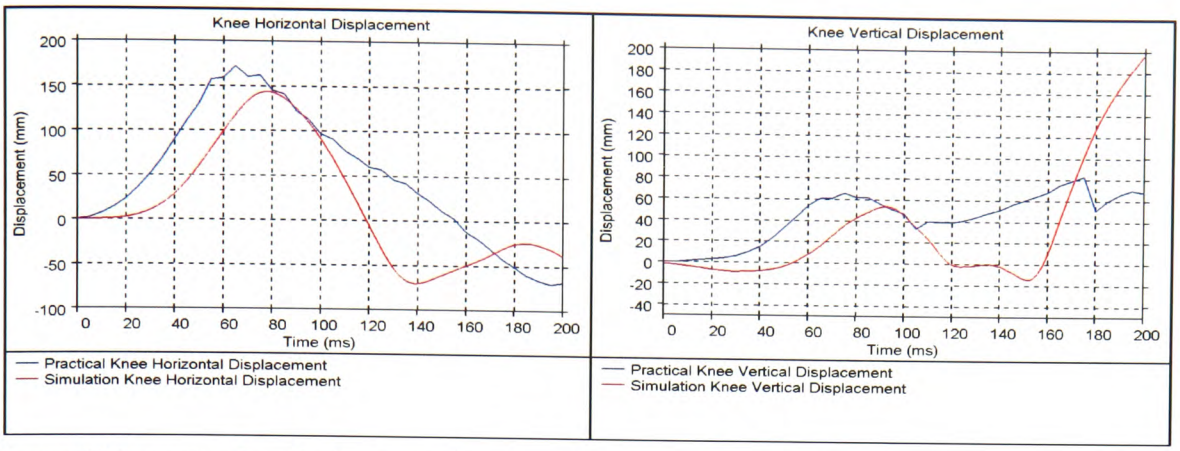

Figure 5.1.8 comparing the horizontal and vertical displacement of the knee for the physical and simulated model

The diagrams in Figure 5.1.9 show the axial force readings for the upper shoulder seatbelt and the rear tie-down. The axial force of the upper shoulder seat belt compared favourably with the practical results with peak readings of 9.67kN and 8.86kN respectively.

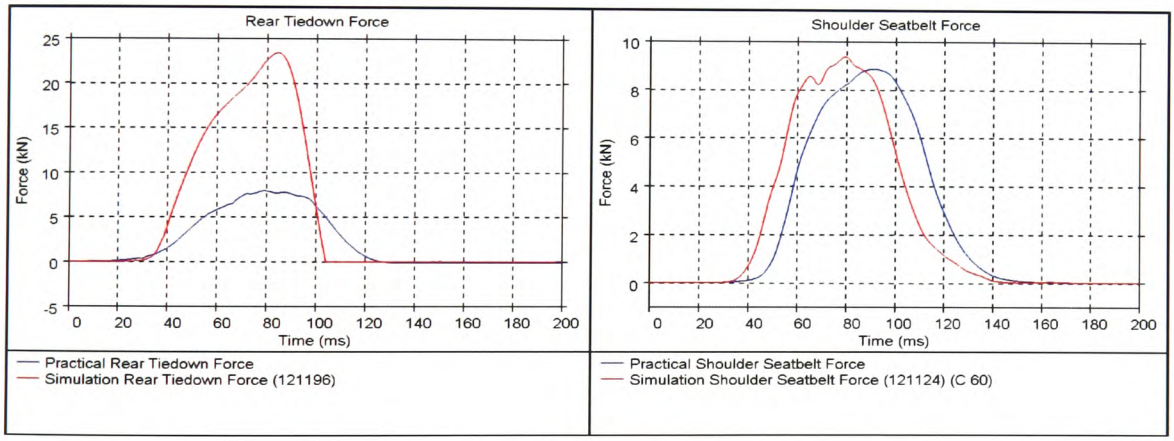

Figure 5.1.9 showing the shoulder belt force (left) and the rear tie-down force (right)

The rear tie-down axial force, however, was far higher than the practical result with a simulated peak force of 21.52kN and a practical peak force of 7.96kN. The method of recording the practical rear tie-down axial force contributed to the large difference. The rear tie-down webbing looped through a cleat attaching the tie-down to the sled, as illustrated in Figure 5.1.10. The load cell was attached to one half of this loop. Assuming that the force in each piece of webbing in the loop was equal then the load

cell was reading half of the total force going through the tie-down. This would suggest a total force of 7.96kN x 2 = 15.92kN, still lower than the simulated result.

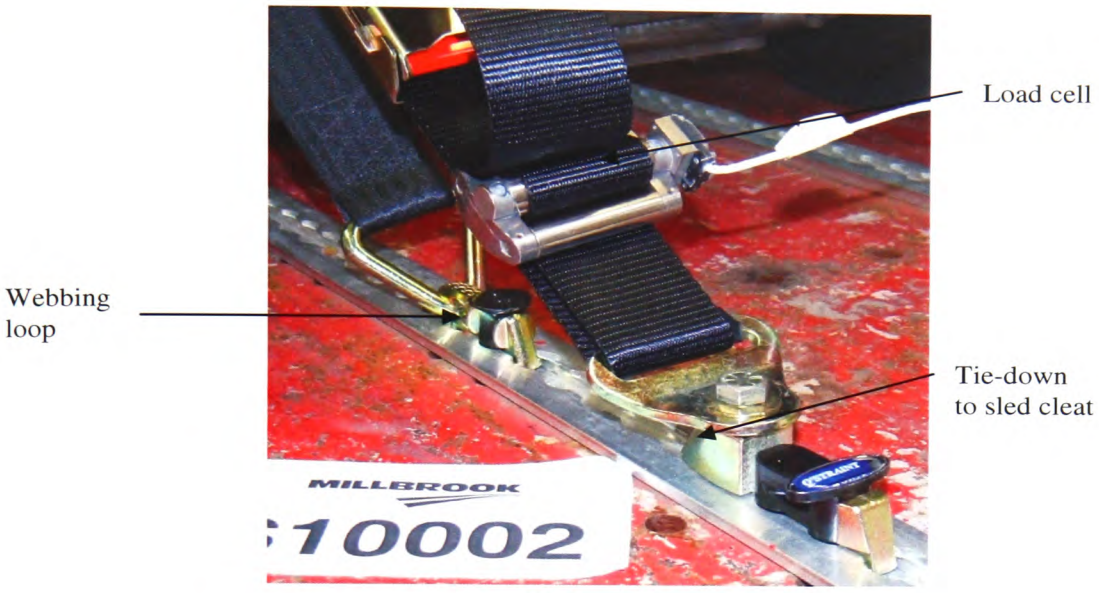

Figure 5.1.10 showing the load cell attached to the rear tie-down

5.2 Rear crash validation

A rear 10g crash test was performed also using the ISO 10542 surrogate wheelchair and Hybrid II dummy. Rear crash testing is not currently required for assessing the transport safety of wheelchairs so consequently has no standard to test to. The test was therefore setup in a similar fashion to that of the frontal 20g crash test except that the wheelchair faced in the opposite direction and the HYGE pneumatic ram, as illustrated in Chapter 3, was setup to deliver a 10g, instead of a 20g, crash pulse. This 10g crash pulse was found to cause the greatest risk of cervical spine injury in car passengers, more commonly referred to as whiplash [43, 44]. The same crash pulse was also used in ISO 17373 [107]; the test procedure of motor vehicle occupants in low speed rear impacts.

The results showed the large dummy neck displacement that a relatively small crash pulse can cause. The rear test, like the frontal one, did not use a head rest. Not all wheelchairs are fitted with head rests but the importance of one can be clearly seen.

The video footage in Figure 5.2.1 of both the practical and simulated sled tests show the dummy and wheelchair moving backwards until restrained by the front tie-downs at 90ms, causing partial compression of the front and rear tyres. The dummy's torso is restrained by the seat back but the head continues to move rearward and, due to the absence of head rest, continues to rotate backwards about the neck joint, Figure 5.2.1 at 90 and 120ms. Elastic energy stored in the front tie-downs and wheels was released causing the wheelchair to rebound into the dummy until restrained by the rear tie-downs (140ms). The dummy rebounded off the wheelchair seat and was restrained from further forward motion by the seatbelt (160 and 200ms in Figure 5.2.1).

Practical 10g rear impact	Time (ms)	Simulated 10g rear impact
	0	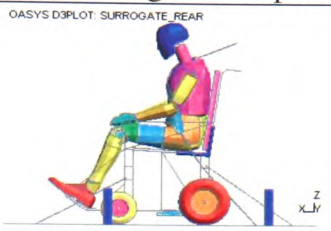
	90	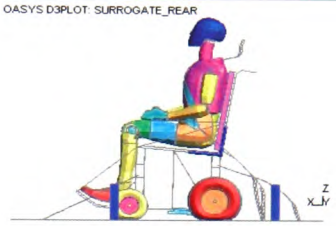
	120	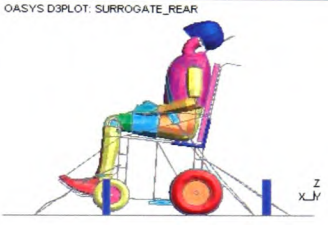
	140	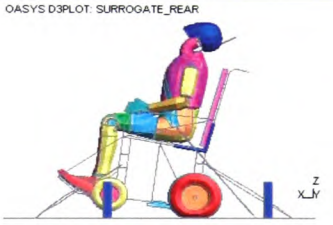
	160	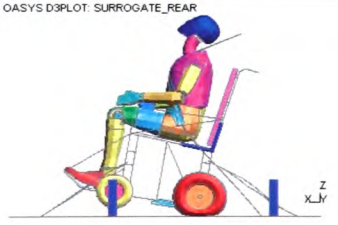
	200	

Figure 5.2.1 showing the comparison between the physical and simulated 10g rear crash test using the ISO 140542 surrogate wheelchair

The graphs in Figure 5.2.2 show the vertical and horizontal displacement of the dummy's head in both the physical and simulated rear crash. As with the frontal crash, the large discrepancy between the physical and simulated head displacements were due to the different head and neck geometries of the Hybrid II and III dummies. The extent by which the dummy's head could move backwards was limited by the head to neck joint and physical contact with the upper back.

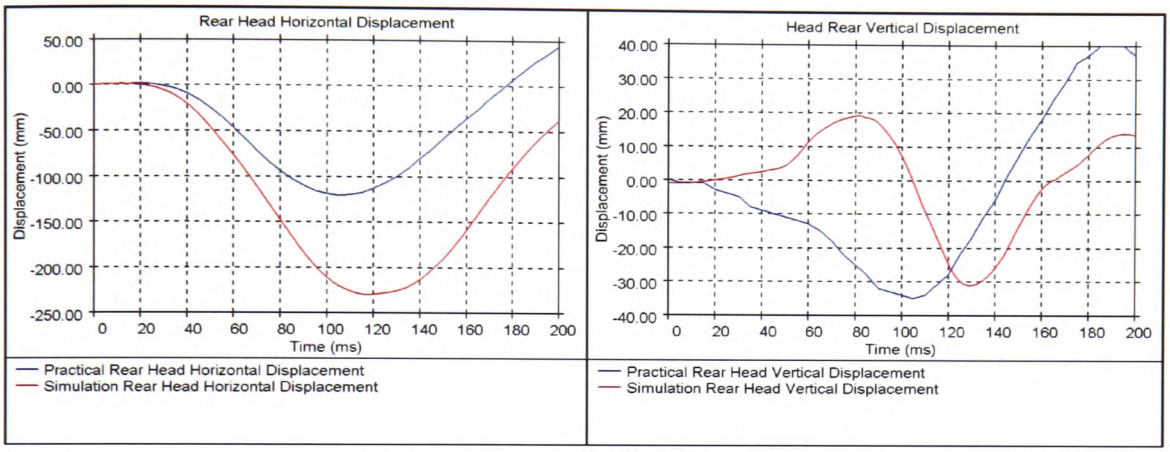

Figure 5.2.2 showing the head horizontal and vertical displacements from the rear simulations and physical crash test

The horizontal maximum head displacements of the practical and simulated values were 120.6mm and 230.3mm respectively. From measurement, and as mentioned when discussing the frontal crash, the Hybrid III dummy's head is positioned 103mm forward of the Hybrid II dummy's head. When the dummy impacts onto the seat back the head continues to move rearward, due to the absence of a head rest, until the neck prevents further rearward motion. The Hybrid III dummy has a more biofidelic (life like) neck than the Hybrid II and is less stiff in extension[8] than in flexion[9], unlike the Hybrid II dummy that has the same stiffness in both flexion and extension [59]. The Hybrid III dummy's neck is therefore less stiff in extension than that of the Hybrid II dummy's. This is clearly illustrated in Figure 5.2.3 where the Hybrid III dummy's

[8] Extension is the movement of a joint that increases the angle between two skeletal members

[9] Flexion is the movement of a joint that decreases the angle between two skeletal members

head can be seen to rotate backwards, to a greater extent than that of the Hybrid II, until the back of the head contacts the base of the neck. The combination of the forward position of the Hybrid III dummy's head, and its greater rearward rotation range, account for the significant difference in head horizontal displacement between the physical and simulated results.

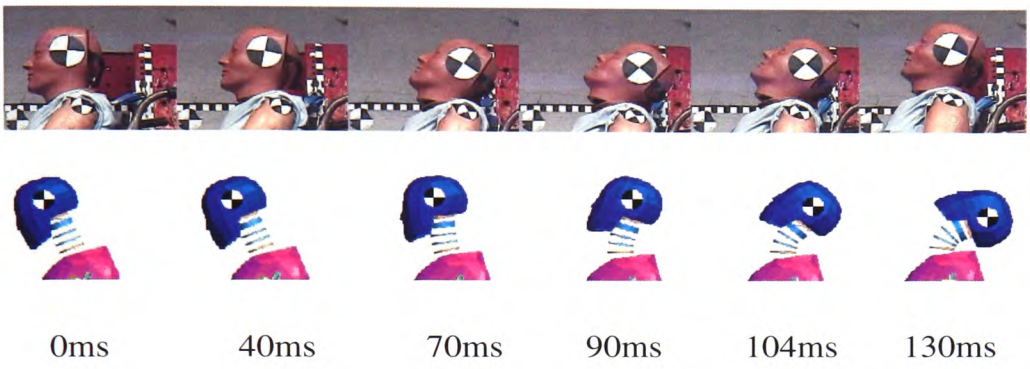

Figure 5.2.3 showing the different neck kinematics of the hybrid II (top) and Hybrid III (bottom) dummies

The maximum vertical head displacement from the practical results was 35.1mm and occurred at the same time as the maximum head horizontal displacement. The simulated results showed a maximum vertical head displacement of 31.0mm. It can be seen from the simulated vertical head displacement results that the head moves upwards before moving down. This occurred due to the forward position of the Hybrid III's neck and head. The way in which the head rotates rearwards about the neck means that it must first extend up, as the neck straightens, before rotating backwards. The Hybrid II's neck is initially in the upright, extended position so does not show a rise in head displacement before rotating backwards and down. The extra horizontal distance travelled by the Hybrid III's head caused a delay of 25ms in it reaching its peak vertical displacement. This motion is best observed in Figure 5.2.1 between the video frames at 0ms, 90ms and 120ms and can also be seen in Figure 5.2.3.

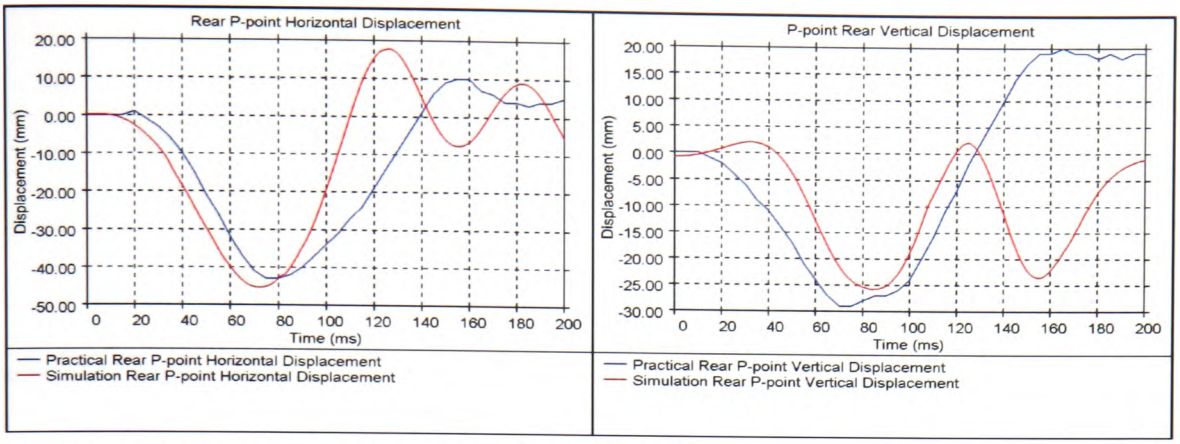

Figure 5.2.4 showing the P-point horizontal and vertical displacements from the rear simulations and physical crash test

The graph in Figure 5.2.4 shows that the maximum practical horizontal P-point displacement of 43.2mm corresponds well with the simulated result of 45.3mm. The minimum vertical P-point displacement for the simulated result is also similar to that of the practical with values of -25.7mm and -29.0mm respectively. After the minimum peak of the vertical P-point value was reached the P-point increased as the rear wheels uncompressed and stored energy in the front tie-downs was released. In the practical experiment the decompression of the rear wheels caused the wheelchair to rebound off the sled, resulting in a positive P-point value. The wheelchair also rotated rearward and, as the P-point is located in front of the rear axle, this also contributed to the increase in the P-point vertical displacement. The simulated model also rebounded upwards after the tyres decompressed but also rebounded further horizontally than the practical results. This led to the rear tie-downs becoming engaged sooner than those in the practical test, which in turn, caused recompression of the rear tyres shown as a decrease in the P-point vertical displacement at 125ms in Figure 5.2.4.

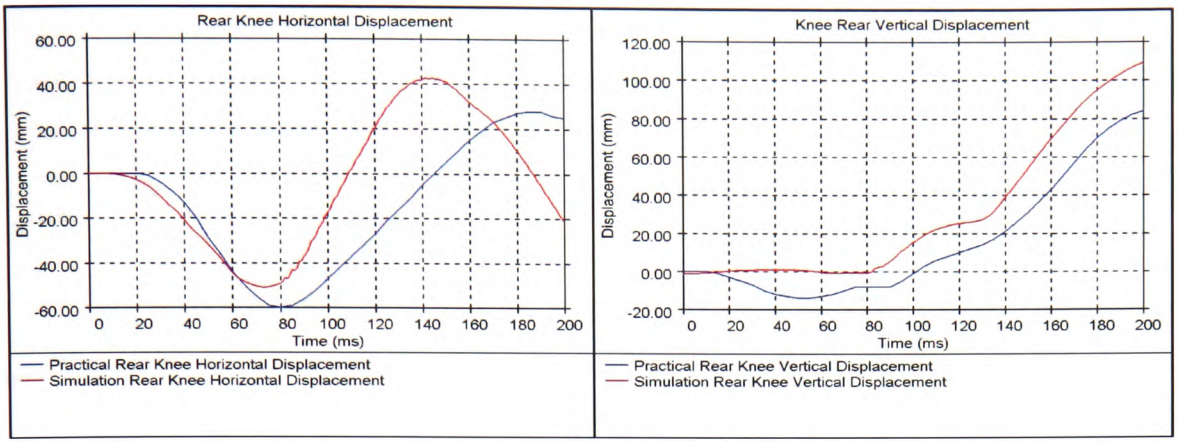

Figure 5.2.5 showing the knee horizontal and vertical displacements from the rear simulations and physical crash test

The simulated horizontal knee displacements show a similar trend to the practical displacement results, with maximums of 51.3mm and 60mm respectively. The vertical knee simulated displacements also correspond well with the practical results.

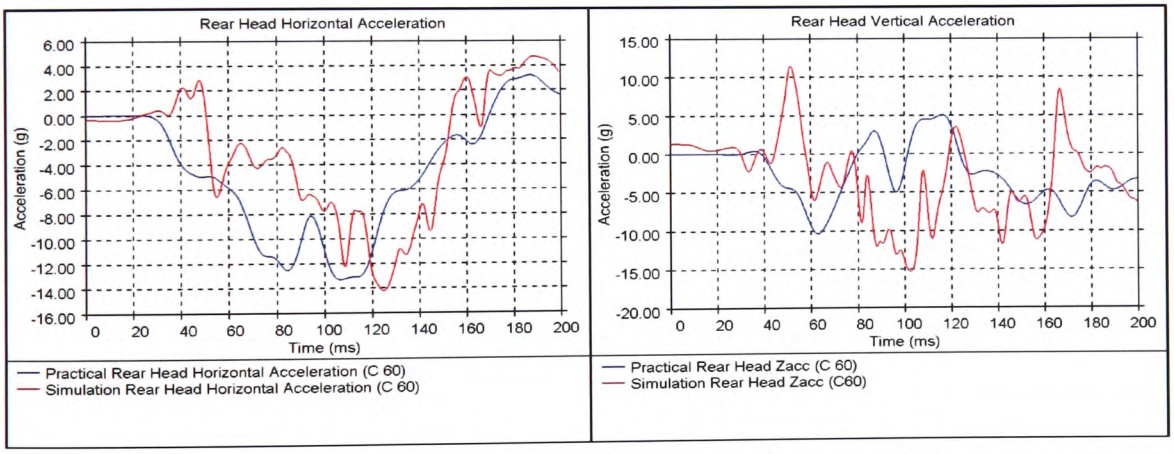

Figure 5.2.6 showing the head horizontal and vertical accelerations from the rear simulations and physical crash test

The simulation results in Figure 5.2.6 show a similar head X (horizontal) acceleration graph shape for both simulated and practical results, with a simulated minimum acceleration of -14.0g, compared to the practical acceleration of -13.4g. The lag in simulated head acceleration, compared to the practical, was attributed to the increased displacement of the Hybrid III dummy's head and different neck stiffness compared with that of the Hybrid II dummy's, as discussed previously.

Also in Figure 5.2.6 the simulated head Z (vertical) acceleration had a minimum value of -12.3g compared to the practical value of -10.6g. The maximum value of 15.3g from the simulation was, however, far greater than the practical value of 5.1g. The head Z simulated acceleration compares rather poorly with the practical results. It is proposed that the difference between the Hybrid II and III dummies maybe more noticeable in such low speed rear impacts.

5.3 Validation of the ISO 16840 surrogate wheelchair

The modelling process was further validated by comparing a previous ISO 16840-4 test, conducted by the RE Unit, with an equivalent FEA simulation. The test used a different surrogate wheelchair to the one used in the ISO 10542-1 tests. The ISO 16840 surrogate was built to test custom seating systems for powered wheelchairs that have already been tested to ISO 7176-19. In this way each different seating system can be crash tested on a standard base without having to destructively test a production wheelchair chassis.

The ISO 16840-4 crash test subjects the wheelchair to the same setup and accelerations as ISO 10542-1 and although currently in draft form is still used by many seat manufactures as a best practice guide to test the crashworthiness of their products [7, 39]. The test itself has the same requirement as both ISO 10542-1 and ISO 7176-19 with additional requirement that "seating system components that may contact the occupant shall not fragment or separate in a manner that produces sharp edges with a radius less than 2mm". Unfortunately no measurement details of the RE Units ISO 16840-4 sled test were available so comparison had to made qualitatively from the video footage and still photographs that were available.

The test was a useful modelling comparison as the seating clamp unit's deformation after the test could be compared with that from the model. Details of the construction of the ISO 16840 surrogate wheelchair have been discussed previously in Chapter 4.

As with the previous simulation and practical comparisons, video stills were compared at meaningful time events. Figure 5.3.1 shows the practical crash test on the left and the equivalent simulation model on the right. The reader will observe that the wheelchair is facing rightwards in these series of tests as opposed to the leftwards facing direction of the previous validation tests. This was purely down to the side of the sled the crash tests were performed on.

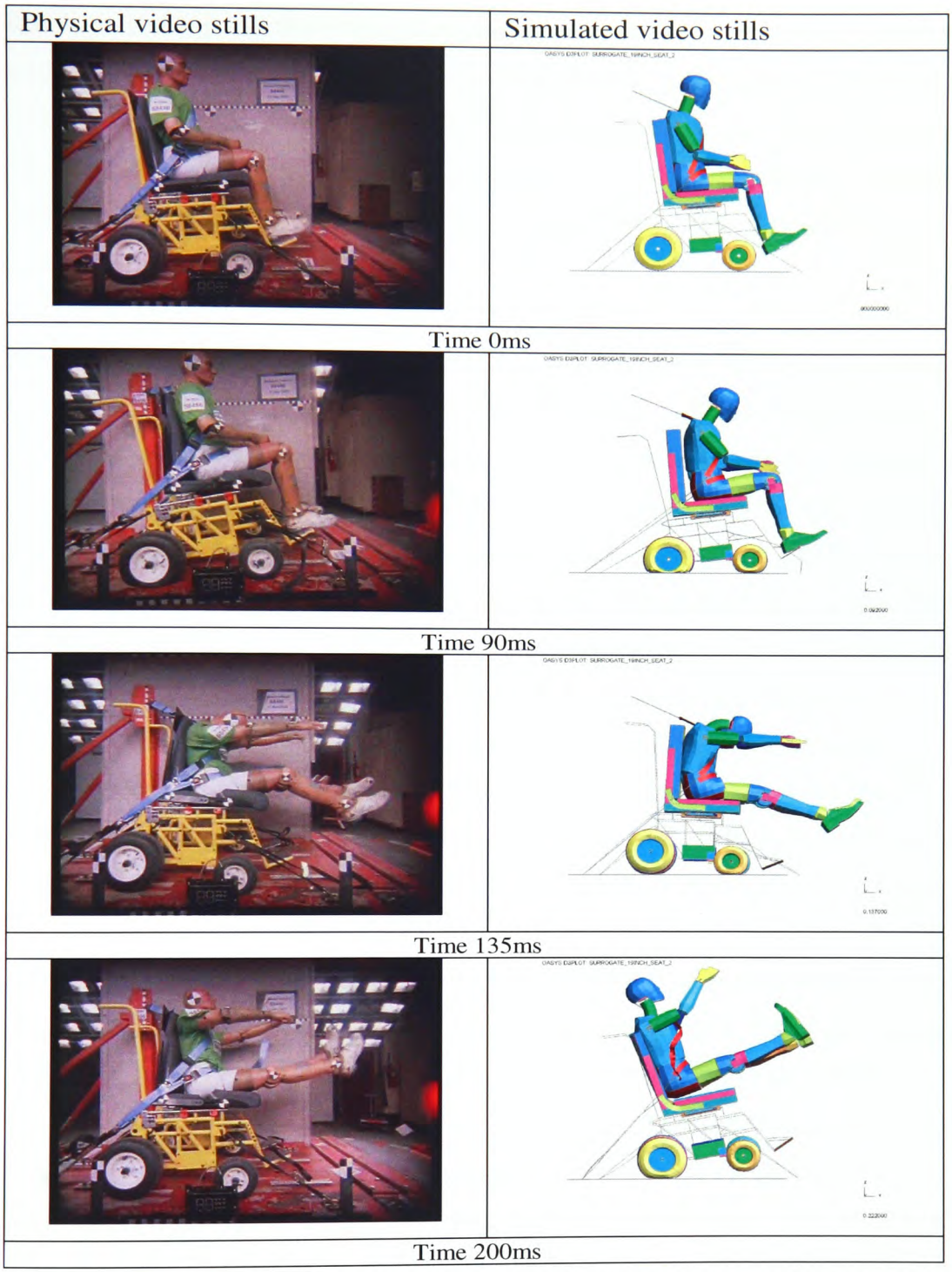

Figure 5.3.1 showing video stills of the physical ISO 16840-4 crash test against the results from the FEA model

The frames at 0ms, in Figure 5.3.1 show both models at rest. The second frame of Figure 5.3.1 at 90ms shows the point of full compression of the rear tyre. As the sled

accelerates to the left of the frame the rear tie-downs exert horizontal and vertical forces on the wheelchair frame causing the rear wheels to compress. The wheelchair moves in the opposite direction relative to the motion of the sled. The seat and occupant slide forward, relative to the wheelchair frame as can be seen by the distance between the seat back and the wheelchair frame arms. The occupant also moves forward relative to the seat.

At 135ms the occupant's motion is resisted by the seatbelt as the legs, arms and head continue to move forward relative to the seat. The rear tyres uncompress and, along with the stored energy in the rear tie-downs, cause the wheelchair to 'rebound' in the direction of the sled motion. The relative forward movement of the dummy, the expansion of the rear tyres and the resistive force of the front tie-downs, as they engage, caused compression of the front tyres. At 200ms the video stills show the dummy rebounding into the seat from the stored energy in the seatbelt and the dummy's chest. The rebound into the seat of the simulated dummy is far more aggressive than that of the physical crash dummy resulting in greater rotation about the rear axle of the simulated wheelchair. The increased rebound forces of the simulated wheelchair model again seems to be caused by a lack of damping in the tyres, tie-downs and seatbelts, as discussed for the frontal ISO 10542-1 test comparison.

The exact cushions used in the practical experiment were unknown so the same foam material as the ISO 10542-1 frontal crash simulation was used. From the screenshots of the practical experiment in Figure 5.3.1 it appears that there are two cushions on the base of the wheelchair seat, the foremost of which slides forward increasing the submarining[10] effect on the dummy. The screen shots at 135ms in Figure 5.3.1 show the simulated dummy far more upright than the practical dummy. It is likely that the increased forward motion of the practical dummy, due to the submarining effect, placed more weight over the front of the wheelchair and inhibits rearward rotation of the physical surrogate wheelchair.

---

[10] See Appendix A for further information and an example of the submarining effect.

5.3.1 Comparison of deformed parts

In order to increase the life of the surrogate wheelchair aluminium bars were used to connect the front wheels to the wheelchair frame. These aluminium bars deformed during the crash test to reduce the damage to the main wheelchair frame. Figure 5.3.2 shows the deformed aluminium bars after a 20g crash test compared to the deformed bars taken from the simulation model. Again, as the data from this particular crash test was acquired second hand and as a by product of a different test the exact extent of the deformation was not recorded. Visual comparison of the aluminium bars from both physical and simulated crash tests did, however, indicate that the modelling process correctly captured the deformation of the bars.

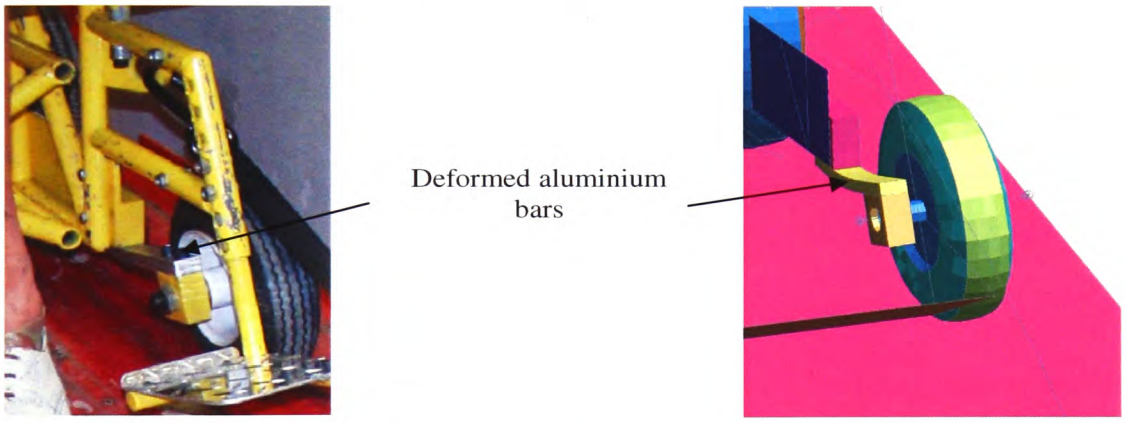

Figure 5.3.2 showing the deformed aluminium bars connecting the front wheels to the ISO 16840 surrogate wheelchair frame

A further visual comparison that was made was for the Rookwood Universal Interface Kit (RUIK) that was specifically being tested in this physical crash analysis. The requirements of the test were simply to ensure that the RUIK was able to adequately secure the wheelchair seating system to the frame in a 20g frontal crash. Figure 5.3.3 shows the comparison between the deformation of the RUIK in the physical and simulated crash tests.

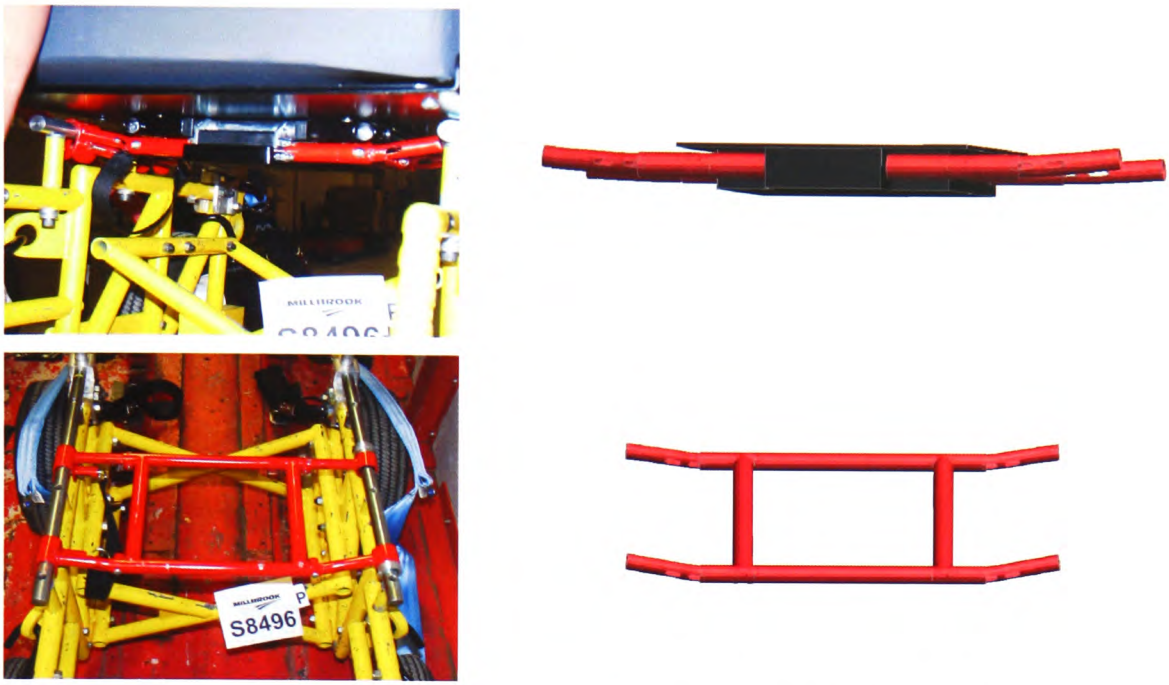

Figure 5.3.3 showing the deformed RUIK (in red) from the ISO 16840-4 practical experiment (left) and from the simulation (right)

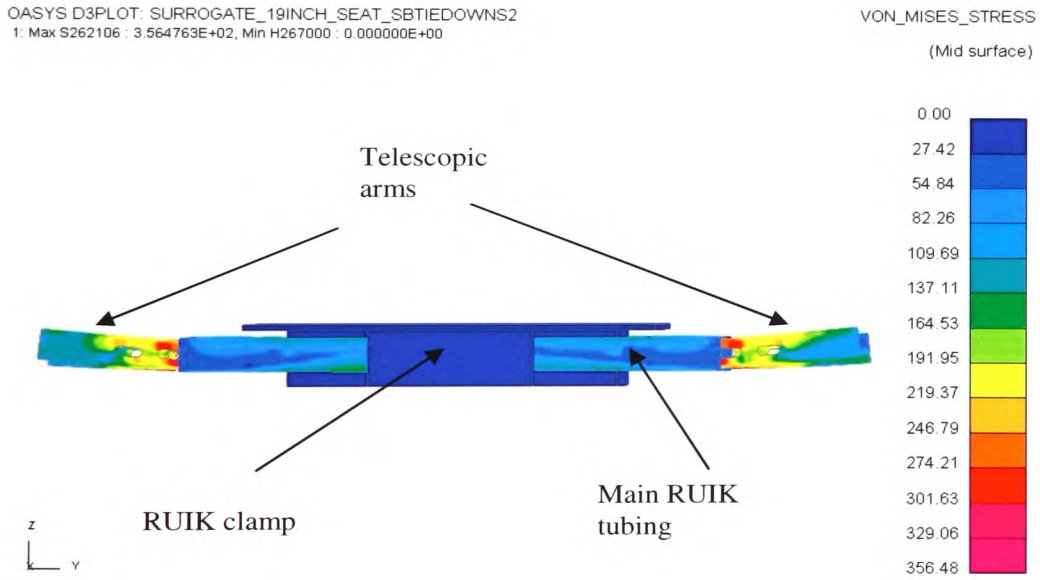

Figure 5.3.4 showing the Von-Mises stress distribution of the deformed RUIK female part at maximum load during the simulated ISO 16840-4 20g frontal crash test

The stress plot in Figure 5.3.4 shows the yield stress of the steel RUIK (200MPa) was exceeded where the telescopic arms enter the main RUIK tubing, causing plastic deformation.

5.4 Model simulation crashworthiness criteria

The various wheelchair crash safety standards (ISO 7176-19, 10542-1 and 16840-4) have criteria that must be satisfied if the wheelchair design, tie-downs or seating system are to be deemed crashworthy. The three standards have excursion limits for the occupant and wheelchair that are broadly similar. They also have additional criteria pertaining to the specific item in question, e.g. tie-downs wear for ISO 10542-1, excessive seat deformation for ISO 16840-4 and battery movement for ISO 7176-19. The results from the virtual crash testing should be compared with these ISO standards if meaningful wheelchair crashworthiness information is to be derived. It makes most sense to compare the virtual results with the crashworthiness criteria from ISO 7176-19 as this is used for testing production wheelchairs that are attached to the test sled with WTORS (wheelchair tie-downs and occupant restraint systems) that should have already been tested to ISO 10542-1 and that are fitted with a seat tested to ISO 16840-4.

To begin with the criteria from ISO 7176-19 will be listed and then each section's relevance to the virtual simulation discussed before proposing a modified test criteria.

Criteria for crashworthiness of a production wheelchair - taken from ISO 7176-19 [3].

1. During the sled crash test

Measurement Point	Excursion variable	Excursion Limit (mm)
Wheelchair P-point	X_{wc}	200
ATD Knee	X_{knee}	375
ATD front of head	X_{headF}	650
ATD rear of head	X_{headR}	400

Table 5.4.1 showing the excursion limits for the dummy (ATD – Anatomical Test Dummy) and wheelchair [3]

The knee excursion must exceed that of the wheelchair P-point excursion, such that $\frac{X_{WC}}{X_{knee}} \geq 1$.

Batteries of powered wheelchairs shall not move completely outside the wheelchair's footprint nor move into the occupant's footprint, i.e. not touch the back of the legs.

2. After the sled crash test

2.1 The wheelchair shall remain upright on the test sled and the dummy shall remain in a seated posture indicated by the dummy's torso not being more than 45^0 to the vertical when viewed from any direction.

2.2 Wheelchair securement points shall not show visible signs of wear.

2.3 Wheelchair components that may contact the occupant shall not fragment or separate in a manner that produces sharp edges, as defined by having a radius less than 2mm.

2.4 Primary load carrying components of the wheelchair shall not show visible signs of failure.

2.5 Locking mechanisms of tilt-in-space mechanisms shall not show visible signs of failure

2.6 Removal of ATD (Anatomical Test Dummy) from the wheelchair shall not require the use of tools.

2.7 Release of wheelchair from the tie-down system shall not require the use of tools.

2.8 The post test height of the average of left and right ATD H-points (the location of the hip joint on the dummy) relative to the wheelchair ground plane shall not decrease by more than 20% from the pre-test height.

Not all the tests listed in ISO 7176-19 are possible to capture using the FEA model. The initial criterion for the project was to improve the risk assessment process not to completely replicate the physical test. Besides, trying to replicate the physical test virtually would still not replace it.

The only difference in occupant and wheelchair excursion limits between the three standards is that ISO 10542-1 does not require rear head displacement to be considered. As a result the rear head displacement for the simulations using the ISO 10542 surrogate wheelchair will not be considered. Similarly the skewed impacts do not have a simple fore and aft movement of the head so taking the maximum forward head motion in X (X_{headF}) and maximum rearward motion in X (X_{headR}) makes little sense. Instead the motion of the head will be taken from the centre of gravity of the head (the position of the target marker on the dummy's head in Figure 5.2.3) in X and Y directions.

Only the first 200ms of the crash event is run in the simulations in this study as this matched the time period of recorded data for the physical crash tests available for comparison. Often times of less than 200ms are used in vehicle crash simulation analysis [28, 47, 120, 123]. The crash pulse returns to zero acceleration after 110ms but from observing the physical crash tests it took up to 3 seconds for the dummy to come to complete rest in the wheelchair. Running the simulations for 3 seconds, to allow measurement of the dummy and wheelchair to be taken 'post test', would take 15 times longer and, with the average simulation run taking between 3-4 hours, could increase the run time up to 60 hours. With it being necessary to conduct several runs, to ensure the various contacts and boundary conditions are behaving correctly, a large run time of 60 hours would significantly lengthen the simulation process and begin to

outweigh the cost benefits of using computer simulation. With this in mind it would be impractical to comply with point 2.1 above and state whether or not the dummy remained in an upright position, being not more than 45^0 to the vertical when viewed from any angle, after the crash. With this in mind it is proposed that the position of the occupant be examined at 200ms to give some indication as to whether or not the occupant is likely to remain upright.

Determining whether a component fragments, leaving a sharp edge with a radius of less than 2mm, was deemed to be an unreasonable level of detail for the model to predict. Signs of failure due to excessively high material stresses were possible to examine, however. Tilt-in-space mechanisms have not been considered in this study.

Assessing whether or not the Dummy or wheelchair needed tools to remove them from the wheelchair and tie-downs respectively is not something that could be achieved easily using computer simulation. An extremely high level of detail would be required to model the tie-down and seatbelt buckles and even then signs of deformation may not indicate failure to undo the buckles by hand. From a risk assessment point of view, jamming buckles do not endanger the occupant during a crash but could well cause problems during a subsequent rescue from a vehicle after a crash. It was decided that modelling of the buckles was beyond the scope of this project.

The final test criteria, 2.8, required that the post H-point height decrease no more than 20% of the initial test height. As mentioned above, running the simulation until the dummy had settled would take too long. Any deformation to the wheelchair that would cause a 20% decrease in dummy H-point height, however, would occur during the maximum loading on the wheelchair in the first 110ms seconds.

The test criteria described above is aimed at wheelchair manufactures. It should be borne in mind that the virtual testing proposed herein is to aid the RE unit in their risk assessment after they have carried out modifications to wheelchairs that have already passed this standard.

An abridged version of the ISO 7176-19 pass criteria is proposed below in Table 5.4.2 and shall be used in Chapter 6 to compare some of the results.

Measurement Point	Excursion Limit (mm)
Wheelchair P-point, X_{wc}	200
ATD Knee, X_{knee}	375
ATD front of head, X_{headF}	650
ATD rear of head, X_{headR}*	400
X_{knee} /X_{wc}	≥ 1
Does the movement of the occupant suggest that they will remain upright?	Occupant angle less than 45^0 from any angle
Battery movement	Within footprint of wheelchair and away from occupant
* Value not used for ISO 10542 surrogate simulations and skewed impacts	

Table 5.4.2 showing the modified ISO 7176-19 crash test criteria for the simulated models

5.5 Validation summary

The above comparison of frontal and rear impacts, using the surrogate ISO 10542 wheelchair, demonstrate both a qualitative and quantitative validation of the computer model against empirical data. The results show that a reasonable degree of confidence can be put in the model predictions of the behaviour of the wheelchair and occupant in a crash using the computer modelling techniques described in the previous Chapter. The ISO 16840 surrogate frontal crash model used the same modelling parameters as the ISO 10542 surrogate runs, but with different wheelchair frame and seat, and compared well with video footage from the ISO 16840-4 frontal crash sled test. The model also captured the deformation of the aluminium bars attaching the front wheels and the RUIK, for which the test was conducted.

From the preceding comparisons between physical and simulated results several common factors causing discrepancies between the two were identified, these are summarised below:

- Different dummies used in the experimental (Hybrid II dummy) and simulated results (Hybrid III dummy).
- Incomplete surrogate wheelchair wheel information; tyre tread thickness and tyre rubber properties.
- Simple air pressure model used for the tyre pressure that did not take into account any energy losses.
- Slippage of seatbelt and tie-downs buckles were not accounted for in the simulated model.
- Cushion details for the ISO 16840 surrogate model. The same cushions as used in the ISO 10542-1 front and rear tests were used instead, reducing the amount of submarining observed in the physical results.

The above factors, affecting the wheelchair behaviour, could be altered to further improve the similarities of the computer models to the physical data. Before such improvements are made it would be prudent to conduct further physical tests to establish a consistent set of results to compare the simulation to. At present the physical results could show behaviour that is inconsistent with the average results of a series of identical tests. Multiple physical tests were not possible in this study due to their high cost.

The above models were subsequently used in the following Chapter to examine a number of different crash scenarios, the results of which were compared with the above validation results and modified ISO 7176-19 crashworthiness criteria, where appropriate, in order to make useful conclusions and demonstrate correlation between model predictions and validated data. As well as using the surrogate wheelchairs some of the crash scenarios were conducted on a model of a Spectra Plus wheelchair. The Spectra model, like the ISO 16840 surrogate model, used the same modelling

parameters but used a different wheelchair frame and wheels. The seatpan and its connection to the frame, used with the Spectra wheelchair model, was the same as that used in the ISO 16840 surrogate wheelchair validation model.

Chapter 6 - Results

The previous Chapter demonstrated the ability of the ISO 10542 surrogate wheelchair and occupant finite element model to predict the behaviour of the equivalent physical crash event. This validated model was used to investigate a number of different crash scenarios and also as a reference to compare with the more complex Spectra wheelchair model. The Spectra model, although not validated, used the same seatbelt and tie-downs as the ISO 10542 surrogate wheelchair and the same seatpan as used in the qualitatively validated ISO 16840 surrogate wheelchair model.

The crash scenarios simulated were as follows:

1. **Frontal 20g impact** – Comparing the ISO 10542-1 frontal 20g simulation discussed in Chapter 5, with the model of the Spectra wheelchair.
2. **Rear 10g impact** – Comparing the ISO 10542-1 rear 10g simulation, discussed in Chapter 5, with the model of the Spectra wheelchair.
3. **Addition of life support equipment** - Attaching life support equipment to ISO 10542 surrogate wheelchair crash test and performing a 20g frontal impact sled test.
4. **Pitching effect** - Pitching effects applied to the sled for both surrogate and Spectra frontal 20g crash tests
5. **Solid tyres** - The effect of adding foam filled solid tyres to both the surrogate and Spectra frontal 20g crash tests.
6. **Skewed impact** - Skewed 60^0 impact of the surrogate and Spectra wheelchairs at 20g. 60^0 is statistically the most common skewed impact [50], also examining the difference of using a right or left shoulder seatbelt.

Of the above crash scenarios only the frontal test, using a 20g crash pulse, is currently required for production wheelchairs in accordance with ISO 7176-19 [3].

For all but the skewed simulations the acceleration and displacements in the Y, or lateral, direction have been ignored for both the sake of brevity and as they tend to be rather small in comparison to those in the X (horizontal) and Z (vertical) directions. A similar assumption was made by Welcher *et al.* [128] in their study of the effects of incremental velocity changes on whiplash associated disorders.

Initially front and rear crashes will be examined for the Spectra wheelchair and compared to the results obtained for the same test using the validated ISO 10542 surrogate wheelchair.

6.1 Frontal 20g impacts

The first test to be conducted was a comparative test between the surrogate and Spectra wheelchairs. The Spectra was one of the more common electric wheelchairs issued by the RE unit. Its relatively simple structure allowed it to be readily modified to meet the needs of each individual client. The most common seat to be attached to the Spectra wheelchair base was the RE seatpan, onto which custom carved seat cushions were mounted to manage the client's posture. This was the same seat as used on the ISO 16840 surrogate wheelchair, qualitatively validated in Chapter 5. The same modelling process, occupant positioning and boundary conditions as the validated ISO 10542 surrogate wheelchair were applied to the Spectra wheelchair. By directly comparing the Spectra wheelchair to the validated surrogate wheelchair a degree of confidence in the behaviour of the Spectra wheelchair model could be achieved. The graphs in Figure 6.1.1 compared the results between the surrogate and Spectra wheelchairs in a 20g frontal sled crash simulation.

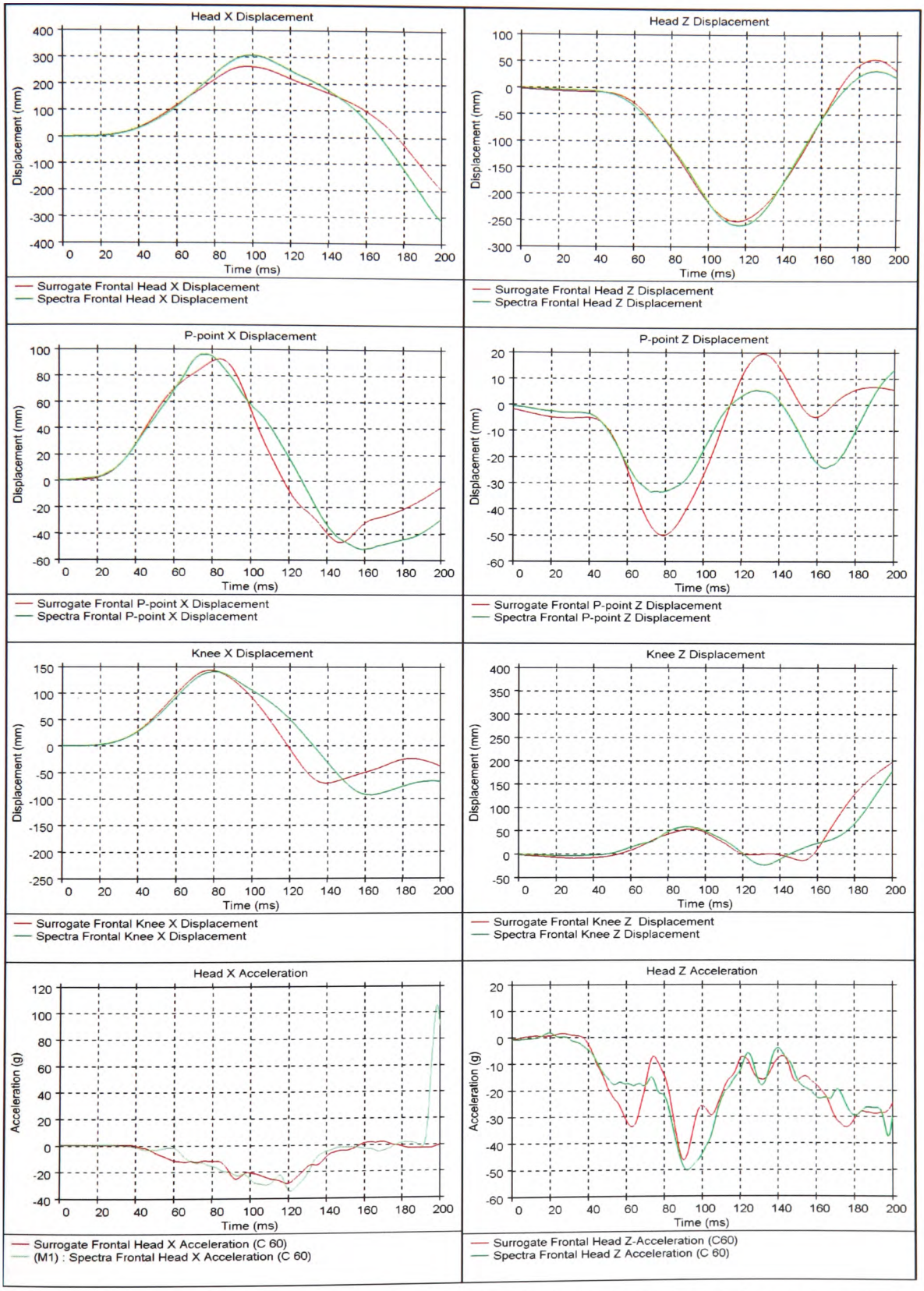

Figure 6.1.1 (a-h) showing the simulation of a frontal 20g impact between the surrogate and Spectra wheelchairs

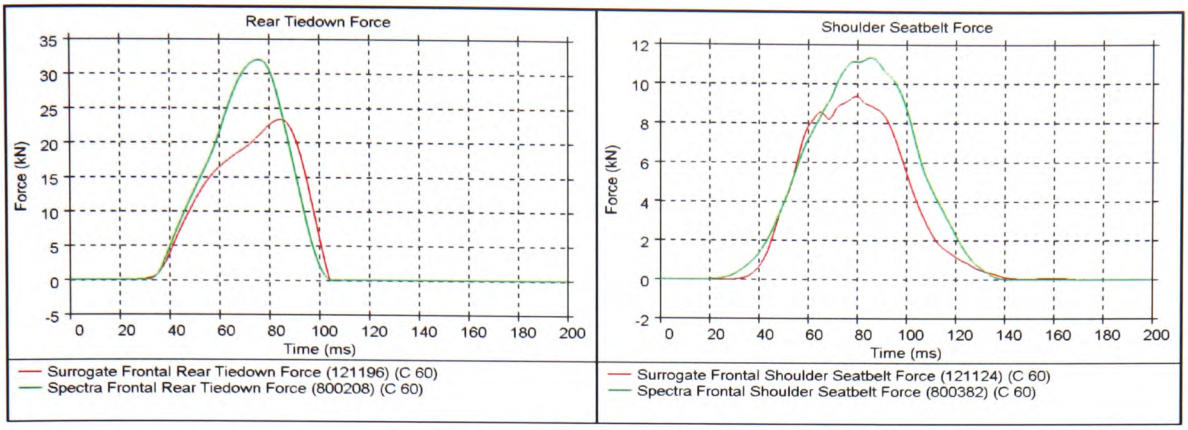

Figure 6.1.1 (i, j) showing the simulation of a frontal 20g impact between the surrogate and Spectra wheelchairs

Comparing the results from the ISO 10542 surrogate and Spectra wheelchair simulations it can be seen that the trends of the displacement, acceleration and force graphs, as well as the screenshots in Figure 6.1.2, are very similar. There was a slight increase in peak head and horizontal P-point displacement for the Spectra wheelchair due to it being 26.7kg heavier than the surrogate wheelchair and occupant. This mass difference also accounts for the increase in rear tie-down and seatbelt force experienced by the Spectra wheelchair.

The P-point vertical displacement for the Spectra wheelchair was 17mm less than that of the surrogate due to the different wheels on the two wheelchairs. The Spectra and surrogate wheels have the same outside diameter of 320mm but have different profiles (tyre thickness from rim to outer tyre edge) of 48mm and 71mm respectively. The thinner profile of the Spectra wheels reduced the amount of compression possible, as shown in the corresponding screen shots in Figure 6.1.2 at 88ms. The effect that tyres of different stiffnesses have is discussed further when considering the addition of solid foam tyres later in this Chapter.

The head vertical acceleration is also similar between the two simulations, as is the horizontal head acceleration up until 196ms where the head of the occupant, in the Spectra wheelchair, makes contact with the head rest, causing a large peak acceleration value of 106g, see Figure 6.1.2 at 200ms. This acceleration value seemed excessively

large. Part of the reason for the large acceleration value value was that the pneumatic wheels of the Spectra wheelchair began to decompress at 165ms (see graph of P-point vertical displacement in Figure 6.1.1) causing the wheelchair and head rest to rebound into the dummy's head as it moved rearward to meet it. Further investigation of this high head acceleration was conducted by setting up a simple simulation whereby the head of the dummy was fired into the rigidly fixed head rest to determine whether the accelerations obtained from the crash simulations were excessively high due to modelling error. The head acceleration recorded in this simple experiment was higher than those observed in the crash analysis, due to the fixed nature of the head rest, indicating that the modelling process was not at fault. Further details of this experiment are presented in Appendix C.

The screenshots in Figure 6.1.2 compare the ISO 10542 surrogate and Spectra frontal wheelchair simulations. The left hand column of Figure 6.1.2, depicting the Spectra results, shows the deformation of the Rookwood seatpan, which is attached to the Spectra chassis. This deformation was similar to that observed in both the practical and simulated ISO 16840-4 sled test discussed in Chapter 5. Apart from the deformable seat, another difference between the two models was the amount of rotation the wheelchairs underwent. The Spectra rear wheels compressed less than those of the surrogate and therefore sprung back to a lesser extent (144ms in Figure 6.1.2). The front casters of the Spectra wheelchair, being made of solid rubber, were considerably stiffer than the front pneumatic tyres of the surrogate wheelchair, which reduced the forward rotation of the Spectra wheelchair and its subsequent rotation rearwards. The surrogate front wheels, on the other hand, compressed fully and then caused the wheelchair to rotate rearwards as the energy was released (174ms and 200ms in Figure 6.1.2). Although the Spectra wheelchair model showed considerably greater seat deformation, in the form of seatpan and RUIK distortion (as can be seen from Figure 5.3.3 and Figure 5.3.4) the surrogate wheelchair, with its pneumatic front wheels, seemed to offer greater energy absorption culminating in a reduced peak dummy head acceleration in the X-direction at 200ms and in the Z-direction at 90ms, as can be seen in Figure 6.1.1 (g, h).

Surrogate 20g frontal impact	Time (ms)	Spectra 20g frontal impact
	0	
	88	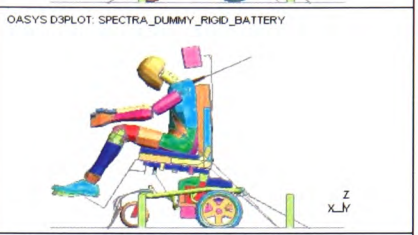
	100	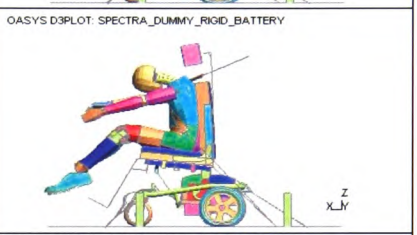
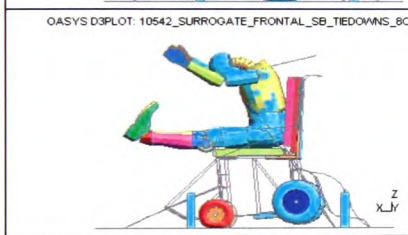	144	
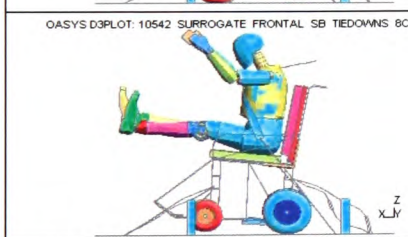	174	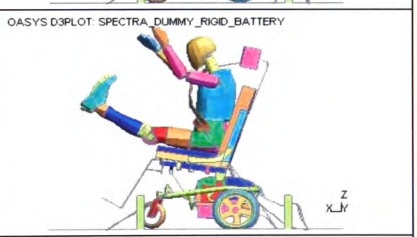
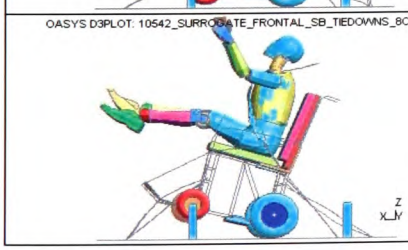	200	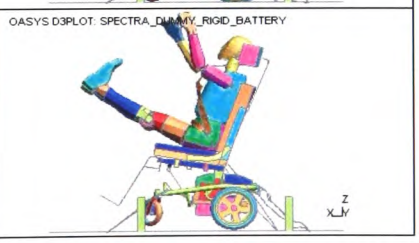

Figure 6.1.2 showing the screenshots of the Spectra frontal 20g test (right) compared with that of the validated ISO 10542 surrogate wheelchair (left)

The results from the simulated frontal crash test for the surrogate and Spectra wheelchairs were compared against the modified ISO 7176-19 test criteria, as discussed in Chapter 5, and presented below in Table 6.1.1. The results show that both tests conformed to the criteria specified.

Measurement Point	Excursion Limit	Surrogate wheelchair	Spectra wheelchair
Wheelchair P-point, X_{wc} (mm)	200	93	97
Dummy Knee, X_{knee} (mm)	375	146	142
Dummy head front, X_{headF} (mm)	650	272	308
Dummy head rear, X_{headR} (mm)	400	N/A	352
X_{knee} /X_{wc}	≥ 1	>1	>1
Does the movement of the occupant suggest that they will remain upright?	Occupant angle less than 45^0 from any angle	Yes	Yes
Battery movement	Within footprint of wheelchair and away from occupant	N/A	Yes

Table 6.1.1 comparing the maximum excursions of the surrogate and Spectra wheelchairs against modified ISO 7176-19 crashworthiness criteria

Another criteria stated in ISO 7176-19 was that the batteries of an electric wheelchair should not move outside the footprint of the wheelchair. The screenshots in Figure 6.1.2 show that the batteries stay with in the wheelchair's foot print. A close up view of the behaviour of the batteries is shown in Figure 6.1.3 where the battery housing and webbing strap can be seen to keep the batteries in position.

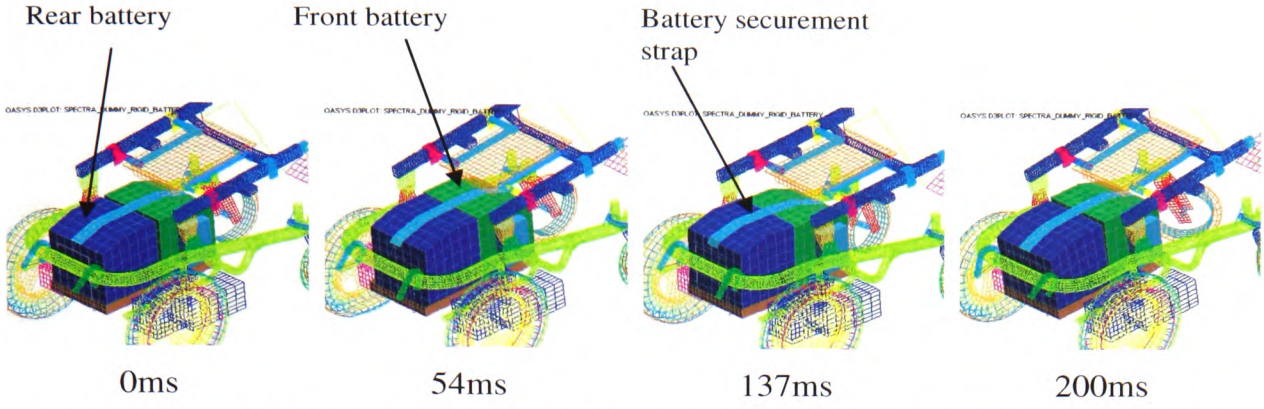

Figure 6.1.3 showing the motion of the Spectra wheelchair batteries during the frontal crash simulation.

Spectra frontal simulation summary

Overall the Spectra model behaved in a very similar fashion to the surrogate model. The differences that did occur are to be expected from the deformable model and different wheel geometries. The Rookwood seatpan of the Spectra wheelchair has been compared with physical results from the ISO 16840-4 [39] test in Chapter 5 and deformed in a similar fashion here. The difference in the rearward rotation of the surrogate and Spectra wheelchairs resulted from the difference in the wheels attached to each wheelchair and the high spike observed in the head acceleration, beginning at 190ms, was attributed to the inclusion of the head rest on the Spectra wheelchair. Comparison of the Spectra model to the validated surrogate model, under the same loading conditions, gave a degree of confidence in the ability of the Spectra model to predict the outcome of crash events.

6.2 Rearward 10g impacts

As with the frontal impacts, the effects of rear impacts on the Spectra Plus wheelchair will be examined. The most noticeable omission from the ISO 10542 surrogate rear crash simulations was the lack of a headrest. A headrest wasn't available for the surrogate wheelchair and consequently allowed for an interesting comparison with the Spectra wheelchair with attached headrest.

It should be remembered that both the Hybrid II and Hybrid III dummy necks are designed for frontal impacts and are less biofidelic in rear impacts, as discussed in some length in Chapter 2. The graphs in Figure 6.2.1 show the comparison between a 10g rear impact on the previously validated surrogate ISO 10542 wheelchair and the Spectra wheelchair.

Initially the sled slid underneath the wheelchairs until the front tie-downs became taught, causing the rear wheels to compress with maximum wheel compression occurring at 80ms, coinciding with minimum P-point vertical displacement.

The most striking difference between the Spectra and surrogate rear impact simulations was the considerable deformation of the Spectra seat. The seat attached to the Spectra frame was the same one used in the ISO 16840-4 frontal validation model, discussed in the Chapter 5. The deformable seat, as opposed to the rigid seat of the surrogate wheelchair, resulted in larger horizontal displacements for the dummy's head.

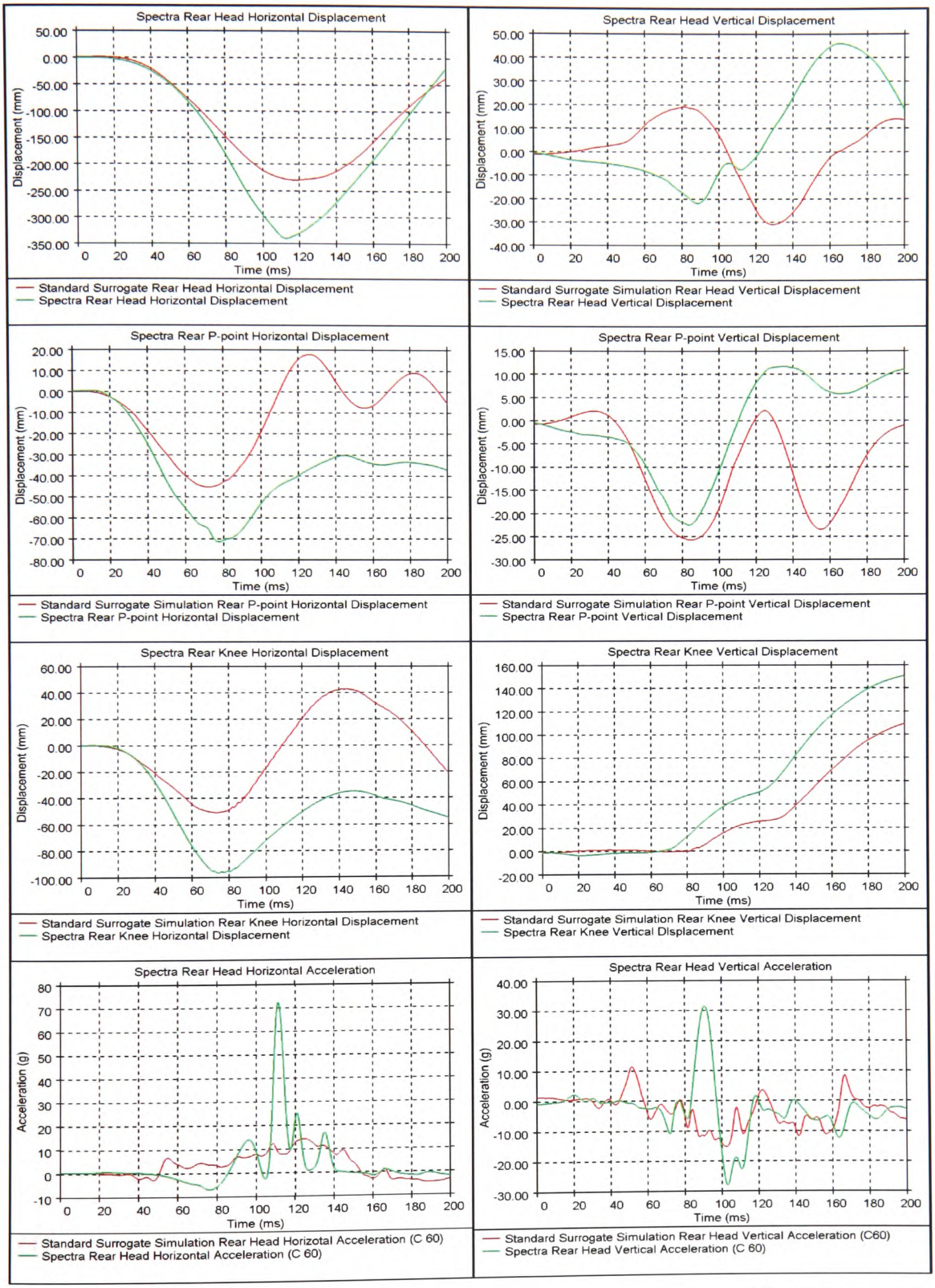

Figure 6.2.1 showing the graphical results of the surrogate and Spectra wheelchairs in a simulated 10g rear impact

The vertical displacement of the dummy's head was also greatly affected by the deformable seat. In Chapter 5, during the comparison between the physical and simulated rear impacts, it was noted that the head of the Hybrid III dummy was positioned forward of the shoulders and, when moving rearward in the rigid surrogate wheelchair, extended up before rotating backwards (see the graph for the vertical head displacement in Figure 6.2.1). The deformation of the Spectra seat allowed the torso of the dummy to move rearward with the head, keeping the neck straighter until impact with the head rest occurred. This effect is also noticeable in the screenshots of Figure 6.2.2 where the head of the Spectra wheelchair dummy moved back with the torso, reducing the bending of the neck. O'Neill [72] noted that as the torso of a motor vehicle occupant was accelerated forward the head lagged behind, causing an S-shape of the neck before the head 'whipped' backwards. Such motion can be seen in the screenshots of Figure 6.2.2 and is commonly associated with 'whiplash' injuries [36, 72, 129].

The head 'whipping' backwards towards the head rest in the Spectra model occurred at the same time as the rear wheels decompressed and the energy stored from the elastic deformation of the seat back was released. This resulted in the head rest moving forward to meet the rearwards moving head, increasing the relative velocity between the two and caused a large horizontal head acceleration of 120g, illustrated in Figure 6.2.1 at 110ms.

As no headrest was present on the surrogate rear simulation model no such acceleration spike from head impacting the headrest was observed. The inclusion of the head rest, although causing a larger head acceleration, significantly reduced hyperextension of the neck (see Figure 6.2.2). The mechanism of injury and the effects that the increased acceleration has on the occupants head are beyond the scope of this study.

A further contribution to the positive vertical displacement of the dummy's head in the surrogate wheelchair simulation was the effect of 'ramping' caused by the dummy's

torso sliding up the seatback. Ramping is an effect commonly associated with rigid seat backs [45]. Comparing the screen shots in Figure 6.2.2, between the surrogate and Spectra wheelchair simulations at 90ms, the dummy on the surrogate wheelchair can be seen to ride up the seatback, unlike the dummy in Spectra wheelchair whose ramping motion is prevented by the deformable seatback. It should be noted that the Hybrid III dummy has been found to underestimate the effects of ramping and so a real life occupant, or a dummy specifically designed to model rear impacts, such as the Rear Impact Dummy (RID2), would most probably show a greater amount of ramping in this instance [35].

The peak values for the P-point and knee horizontal displacement of the Spectra wheelchair were 17mm and 37mm greater, respectively, than that of the ISO 10542 surrogate wheelchair. This increase was a result of the heavier Spectra wheelchair, as also noticed in the frontal impacts, and the deformation of the Spectra seatpan. The vertical P-point displacement of wheelchair reduced as the front tie-downs became taught causing compression of the rear wheels. The energy stored in the compressed tyres was released and caused the wheelchair to rebound thus increasing the P-point value. This rebound was resisted by the rear tie-downs. In the case of the Spectra wheelchair the tension in the rear tie-downs caused slight compression in the rear wheels at 165ms, indicated as a decrease in P-point vertical displacement of 6mm. The surrogate wheelchair followed a similar trend to the Spectra up until 123ms where the tension in the rear tie-downs, resisting the rebound, caused much greater compression of the surrogate rear tyres, resulting in a reduction of P-point vertical displacement of 25mm.

The vertical knee displacements of the surrogate and Spectra wheelchair dummies followed a similar trend with the Spectra dummy's knee value being consistently higher than that of the surrogate dummy's, in line with the increased value of Spectra vertical P-point displacement.

The large peak in horizontal head acceleration of the Spectra model seemed excessive so the mechanism of the head contacting the headrest was looked at more closely. On impact the Spectra wheelchair moved rearwards causing the front tie-downs to become taught and in doing so compressed the rear wheels, with full tyre compression occurring at 80ms. The lumbar spine of the dummy was resisted by the base of the seatback as the upper torso rotated rearward, causing the seatback to deflect. During this period, from 80ms to 104ms, the head lagged behind the torso causing a forward bend of the neck. The seatback stopped deflecting, resisting any further rear rotation of the torso. The elastic energy stored in the deformed seatback was released and started to spring back. This motion coincided with the decompression of the rear wheels, which forced the wheelchair up and forwards. These combined effects forced the torso forward while the head was still moving rearward, causing the neck to bend backwards until it contacted with the headrest at 109ms. The rebound of the wheels had a similar effect, as observed in the frontal 20g simulation, in that it increased the relative velocity of the headrest and head, resulting in high head accelerations upon impact. This forward motion of the dummy's chest upon rebound, while the head was still moving rearwards, was also noted by Park and Park [49] who found that using integrated seatbelt seats reduced the effect by also supporting the occupant during rebound.

Rear impact summary

Along with the frontal surrogate and Spectra wheelchair comparisons the rear impact results show that the Spectra model followed similar trends to the surrogate model. The differences were far greater between the two rear models than the frontal simulations and this was largely due to the deformation of the Rookwood seatpan attached to the Spectra wheelchair. The deformation of the Rookwood seatpan acted in much the same way as the Volvo Whiplash Injury Prevention System (WHIPS) vehicle seat, whose seatback hinge yields to reduce the relative motion between the head and torso. This reduction of relative head to torso motion was found by O'Neill [72] to significantly reduce neck injury.

A further advantage that the Rookwood seatpan had over normal seating systems was their customisation to the individual. Correctly fitting backrests and headrests in close proximity to the occupant have been found to reduce neck injury in rear impacts by ensuring that the occupant is not out of position in the seat and that they are close to the head and back rest. Strother *et al.* [130] also found out of position occupants in rear crashes are more prone to ramping up the seat back [43, 72, 130].

Surrogate 10g Rear Impact	Time (ms)	Spectra 10g Rear Impact
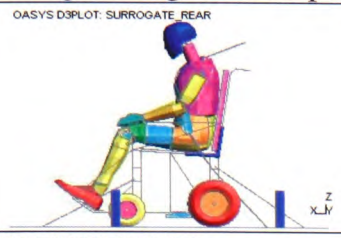	0	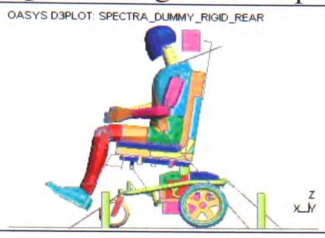
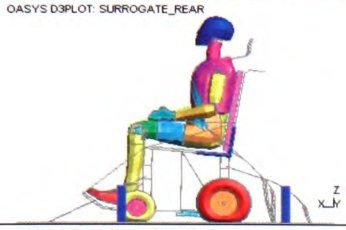	90	
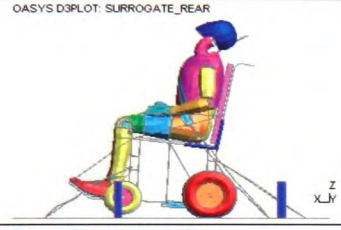	120	
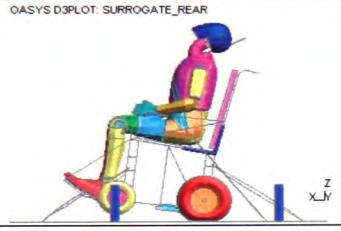	140	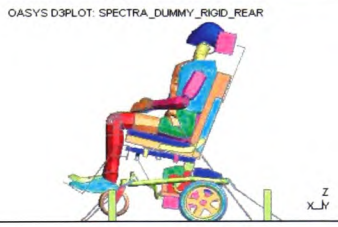
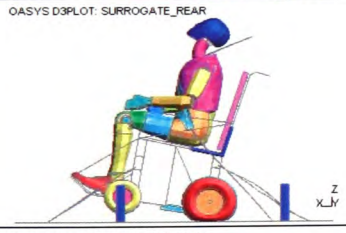	160	
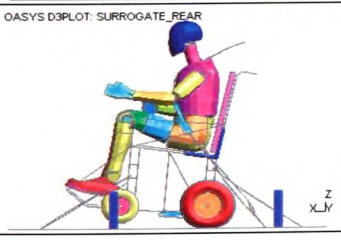	200	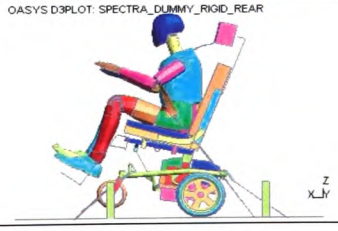

Figure 6.2.2 showing the screenshots comparing the simulated rear impact of the surrogate and Spectra wheelchairs

An important consideration with deformable seatbacks is the increased possibility of secondary impacts, e.g. vehicle interior, from larger occupant excursion. There also exists the possibility of seat failure, resulting in the collapse of the seat back [11]. The frame shots in Figure 6.2.3 were taken from a test conducted at Millbrook Proving Grounds whereby the Rookwood seatpan was attached to a manual wheelchair with the side support arms of the Rookwood seatpan removed. The impact forces were the same as for the rear ISO 10542 surrogate test with a 10g crash pulse. The failure of the seatpan in this test, although contrived, demonstrated the importance of sufficient seat back strength.

Rookwood seatpan, without side supports, mounted on a manual wheelchair in a rear 10g sled test

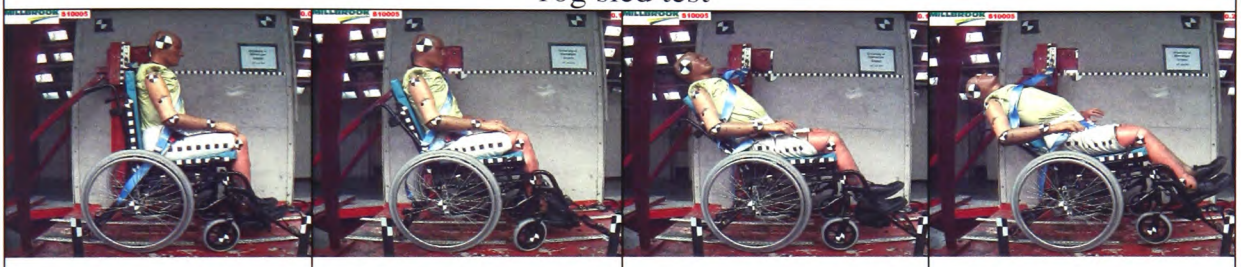

0ms	100ms	150ms	200ms

Figure 6.2.3 showing the result of seat failure in a rear 10g sled test

Although not within the scope of this project, it is recommended that the behaviour of the Rookwood seatpan in rear impact be looked at more closely. The crash pulse used here has a peak acceleration of 10g but the effect that a higher peak acceleration crash pulse could have, e.g. a 20g crash pulse, has not been considered.

Measurement Point	Excursion Limit	Surrogate wheelchair	Spectra wheelchair
Wheelchair P-point, X_{wc} (mm)	200	45	72
Dummy Knee, X_{knee} (mm)	375	50	97
Dummy head front, X_{headF} (mm)	650	0	0
Dummy head rear, X_{headR} (mm)	400	249	349
X_{knee} /X_{wc}	≥ 1	>1	>1
Does the movement of the occupant suggest that they will remain upright?	Occupant angle less than 45^0 from any angle	Yes	Yes
Battery movement	Within footprint of wheelchair and away from occupant	N/A	Yes

Table 6.2.1 assessing the crashworthiness of the ISO 10542 surrogate and Spectra wheelchairs in a rear 10g impact simulation

Table 6.2.1 compares the results from the surrogate and Spectra wheelchairs against the modified ISO 7176-19 crashworthiness criteria. Notice that both values for the forward head displacement, X_{headF}, are zero as it is a rear impact. The rearward head displacement, X_{headR}, for the surrogate wheelchair occupant was not ignored in this case. Although rearward crash tests are not yet required by ISO 7176-19 the results shown in Table 6.2.1 indicate that both the surrogate and Spectra wheelchairs would pass such a test if the excursion limits were the same as for the frontal 20g impact. An important caveat when considering rear impacts is that the Hybrid II and III dummy models have been found to have poor biofidelity due to overly stiff necks [35, 36]. This does not mean, however, that useful comparative data cannot be gained from their use.

6.3 Frontal impacts with the addition of life support equipment

One of the areas that the Rehabilitation Engineering Unit at Rookwood Hospital specialise in is adding life support equipment to wheelchairs. The equipment typically added to the wheelchairs was discussed in Chapter 4 and vary from patient to patient. The location at which this equipment is mounted affects the wheelchair's centre of gravity and also stability.

A typical setup of oxygen and suction pump, attached to the push bars behind the seat, was examined here. The equipment and support bracket had a combined mass of 13.6kg, see Chapter 4 for further details.

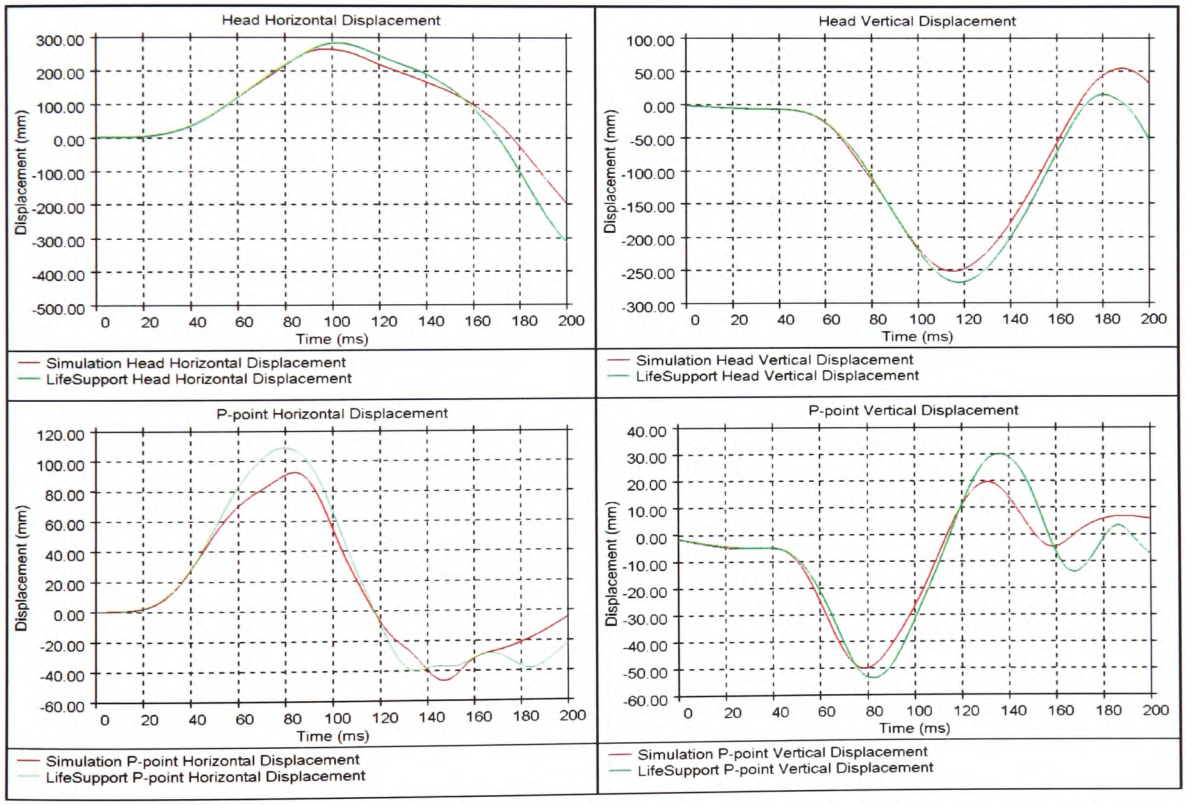

Figure 6.3.1 (a-d) showing the graphical results of a surrogate frontal impact with added Life Support equipment compared with standard frontal impact simulation

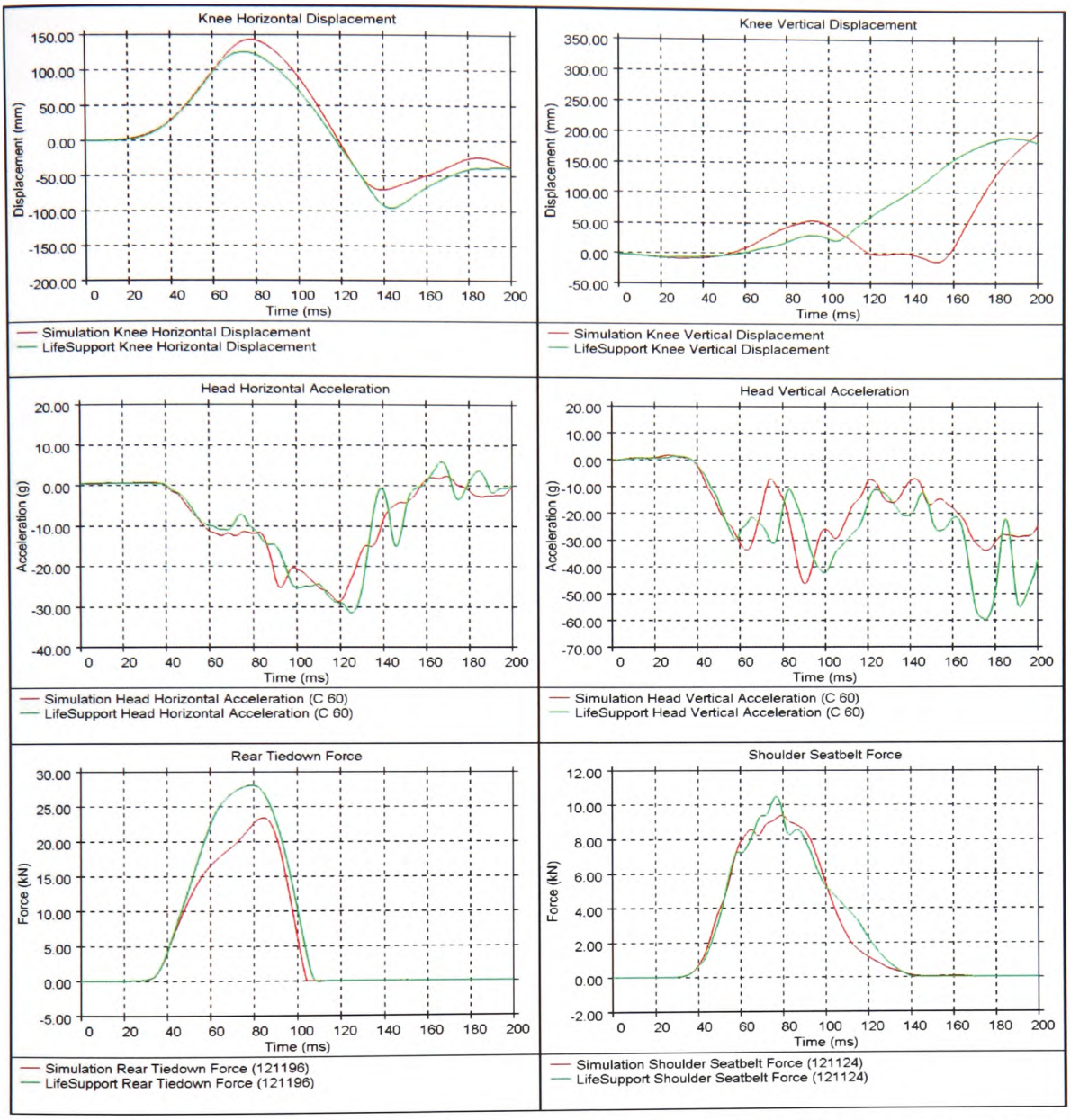

Figure 6.3.1 (e-j) showing the graphical results of a surrogate frontal impact with added Life Support equipment compared with standard frontal impact simulation

P-point horizontal and vertical displacements were observed to increase by 15mm and 14mm respectively due to the additional mass of the life support equipment. Head horizontal displacement also increased by 14mm. The increase in wheelchair excursion (P-point) caused increased stretch of the rear tie-downs and seatbelt resulting in increased axial load of 3.5kN for the tie-downs and 1.5kN for the seatbelt. The additional mass of the life support equipment at the rear of the wheelchair reduced the

forward rotation, as shown in Figure 6.3.2 at 144ms, causing a decrease of 15mm in horizontal knee displacement.

The peak head horizontal acceleration increased by 4g. The head vertical acceleration at 90ms was slightly less than without the addition of life support equipment but had a large peak at 175ms of -60g, a 56.7% increase from the standard frontal simulation. This corresponded to the point where the dummy was thrust back into the wheelchair seat back as the wheelchair itself was pulled forward from energy stored in the front tie-downs. This effect was far more aggressive than observed from the model without the addition of the life support equipment.

Simulated Surrogate 20g frontal impact	Time (ms)	Surrogate with life support equipment
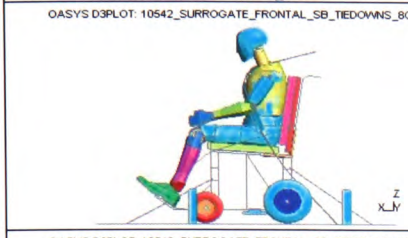	0	
	88	
	100	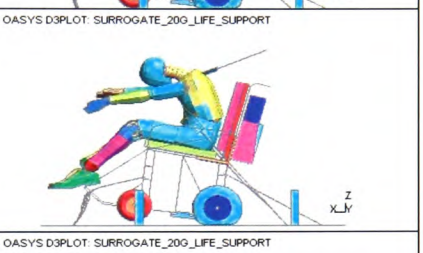
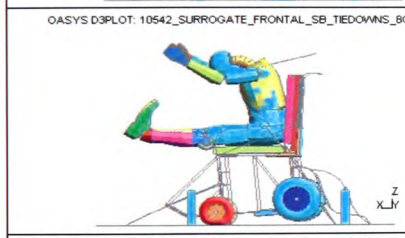	144	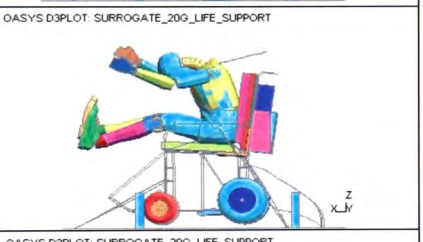
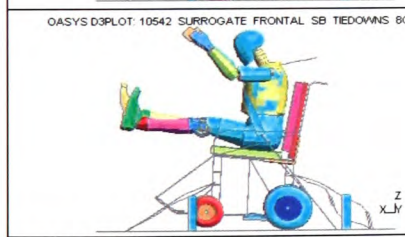	174	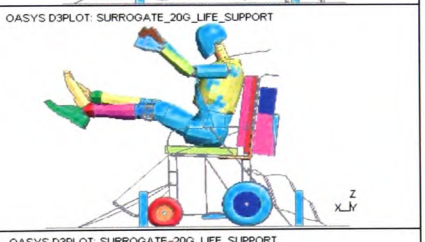
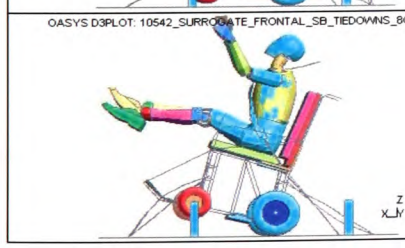	200	

Figure 6.3.2 showing Screen shots comparing the ISO 10542 surrogate frontal impact with added Life Support equipment with the standard frontal impact simulation

Life support summary

The results demonstrate that the effects of adding life support equipment to the wheelchair model can be captured accurately by the simulation process. It also shows that in the instance described, the additional equipment increased head and wheelchair excursion as well as increasing the tension on the rear tie-downs and occupant shoulder seatbelt.

As discussed in the literature review, Kang and Pilkey [47] as well as Bertocci *et al.* [14], looked at the least injurious position to attach the tie-downs with respect to the wheelchair's centre of gravity. Kang and Pilkey found the optimum attachment position of the tie-downs to be level with the centre of gravity while Bertocci *et al.* [14] found it to be slightly above (38-64mm above the centre of gravity). The addition of the life support equipment in the position described, i.e. behind the seat back, raised the centre of gravity, which in effect, lowered the distance of the rear tie-downs attachment point in relation to the wheelchair's centre of gravity. Unlike Bertocci *et al's* [14] findings the simulation herein caused an increase in the P-point horizontal displacement and no noticeable increase in the forward rotation of the wheelchair. This would tend to suggest that the additional mass attached to the wheelchair, in the form of the life support equipment, has a greater effect on the wheelchair's behaviour than the movement of the centre of gravity relative to the rear tie-down attachment point.

Measurement Point (mm)	Excursion Limit	Surrogate with equipment
Wheelchair P-point, X_{wc}	200	108
Dummy Knee, X_{knee}	375	125
Dummy head, X_{headF}	650	292.9
Dummy head rear, X_{headR}	400	N/A
X_{knee}/X_{wc}	≥ 1	>1
Does the movement of the occupant suggest that they will remain upright?	Occupant angle less than 45^0 from any angle	Yes
Battery movement	Within footprint of wheelchair	N/A

Table 6.3.1 assessing the crashworthiness of the ISO 10542 surrogate wheelchair with attached life support equipment in a rear 10g impact simulation

From comparing the changes to the wheelchairs behaviour, using the modified crash criteria table in Table 6.3.1, the addition of the life support equipment, in this instance, did not appear to compromise the crash safety of the wheelchair and occupant.

The other consideration when adding life support equipment to a wheelchair is whether or not the equipment will stay securely fixed to the wheelchair during a crash. The result of equipment becoming detached is a serious risk to the wheelchair occupant and other users of the vehicle. To accurately predict failure of support brackets and fixtures requires a high level of model detail that is beyond the scope of this project.

To analyse the support brackets in detail, or any other piece of equipment for that mater, the displacements of the push arms, to which they are attached, can be recorded. This displacements can then be applied to a detailed model of the support bracket without the need to model the wheelchair and occupant system. Such sub-system modelling is commonplace in the automotive industry and was used to record the pitch rate of a vehicle chassis, which was then applied to the test sled, as discussed in Chapter 4.

6.4 Pitching

All ISO wheelchair crash tests, as well as the published physical and simulated tests conducted, use sled based testing whereby lateral and vertical movement of the sled base are fixed. The following results show the effects that including the pitching of the transporting vehicle has on the dynamics of the wheelchair and occupant.

A pitch angle of 5.7^0, as found from truck simulation test conducted in Chapter 4, was used along with a scaled up pitch angle of 12.5^0, the pitch angle of the Ford Explorer in a 48km/hr frontal barrier test. Both pitch angles were compared with the standard horizontal sled test with zero pitch. Using two different pitch angles made it easier to identify the influence that the pitching effect had.

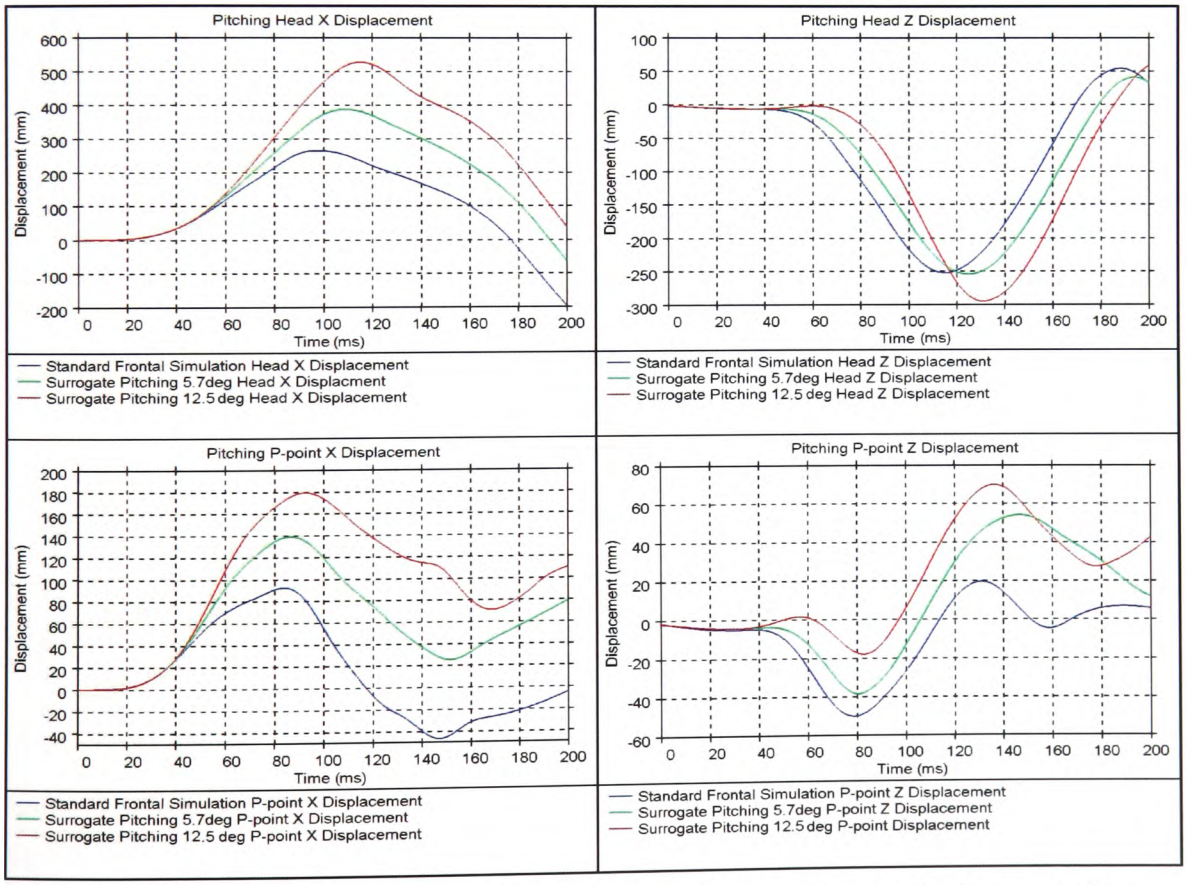

Figure 6.4.1 (a-d) showing the graphical results from the 0, 5.7 and 12.5 degree pitching simulations

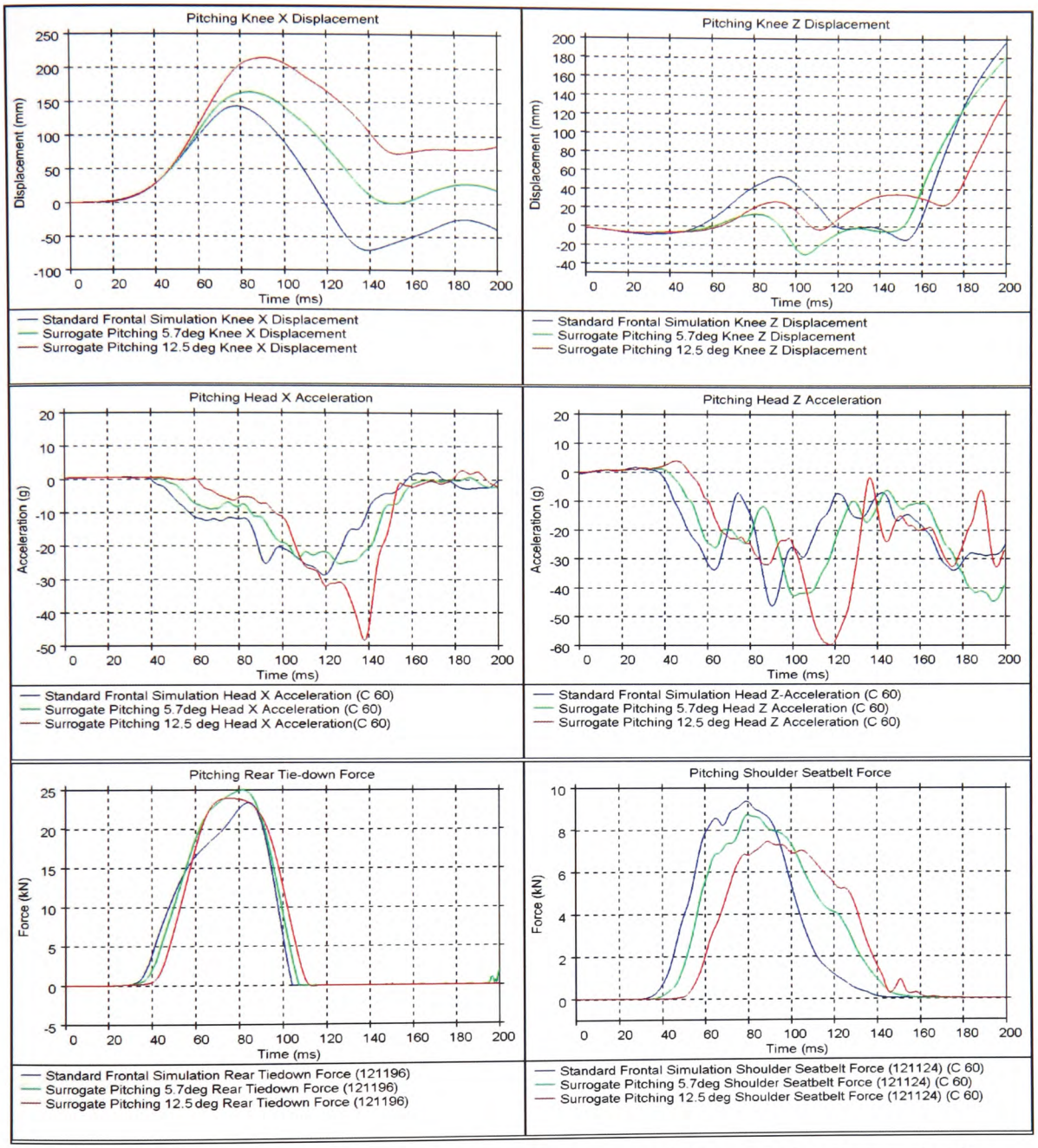

Figure 6.4.1 (e-j) showing the graphical results from the 0, 5.7 and 12.5 degree pitching simulations

The pitching wheelchair models had less initial reward rotation about their rear axle than the non-pitching model due to the sled dropping away beneath the front wheels. This caused the pitching models to rotate forward, counteracting the rear rotation from the compression of the rear wheels and the tightening of the rear tie-downs. From the graphs in Figure 6.4.1 this can be seen to have resulted in increased head and P-point

displacement in the X-direction. The screenshots at 88ms and 100ms, in Figure 6.4.2, show an increase in the dummy's back angle relative to the seatback and a decrease in angle between the dummy's torso and thigh as the pitch angle increased. As the rear wheels uncompressed and the front tie-downs became taught the wheelchair rotated forward. The 5.7^0 and, to a greater extent, the 12.5^0 pitching angles allowed the wheelchairs to rotate further forward before the front wheels came into contact with the sled (see the screen shots at 144ms in Figure 6.4.2). The forward rotation also coincided with the maximum values of P-point Z-displacements and minimum values of head Z-displacement, illustrated in Figure 6.4.1 (d and b). The decompression of the front wheels and the dummy rebounding into the seatback, caused secondary rear rotation of the wheelchair and occupant. As the front wheels of the non-pitching wheelchair came into contact with the sled first they were also the first to uncompress resulting in the screen shots at 174ms and 200ms in Figure 6.4.2, showing that the rear rotation of the non-pitching model occurred ahead of the 5.7^0 pitching model which in turn occurred before the 12.5^0 pitching model.

The head vertical and horizontal acceleration increased considerably with the 12.5^0 pitch angle but the 5.7^0 pitch angle, as with the vertical head displacement, showed little change in head acceleration, although, like the displacement, it did cause a slight delay of around 10ms.

Both the pitching models had higher rear tie-down peak forces than the non-pitching model with the 5.7^0 pitching model having a 1.4kN increase in tensile force and the 12.5^0 model having a 0.8kN increase. The shoulder seatbelt force of the 5.7^0 pitch model had a peak value of 8.6kN and the 12.5^0 pitch model had a peak value of 7.4kN, both lower than the peak value of 9.3kN for the non-pitching model.

Frontal Surrogate simulation	Time (ms)	Frontal Surrogate Simulation with 5.7^0 pitching effect	Frontal Surrogate Simulation with 12^0 pitching effect
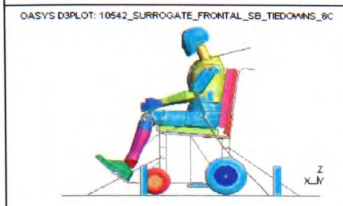	**0**		
	**88**		
	**100**		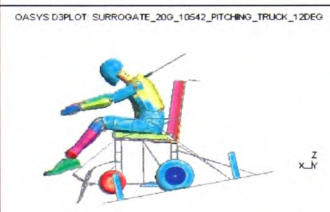
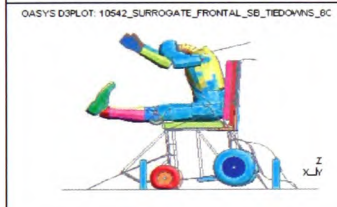	**144**		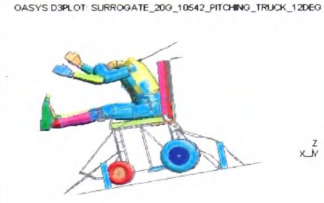
	**174**		
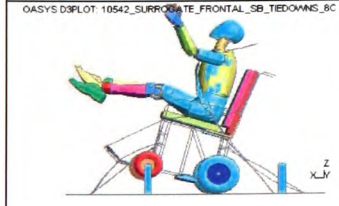	**200**		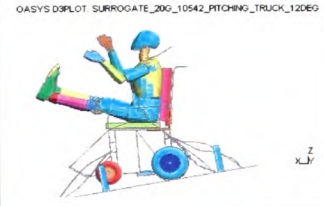

Figure 6.4.2 containing screenshots comparing 5.70 and 120 pitch angle with zero pitching

Pitching summary

The results show that the occupant's horizontal and vertical displacements and accelerations maybe underestimated if the pitching effect is not accounted for. The forward rotation of the wheelchair also increases with included pitching, as the screenshots at 144ms in Figure 6.4.2 show. Ignoring the effects of pitching could lead to an incorrect assumption regarding the safe carrying load of the wheelchair. The inclusion of pitching also shows that the sled test overestimates the seatbelt force on the occupant.

Measurement Point	Excursion Limit	Surrogate wheelchair with pitch angle 5.7^0	Surrogate wheelchair with pitch angle of 12.5^0
Wheelchair P-point, X_{wc} (mm)	200	139	180
Dummy Knee, X_{knee} (mm)	375	162	215
Dummy head front, X_{headF} (mm)	650	401.2	535.3
Dummy head rear, X_{headR} (mm)	400	N/A	N/A
X_{knee}/X_{wc}	≥ 1	>1	>1
Does the movement of the occupant suggest that they will remain upright?	Occupant angle less than 45^0 from any angle	Yes	Yes
Battery movement	Within footprint of wheelchair and away from occupant	N/A	Yes

Table 6.4.1 assessing the crashworthiness of the ISO 10542 surrogate wheelchair with pitch angle of 5.7^0 and 12.5^0 in a frontal 20g impact simulation

Despite the increase in occupant and wheelchair excursion, from the inclusion of sled pitching, the results are still within the modified ISO 7176-19 crashworthiness criteria, as shown in Table 6.4.1.

6.5 Addition of Solid tyres to wheelchair model

Both the wheels fitted to the surrogate wheelchairs during the physical sled tests had pneumatic tyres. The wheelchairs issued by the RE Unit vary between pneumatic and solid tyre wheels. In Chapter 3 both solid and pneumatic Spectra wheels were statically tested in compression. The results showed that the solid tyres were stiffer than their pneumatic equivalents. It was proposed that this would have an effect on the crash response of the wheelchair and occupant. Indeed, such sensitivity to wheel and tyre stiffness has been highlighted, to a somewhat lesser extent, by Kang *et al.* [47] whose simplified wheelchair and occupant model, used to model the behaviour of wheelchair tie-downs and seatbelt restraints, found that an increase in wheel stiffness caused a decrease in wheelchair excursion. Solid tyres were added to both the ISO 10542 surrogate and Spectra wheelchair models, with the surrogate model being examined first.

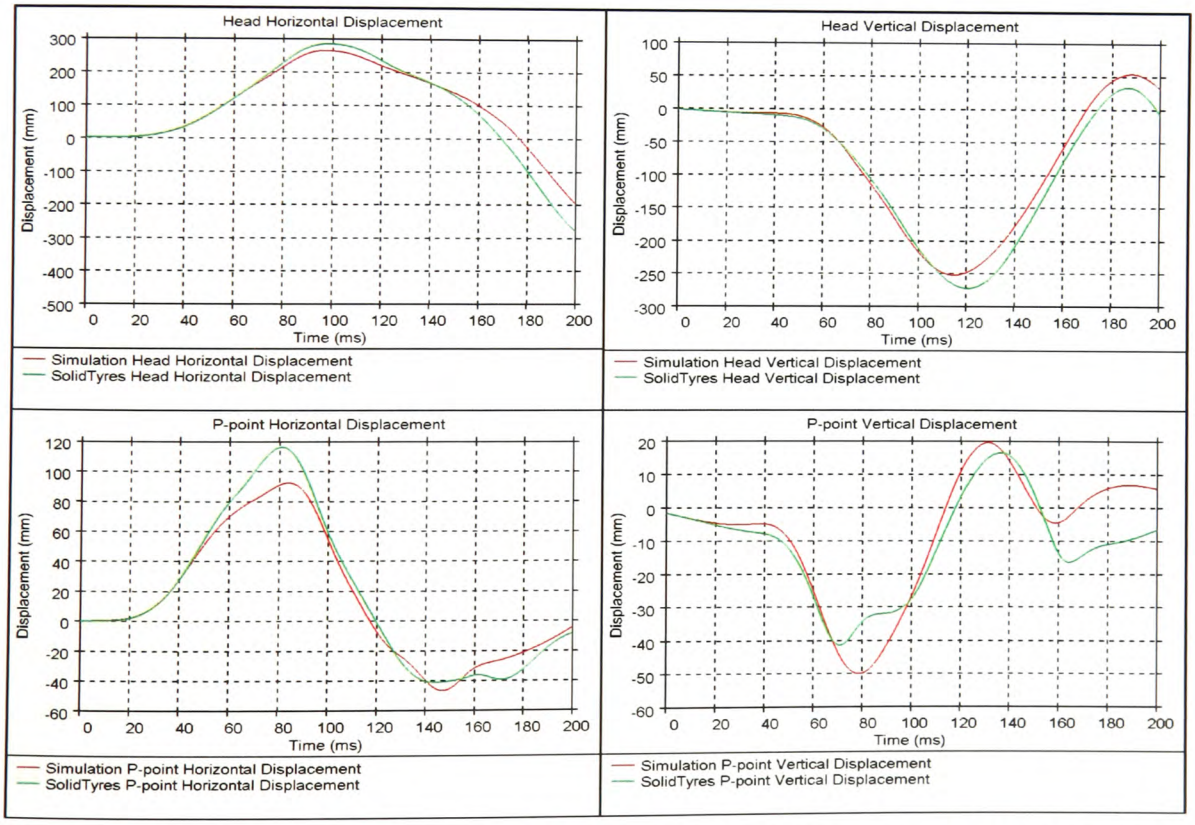

Figure 6.5.1 (a-d) showing the behavioural difference between the surrogate wheelchair with pneumatic and solid foam tyres

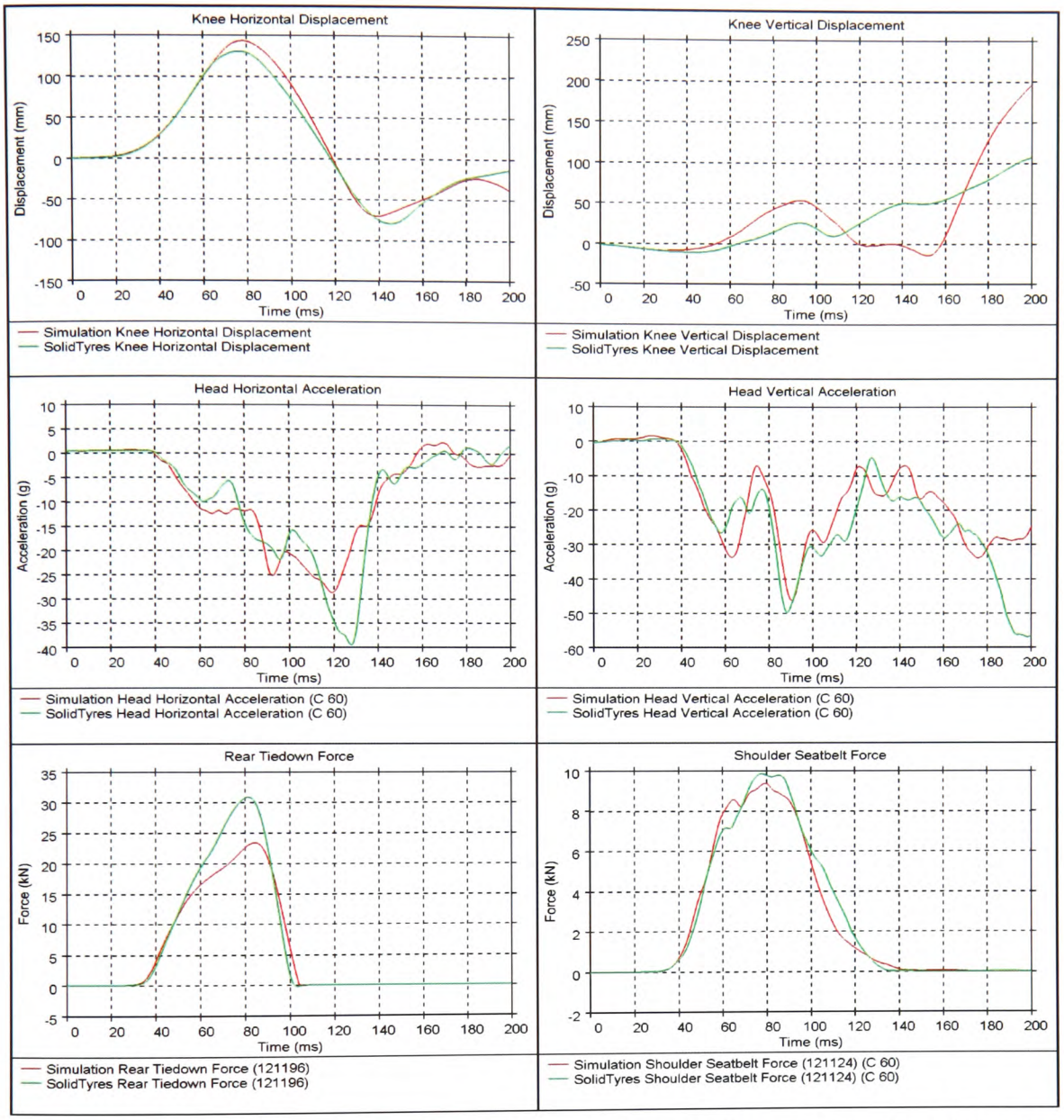

Figure 6.5.1 (e-j) showing the behavioural difference between the surrogate wheelchair with pneumatic and solid foam tyres

The most striking difference with the addition of the solid tyres to the ISO 10542 surrogate wheelchair was the reduction in P-point vertical displacement. The solid foam tyres are stiffer than the air filled tyres so consequently compressed less. This can be seen by the 10mm reduction in P-point vertical displacement in Figure 6.5.1 (d).

A considerable increase in head horizontal acceleration of 30% occurred at 128ms as the solid tyres offered less damping effect than the pneumatic tyres. The increased wheel stiffness resulted in a 2% increase in vertical head acceleration at 88ms. The large increase in vertical head acceleration at 200ms corresponds with the upper back of the dummy impacting with the top of the wheelchair seat, as can be seen in the screenshots in Figure 6.5.2 at the same time interval. The maximum horizontal P-point displacement was 117mm with the addition of solid tyres as compared to 92mm for the frontal sled simulation with pneumatic tyres. The force on the rear tie-downs also increased by 25.8%.

The results show that the solid tyres increase the horizontal displacement of the wheelchair and thereby the extension of the rear tie-downs. This can be explained if we consider the energy of the system. During compression of the deformable tyres more energy is absorbed than that of the solid tyres. This is energy that would otherwise have been absorbed by the tie-downs. The energy absorbed by the deformable tyres, as also observed by Hunter-Zawarski and Zawarski [24], is stored as elastic energy and then subsequently released, causing the wheelchair to be forced upwards. The increased compression of the pneumatic tyres can be seen at 88ms in Figure 6.5.2 and the subsequent spring back of the tyres can be seen at 144ms again in Figure 6.5.2.

Simulated 20g frontal impact	Time (ms)	Simulated frontal impact with solid tyres
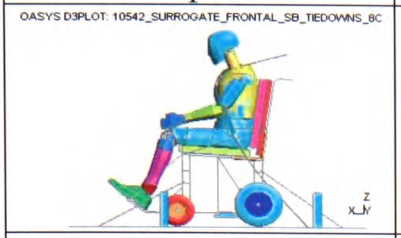	0	
	88	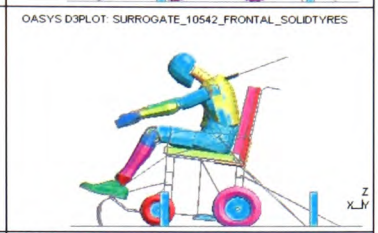
	100	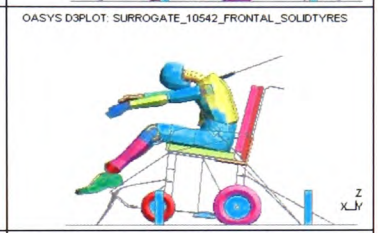
	144	
	174	
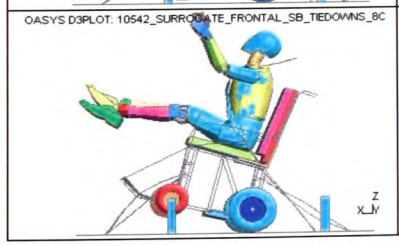	200	

Figure 6.5.2 showing the surrogate wheelchair with pneumatic tyres (left) and solid foam tyres (right) in a frontal 20g simulation

The effect of putting solid foam tyres on the Spectra wheelchair was also examined by comparing the results with those of the Spectra wheelchair fitted with pneumatic tyres.

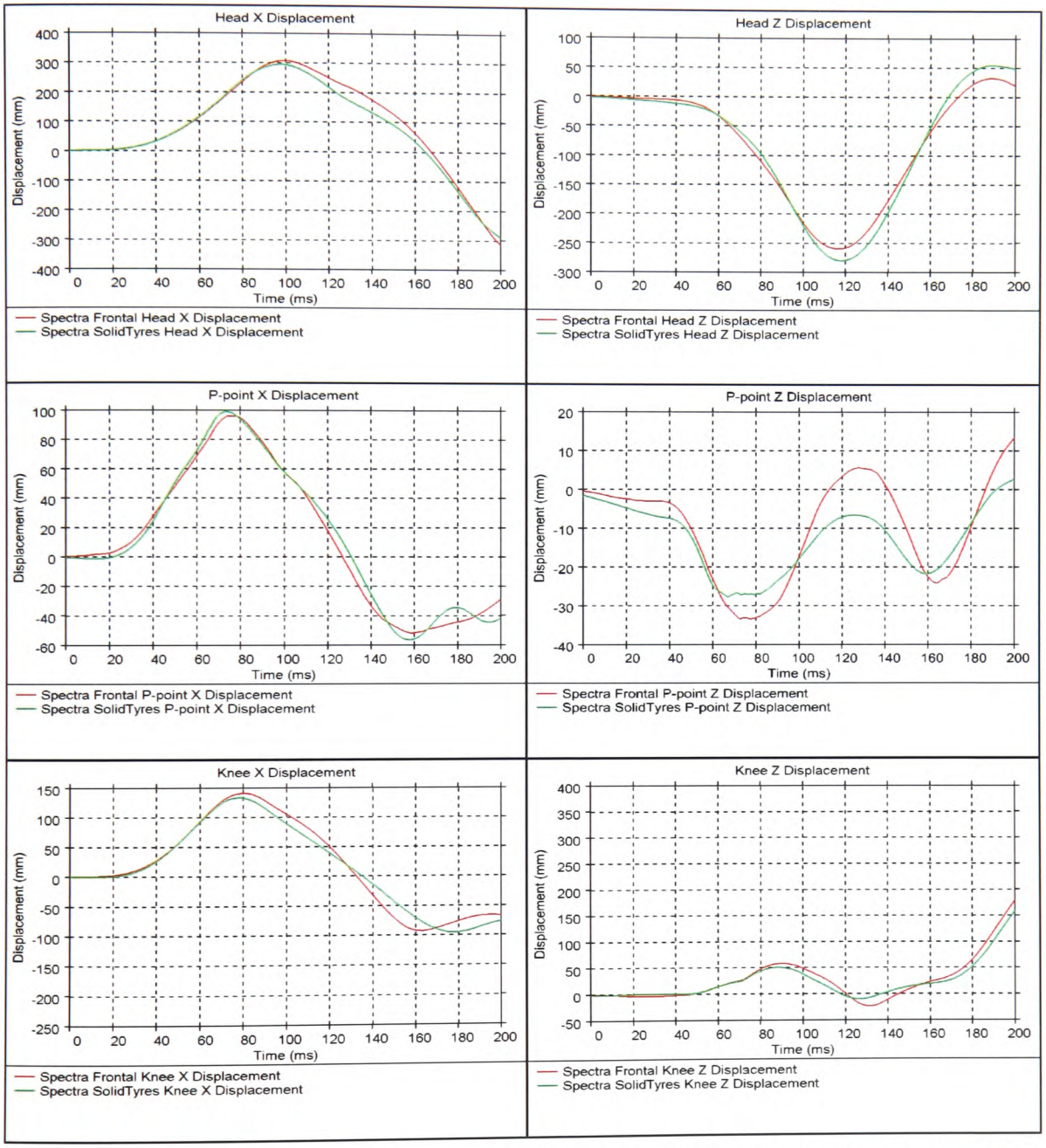

Figure 6.5.3 (a-f) showing the graphical results of adding solid tyres of the Spectra wheelchair model

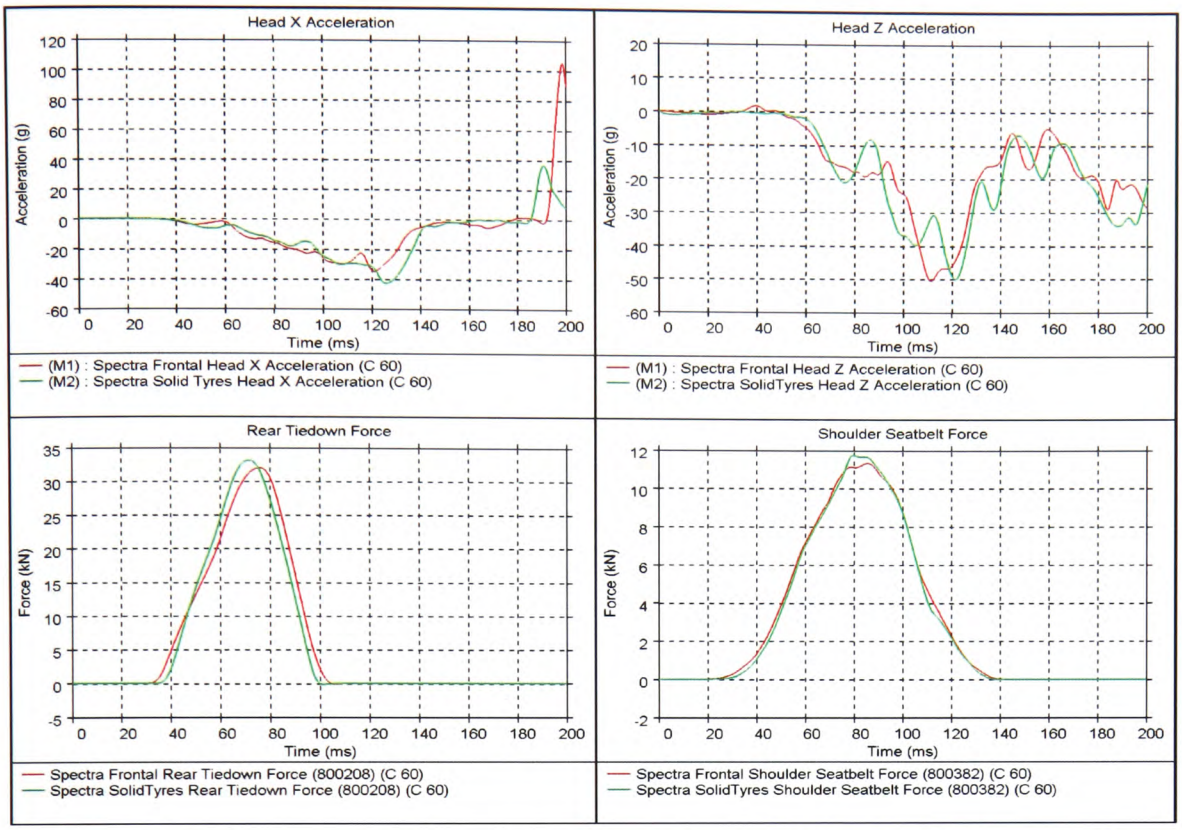

Figure 6.5.3 (g-j) showing the graphical results of adding solid tyres of the Spectra wheelchair model

Comparing the behaviour of solid tyres on the Spectra wheelchair, as well as that of the surrogate, was useful to determine whether the change in tyres had the same influence on the different wheelchair models, thus confirming the robustness of the solid wheel model. The materials of both the surrogate and Spectra wheels were the same but their geometries differed, with the surrogate tyre having a larger volume than the Spectra. Never the less, the graphs, in Figure 6.5.3, show that the trends do indeed match those observed when adding the solid tyres to the surrogate wheelchair.

With the exception of the head acceleration, adding solid tyres to the Spectra wheelchair had less of an affect than adding them to the surrogate wheelchair. The Spectra wheels, as previously discussed, had a lower profile and were narrower than the surrogate wheels, i.e. they have a lesser volume. Changing the Spectra tyres to solid foam filled tyres resulted in a lower change in stiffness as compared to the larger volume surrogate tyres.

The minimum head horizontal acceleration at 126ms, as with the surrogate wheelchair model, also increased with the addition of the solid tyres, although to a lesser extent. The maximum peak head acceleration upon the head striking the head rest, however, decreased considerably with the addition of the solid tyres and also occurred before that of the pneumatic wheeled model.

The considerable difference of the horizontal peak head accelerations, where the head impacted the headrest, between the pneumatic and solid wheeled models, at 198ms and 190ms respectively, was due to the potential energy stored by the rear tyres in compression, as discussed for the surrogate wheelchair model. The reduced compression of the stiffer solid tyres was responsible for the increase in horizontal head acceleration at 125ms. The potential energy (equal to $1/2kx^2$, where k is the tyre stiffness and x is the compressive displacement) of the solid tyres was less, despite being more stiff than the pneumatic tyres, due to the lower x^2 term. On decompression this caused a less aggressive rebound of the wheelchair and subsequent reduction in headrest rebound into the occupant's head.

Spectra (Pneumatic Tyre) Frontal Simulation	Time (ms)	Spectra Solid Tyre Simulation
	0	
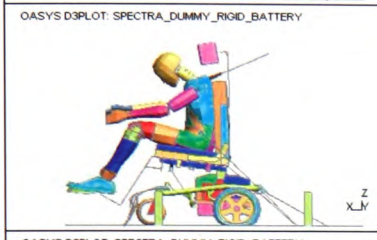	88	
	100	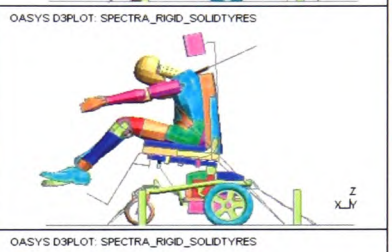
	144	
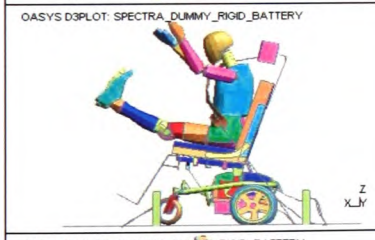	174	
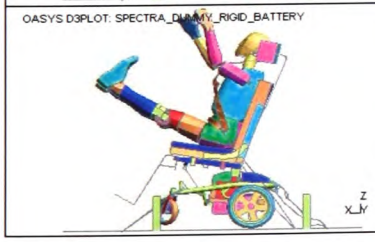	200	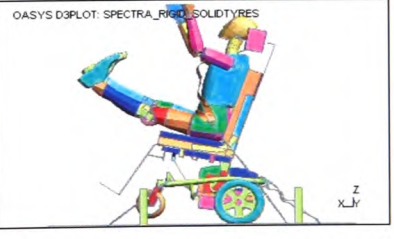

Figure 6.5.4 showing the screenshots of the Spectra wheelchair with pneumatic and solid tyres

Solid Tyre summary

The addition of solid tyres to both surrogate and Spectra wheelchairs produced little difference in occupant excursion, although the dummies in both cases tended to rebound into the seat back before that of the pneumatic tyre simulations. The forces on the rear tie-downs in both cases increased, as did the head accelerations. The solid tyres were observed to reduce the amount of spring back of the wheelchairs, the effect caused by energy from the compressed tyres being released. This effect was far more noticeable with the surrogate wheelchair. As a result of this there is little change in the crashworthiness criteria shown in Table 6.5.1.

The results show a different outcome to the ones found by Kang *et al.* [47] who observed a decrease in wheelchair horizontal excursion with stiffer tyres. Precise details of the wheelchair computer model used by Kang *et al.* [47] are unknown but from their published work their model appears to be simplified to a greater extent than the one used here.

Measurement Point (mm)	Excursion Limit	Surrogate wheelchair with solid tyres	Spectra wheelchair with solid tyres
Wheelchair P-point, X_{wc}	200	117	99
Dummy Knee, X_{knee}	375	130	137
Dummy head front, X_{headF}	650	296	310
Dummy head rear, X_{headR}	400	N/A	294
X_{knee}/X_{wc}	≥ 1	>1	>1
Does the movement of the occupant suggest that they will remain upright?	Occupant angle less than 45^0 from any angle	Yes	Yes
Battery movement	Within footprint of wheelchair and away from occupant	N/A	Yes

Table 6.5.1 assessing the crashworthiness of the ISO 10542 surrogate and Spectra wheelchairs with solid tyres in a frontal 20g impact simulation

6.6 Skewed frontal impacts at 60^0

As with the pitching simulations, neither physical nor computer simulated tests of skewed wheelchair and occupant impacts have been investigated, from the literature reviewed. The majority of impacts will contain some degree of lateral loading, unless perfectly head on, so it is important that the behaviour of both the wheelchair and occupants in skewed impacts be considered.

The graphs in Figure 6.6.1 and screenshots in Figure 6.6.2 and Figure 6.6.3 show the results of the surrogate and Spectra skewed impacts at 60^0 to the front of the vehicle. This is representative of an impact directed towards the right hand side of the occupant. In this instance the displacements and accelerations in the Y-direction are considered. The forces on the right and left rear tie-downs are also considered separately due to the uneven loading on them from a skewed impact.

As mentioned in the Chapter 4, the skewed simulations were conducted with the seatbelt over the left and then over the right shoulder. Rather than remodelling the seatbelt the load vector was changed from 60^0 (simulating seatbelt over right shoulder) to 300^0 (simulating seatbelt over left shoulder). The same 20g crash pulse as the frontal impacts was used.

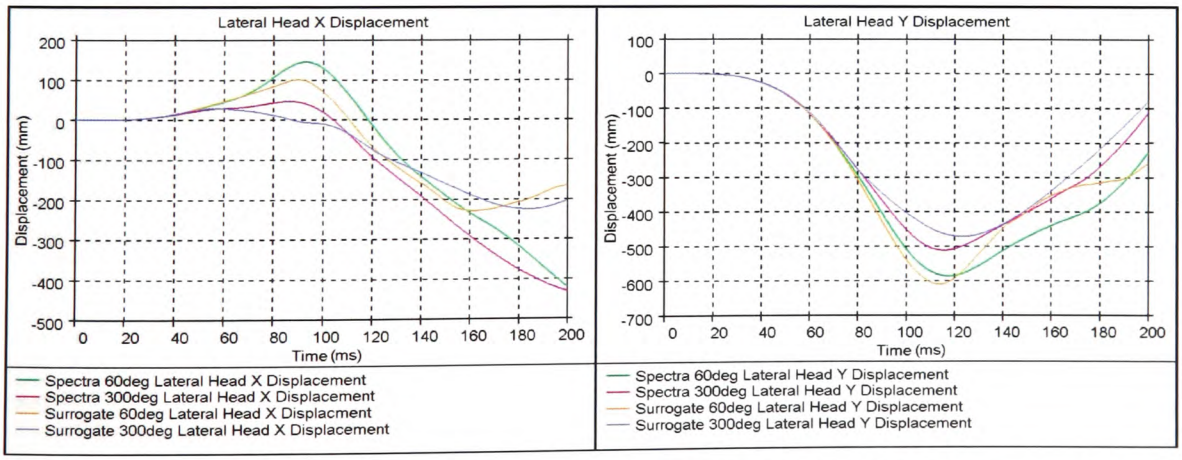

Figure 6.6.1 (a,b) showing the graphical results of the lateral impacts for the surrogate and Spectra wheelchair models with left and right shoulder seatbelts

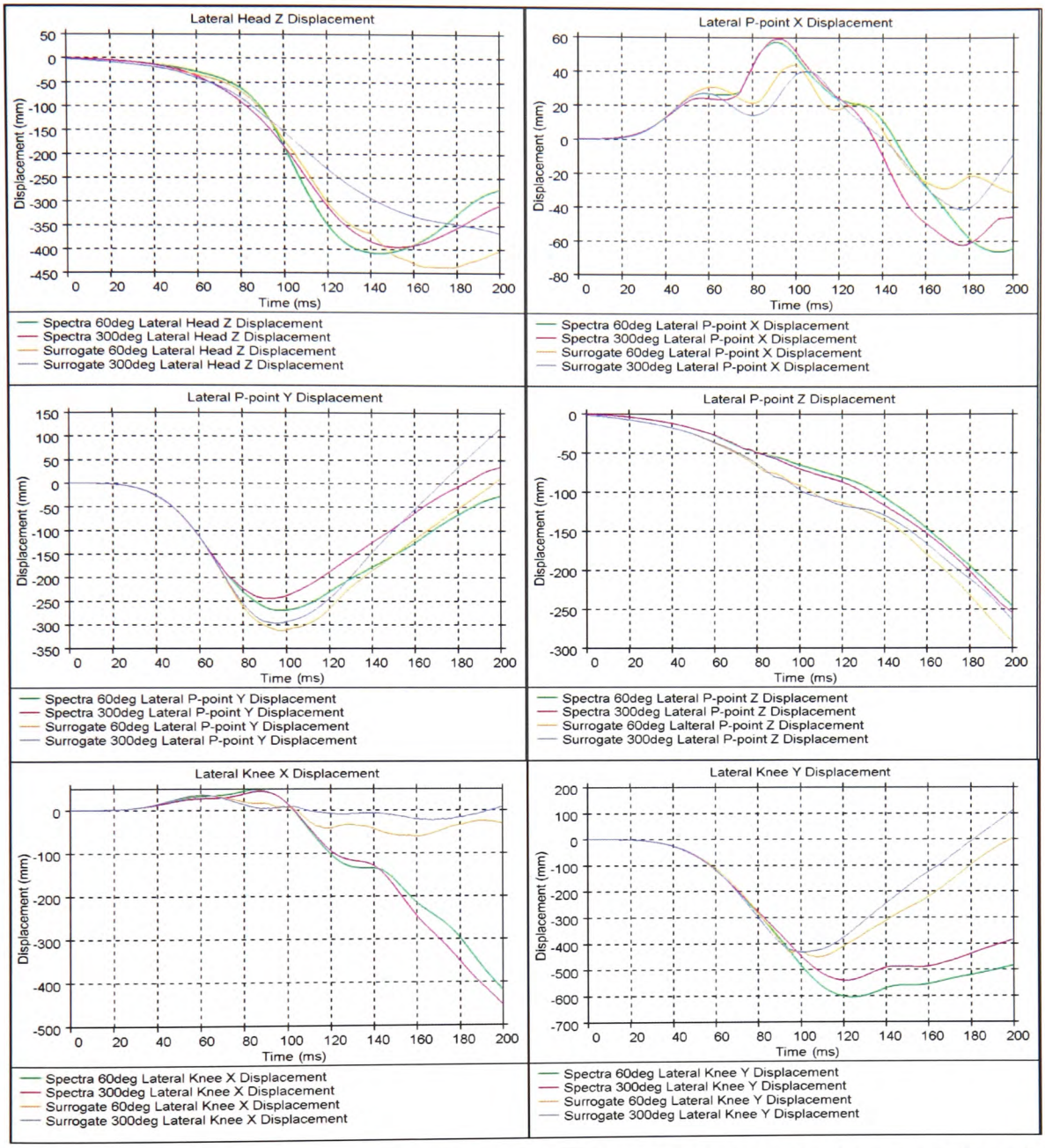

Figure 6.6.1 (c-h) showing the graphical results of the lateral impacts for the surrogate and Spectra wheelchair models with left and right shoulder seatbelts

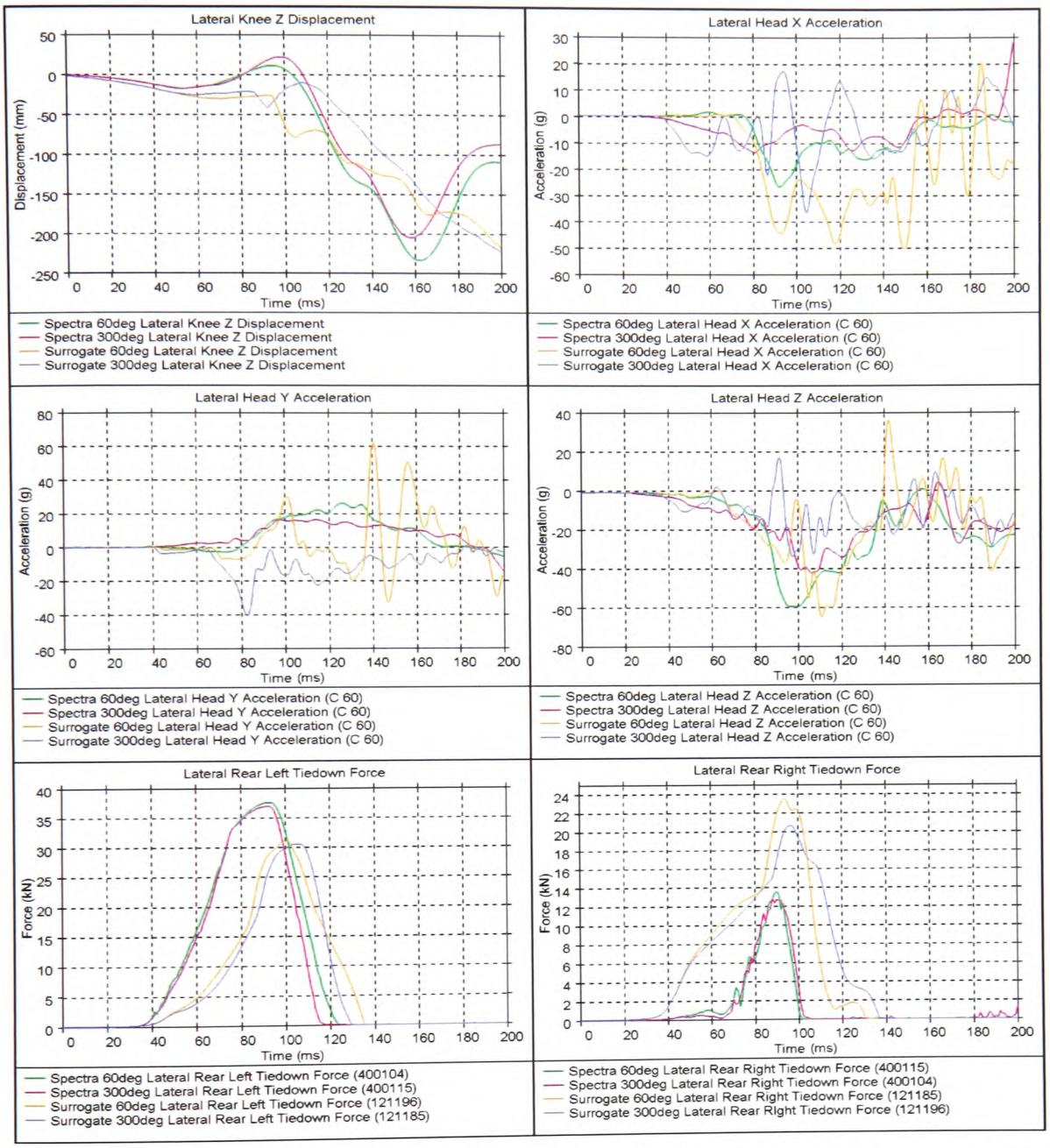

Figure 6.6.1 (i-n) showing the graphical results of the lateral impacts for the surrogate and Spectra wheelchair models with left and right shoulder seatbelts

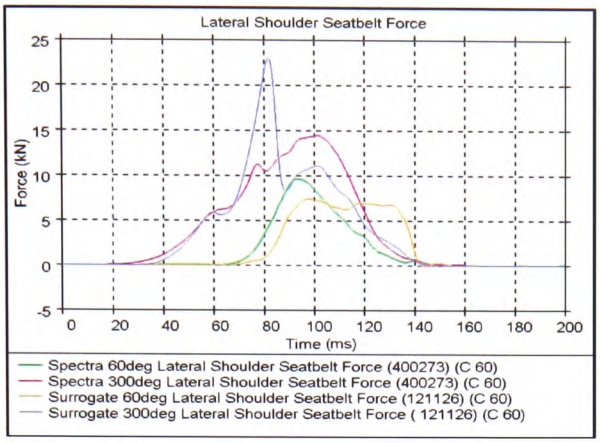

Figure 6.6.1 (o) showing the graphical results of the lateral impacts for the surrogate and Spectra wheelchair models with left and right shoulder seatbelts

The series of screen shots in Figure 6.6.2 illustrate the behaviour of the surrogate wheelchair and dummy in a 60^0 skewed impact and Figure 6.6.3 illustrates the same impact scenario for the Spectra wheelchair and occupant. The screenshots on the left have the seatbelt positioned over the occupant's left shoulder and the screenshots on the right have the seatbelt positioned over the occupant's right shoulder.

The orientation of the front and rear tie-downs are designed to primarily stabilise the wheelchair in fore and aft directions. The specified angle of the rear tie-downs to the vertical Z-plane, from ISO 10542-1, was 10^0 [1], offering little lateral support, see Figure 4.3.2.

As the skewed simulation began the wheelchair slid sideways. Considerable lateral distortion of the wheelchair tyres was observed at 80ms in both surrogate and Spectra models (Figure 6.6.2 and Figure 6.6.3). At this point the tie-downs became taught as they resisted further movement of the wheelchair. This corresponded with the peak value in tie-down axial force observed in the graph in Figure 6.6.1 (n), with the peak force of the surrogate tie-downs lagging those of the Spectra tie-downs by 20ms.

Surrogate wheelchair – Skewed impact at 60^0 to front		
Left shoulder seatbelt	Time(ms)	Right shoulder seatbelt
	0	
	80	
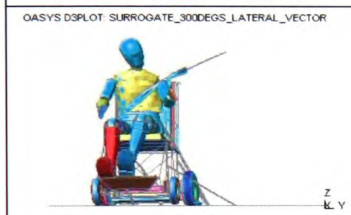	94	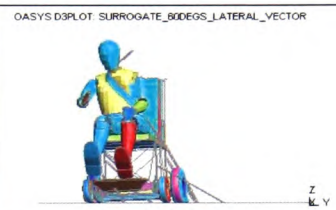
	104	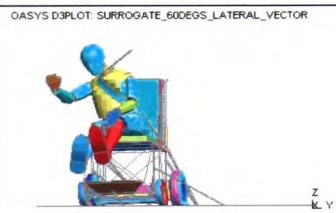
	120	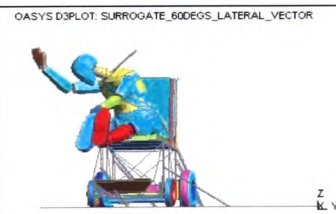
	166	
	200	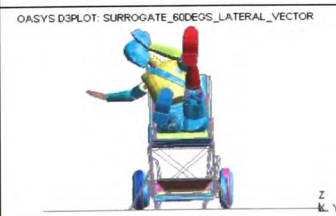

Figure 6.6.2 showing the screenshots of the 60^0 lateral impact on the surrogate wheelchair with right and left shoulder seatbelts

The screenshot frames at 80ms and 94ms in Figure 6.2.2 and Figure 6.2.3 show the seatbelt sliding up the shoulder and onto the neck of the right hand model whereas the right shoulder of the left hand model rotated forward about the left shoulder. From the graphs in Figure 6.6.1 this can be seen to result in a greater head displacement in all directions for the left shoulder belt model when compared to the model with right hand shoulder belt. Having the seatbelt across the shoulder opposite to the side of impact would therefore seem to reduce excursion of the occupants head by limiting the rotation of the torso.

Comparing the head accelerations between the two wheelchair models it can be seen that the head of the dummy in the Spectra wheelchair experiences considerably lower accelerations in both the X and Y directions (see Figure 6.6.1). This can be explained when the motion of the dummies torso and lower body is considered. The rigid side support of the surrogate wheelchair, in the form of the fixed armrest, restrained the lateral motion of the dummy's body but not the head, which was free to move after the body had been restrained. The Spectra wheelchair, on the other hand, offered limited torso and lower body lateral restraint so allowed the body to move laterally along with the head, consequently reducing the acceleration experienced by the head. The effect was similar to the deforming seatback, observed in the Spectra rear impacts, which allowed the torso to move with the head.

The highest peak values for head Z acceleration occurred with the right shoulder seatbelt models. The action of the right shoulder seatbelt riding up onto the neck resisted further movement of the upper body and neck but allowed the head to whip across the right shoulder, hence causing the high head Z acceleration. This effect can be observed clearly in the surrogate wheelchair model at 104ms, 120ms and 166ms in Figure 6.6.2.

The P-point displacements were similar for all runs, as one would expect. The Spectra wheelchair had a greater X displacement but lower Y and Z displacements as compared to the surrogate wheelchair. The components affecting the movement of the

wheelchairs were the tie-downs and wheels. The Spectra wheels had a lower profile than the surrogate wheels, making them less prone to lateral (Y-displacement) and compressive (Z-displacement) deformation.

The X and Y displacements of the knee varied considerably between the two wheelchairs. The surrogate wheelchair, with its rigid arm rest, offered far greater lateral restraint to the occupant than that of the Spectra wheelchair. The arm rest of the Spectra wheelchair, consisting of a single vertical bar, deformed considerably and allowed a large lateral movement of the occupant.

The graph of force against time, for the shoulder seatbelt over the left shoulder seatbelt models, had a peak value of 22.6kN and 14.5kN for the surrogate and Spectra wheelchairs respectively. The right shoulder seatbelt forces were lower at 7.4kN for the surrogate wheelchair and 9.5kN for the Spectra wheelchair. At 104ms the right shoulder of the right hand model dummy was restrained by the seatbelt, allowing the left shoulder to rotate rightwards. The seatbelt of the left hand model restrained the dummy across its chest without riding up the shoulder, thus limiting the torso rotation. The right hand model's dummy continued to rotate to the right at 120ms with a distinct rotation of the neck about the seatbelt. The left hand model showed lateral bending of the neck but without the rotation. The occupants rebounded into their seats at 166ms and the wheelchairs were pulled back towards their initial position as the energy built up in the tie-downs was released.

The graph in Figure 6.6.1 (o), showing the seatbelt force for the left shoulder surrogate wheelchair model, has a spike at 82ms of 22.6kN. This was caused by 1D seatbelt element penetration of both the dummy shoulder joint and the 1D beam element wheelchair frame. The penetration was observed in earlier frontal impact models and corrected by adjusting the contact stiffness and modelling the wheelchair frame with 2D elements where contact occurred. Although these steps reduced the penetration in this instance a certain amount of penetration still occurred that would need further model adjustment to correct.

Spectra wheelchair – Skewed impact at 60^0 to front		
Left shoulder seatbelt	Time(ms)	Right shoulder seatbelt
	0	
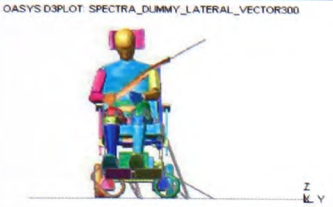	80	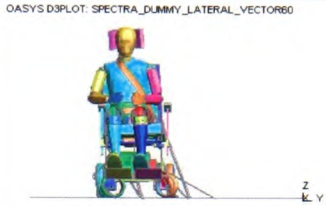
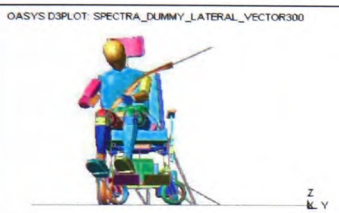	94	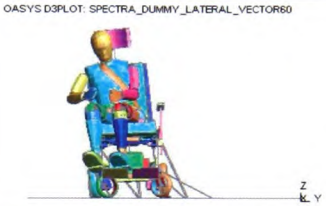
	104	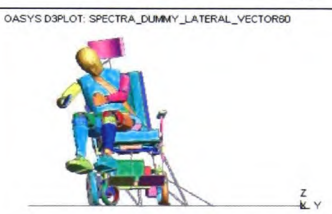
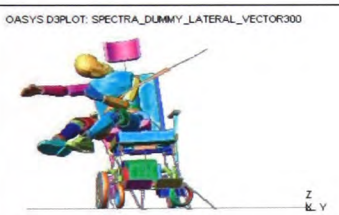	120	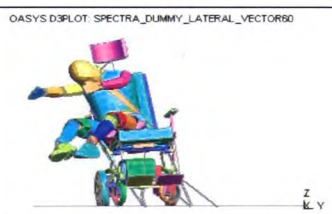
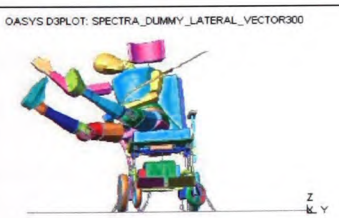	166	
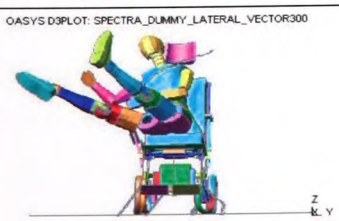	200	

Figure 6.6.3 showing the screenshots of the 600 lateral impact on the Spectra wheelchair with right and left shoulder seatbelts

Measurement Point	Excursion Limit	Surrogate wheelchair Left shoulder belt	Surrogate wheelchair Right shoulder belt	Spectra wheelchair Left shoulder belt	Spectra wheelchair Right shoulder belt
Wheelchair P-point, X-Y_{wc} (mm)	200	X: 40, -41 Y: -297	X: 44, -29 Y: -313	X: 59, -62 Y: -243	X: 58, -66 Y: -270
Dummy Knee, X-Y_{knee} (mm)	375	X: 37, -25 Y: -432	X: 36, -61 Y: -452	X: 45, -451 Y: -540	X: 50, -416 Y: -606
Dummy head, X-Y_{head} (mm)	X: -400 to 650 Y: -650 to 650	X: 28, -226 Y: -470	X: 100, -230 Y: -610	X: 47, -433 Y: -511	X: 146, -421 Y: -586
X_{knee} /X_{wc}	≥ 1	<1	<1	<1	<1
Does the movement of the occupant suggest that they will remain upright?	Occupant angle less than 45^0 from any angle	Yes	Yes	No	No
Battery movement	Within footprint of wheelchair and away from occupant	N/A	N/A	Yes	Yes

Table 6.6.1 comparing the maximum excursions of the surrogate and Spectra wheelchairs against ISO 7176-19 crashworthiness criteria

Table 6.6.1 shows the comparison of the skewed impact displacements with the modified crashworthiness criteria from ISO 7176-19 [3]. Both X and Y values were considered due to the extra dimension that skewed impacts imply. From the graphs in Figure 6.6.1 it can be seen that the X-displacements have distinctive maximum and minimum values whereas the Y-displacement values tended to have only a distinctive minimum value. To account for this both maximum and minimum peak values were entered for the X-displacements. The results in Table 6.6.1 show that all the skewed crash simulations tested exceed the P-point limit of 200mm in the Y-direction. Similarly, all the knee excursions in the Y-direction also exceed the limit of 375mm.

The head displacements were altered slightly for the skewed simulations. As the head moved in both X and Y directions it was decided to take the displacement measurements from the centre of gravity of the head rather than the foremost and rearmost points, as used in the frontal crash scenarios. The displacement limits for the

X-displacement were set to be between -400mm (representing rearward head motion) to 650mm (representing forward head motion), in line with the previous compared simulations. The Y-displacement limits were set between -650 to 650mm, the same as the forward head displacement limits. Table 6.6.1 shows that the rearward head motion for both Spectra skewed simulations (left and right shoulder belt setups) exceed the excursion limit of 400mm. The ratio of knee displacement to wheelchair (P-point) displacement (X_{knee}/X_{WC}) was taken between both X and Y corresponding maximum values. In each scenario the worst case result was used. All four of the scenarios in the skewed simulations had values where $X_{knee}/X_{WC} < 1$, failing the criteria of $X_{knee}/X_{WC} \geq 1$. From Table 6.6.1 it can be seen that all the skewed simulations failed the modified ISO 7176-19 crashworthiness criteria.

Skewed impact summary

Unless a vehicle crash is perfectly head-on there will be some lateral component to the impact. The simulations demonstrate the vulnerability of the occupant in such a crash, the inability of the wheelchair to offer adequate occupant protection (excessive deformation of the Spectra arm rests) and the ineffectiveness of the tie-downs to offer sufficient lateral support. The skewed simulations conducted agree with the findings of Gavelin *et al.* [91] who found that motor vehicle occupants restrained by a 3-point harness tended to rotate towards the impact zone.

The increased displacement of the lower body due to insufficient arm rest/side support in the Spectra wheelchair could result in secondary impact between the occupant and the vehicle interior. The simulation of the 60^0 skewed impact, with the seatbelt over the left shoulder, was re-run with the interior space of a Citroën Dispatch van (a typical wheelchair transporting vehicle, see Figure 1.3.2) surrounding it. The results in Figure 6.6.4 and Figure 6.6.5 clearly show secondary impact between the side of the vehicle and the occupant's arm and leg.

The modified ISO 7176-19 crashworthiness criteria used to assess the skewed results was the same as that used for the frontal simulations except with the addition of

Y-displacements. It could be that the criteria needs to be modified in order to compensate for skewed impacts but at present no such recognised standard exists to base it on. A further consideration is the lack of biofidelity of the Hybrid III dummy's neck in lateral and rear impact [54, 59]. Vehicle manufactures use specialist dummies such as the EuroSID or BioSID when analysing side impact injury [54, 66].

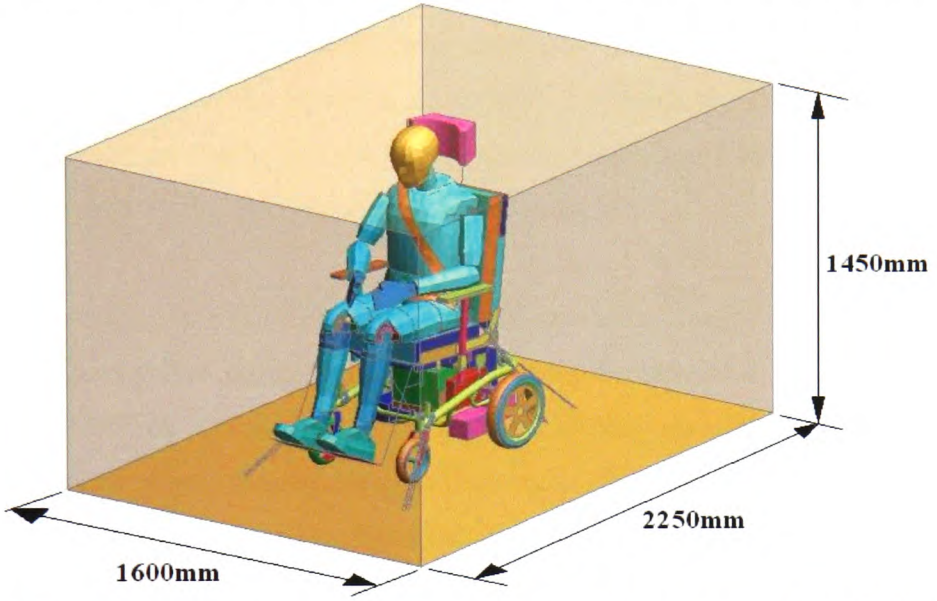

Figure 6.6.4 showing the dimensions of the rear compartment of a Citroen Dispatch [131].

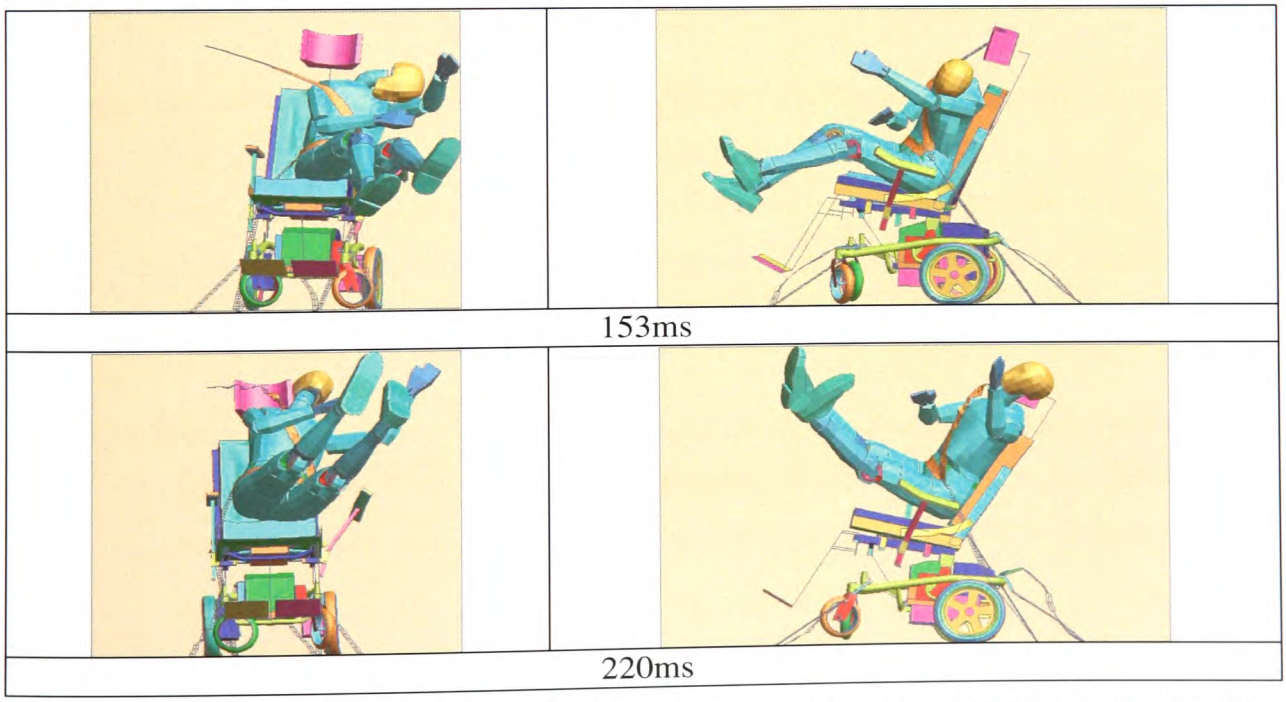

Figure 6.6.5 showing the secondary impact between the interior of the vehicle (orange box) and the occupant.

6.7 Results summary

The results demonstrate the ability of the simulation process to capture many of the requirements of ISO 7176-19, allowing an informed risk assessment of the wheelchair's crashworthiness to be made.

The ISO 10542 surrogate wheelchair was validated in Chapter 5 and was used in this Chapter as a reference for the Spectra wheelchair simulations. This logical progression gives support to use of the Spectra wheelchair model to make informed judgements on the crashworthiness of the wheelchair and occupant.

A number of other crash scenarios were performed and their outcome analysed. The addition of life support equipment was particularly pertinent to the RE Unit and showed that the effects on crashworthiness from adding mass to the wheelchair, in the form of life support equipment, could be captured. Although in the case investigated it was not to the detriment of the crashworthiness of the wheelchair.

The results can be summarised as follows

Comparison of frontal impact between surrogate and Spectra wheelchair models

Small increase in Spectra occupant head displacement.

Reduced Spectra P-point vertical displacement as a result of stiffer tyres.

Increased mass of Spectra wheelchair resulted in larger horizontal displacement and greater tie-down and seatbelt forces.

Comparison of rear impact between surrogate and Spectra wheelchair models

Considerable difference in occupant head displacement due to deformable Spectra seat back, as opposed to the rigid seat of the surrogate wheelchair.

Addition of life support equipment in a frontal impact

Increase in wheelchair mass caused an increase in wheelchair and occupant excursion along with increased tie-down and seatbelt forces.

Effects of Pitching

Increased occupant head displacement and acceleration as well as increased frontal wheelchair rotation.

Small increase in rear tie-down forces and small decrease in shoulder seatbelt forces.

Solid tyres

Decrease in P-point vertical displacement and increase in P-point horizontal displacement. Head horizontal acceleration decreased considerably. There was also an increase in tie-down and seatbelt forces.

Little change in dummy head and knee displacement.

Skewed Impact

Insufficient lateral support offered by the Spectra arm rests.

Large lateral displacement of the occupant increased the chance of secondary impact with the vehicle interior.

The seatbelt positioned over the right shoulder (the shoulder on the side of the impact) caused higher acceleration to the head than the seatbelt over the left shoulder. Higher head accelerations were recorded in both the surrogate runs, as compared to the Spectra runs, due to reduced occupant excursion from the stiffer side supports.

The four skewed simulations analysed failed the modified ISO 7176-19 crashworthiness criteria.

Chapter 7 - Conclusions and Recommendations for Future work

The aim of this thesis was to investigate the feasibility of computer modelling to aid the RE Unit's risk assessment of the crash safety of their specialist wheelchair and seating devices. The results from the validation in Chapter 5 indicate that the computer simulation techniques described are indeed capable of replicating real life sled test results. The validation results do have room for improvement, however, especially in the case of the ISO 10542 surrogate wheelchair wheels that caused excessive rebound when uncompressed. Consequently the models discussed in this thesis should be assumed to overestimate the rebound phase of the impact (at approximately 120ms) and consequently cause increased values of head acceleration upon contact with the headrest, where fitted. Further work developing an improved surrogate wheel model is therefore recommended. This should include static compression testing, as with the Spectra wheels described in Chapter 3, and an improved airbag algorithm to replicate the hysteresis nature of the tyre decompression.

Modelling the air in the tyres with the 'Simple Pressure-Volume' airbag definition in LS-Dyna is recommended due to its simplicity. Problems occur, however, during rebound. When looking at car impacts the rebound is often of less interest so the simple pressure-volume model will suffice. Compared with the weight of a vehicle, the effect of rebound energy will be less than on the much lighter wheelchair setup. In the case of the wheelchair, the release of energy from the compressed tyres was seen to be considerable. In practise the full compression of a tyre in a crash and its subsequent expansion is not 100% efficient. Energy will be lost due to the heating of the tyre and air loss through the tyre bead. Such energy losses can be modelled by using a more sophisticated airbag algorithm within LS-Dyna. The 'Simple_Airbag_Model' airbag algorithm allows an exit hole to be defined, which represents air loss during tyre compression, and also allows for energy loss through heat transfer [85].

Regrettably there was no physical data to compare the Spectra wheelchair model against. This model was therefore compared against the front and rear ISO 10542 surrogate wheelchair models. Only the wheelchair itself varied between the Spectra and surrogate models with the occupant, seatbelt, tie-downs and sled remaining the same. Although the results from the two models differed, the Spectra model was observed to function correctly, with any differences between the two models being accounted for. It is proposed that the same technique of comparison against the surrogate wheelchair models be used to assess the behaviour of other wheelchair systems constructed by the RE Unit. In this way a systematic link is maintained between physical and virtual crash tests.

The production wheelchair crashworthiness criterion from ISO 7176-19 [3] was modified to produce a guide for assessing crashworthiness for the simulated models. The sections of the ISO 7176-19 crashworthiness criterion that were omitted were mostly the examination of post-crash test measurements as it was deemed too costly to run the simulation to cover a 3 second time interval, which would allow the dummy and wheelchair to come to a complete rest. With improved computer resources longer run times would become more economical. It is therefore recommended that a multi-processor computer be used for subsequent work. A further cost implication, aside from that of the computer, is the licensing of LS-Dyna, which is charged for per processor.

The crash scenarios examined, such as skewed impact and sled pitching, explored loading conditions that could be expected in an actual crash. Although such crash scenarios are not required by current wheelchair crash test standards they could be used to enhance the RE units transport risk assessment, increasing confidence in the RE unit to issue their modified wheelchairs for use in transport and ultimately improve the safety of the wheelchair occupants. It should be reiterated at this point that the crash simulations discussed are not intended to replace physical sled testing but to provide the RE unit with a more informed method of assessing wheelchair transport safety where physical sled testing is not possible. The wheelchair models created were

used to highlight areas in wheelchair crash safety, hitherto untested, that are cause for concern.

Rear impact simulations between the surrogate and Spectra wheelchairs demonstrated that some deformation of the seat back reduces occupant ramping and neck bending, as found by previously published work on vehicle seats by Warner *et al.* [45]. The importance of using a head rest during transportation could be seen from the results of the surrogate rear impact, without head rest, which caused the typical S-shape bending of the occupant neck commonly associated with whiplash injuries [72].

The results from the addition of life support equipment in a frontal crash showed an adverse affect on the behaviour of the occupant and wheelchair by increasing tie-down and seatbelt forces and increased occupant excursion. The added mass did not, in the specific setup examined, cause the wheelchair to fail the modified ISO 7176-19 crash criteria. Although the equipment was modelled as lumped mass the forces on the equipment and retaining tray could be examined more closely by taking nodal displacements histories from the attaching nodes and applying them to a more detailed model of just the life support equipment and retaining tray. This method of node history was used to examine the behaviour of the Rookwood seatpan and is discussed in more detail in Appendix B. A Further consideration of adding life support equipment to wheelchairs is the additional force exerted on the tie-downs. The tie-downs are tested to ISO 10542-1 [1] using an 85kg surrogate wheelchair and a 75kg dummy. It is not uncommon for wheelchairs and occupants to exceed these weights and considerable care should be taken in such cases.

The novel investigation into skewed impacts highlighted the vulnerability of occupants from insufficient lateral support, resulting in a high chance of secondary impact. Large lateral excursion of the wheelchair was also observed from the fore and aft bias of the tie-down setup. Unless an impact occurs perfectly head-on there will be some degree of lateral motion and the findings show that the Spectra wheelchair design and its securement method are ill equipped to deal with this.

A further contribution to the large lateral excursion of the wheelchair in the skewed impacts was the lateral deformation of the pneumatic tyres. Further work to investigate whether or not solid foam wheels would reduce this effect would be worthwhile.

Legislation does not currently require skewed or rear testing to be carried out so there is little incentive for manufactures to address these short failings in wheelchair safety. It is the authors opinion, however, that any side support arms that are modified by the RE unit should also have their ability to resist lateral movement of the occupant considered.

The mechanism of how side impacts in vehicles differ from frontal impacts was touched upon in the literature review in Section 2.3.1. In the simulations of skewed impacts, presented in Chapter 5, the frontal 20g crash pulse was used. In reality this crash pulse would be different as the mechanism of the deceleration through the deformation of the vehicle body would be dependent on the position of the impact on the vehicle body. To increase the realism of the skewed simulations a crash pulse modelled on the deceleration of the vehicle at the particular skewed impact should be applied to the sled. This could be done by utilising the model of the Chevrolet truck that was used to find the pitch rate in Chapter 4. A skewed barrier impact of the truck could be set up and the deceleration rate recorded then applied to the sled of the skewed wheelchair impact model.

The non-standard ISO tests demonstrated the wheelchair computer model's sensitivity to different crash scenarios and also highlighted potential limitations in the wheelchair's ability to adequately protect the occupant, especially in the case of skewed impacts.

The wheelchair model with added life support equipment could be used in future work to assess the wheelchair's static and dynamic stability in normal use. The static stability of the each custom wheelchair produced by the RE Unit is currently tested by

inclining it to an angle of 16^0 with the occupant insitu. This practice, although common place, can be harrowing for the wheelchair user and requires a number of people to be present to prevent the wheelchair from tipping over should it become unstable. If the wheelchair is found to be unstable the user will have to be sent away whilst the wheelchair is modified. Considerable cost and time could be saved if such a test could be done virtually. Dynamic stability is considerably harder to test for in practice. A wheelchair that would be stable on an incline at rest or at constant velocity could become unstable if accelerated up the same incline. Again this can be tested for virtually using the same model as used for the virtual crash testing. Preliminary work on both static and dynamic testing has already been investigated by the author and presented to the Institute of Physics, Engineering and Medicine (IPEM) in York [132].

Thesis References

1. ISO 10542-1, Technical systems and aids for disabled or handicapped persons - Wheelchair tie-down and occupant-restraint systems, International-Organization-for-Standardization, 2001
2. Gibson, C. *Risk Management - Why? How? Who?* in *Risk Management in Vehicle Transportation for People in Wheelchairs meeting*. 2000. Botanical Gardens, Birmingham: Institute of Physics and Engineering in Medicine.
3. ISO 7176-19, Wheeled mobility devices for use as seats in motor vehicles, International-Organization-for-Standardization, 2005
4. Bertocci, G., Wheeled Mobility Device Database for Transportation Safety Research. *Assistive Technology*, 1997. **9**(2): p. 102-115.
5. Bertocci, G. *Transport Safe Wheelchair Seating*. in *State of Science*. 2001. Washington, D.C: RESNA Press.
6. Bertocci, G., Digges, K., and Hobson, D., Shoulder belt anchor location influences on wheelchair occupant crash protection. *Journal of Rehabilitation Research & Development*, 1996. **33**(3): p. 279-289.
7. Bertocci, G., Ha, D., Van Roosmalen, L., Karg, P., and Deemer, E., Evaluation of wheelchair drop seat crashworthiness. *Medical Engineering and Physics*, 2001. **23**(4): p. 249-257.
8. Bertocci, G., Manary, M., and Ha, D., Wheelchairs used as motor vehicle seats: Seat loading in frontal impact sled testing. *Medical Engineering and Physics*, 2001. **23**(10): p. 679-685.
9. Bertocci, G., Souza, A.L., and Szobota, S., The effects of wheelchair-seating stiffness and energy absorption on occupant frontal impact kinematics and submarining risk using computer simulation. *Journal of Rehabilitation Research and Development*, 2003. **40**(2): p. 125-130.
10. Bertocci, G.E., Szobota, S., Hobson, D.A., & Digges, K, Computer Simulation and Sled Test Validation of a Powerbase Wheelchair and Occupant Subjected to Frontal Crash Conditions. *IEEE Transport Rehabilitation Engineering*, 1999. **7**(2): p. 234-244.

11. Bertocci, G.E., Szobota, S, Ha, D.R., Van Roosmalen, L, Development of Frontal Impact Crashworthy Wheelchair Seating Design Criteria Using Computer Simulation. *Journal of Rehabilitation and Development*, 2000. **37**(5): p. 565-572.

12. Bertocci, G.E., Esteireiro, J., Cooper, R.A., Young, T.M., and Thomas, C., Testing and evaluation of wheelchair caster assemblies subjected to dynamic crash loading. *Journal of Rehabilitation Research and Development*, 1999. **36**(1): p. 32-41.

13. Bertocci, G.E. and Evans, J., Injury risk assessment of wheelchair occupant restraint systems in a frontal crash: A case for integrated restraints. *Journal of Rehabilitation Research and Development*, 2000. **37**(5): p. 573-589.

14. Bertocci, G.E., Hobson, D.A., and Digges, K.H., Development of transportable wheelchair design criteria using computer crash simulation. *IEEE Transactions on Rehabilitation Engineering*, 1996. **4**(3): p. 171-181.

15. Bertocci, G.E., Hobson, D.A., and Digges, K.H., Development of a wheelchair occupant injury risk assessment method and its application in the investigation of wheelchair securement point influence on frontal crash safety. *IEEE Transactions on Rehabilitation Engineering*, 2000. **8**(1): p. 126-139.

16. Colvin, D.P., McKinney, R.A., and Shaw, G., Crash-safe wheelchair seating systems for children. *American Society of Mechanical Engineers, Bioengineering Division (Publication) BED*, 1999. **42**: p. 459-460.

17. Cooper, R.A., O'Connor, T.J., Gonzalez, J.P., Boninger, M.L., and Rentschler, A., Augmentation of the 100kg ISO wheelchair test dummy to accomodate higher mass: A technical note. *Journal of Rehabilitation Research & Development*, 1999. **36**(1).

18. Digges, K., Occupant restraints and wheelchair tie-downs. *Annals of Biomedical Engineering*, 1991. **19**(5): p. 645.

19. SAE J2249: Wheelchair tiedowns and occupant restraint systems - surface vehicle recommended practice., Engineers, S.o.A., 1999

20. Geyer, M.J., Brienza, D.M., Bertocci, G.E., Crane, B., Hobson, D., Karg, P., Schmeler, M., Trefler, E., Wheelchair seating: a state of the science report. *Assistive Technology*, 2003. **15**(2): p. 120-128.

21. Gu, J., Roy, P. *Optimization of the wheelchair tiedown and occupant restraint system.* in *15th International Technical Coference on Enhanced Safety of Vehicles*. 1996. Melbourne (Australia).

22. Ha, D., Bertocci, G., Deemer, E., van, R., Linda, and Karg, P., Evaluation of wheelchair back support crashworthiness: combination wheelchair back support surfaces and attachment hardware. *Journal of Rehabilitation Research and Development*, 2000. **37**(5): p. 555-563.

23. Ha, D., Bertocci, G., Karg, P., and Deemer, E., Evaluation of wheelchair sling seat and sling back crashworthiness. *Medical Engineering and Physics*, 2002. **24**(6): p. 441-448.

24. Hunter-Zaworski, K.M. and Zaworski, J.R., Progress in wheelchair securement: Ten years after the Americans with disabilities act. *Transportation Research Record*, 2001(1779): p. 197-202.

25. Kang, S.J. and Chun, B.K., Strength Analysis of Automotive Seat Belt Anchor. *International Journal of Vehicle Design*, 2001. **26**(5): p. 496-508.

26. Le Claire, M., Visvikis, C., Oakley, C., Savill, T., & Edwards, M, *The Safety of Wheelchair Occupants in Road Passenger Vehicles*. 2003, Department for Transport: UK.

27. Shaw, G. and Gillispie, T., Appropriate protection for wheelchair riders on public transit buses. *Journal of Rehabilitation Research and Development*, 2003. **40**(4): p. 309-319.

28. Shaw, G., Lapidot, A., Scavnicky, M., Schneider, L.W., and Roy, P. *Interlaboratory study of proposed compliance test protocol for wheelchair tiedown and occupant restraint systems.* in *Proceedings of the 38th Stapp Car Crash Conference*. 1994. Fort Lauderdale, FL, USA: SAE, Warrendale, PA, USA.

29. Van Roosmalen, L., Wheelchair Integrated Occupant Restraints: Feasibility in Frontal Impact. *Medical Engineering and Physics*, 2001. **23**: p. 687-698.

30. Van Roosmalen, L., Preliminary Evaluation of Wheelchair Occupant Restraint System Usage in Motor Vehicles. *Journal of Rehabilitation Research and Development*, 2002. **39**(1): p. 83-93.

31. Van Roosmalen, L., Bertocci, G., Ha, D., Karg, P., and Szobota, S., Proposed test method for and evaluation of wheelchair seating system (WCSS) crashworthiness. *Journal of Rehabilitation Research and Development*, 2000. **37**(5): p. 543-553.

32. Van Roosmalen, L. and Bertocci, G.E., Adaptation of integrated restraint (IR) technology for use in the wheelchair transportation industry. *Annual International Conference of the IEEE Engineering in Medicine and Biology - Proceedings*, 1999. **1**: p. 605.

33. Van Roosmalen, L., Bertocci, G.E., Ha, D., and Karg, P., Wheelchair integrated occupant restraints: feasibility in frontal impact. *Medical Engineering & Physics*, 2001. **23**(10): p. 687-698.

34. Walker, B., *Conversation regarding the free on-line computer model of the Hybrid III anthropomorphic test dummy*. 2006: Solihull, Birmingham.

35. Cappon, H., Philippens, M., van Ratingen, M., Wismans, J, Development and Evaluation of a new Rear-Impact Crash Dummy: the RID2. *Stapp Car Crash Journal*, 2001. **45**: p. 1-14.

36. Szabo, T.J.W., J. B.; Anderson, R. D.; Rice, M. M, Human Occupant Kinematic Response to Low Speed Rear-End Impacts. *SAE Transactions*, 1994. **103**(6): p. 630-642.

37. Levick, N., Biomechanics of the patient Compartment of Ambulance vehicles. *SAE Transactions*, 2001. **110**(6): p. 1329-1335.

38. *Disability Discrimination Act 1995: Elizabeth II, Chapter 50*. 1995: HMSO.

39. ISO 16840-4, Seating Devices For Use In Motor Vehicles, International-Organization-for-Standardization, 2002

40. Bleck, W., Larour, P., Bäumer, A., High Strain Rate Tensile Testing of Modern Car Body Steels. *Materials Forum*, 2005. **29**: p. 21-28.

41. Cunat, P.J. *Stainless Steel Properties for Structural Automotive Applications.* in *Metal Bulletin International Automotive Materials Conference.* 2000. Cologne: Euroinox.

42. FMVSS Seating System (49CFR Part 571.207), Department-of-Transportation, 1993

43. Hell, W.L., K.; Walz, F.; Muser, M.; Kramer, M.; Hartwig, E. *Consequences for Seat Design Due to Rear End Accidnet Analysis, Sled Tests and Possible Test Criteria for Reducing Cervical Spine Injuries After Rear End Collision.* in *Biomechanics of impact.* 1999. Barcelona, Spain: Bron Cedex; IRCOBI.

44. Prasad, P., Kim, A., Weerappuli, D.P.V., Roberts, V., and Schneider, D., Relationships Between Passenger-Car Seat Back Strength and Occupant Injury Severity in Rear-End Collisions: Field and Laboratory Studies. *SAE Transactions*, 1997. **106**(2): p. 3935-3967.

45. Warner, C.Y., Stother, C.E., James, M.B., Decker, R.L., Occupant Protection in Rear-end Collisions: II. The Role of Seat Back Deformation in Injury Reduction. *SAE International*, 2003. **106**: p. 370-381.

46. Benson, B.R., Effect of seat stiffness in out of position occupant. *SAE International*, 2003. **106**: p. 244-257.

47. Kang, W. and Pilkey, W.D., Crash simulations of wheelchair-occupant systems in transport. *Journal of Rehabilitation Research & Development*, 1998. **35**(1): p. 73-84.

48. 42 U.S.C. 12101, Americans with Disability Act (ADA), Americans-Disibilities-Act, 1990

49. Park, Y.-S., Park, G-j., Crash Analysis and design of a belt integrated seat for occupant safety. *IMechE*, 2001. **215**(D): p. 875-889.

50. Otte, D., Comparison and realism of crash simulation tests and real accident situations for the Biomechanical movements in car collisions. *SAE International*, 2003. **92**: p. 256-272.

51. Lund, A.K., Changes in Vehicle Designs from Frontal Offset and Side Impact Crash Testing. *SAE International*, 2003. **1775**: p. 75-80.

52. Planath-Skogsmo, I.N., R, Frontal Crash Tests - A Comparison of Methods. *SAE Transactions*, 1994. **103**(6): p. 1887-1895.

53. Zaouk, A.K.M., D.; Bedewi, N. E, Development of a detailed vehicle finite element model Part I: Methodology. *International Journal of Crashworthiness*, 2000. **5**(1): p. 25-36.

54. Rush, C., Crash Testing Part 2: Predicting Human Injury with Computerized. *International Journal of Trauma and Nursing*, 2000. **6**(3): p. 91-94.

55. Wheeler, L.K. *Biofidelity of dummy legs for use in Legislative car crash testing*. in *IMechE Conference Transactions*. 2000: Great Britain Professional Engineering.

56. Bermond, F.V., P.; Ramet, M.; Bouquet, R.; Caire, Y.; Verriest, J. P.; Voiglio, E. *Human Response to a Frontal Sled Deceleration Test for the Validation of a Car Occupant Mathmatical Model*. in *Biomechanics of impact*. 2000. Montpellier, France: International Research Council on the Biomechanics of Impact.

57. Huang, Y.K., A. I.; Cavanaugh, J. M, Finite Element Modeling of Gross Motion of Human Cadavers in Side Impact. *SAE Transactions*, 1994. **103**(6): p. 1604-1622.

58. Kallieris, D.S., K. M.; Mattern, R.; Morgan, R, The Performance of Active and Passive Driver Restraint Systems in Simulated Frontal Collisions. *SAE Transactions*, 1994. **103**(6): p. 1727-1737.

59. Spittle, E.K.M., Donna J. ; Shipley, Buford W., Jr. ; Kaleps, Ints, *Hybrid II and Hybrid III Dummy Neck Properties for Computer Modeling*. 1992, Wright-Patterson Air Force Base: Ohio, US. p. 1-140.

60. Oshita, F. *Development of a Finite Element Model of the Human Body*. in *7th International LS-Dyna Conference*. 2002. Dearborn, Michigan, USA: Livermore Sodtware Technology Corporation.

61. Kirkpatrick, S.W. *Development of a LS-Dyna Occupant Model for use in Crash Analysis of Roadside Safety Features*. in *Transportation Review Board 82nd annual meeting*. 2002. Washington D.C. U.S.

62. Mehta, B.V.C., S. H.; Patlu, S.; Petkar, P. N.; Williams, R. L.; Bindeman, L. P.; Kennedy, J. M.; Pellettiere, J. *Integration of Finite Element Analysis (LS-DYNA) with Rigid Body Dynamics (ATB) for Crash Simulation.* in *International LS-DYNA users conference; "Simulation 2000".* 2000. Dearborn, MI: Livermore Software Technology Corporation.

63. Bradshaw, D. *The Development of an LS-Dyna3D Model of the Hybrid III 5th Percentile Dummy.* in *First European LS-DYNA Conference.* 1997. Stratford-Upon-Avon, England.

64. Moffatt, E.A. *Head Excursion of Seat Belted Cadaver, Volunteers and Hybrid 3 ATD in a dynamic/Static Rollover fixture.* in *SAE Conference Proceedings.* 1997. USA.

65. Fast, A., Forces, moments, an accelerations acting on a restrained dummy during simulation of a wheelchair negotiating a curb. *American Journal of Physical Medicine and Rehabilitation*, 1997. **76**: p. 370-377.

66. Arnoux, P.J.J., S.; Thollon, L.; Kayvantash, K, Radioss finite element model of the Thor dummy. *International Journal of Crashworthiness*, 2003. **8**(6): p. 529-542.

67. Zaouk, A.K., Occupant Injury Patterns in Side Crashes. *SAE SP*, 2001(1616): p. 77-81.

68. Fugger, T.F., Vehicle and Occupant Kinematics in Low-Speed Overide/Underride Collisions. *Society of Automotive Engineers*, 2003. **1784**: p. 37-46.

69. Buzeman, D.G.V., D. C.; Lovsund, P, Injury Probability and Risk in Frontal Crashes: Effects of Sorting Techniques on Priorities for Offset Testing. *Accident Analysis and Prevention*, 1998. **30**(5): p. 583-595.

70. Gallacher, C. *A methodology for creating a simplified Side Impact Model using LS-Dyna3D Based on Dynamic Test Data.* in *First European LS-DYNA conference.* 1997. Stratford-Upon-Avon, England.

71. Aekbote, K., A New Component Test Methodology Concept for Side Impact Simulation. *Society of Automotive Engineers*, 1999: p. 11-26.

72. O`Neill, B., Head restraints-the neglected countermeasure. *Accident Analysis and Prevention*, 2000. **32**(2): p. 143 - 150.

73. Suh, J.K.H., B. R.; Hong, S. G, Occupant Simulation of SUV by LS-Dyna for NCAP & 25mph. *SAE International*, 2003. **1774**: p. 39-44.

74. Williamson, P. *Aspects of Simulation of Automobile Seating Using LS-Dyna 3D*. in *LS-Dyna Forum*. 2005. Bamberg, Germany: Dynamore.

75. DeLeeuw, M., New automotive crash sled adds pitching simulation to standard tests. *Test Engineering and Management*, 2003. **65**(5): p. 14-17.

76. Babu, V.T., K. R.; Sakatis, C, LS-Dyna 3D Interface Component Analysis to Predict FMVSS 208 Occupant Response. *SAE SP*, 2003. **1774**: p. 55-60.

77. Whirley, R.G.E., B. E., Crashworthiness Simulation in Electric Vehicle Development. *ASME Applied Mechanical Division-Publications-AMD*, 1995. **210**: p. 287-306.

78. Reid, J.D.H., M. W.; Paulson, S. L, LS-DYNA: A Computer Modeling Success Story. *Public Roads*, 2001. **64**(4): p. 21-25.

79. Zienkiewicz, O.C., Taylor, R.L., Zhu, J.Z., *The finite element method : its basis and fundamentals*. 6th ed. 2005: London : Elsevier Butterworth-Heinemann.

80. Rockey, K.C., *The Finite element method : a basic introduction*. 2nd ed. 1983: London : Granada.

81. Fagan, M.J., *Finite element analysis : theory and practice*. 1957: Harlow : Longman Scientific & Technical.

82. Grandin, H., *Fundamentals of the finite element method*. 1986: London : Macmillan Publishing Company.

83. Moaveni, S., *FInite Element Analysis: Theory and Application with Ansys*. 2nd ed. 2003: Pearson Education.

84. Arup, *LS-Dyna Training Course Notes*. 2006.

85. Hallquist, J.O., *LS-Dyna Theoretical Manual*. 1998: Livermore Software Technology Corporation, Livermore, California.

86. Khalil, T.B.L., T. C, Simulation of the Hybrid III Dummy Response to Impact by Nonlinear Finite Element Analysis. *SAE Transactions*, 1994. **103**(6): p. 1868-1886.

87. ARUP, *Oasys Primer User Manual.* 9.2 ed. 2006: Arup.

88. Zaouk, D., Development of a Detailed Vehicle Finite Element Model Part II: Material Characterization and Component Testing. *International Journal of Crashworthiness*, 2000. **5**(1): p. 37-50.

89. Song, D., Mack, P., Tarriere, C., Brun-Cassan, F., Le Coz, J.Y., Lavaste, F, Finite Element Simulation of the Occupant/ Belt Interaction: Chest and Pelvis Deformation, Belt Sliding and Submarining. *SAE International*, 2003. **92**: p. 817-835.

90. Rouhana, S.W., Assessment of Lap-Shoulder Belt Restraint Performance in Laboratory Testing. *Progress in Technology*, 2003: p. 135-145.

91. Gavelin, A., *Seat Integrated Safety belts, A parametric Study using Finite Element Simulations (LS-Dyna),* in *Department of Applied Physics and Mechanical Engineering*. 2006, Lulea University of Technology: Lulea.

92. Williams, T.D., Pennington, A., Barton, D.C., The Frontal Impact Response of a Spaceframe Chassis Sportscar. *Proceedings - Instituteof Mechanical Engineers, Journal of Automobile Engineers*, 2000. **214**(D): p. 865-873.

93. Kirkpatrick, S.W. *Development of a Computer Model for Prediction of Collision Response of a Railroad Passenger Car.* in *ASME/IEEE Joint Rail Conference*. 2002. Washington, D.C.: ASME.

94. Bolarinwa, E.O., Olatunbosun, O.A., Finite Element Simulation of the Tyre Burst Test. *Proceedings - Instituteof Mechanical Engineers, Journal of Automobile Engineers*, 2004. **218**(D): p. 1251 - 1258.

95. Pelc, J., Static three-dimensional modelling of pneumatic tyres using the technique of element overlaying. *Journal of Automobile Engineering*, 2002. **216**(9): p. 709-716.

96. Hölscher, H., Modelling of Pneumatic tires by a Finite Element Model for the Development of a Tire Friction Remote Sensor. 2004.

97. Fukushima, T., Shimonishi, H., Hayashi, K., Shiraishi, M. *Simulation of a Vehicle Running on to a Curb by Using Tire and Vehicle FE Models.* in *4th European LS-Dyna Users Conference*. 2003. Ulm, Germany: Dynamore.

98. Reid, J.D. *Detailed Tire Modelling for Crash Applications.* in *ICrash.* 2006. Athens, Greece.

99. Non-Linear Modal Rolling Tyre Model for Dynamic Simulation with ADAMS, 1998, Mancosu, F., http://www.msc.software.com/support/library/conf/adams/euro/1998/euc98_04.pdf, Accessed: 12/07/2007

100. Shiraishi, M. *Making FEM Tire Model and Applying it for Durability Simulation.* in *International LSDyna Users Conference.* 2000. Dearborn: Livermore.

101. Lorenzo, J.M., FMVSS201 "A" Pillar Impact Simulation and Verification Study. *Society of Automotive Engineers*, 1999: p. 51-56.

102. Nordberg, H., *Note on the Sensitivity of Stainless Steel to Strain Rate.* 2004, Sheffield Hallam University. p. 1-10.

103. Dietenberger, M., Buyuk, M., Kan, C. *Development of a High Strain-Rate Dependant Vehicle Model.* in *LS-Dyna Anwenderforum.* 2005. Bamberg, Germany: DynaMore.

104. Gokstrop, A. *Material Models for Metals Subjected to High Strain Rates.* in *First European LS-Dyna Conference.* 1997. Stratford-Upon-Avon, England, UK.

105. Sato, K., Yoshitake, A., Hosoya, Y.,. *FEM Simulation to Estimate Crashworthiness of Automotive Parts.* in *Society of Automotive Engineers.* 1998.

106. Huang, M., *Vehicle Crash Mechanics.* 2000: CRC Press.

107. ISO 17373, Road vehicles - Sled test procedure for evaluating occupant head and neck interactions with seat/head restraint designs in low-speed rear-end impact, International-Organization-for-Standardization, 2005

108. Forrington, K., *Discussion regarding vehicle pitch angle.* 2007.

109. Decelerator Sled Testing System, 2006, LLC, S.S., http://www.seattlesafety.com/products/, Accessed: 09/01/2008

110. Hyge Operating Principal, 2007, Hyge, http://www.hyge.com/operatingprinciple.shtml, Accessed: 02/08/2007

111. Yanjin, G., GuoQun, Z., FEA and Testing Studies on Static Camber Performance of the Radial Tire. *Journal of Reinforced Plastics and Composites*, 2007: p. 1-16.

112. Hallquist, J.O., *LS-Dyna Keyword User's Manual*. Version 970 ed. 2003: Livermore Software Technology Corporation, Livermore, California.

113. Fukushima, T., Shimonishi, H., Hayashi, K., Shiraishi, M. *Vehicle Turn Simulation Using FE Tire Model*. in *3rd German LS-Dyna Conference*. 2004. Bamberg, Germany: DYNAmore.

114. Adams, V., Askanazi, A., *Building Better Products with Finite Element Analysis*. 1999: Thomson Delmar Learning.

115. Caldicott, S.J., Shapcott, N., Validation of a Software-Based Stability Assessment System for WHeelchairs and their Occupants. *Journal of Medical Engineering and Technology*, 2008: p. 1-8.

116. Shiraishi, M., Hayashi, K. *Developing FE-TIRE Model for Road Noise Simulation*. in *5th European LS-Dyna Users' Conference*. 2005. Birmingham, UK: ARUP.

117. National Crash Analysis Centre, 1992, National Crash Analysis Centre, G.W.U., http://www.ncac.gwu.edu/vml/models.html, Accessed: 10/06/2008

118. Finite Element Model Archive, 2008, Centre, N.C.A., http://www.ncac.gwu.edu/vml/archive/ncac/vehicle/explorer-0.2.pdf, Accessed: 05/03/2008

119. Schwer, L.E. *An Overview of the ASME Guide for Verification and Validation in Computational Solid Mechanics*. in *LS-Dyna Conference*. 2006. Ulm, Germany: The American Society of Mechanical Engineers.

120. Mao, M., Chirwa, E.C., Chen, T., and Latchford, J., Static and dynamic roof crush simulation using LS-DYNA3D. *International Journal of Crashworthiness*, 2004. **9**(5): p. 495-504.

121. McKie, T. *Simulation of Body Block Steering Wheel Impacts using LS-Dyna3D*. in *First European LS-Dyna conference*. 1997. Stratford-Upon-Avon.

122. Musale, G., Versatile Occupant Analysis Model (V.O.A.M) for Frontal Impacts Using LS-DYNA and MADYMO. *SAE International*, 2005. **1958**: p. 157-162.

123. Solanki, K.O., D. L.; Burton, C. L.; Fang, H.; Horstemeyer, M. F. *Crashworthiness Simulations Comparing PAM-CRASH and LS-DYNA*. in *Society of Automotive Engineers; SAE 2004 world congress*. 2004. Detroit, MI: SAE; 2004.

124. Wu, J.Z., Simulating Neck Injury in Frontal Impact using LS-DYNA. *SAE International*, 2007. **2117**: p. 227-240.

125. Xiao, X. *Plastic Material Modelling for Vehicle Crash Simulation using LS-Dyna*. in *ANTEC - CONF 59*. 2001.

126. Moumni, Z. and Axisa, F., Simplified modelling of vehicle frontal crashworthiness using a modal appraoch. *International Journal of Crashworthiness.*, 2004. **9**(3): p. 285-298.

127. Development of a detailed Nonlinear Finite Element Analysis Model of Colliding Trains, 2005, Martinez, E., http://www.fra.dot.gov/downloads/Research/rr0509.pdf, Accessed: 15/06/2006

128. Welcher, J.B., Szabo, T.J., Voss, D.P., Human Occupant Motion in Rear-End Impacts: Effects of Incremental Increases in Velocity Change. *SAE Transactions*, 2001. **110**(6): p. 1129-1137.

129. Van-Lopik, D.W., Acar, M., A computational model of the human head and neck system for the analysis of whiplash motion. *International Journal of Crashworthiness*, 2004. **9**(5): p. 465-474.

130. Strother, C.E.J., M. B.; Gordon, J. J., Response of out-of-position dummies in rear impact. *Progress in Technology*, 2003. **106**: p. 272-300.

131. Citroen Dispatch Dimensions, 2008, CITROËN, http://www.citroen.com.sg/html/pages/subpage_dispatch_dimensions.asp, Accessed: 03/11/2008

132. Rogers, P.D., Wilcox, S.J., Chong, A.Z., Gibson, C. *Virtual Crash Testing of Wheeled Mobility Devices Used in Transport*. in *Wheelchair Stability*. 2008. York, UK: Institute of Physicas and ENgineeirng in Medicine.

133. Hodgson, V.R., Thomas, L.M. *Effects of Long-Duration Impacts on the Head*. in *16th Stapp Car Crash Conference*. 1972. Detroit, USA.

Appendix A – Submarining

During the creation of the ISO 16840 surrogate wheelchair model the seatbelt around the dummy was applied with an excessively loose fit. When the model was run the slack belt caused the lap belt to ride up over the dummy's iliac crest, at the front of the pelvis, and ride up to the dummy's abdomen allowing the dummy to slide underneath the belt, see Figure A.1. This action is known as 'submarining' [7, 9, 11, 47, 89, 90]. Although in this instance the fit of the belt was at fault it was useful to find that the model, and indeed the modelling process, was able to adequately capture such events. By way of comparison Figure A.2 shows a frontal crash test of an ISO 10542 surrogate wheelchair, conducted by Rookwood Hospital at Millbrook Proving Grounds, which failed due to submarining.

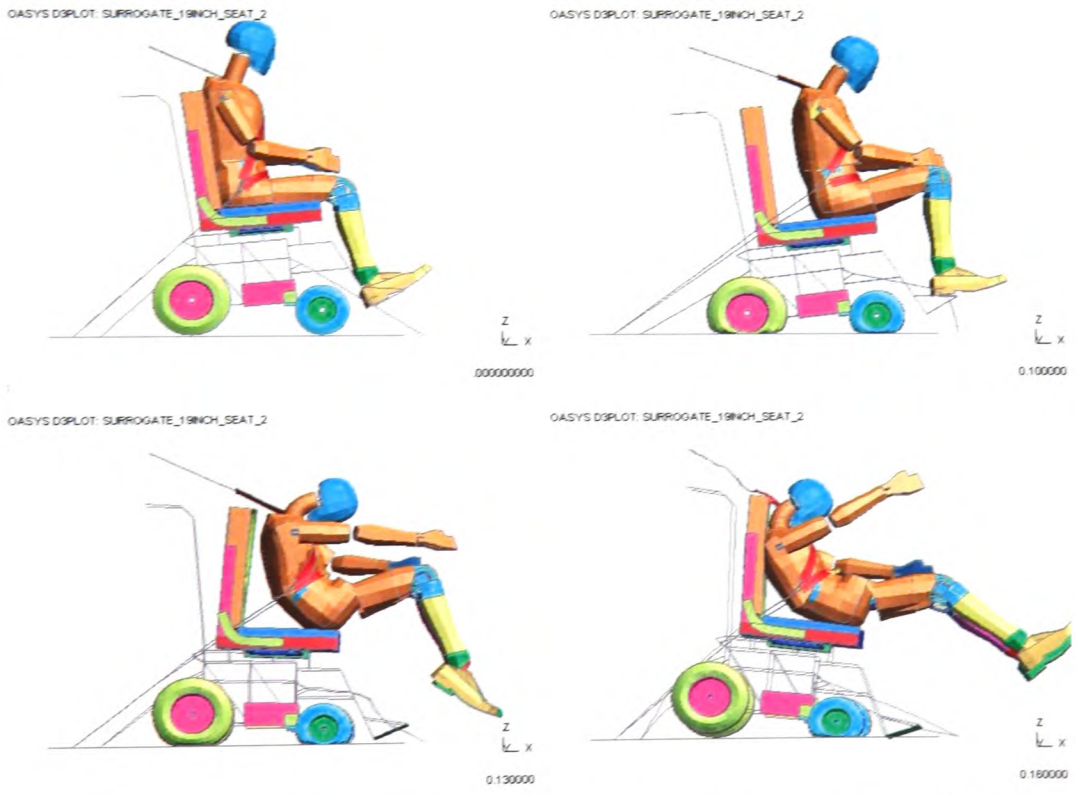

Figure A.1 showing submarining caused by an excessively loose seatbelt.

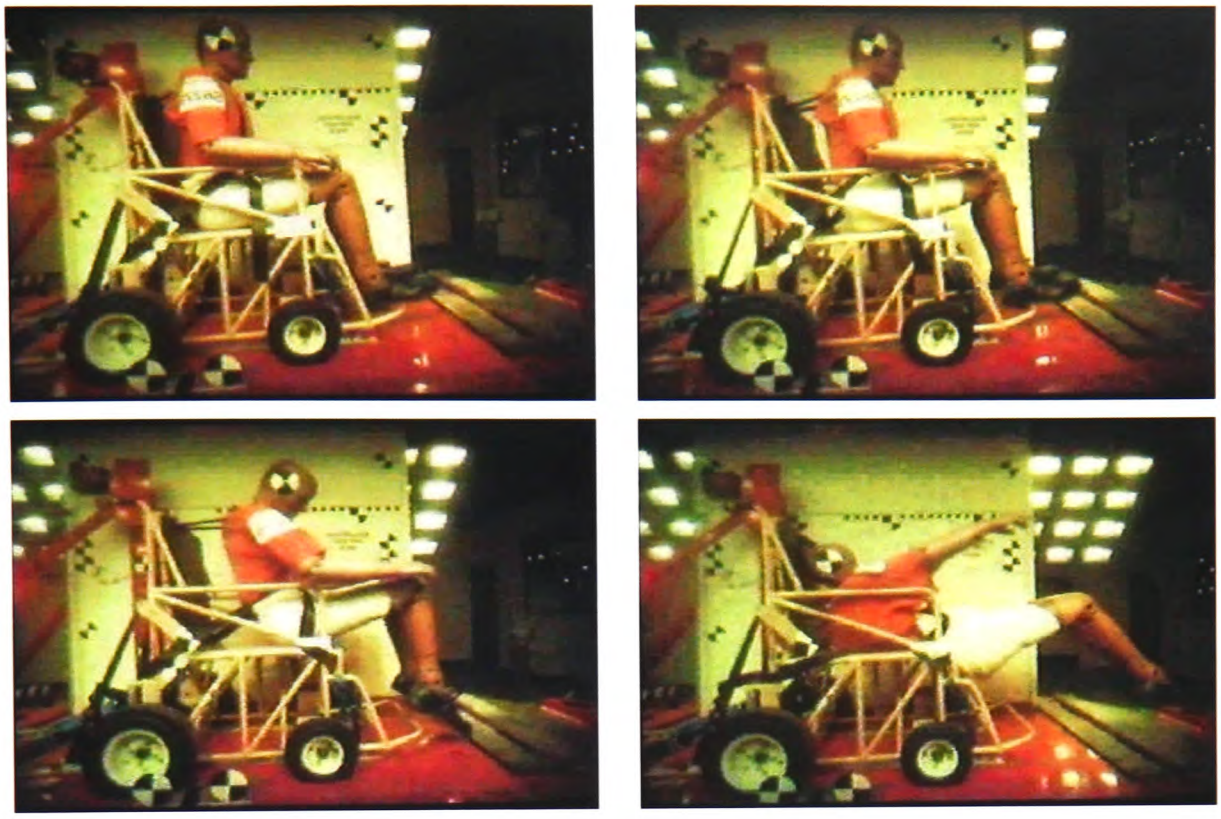

Figure A.2 showing the submarining effect during an ISO 10542-1 frontal 20g crash test with an ISO 10542 surrogate wheelchair.

Wheelchairs are often prone to poor belt fit. Bertocci *et al.* [13] discuss the causation of poor belt fit around a seated wheelchair occupant stating that the fixed arm rests and clothing shields prevent the waist belt from following a close fitting path across the pelvis, resulting in an increased risk of submarining.

Appendix B – Node History

The displacement of various nodes can be recorded from a full simulation to examine a sub-part of the model independently. This technique was used in Chapter 4 for recorded the pitching of the truck chassis. An obvious application in the wheelchair crash simulations is the simulation of the seat and occupant without the wheelchair chassis. This method is especially relevant in the case of the Rehabilitation Engineering Unit who use a common interface between the wheelchair chassis and the seats on many of their wheelchairs. The primary advantage of this sub-part simulation method is the reduction in processing speed. If the performance of a new seat design needed to be checked it could be done initially independently of the wheelchair chassis. Care must be taken, however, as although the behaviour of the chassis of the wheelchair affects the behaviour of the occupant and seat so the occupant and seat, being of comparable mass, will affect the behaviour of the wheelchair chassis.

The nodes of interest were defined in the 'Database_History' option, in LS-Dyna, so that their details were written to the output file. On completion of the simulation graphs of displacement against time for each node were saved in the post-processor (nodal velocities or accelerations could have been used instead if required). The model was then modified in the pre-processor to show the required sub-assembly of the model. The motion of the nodes of interest were defined by applying the recorded displacement against time graphs using the 'Boundary_Prescribed_Motion' function within LS-Dyna [112].

Figures B.1 and B.2 show two examples of seat and occupant simulations independent of the wheelchair chassis. Figure B.1 was used to test the correct function of the initial Rookwood seatpan design and Figure B.2 was used to examine the thigh and pelvis joint of the Hybrid III dummy.

Figure B.1. showing the Rookwood seatpan without a head rest and dummy in a frontal 20g impact independent of the wheelchair chassis.

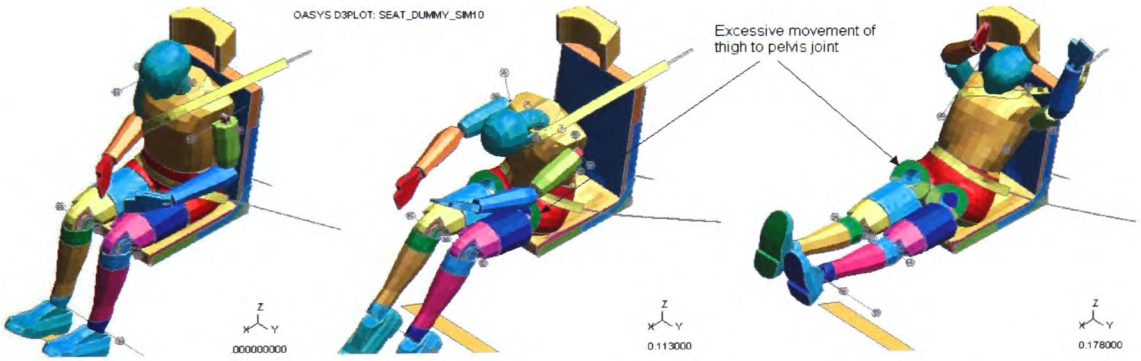

Figure B.2 showing the simulation of the Rookwood seatpan and dummy in a frontal simulation showing submarining tendencies.

Appendix C – Head to head rest contact acceleration

The graphs of the Spectra wheelchair simulations, illustrated in Chapter 6, show large spikes in occupant head acceleration at the points where the head contacted the head rest. In order to check that these high acceleration values were reasonable a simple head to headrest simulation was conducted and compared with the results from the Spectra frontal 20g simulation. Graphs of the velocity of the head and headrest from the frontal 20g Spectra simulation and rearward 10g Spectra simulation were plotted and the relative velocity of the head to headrest, just before impact, were found, see Figures C.1. The head rest, comprising of backing plate and foam, was fixed rigidly in space and the head fired towards it with a velocity of 7.8m/s, for the rear impact, and 10.5m/s, for the frontal impact. The setup of the simulation is shown in Figure C.2. The velocity of the head was applied using the 'initial_velocity' card in LS-Dyna [85]. In the full simulation the headrest was attached to the seat back, which allowed a certain amount of deformation when struck by the dummy's head. The head to headrest simulation, with its rigidly fixed head rest, was therefore expected to produce significantly higher head accelerations.

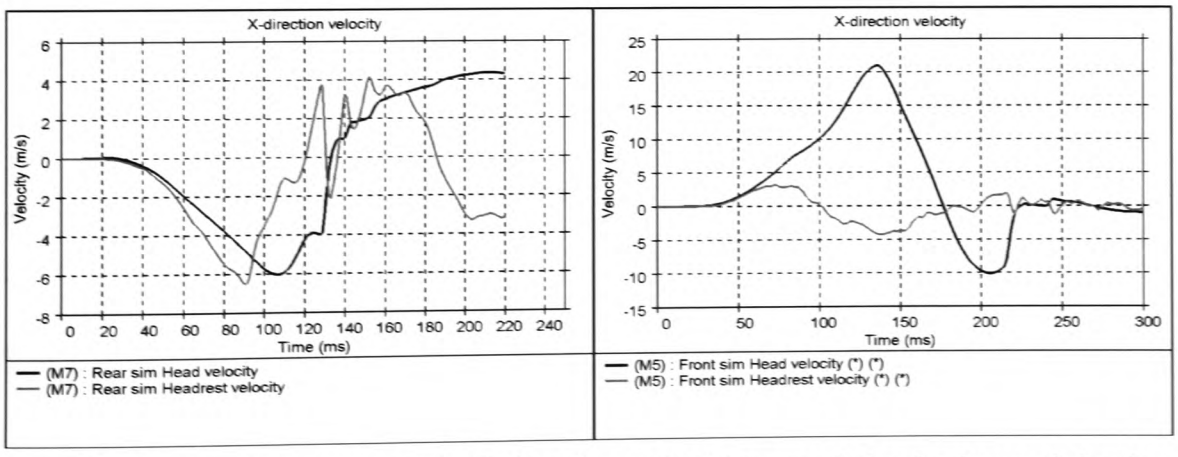

Figure C.1 showing the velocity in the X-direction against time graph for the dummy's head and headrest in the Spectra rearward 10g simulation (left) and the Spectra frontal 20g simulation (right).

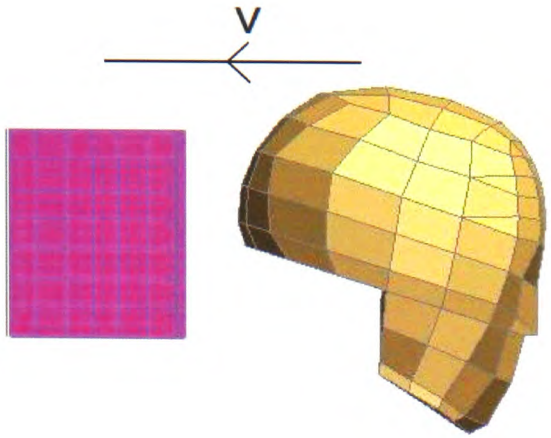

Figure C.2 showing the setup of the head to headrest simulation.

Results

Rear simulation head to headrest impact occurred at 129ms.

The head velocity at 129ms = 4.0ms

The headrest velocity at 129ms = -3.8ms

The relative velocity of the head to headrest = 4.0-(-3.8) = 7.8m/s

Frontal simulation head to headrest impact occurred at 215ms.

The head velocity at 215ms = -8.7ms

The headrest velocity at 215ms = 1.8ms

The relative velocity of the head to headrest = -8.7-1.8 = -10.5m/s

The finite element head to headrest simulation for the rear impact produced a maximum acceleration of 138g, see Figure C.3 (a),

The finite element head to headrest simulation for the frontal impact produced a maximum acceleration of 190g, see Figure C.3 (b),

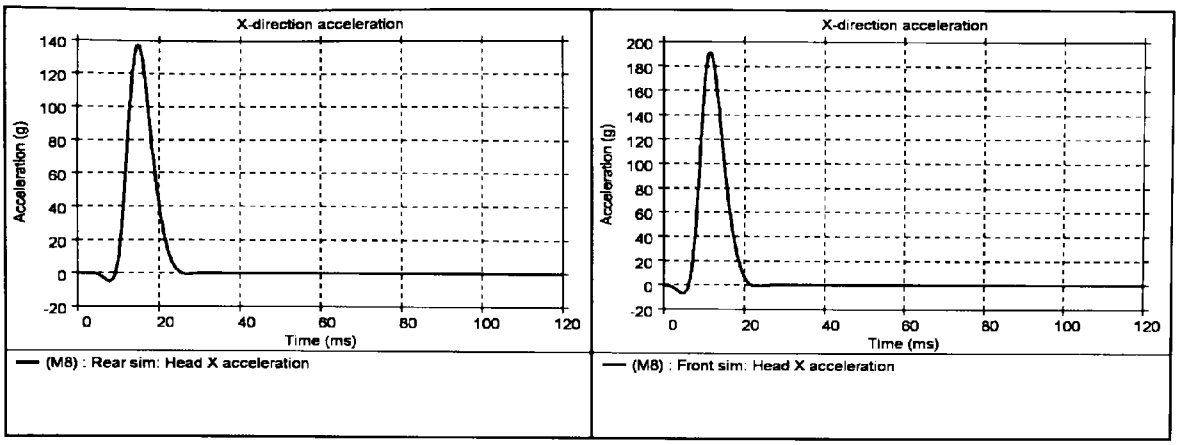

Figure C.3 (a) showing the head acceleration for the rear head to headrest simulation (left), (b) showing the front head to headrest simulation (right).

Discussion

The head to headrest simulation for the rear impact gave a maximum acceleration of 138g compared with 72g from the full scale rear Spectra impact simulation. The head to headrest simulation produced a higher peak acceleration, as expected, due to the rigid fixing of the head rest. The frontal head to headrest simulation behaved similarly with a maximum acceleration of 190g compared to the full scale frontal Spectra impact simulation of 105g.

The impact of the head to headrest in the rearward simulation is shown in detail in Figure C.4. The Figure shows that the torso remained stationary, relative to the head rest, while the head rotated rearwards into the headrest, illustrating the typical whipping back of the head and neck seen in other studies of occupant rear impact [31, 36, 43, 44, 54, 72, 129]. If this motion is compared with the motion of the dummy in the frontal 20g impact simulation of the Spectra wheelchair, it can be seen that, unlike the rearward impact, both the dummy's torso and head moved rearward into the headrest.

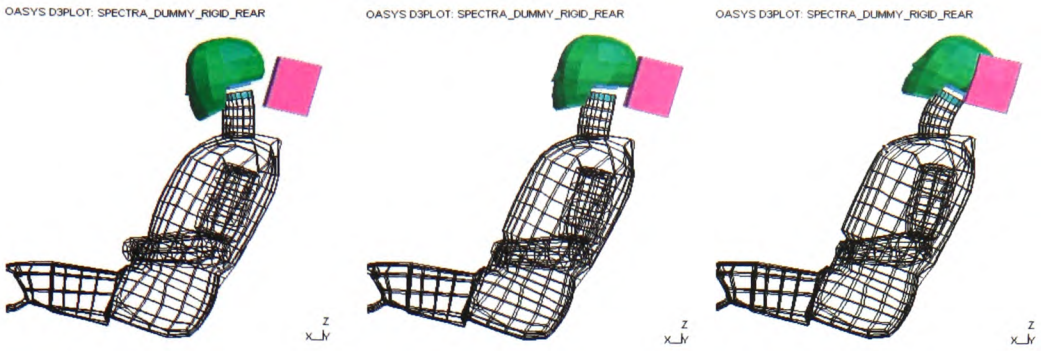

Figure C.4 showing movement of the head and neck striking the headrest during the Spectra 10g rear impact

Figure C.5 showing movement of the head and neck striking the headrest during the Spectra 20g frontal impact

In drop tests of human cadaveric heads, Hodgson and Thomas [133], measured peak uniaxial acceleration of between 190g and 340g from drop heights of 320mm to 1050mm respectively onto a rigid surface. Using simple motion equations the time taken for the cadaveric head dropped from the height of 320mm to decelerate from its initial velocity of 2.5m/s ($v^2=u^2+2as$ = $(2x9.81x0.32)^{1/2}$ = 2.5m/s) to zero, with a deceleration of 190g, was 1.36ms (t=v/a) whereas the time taken for the dummy's head to decelerate, at 72g, from 7.8m/s to zero, in the case of the rear head simulation, was 11.0ms and the deceleration time for the frontal impact from 10.5m/s to zero, with deceleration of 105g, was 10.2ms. So although the initial velocity in the crash scenario was greater than that of the cadaveric drop test the foam head rest of the crash simulation increased the deceleration time of the head hence reduced the deceleration.

Conclusion

The high peak head accelerations recorded in the simulations seem reasonable when compared to the simple head to headrest simulation and also to those experienced by the human head drop tests conducted by Hodgson and Thomas [133].

Modelling the crashworthiness of wheelchair and special seating systems

Paul D. Rogers[a], Steve J. Wilcox[a], Alex Chong[a], Colin Gibson[b]

[a]*University of Glamorgan, Department of Engineering, Treforest, Wales, UK*
[b]*Cardiff and Vale NHS Trust, Rehabilitation Engineering Unit, Rookwood Hospital, Cardiff, Wales, UK*

Abstract

The crashworthiness of occupied proprietary wheelchairs, which are transported in motor vehicles, is currently assessed by physical crash testing in accordance with ISO 7176-19. If such wheelchairs are modified to meet the needs of the occupant, e.g. the addition of special seating, environmental control systems or life support equipment, then those making the modifications take on the manufacturer's responsibilities, one of these being the assessment of the modified wheelchair's ability to withstand vehicle crash forces. Destructively testing bespoke wheelchair designs is not practical so, currently, the transport-related risk is assessed using best engineering judgement. To improve this process virtual crash testing of the wheelchair and occupant was used. A modified crash criteria from ISO 7176-19 is proposed to enable assessment of the wheelchair's crashworthiness and provide the clinical engineer with an informed judgement of how both wheelchair alone and occupant and wheelchair together will behave in a crash.

Keywords: Wheelchair; Special Seating; Crashworthiness; ISO 7176-19

1. Introduction

Risk management is the process of ensuring that risk is reduced to an acceptable level. Risk assessment provides a methodology by which this aim may be achieved albeit its application to posture and mobility equipment (such as wheelchairs and special seating systems) poses many challenges for manufacturers, clinical prescribers and NHS service providers alike [1]. Wheelchair manufacturers undertake generic risk assessments for their products as an integral part of their risk management. However, should a NHS service provider modify a proprietary wheelchair, for example, by adding a bespoke special seat to meet the needs of a specific patient then that NHS service provider takes on the risk management responsibilities of the manufacturer.

These responsibilities necessarily include an assessment of the ability of a wheelchair to offer adequate protection to its occupant in the event of a crash while being transported in a vehicle. The current standard for assessing the "crashworthiness" of wheelchairs in transport is physical crash testing, as described in ISO 7176-19 [2]. As the name implies, crash tests are destructive and the cost of crash testing is high in terms of the test itself and the destruction of the test specimen. For example, a break down of the physical crash testing costs for a wheelchair modified to carry life support equipment (as has been prescribed for a specific client by the Rehabilitation Engineering Unit at Rookwood Hospital in Cardiff) is shown in Table 1.1. Such costs can be easily absorbed where there are economies of scale, however, the very nature of bespoke wheelchair design makes this very difficult for NHS service providers noting, of course, that there would have to be two identical modified wheelchairs, one to crash test and one to issue to the patient. At present, NHS service providers must use engineering judgement as to whether their modified wheelchairs are safe for transport or not. It has been proposed that a computer model of the wheelchair and occupant could be virtually crash tested to aid a NHS service providers risk assessment process. A bi-product of the computer simulation of a wheelchair and occupant in a crash situation may not only be to allow the NHS service provider to have confidence in the crashworthiness of that wheelchair but ultimately it may be to improve the safety afforded to the occupant of that wheelchair. Virtual crash testing can not replace physical testing and, as will be seen, it can not account for all the requirements of ISO 7176-19, but it is a useful tool when physical testing is impractical.

Item		Cost
Wheelchair modified to accept Life Support equipment		£4000
WTORS		£312.55
Life Support equipment		
	Breas Ventilator PV 403	£4898.58
	Leardal Suction Unit	£757.88
	Oxygen cylinder	£164.50
	Connection and fittings	£100.00
Crash Test		£2000.00
1 day for two members of staff		£200.00
Transport, accommodation and expenses		£300.00
Total		£12,733.51

Table 1.1 showing the cost of physical crash testing using a custom made stretched wheelchair with life support equipment as an example (source: Rehabilitation Engineering Unit, Rookwood Hospital, Cardiff).

2. Methods

2.1 Physical Crash Testing

When creating a computer model to investigate crashworthiness it is necessary to validate it against physical data to ensure correct behaviour.

Physical sled crash tests using an ISO 10542 surrogate wheelchair and Hybrid II dummy were conducted at Millbrook Proving Grounds (www.millbrook.co.uk). The sled was mounted on a track and accelerated by a large pneumatic ram. Rather than decelerating from a constant velocity to zero the sled is accelerated from zero velocity with the equivalent acceleration that would be experienced in a crash.

The rigidly constructed ISO 10542 surrogate wheelchair [3] allowed for the movement of the dummy, the behaviour of the seatbelt and tie-downs and the compression of the wheels in a crash situation to be examined in isolation of wheelchair chassis deformation. Due to the rigid structure of the ISO 10542 wheelchair, the FEA model wheelchair chassis could be modelled as a rigid body, decreasing both the modelling and run time.

A frontal crash test, using a 20 g crash pulse, and a rearward crash test, using a 10 g crash pulse, were conducted. The crash pulse used for the frontal crash testing was styled on a passenger car travelling at a constant velocity of 48 km/hr impacting into a rigid barrier. The initial velocity for the rear impact was 15 km/hr [4] (see Figure 2.1). The crash pulse describes the change in acceleration over time from the moment the vehicle contacts the solid barrier until it comes to rest.

The 20 g crash pulse was chosen for the frontal test as this is the acceleration required for all ISO frontal wheelchair crash tests. The 10 g crash pulse was used in ISO 17373 for evaluating occupant head and neck interactions with seat/head restraint designs in motor vehicles and is believed to be optimum for producing whiplash in the occupant [5, 6]. Although an acceleration of 10 g is not as injurious as higher accelerations it is certainly more common [7].

A Hybrid II dummy was seated in the surrogate wheelchair and restrained with a 3-point harness in line with ISO 10542-1. The wheelchair was secured to the sled with a 4-point tie-down system, again in line with ISO 10542-1.

Two accelerometers (Endevco 2262CA) were placed in the dummy's head to record X and Z accelerations (with the X-axis being in the horizontal direction of sled travel and the Z-axis being the vertical direction). Seatbelt load cells (FGP FN 4090) were placed on the upper shoulder belt and on one of the rear tie-downs to measure the tensile load. These load cells were of light-weight aluminium construction, adding minimal weight to the seatbelt. A high speed camera was mounted on a boom attached to the side of the sled. The camera could acquire 1000 frames per second and was triggered when the pneumatic cylinder fired. Data of the vertical and horizontal motion of the head, knee and P-point[1] were measured after the test by video capture software at a sample rate of 200 Hz (sample period of 5ms). Still photos were also taken before and after the crash.

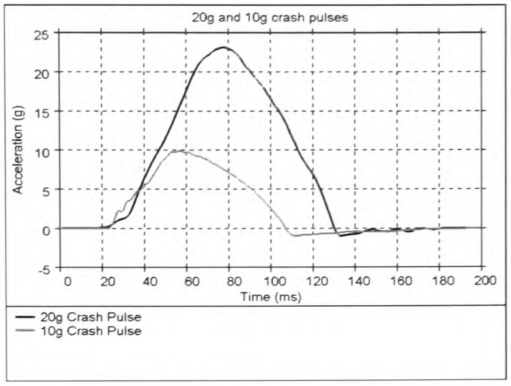

Figure 2.1 showing the 10g and 20g crash pulses produced by the pneumatic cylinder in frontal and rearward sled tests respectively.

2.2 Material Properties

Before the finite element model of the wheelchair and occupant was created the material properties of the wheelchair and associated components were found. Material tests were conducted for material properties that could not be found from literature or from the manufacturer, such as the stiffness of the wheels, tie-downs and seat foam.

2.3 Model construction

The wheelchair and components were measured and drawn in SolidWorks™, as shown in Figure 2.2. The CAD drawings were modified to simplify the meshing process. The modification involved the removal of any non-critical detail from the model, e.g. chamfers and rounded edges from non-critical parts, and alteration for shell element meshing. Parts that were not expected to deform during the crash simulation were modelled as rigid.

Part of the modelling process involved correct location of the wheelchair's centre of gravity, which was found by using similar techniques as described by Caldicott and Shapcott [8]. The wheelchair was put on scales and the force through each wheel was measured. The front wheels were then raised by a certain angle and the forces through each wheel were measured again. Using simple moment calculations, the centre of gravity was found. The centre of gravity of the wheelchair computer models was adjusted, where necessary, by re-distributing the mass of the computer model.

The CAD geometry was exported as an IGES (Initial Graphics Exchange Specification) file into Hypermesh™ where a finite element mesh of the geometry was created. The meshed geometry was then transferred to Oasys Primer™, a pre-processor for LS-Dyna. LS-Dyna

[1] The P-point is an arbitrary point on the wheelchair defined by ISO 10542 and ISO 7176-19. It is found by placing a cylinder of 100mm diameter and 200mm length on the wheelchair seat so that the cylinder surface touches both the seat and seatback. The P-point is the centre point of the cylinder at this position.

is an explicit finite element solver and is an industrial standard for modelling vehicle crash simulations.

A Finite element model of the Hybrid III dummy was placed in the wheelchair seat. A pre-run of the model was performed to compress the dummy into the seat, allowing the seat cushion to compress into the shape of the dummy. The seatbelt was then fitted around the dummy using an inbuilt fitting algorithm in the pre-processing software that fitted a spline through a defined path. A combination of 1D and 2D seatbelt elements, which produce zero stress with negative strain, were attached to the spline making up the seatbelt. 2D elements were used where the belt contacted the dummy's body as they provided more realistic contact whereas the 1D seatbelts made up the rest of the belt as they were quicker to solve. The seatbelt was moved towards the dummy until contact was achieved and then moved back out to satisfy the penetration limits set.

Figure 2.2 showing the ISO 10542 surrogate wheelchair (left) and the Invacare Spectra Plus production wheelchair with Rookwood seatpan attached (right).

The most noticeable limitation of the validation process described was the use of a physical Hybrid II dummy in the practical tests and a virtual Hybrid III dummy in the virtual tests. The use of a Hybrid III dummy, with its increased biofidelity and sensor location, was out of the budget range for this study so the cheaper and more robust Hybrid II dummy was used.

The sled was modelled using rigid shell elements and constrained in all but the horizontal plane. The crash pulse was applied to the sled using the 'Boundary Prescribed Motion' function in LS-Dyna.

2.4 Construction of crashworthiness criteria

The various wheelchair crash safety standards (ISO 7176-19, 10542-1 and 16840-4) have criteria that must be satisfied if the wheelchair design, tie-downs or seating system are to be deemed crashworthy. The results from the virtual crash testing should be compared with these ISO standards if meaningful wheelchair crashworthiness information is to be derived. It made most sense to compare the virtual results with the crashworthiness criteria from ISO 7176-19 as this is used for testing production wheelchairs that are attached to the test sled with WTORS (wheelchair tie-downs and occupant restraint systems) that should have already been tested to ISO 10542-1.

Not all the tests listed in ISO 7176-19 are possible to capture using the FEA model. The initial criterion for the project was to improve the risk assessment process not to completely replicate the physical test. Besides, trying to replicate the physical test virtually would still not replace it.

Only the first 200 ms of the crash event was run in the simulations in this study as this matched the time period of recorded data for the physical tests available for comparison. Often times of less than 200 ms are used in vehicle crash simulation analysis [9-12]. The crash pulse returns to zero acceleration after 110 ms but from observing the physical crash tests it took up to 3 seconds for the dummy to come to complete rest in the wheelchair. Running the simulations for 3 seconds, to allow measurement of the dummy and wheelchair to be taken 'post test', would take 15 times longer and, with the average simulation run taking between 3-4 hours, could increase the run time up to 60 hours. With it being necessary to conduct several runs, to ensure the various contacts and boundary conditions are behaving correctly, a large run time of 60 hours would significantly lengthen the simulation process and begin to outweigh the cost benefits of using computer simulation. With this in mind, it would be impractical to comply with points 5.2.2(a) and 5.2.2(i) of ISO 7176-19; that the wheelchair and occupant remain upright after the crash with the occupant, being not more than 45° to the vertical when viewed from any angle and that the post test height of the wheelchair H-point above the ground shall not decrease by more than 20%. Therefore, it is proposed that the position of the occupant in relation to the wheelchair seat and securement system be examined at 200 ms to give some indication as to whether or not the occupant is likely to remain upright. The H-point, being the position of the hip joint of the occupant, is affected by the compression of the tyres. The H-point is also affected by ill fitting waist belts, and also seat deformation, which can cause submarining, where the waist belt rides up over the iliac crest allowing the pelvis so slide under the belt causing abdominal trauma [11, 13-17]. From the simulations performed and from the practical sled tests conducted the minimum H-point values occurred within the first 200 ms (an H-point reduction of 8.7% at 182 ms for the ISO 10542 frontal surrogate wheelchair simulation, 2.2% reduction for the ISO 16840 frontal simulation and a 2.4% reduction at 87 ms for the Spectra frontal simulation).

Further items from ISO 7176-19 that could not be tested for was the fracture of parts that would a sharp edge of less than 2 mm diameter. Such detail is not practical here. Nor was it practical to determine whether the wheelchair or dummy require tools to remove them after

the crash or indeed if excessive wear had occurred to the primary load and securement points of the wheelchair. The excursion of the dummy and wheelchair could, however, be recorded as could the movement of the batteries, in the case of electric wheelchairs.

Measurement Point	Excursion Limit (mm)
Wheelchair P-point, X_{wc}	200
ATD Knee, X_{knee}	375
ATD front of head, X_{headF}	650
ATD rear of head, X_{headR}*	400
X_{knee}/X_{wc}	≥ 1
Decrease in H-point above ground	<20%
Does the movement of the occupant suggest that they will remain upright?	Occupant angle less than 450 from any angle
Battery movement	Within footprint of wheelchair and away from occupant
* Value not used for ISO 10542 surrogate simulations and skewed impacts	

Table 2.1 showing the modified crash criteria for the virtual crash simulations.

The test criteria of ISO 7176-19 is aimed at wheelchair manufacturers. It should be borne in mind that the virtual testing proposed herein is to aid NHS service providers in their risk assessment after they have carried out modifications to wheelchairs that have already passed this standard.

3. Results

The finite element models of the ISO 10542-1 sled test were compared with the equivalent practical results. The models showed good correlation, although differences in some of the dummy displacements were observed due to the differences between the Hybrid II and Hybrid III dummies. Figure 3.2 shows video stills of the frontal 20g crash test between the practical and virtual results. From the frame at 0 ms it can be seen that there is a difference between the postures of the two different Hybrid dummies where the head of the Hybrid III dummy is positioned further forward than that of the Hybrid II dummy. The horizontal head displacement for both results show a similar trend although the peak value for practical Hybrid II dummy was 85mm greater than that of the virtual Hybrid III dummy. Much of the difference is due to the Hybrid II dummy's head being located 103mm further back, relative to the dummies shoulder, than that of the Hybrid III.

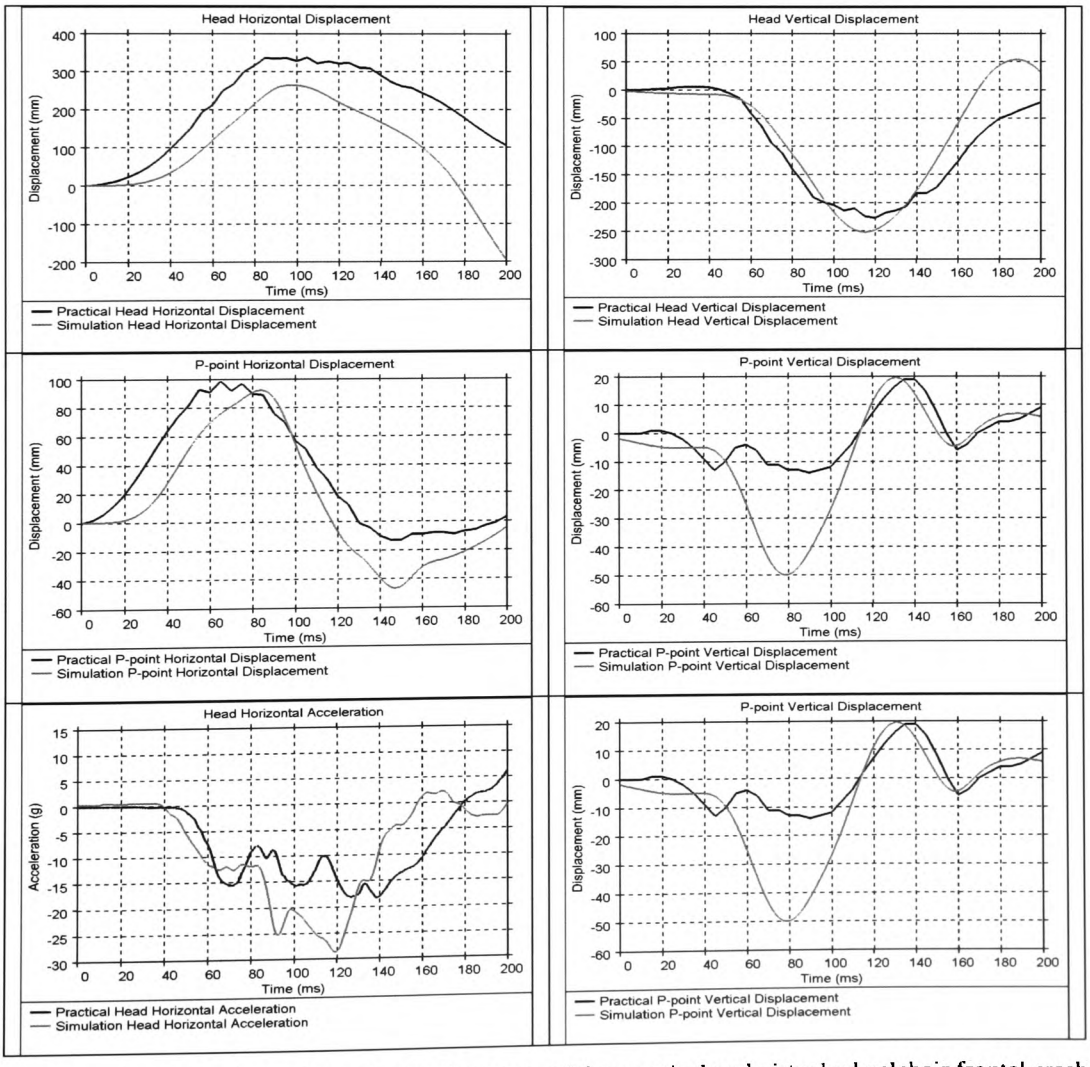

Figure 3.1 showing the horizontal P-point displacement of the practical and virtual wheelchair frontal crash test.

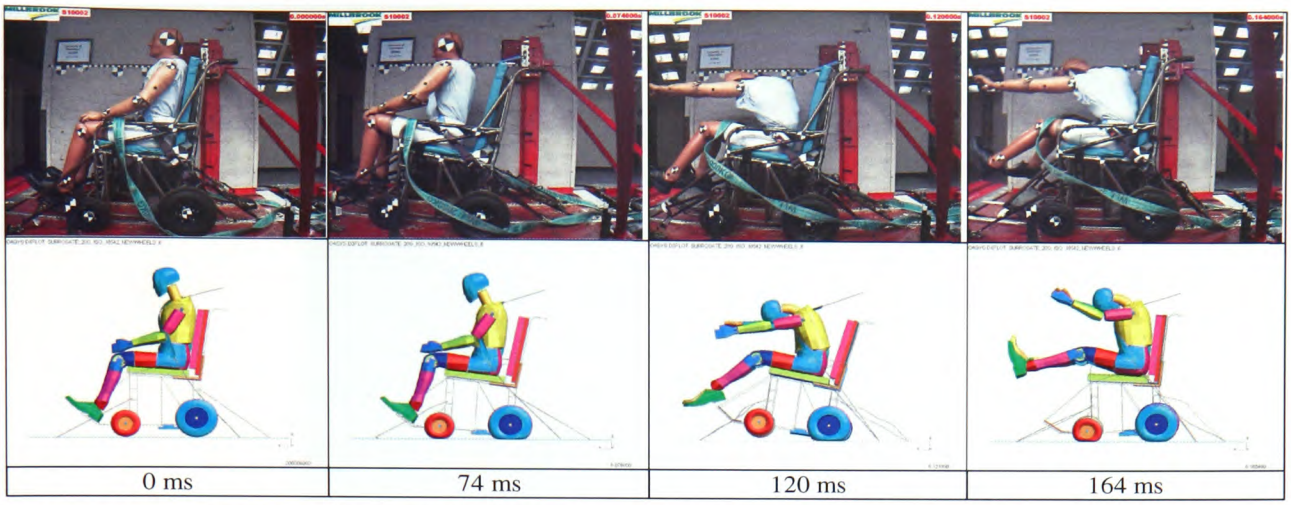

Figure 3.2 showing video stills comparing the practical and simulated 20g frontal ISO 10542 surrogate sled test.

The head horizontal and vertical accelerations again show good correlation although the simulated results show higher peak acceleration in the horizontal direction.

The P-point displacement of the wheelchairs corresponded well, as shown from the graph in Figure 3.1. The virtual wheelchair model can be seen from Figure 3.2 to rebound further than that of the practical wheelchair. This is due to a lack of damping in the rear tie-downs during unloading.

There was a considerable difference between the P-point vertical displacements of the simulated and physical tests despite the video stills in Figure 3.2 showing good agreement. The rear wheels of both tests were observed to bottom out at 80 ms and it is this compression of the rear wheels that is responsible for the P-point vertical movement.

The results and video footage of the simulated and practical sled tests were deemed close enough to give confidence in the simulation model's ability to predict physical events

This validated model was used as the basis of other models as the wheelchair tie-downs, dummy and occupant restraints remained the same for all subsequent models.

A model of the Invacare Spectra Plus wheelchair was created based upon the validated model of the ISO 10542 surrogate wheelchair. The Spectra Plus wheelchair was chosen as it is the most common wheelchair chassis issued by the Rehabilitation Engineering Unit at Rookwood Hospital, Cardiff who collaborated with this work.

The results from the two surrogate wheelchairs and Spectra wheelchair frontal crash tests are presented in Table 4.1 using the modified crashworthiness criteria.

All of the simulations meet the necessary limits in Table 4.1.

The practical results for the ISO 10542 surrogate wheelchair also satisfied its respective test standard.

4. Discussion

Ideally, further physical testing would be carried out to improve the validation process but due to funding constraints it was only possible to conduct two full wheelchair crash tests. The use of different Hybrid dummies in the physical and virtual tests was not ideal but did allow the trends of the occupant motion to be compared. A further disadvantage of the validation process was the lack detail of the surrogate tyres. The thickness of the surrogate tyre tread was not known so was given the same thickness as that of the tested Spectra tyres, i.e. 6mm. If the surrogate tyres were thicker then this would reduce the large disparity observed in the vertical P-point displacement between the practical and simulated frontal sled tests in Figure 3.2.

The logical progression between the validated ISO 10542 surrogate model and subsequent computer models was the assumption that all wheelchairs tested were restrained using the same 4-point tie-down system and all occupants were restrained using the same 3-point harness. The test sled and dummy also remained the same.

The results in Table 4.1 show that many of the parameters of the ISO 7176-19 crashworthiness criteria can be checked for virtually. This would not only allow the NHS service providers to assess their bespoke wheelchair designs but also to assess the crashworthiness of their designs before fabrication.

Measurement Point	Excursion Limit (mm)	ISO10542 surrogate wheelchair frontal 20g	Spectra wheelchair frontal 20g
Wheelchair P-point, X_{wc}	200	93	97
ATD Knee, X_{knee}	375	146	142
ATD front of head, X_{headF}	650	272	308
ATD rear of head, X_{headR}*	400	N/A	352
X_{knee}/X_{wc}	≥ 1	>1	>1
Decrease in H-point above ground	<20%	8.7%	2.4%
Does the movement of the occupant suggest that they will remain upright?	Occupant angle less than 45^0 from any angle	Yes	Yes
Battery movement	Within footprint of wheelchair and away from occupant	N/A	Yes
* Value not used for ISO 10542 surrogate simulations and skewed impacts			

Table 4.1 showing the results of the three simulations with respect to the modified crashworthiness criteria.

Each wheelchair and special seating system that NHS service providers produce has a number of components that maybe adjusted to the needs of the particular client, such as seat back angle, seat recline, position of wheelchair and environmental controls, footplate design and position and the addition of other ancillary equipment. Currently, the effects that any one of these items has on the crash safety of the wheelchair and occupant in transport are guessed at. By virtually simulated different set ups and, indeed, different designs, a more informed judgement of a wheelchair's crashworthiness and the safety afforded to the occupant can be made.

The first few wheelchair models took considerable time to create and mesh but as each additional wheelchair and associated piece of equipment is modelled so the database of parts will increase allowing for faster model creation.

A further benefit of the virtual crash testing is the ability to set up different crash test scenarios, e.g. rear and side impacts. Although not currently required by current ISO standards the behaviour of lateral and rear impacts should be considered if the best possible safety is to be afforded to the wheelchair occupant.

References

1. Gibson, C. *Risk Management - Why? How? Who?* in *Risk Management in Vehicle Transportation for People in Wheelchairs meeting*. 2000. Botanical Gardens, Birmingham: Institute of Physics and Engineering in Medicine.
2. ISO 7176-19, Wheeled mobility devices for use as seats in motor vehicles, International-Organization-for-Standardization, 2005
3. ISO 10542-1, Technical systems and aids for disabled or handicapped persons - Wheelchair tie-down and occupant-restraint systems, International-Organization-for-Standardization, 2001
4. Huang, M., *Vehicle Crash Mechanics*. 2000: CRC Press.
5. Hell, W.L., K.; Walz, F.; Muser, M.; Kramer, M.; Hartwig, E. *Consequences for Seat Design Due to Rear End Accidnet Analysis, Sled Tests and Possible Test Criteria for Reducing Cervical Spine Injuries After Rear End Collision*. in *Biomechanics of impact*. 1999. Barcelona, Spain: Bron Cedex; IRCOBI.
6. Prasad, P., Kim, A., Weerappuli, D.P.V., Roberts, V., and Schneider, D., Relationships Between Passenger-Car Seat Back Strength and Occupant Injury Severity in Rear-End Collisions: Field and Laboratory Studies. *SAE Transactions*, 1997. **106**(2): p. 3935-3967.
7. Warner, C.Y., Stother, C.E., James, M.B., Decker, R.L., Occupant Protection in Rear-end Collisions: II. The Role of Seat Back Deformation in Injury Reduction. *SAE International*, 2003. **106**: p. 370-381.
8. Caldicott, S.J., Shapcott, N., Validation of a Software-Based Stability Assessment System for WHeelchairs and their Occupants. *Journal of Medical Engineering and Technology*, 2008: p. 1-8.
9. Shaw, G., Lapidot, A., Scavnicky, M., Schneider, L.W., and Roy, P. *Interlaboratory study of proposed compliance test protocol for wheelchair tiedown and occupant restraint systems*. in *Proceedings of the 38th Stapp Car Crash Conference*. 1994. Fort Lauderdale, FL, USA: SAE, Warrendale, PA, USA.
10. Solanki, K.O., D. L.; Burton, C. L.; Fang, H.; Horstemeyer, M. F. *Crashworthiness Simulations Comparing PAM-CRASH and LS-DYNA*. in *Society of Automotive Engineers; SAE 2004 world congress*. 2004. Detroit, MI: SAE; 2004.
11. Kang, W. and Pilkey, W.D., Crash simulations of wheelchair-occupant systems in transport. *Journal of Rehabilitation Research & Development*, 1998. **35**(1): p. 73-84.
12. Mao, M., Chirwa, E.C., Chen, T., and Latchford, J., Static and dynamic roof crush simulation using LS-DYNA3D. *International Journal of Crashworthiness*, 2004. **9**(5): p. 495-504.
13. Song, D., Mack, P., Tarriere, C., Brun-Cassan, F., Le Coz, J.Y., Lavaste, F, Finite Element Simulation of the Occupant/ Belt Interaction: Chest and Pelvis Deformation, Belt Sliding and Submarining. *SAE International*, 2003. **92**: p. 817-835.
14. Bertocci, G.E., Szobota, S, Ha, D.R., Van Roosmalen, L, Development of Frontal Impact Crashworthy Wheelchair Seating Design Criteria Using Computer Simulation. *Journal of Rehabilitation and Development*, 2000. **37**(5): p. 565-572.
15. Bertocci, G., Ha, D., Van Roosmalen, L., Karg, P., and Deemer, E., Evaluation of wheelchair drop seat crashworthiness. *Medical Engineering and Physics*, 2001. **23**(4): p. 249-257.
16. Bertocci, G., Souza, A.L., and Szobota, S., The effects of wheelchair-seating stiffness and energy absorption on occupant frontal impact kinematics and submarining risk using computer simulation. *Journal of Rehabilitation Research and Development*, 2003. **40**(2): p. 125-130.
17. Rouhana, S.W., Assessment of Lap-Shoulder Belt Restraint Performance in Laboratory Testing. *Progress in Technology*, 2003: p. 135-145.